THE UNIVERSITY
of EDINBURGH

STING at the Nuclear Envelope: Novel Partners Contribute to Innate Immune Responses

Charles R. Dixon

Thesis submitted for the degree of

Doctor of Philosophy

The University of Edinburgh

School of Biological Sciences

May 2021

Declaration

I declare that this thesis is composed by myself and the work presented within is my own, except where stated otherwise. This research has not been submitted for any other degree except for the degree of Doctor of Philosophy at The University of Edinburgh.

Charles Dixon

Edinburgh

May 2021

Lay Summary

Most cells have the intrinsic ability to detect and defend against infection from viruses or bacteria, this is called the innate immune response. This response relies on the detection of molecular patterns unique to viruses and bacteria by host cell sensor proteins. As well as external threats, the innate immune response can also be activated by damage to host cells which results in the leakage of host cell DNA into the cytoplasm. cGAS is one such sensor protein which recognises DNA from invading viruses and bacteria, or self-DNA if it is aberrantly localised. Upon recognising DNA in the cytoplasm, cGAS activates a signalling cascade which results in the expression of genes to combat infection/cell damage and the recruitment of specialised cells of the immune system. STING is an essential molecule in this signalling cascade and propagates signalling started by cGAS. STING resides in a compartment of the cell called the endoplasmic reticulum, an interconnected membrane system within the cell cytoplasm, but when activated during an innate immune response it leaves the endoplasmic reticulum to activate downstream signalling factors. STING was initially identified in another cellular compartment known as the nuclear envelope, which is connected to the endoplasmic reticulum and encapsulates host cell DNA in the nucleus protecting it from the cytoplasm. However, most research has focussed on STING's functions in the endoplasmic reticulum and not investigated its functions in the nuclear envelope. Therefore, in this study I sought to investigate STING localisation and functions within the nuclear envelope.

The nuclear envelope is a double membrane system comprising inner and outer nuclear membranes and, in this thesis, I present work showing for the first time that STING is present in both the inner and outer membranes. Moreover, live-cell microscopy of fluorescently tagged STING reveals that it increases mobility and redistributes to the outer nuclear membrane upon innate immune response stimulation by DNA or a synthetic RNA which mimics viral infection. Previously, isolation of STING from purified nuclear envelopes coupled with mass spectrometry, a technique used to identify proteins, found new potential partners of STING at the nuclear envelope. Seventeen of these potential STING partners interact indirectly with key innate immune signalling factors, and so it was hypothesised that they may also be involved in innate immune responses through STING at the nuclear envelope.

Therefore, I interrogated a subset of these proteins for a role in the innate immune response, finding that several STING partners are novel modulators of DNA triggered innate immune responses. Moreover, I found that one partner is a novel antagonist of the RNA virus, influenza A virus, potentially shedding light on reports of STING-mediated inhibition of RNA viruses. Thus, the work presented in this thesis expands our knowledge of STING's role in the innate immune response and adds to a growing literature which shows that STING's functions are more extensive than its role in the cytoplasmic DNA sensing pathway.

Abstract

The innate immune response (IIR) is the first line of defence against pathogen infection and relies on the recognition of pathogen associated molecules by host cell sensors. STING (STimulator of INterferon Genes) is the essential adaptor protein in IIRs triggered by the recognition of cytoplasmic double-stranded DNA, a potent signal of pathogen infection or host cell DNA damage. Most STING resides in the endoplasmic reticulum and propagates IIR signalling cascades upon binding the second messenger, cGAMP, produced by the upstream cytosolic DNA sensor, cGAS. However, STING was initially identified as a nuclear envelope transmembrane protein and yet the function of STING within the nuclear envelope has been relatively understudied. Therefore, in this study I sought to investigate STING localisation and functions within the nuclear envelope.

The nuclear envelope is a double membrane system comprising inner and outer nuclear membranes and, in this thesis, I present work showing for the first time that STING is present in both the inner and outer membranes by immunogold electron microscopy. Moreover, live-cell microscopy of GFP-tagged STING reveals that it increases mobility and redistributes to the outer nuclear membrane upon IIR stimulation by transfected dsDNA or the dsRNA mimic poly(I:C). Previously, immunoprecipitation of STING from isolated nuclear envelopes coupled with mass spectrometry identified a nuclear envelope-STING proteome consisting of known nuclear membrane proteins and enriched in DNA- and RNA-binding proteins. Seventeen of these nuclear envelope STING partners are known to bind direct interactors of the immune transcription factors, IRF3/7, and so it was hypothesised that these proteins could contribute to IIR through STING at the nuclear envelope. Therefore, I interrogated a subset of these for a role in IIR, finding that STING partners SYNCRIP, MEN1, DDX5, SNRNP70, RPS27A, and AATF are novel modulators of dsDNA triggered IIR. Moreover, through siRNA-mediated knockdown and CRISPR/Cas9 gene editing I found that SYNCRIP is a novel antagonist of the RNA virus, influenza A virus, potentially shedding light on reports of STING-mediated inhibition of RNA viruses.

Thus, the work presented in this thesis expands our knowledge of STING's role in IIR and adds to a growing literature which shows that STING's functions are more extensive than its role in the cytoplasmic DNA sensing pathway.

Acknowledgements

Firstly, I would like to thank The Wellcome Trust for funding my PhD and making this research possible. Secondly, I would like to thank my supervisor, Eric, for his guidance and support throughout. The freedom he gave me in the lab to experiment and learn different techniques has, I believe, made me a better scientist. Thanks should also go to my second supervisor, Martin Goldberg, and other members of my thesis committee - Bill Earnshaw, Sara Macias-Ribela, David Gray - for their comments and critique of my work. I would also like to thank several collaborators and facility managers, without whom, much of this work would not have been possible. Special thanks to Paul Digard who welcomed me into his lab to learn all things Flu-related and Elly Gaunt who supervised and encouraged me while in his lab. Thank you to David Kelly who taught me most things microscope-related and whose cheery demeanour always made COIL an enjoyable place to work. Thanks to Jessica Valli who assisted FRET-FLIM microscopy and Martin Waterfall for FACS. Thank you to Mark Tingey and Weidong Yang who conducted smFRAP experiments after my many attempts to distinguish inner and outer nuclear membranes using various alternative fluorescence microscopy approaches failed. Thanks also to Christine Richardson and Martin Goldberg whose expertise and supervision were essential for immunogold electron microscopy.

Next, I would like to thank all members of the Schirmer Lab, past and present, who have been not just colleagues but friends during my time in Eric's lab – not only did they teach me so much, but they also gave me many laughs along the way. So, thank you especially to Rafal, Aishwarya, José, Andrea, Dario, Douglas, and Alex with whom I shared much of this journey. Thanks also to members of the Earnshaw, JP, Ly, and Heun labs who had to suffer my lab meetings, their critique and suggestions were always helpful. I would also like to thank the many friends I have made in the Michael Swann Building who made the day-to-day more enjoyable.

Outside of the lab I would like to thank all my friends, old and new, who encouraged me and kept me going, particularly over these last few months where their motivating me to finish my thesis was especially helpful. I would like to give special thanks to my partner, Becky, for her unwavering support and belief in me. Finally, I would like to thank my parents and family who have given me so much and always been there for me, no matter what.

Abbreviations

3D SIM	3D Structured illumination microscopy
AGS	Aicardi-Goutieres syndrome
AIM2	Absent in melanoma 2
ALR	AIM2-like receptor
APC	antigen-presenting cell
ATP	Adenosine triphosphate
bp	Basepairs
CARD	caspase activation and recruitment domain
cGAS	cyclic GMP-AMP synthase
cGAMP	2'3'-Cyclic GMP-AMP
CHIKV	Chickungunya virus
CLR	C-type lectin receptor
CRISPR	clustered regularly interspaced short palindromic repeats
CTT	C'-terminal tail
Da	Dalton
DAPI	4’,6’-diamidino-2-phenylindole
DDX	DEAD box helicase
DENV	Dengue virus
DNA	Deoxyribonucleic acid
EDTA	ethylenediaminetetraacetic acid
EM	electron microscopy
EMCV	encephalomyocarditis virus
ER	endoplasmic reticulum
ERGIC	Endoplasmic reticulum-Golgi intermediate compartment
ESCRT	endosomal sorting complex required for transport
FLIM	Fluorescence lifetime imaging
FRAP	Fluorescence recovery after photobleaching
FRET	Förster resonance energy transfer
GFP	Green fluorescent protein
GTP	Guanosine triphosphate
h	Hour
HA	haemagglutinin
HCV	hepatitis C virus
HGPS	Hutchinson-Gilford progeria syndrome
HIV	human immunodeficiency virus
HP1	Heterochromatin protein 1
hpi	hours post-infection
HSV	herpes simplex virus
IAV	influenza A virus

IF	immunofluorescence
IFN	interferon
IFNAR	IFN-alpha/beta receptor
IKK	IκB kinase
IL	Interleukin
INM	Inner nuclear membrane
IRF	Interferon response factor
ISG	interferon stimulated gene
JAK	Janus kinase
kb	Kilobase
kDa	kilodalton
LAP1/2	Lamina associated polypeptide 1/2
LBR	Lamin B receptor
MAPK	mitogen-activated protein kinase
MAVS	Mitochondrial antiviral-signalling protein
MDA5	melanoma differentiation-associated protein 5
min	Minutes
MOI	multiplicity of infection
mRNA	Messenger RNA
mt	mitochondria
MYXV	Myxoma virus
NDV	Newcastle disease virus
NE	nuclear envelope
NEMO	NFκB essential modulator
NES	nuclear export signal
NET	Nuclear envelope transmembrane proteins
NFκB	nuclear factor kappa-light-chain-enhancer of activated B cells
NLS	nuclear localisation sequence
nM	nanomolar
nm	nanometre
NPC	Nuclear Pore Complex
Nup	nucleoporin
OAS	2'-5'-oligoadenylate synthetase
ONM	Outer nuclear membrane
PAMP	Pathogen-associated molecular pattern
PBS	Phosphate buffer saline
PCR	Polymerase chain reaction
PEDV	Porcine Epidemic disease virus
PFU	plaque forming units
PKR	Protein kinase R
PLA	proximity ligation assay

poly(I:C)	(polyinosinic:polycytidylic) acid
PRR	Pattern recognition receptor
qPCR	Quantitative polymerase chain reaction
RFP	Red fluorescent protein
RIG-I	Retinoic acid-inducible gene 1
RLR	RIG-I-like receptor
RNA	Ribonucleic acid
SASP	senescence associated secretory phenotype
SAVI	STING-associated vasculopathy with onset in infancy
SDS	Sodium dodecyl-sulphate
SeV	Sendai virus
SINV	Sindbis virus
siRNA	Short interfering RNA
smFRAP	single molecule FRAP
STAT	signal transducer and activator of transcription
STING	STimulator of Interferon Genes
TBK1	TANK-binding kinase 1
TLR	Toll-like receptor
TNF	Tumour necrosis factor
TRAF	TNF receptor associated factor
TRIM	Tripartite motif-containing protein
U	Enzyme units
VSV	vesicular stomatitis virus
WNV	West-Nile virus
YFV	Yellow fever virus
ZIKV	Zika virus

Table of Figures

Contents

Chapter 1

Introduction

STING (stimulator of interferon genes; also called ERIS, MITA, MPYS, and NET23) is the critical adaptor protein in innate immune signalling cascades triggered by cytosolic dsDNA, which culminate in the induction of type-I interferons (IFNs) (Ishikawa and Barber 2008; Zhong et al. 2008; Ishikawa et al. 2009; Sun et al. 2009; Ahn and Barber 2019; Motwani et al. 2019). STING is a ubiquitously expressed transmembrane protein (Ishikawa and Barber 2008; Zhong et al. 2008; Sun et al. 2009) and while early studies reported that STING localised throughout the endoplasmic reticulum (ER) (Ishikawa and Barber 2008; Ishikawa et al. 2009; Sun et al. 2009), at mitochondria (Jin et al. 2008; Zhong et al. 2008), and at the plasma membrane (Jin et al. 2008), it is now widely stated that STING is an ER protein with a small pool interacting with the mitochondria likely at mitochondria-associated ER membranes (Ishikawa and Barber 2008; Ishikawa et al. 2009; Sun et al. 2009). However, prior to its identification as an ER resident protein, STING was identified as a candidate nuclear envelope (NE) protein based on proteomics of NEs isolated from rat liver (Schirmer et al. 2003). Despite this, most research into STING has focussed on its role at the ER in innate immune signalling cascades triggered by cytosolic DNA. I am interested in investigating the localisation of STING within the NE and the role of STING at the NE, an area of research which has been largely neglected except by the Schirmer Laboratory which previously reported STING's presence in the NE (Schirmer et al. 2003; Malik et al. 2010) and discovered that overexpression of STING induced a chromatin compaction phenotype radiating from the NE (Malik et al. 2014).

In this chapter, I will begin by describing the NE and mechanisms by which transmembrane proteins are targeted there. I will then give an overview of the innate immune response and the role STING plays in it, as well as emerging roles for STING. Finally, I will describe the extent of our knowledge of STING at the NE and define the aims of this study.

1.1 - The Nuclear Envelope

The segregation of genomic material within a distinct cellular compartment, the nucleus, is the eponymous feature of eukaryotic cells, distinguishing them from prokaryotes. The nucleus is encapsulated by a double membrane system known as the NE, which physically

separates most of the cell's genetic material (DNA) from the cytoplasm. Structurally, the NE consists of two lipid bilayers, the outer and inner nuclear membranes (ONM and INM) which are separated by an approximately 50 nm luminal space and connect at discrete locations forming pores between the nucleus and cytoplasm (Callan et al. 1949; Callan and Tomlin 1950). Within these pores sit the multi-protein structures called nuclear pore complexes (NPCs) (Aitchison and Rout 2012; Grossman et al. 2012), which form proteinaceous channels that allow for regulated transport between the nucleus and cytoplasm. On its nucleoplasmic face, the NE is supported by the nuclear lamina, a matrix of intermediate filament lamin proteins which line the INM providing mechanical stability (Gerace et al. 1978; Gruenbaum and Foisner 2015). While on its cytoplasmic face, the ONM is contiguous with the ER and not only doubles as a functional subdomain of the ER studded with ribosomes, but also has ONM-specific proteins (Crisp et al. 2006; Meinke and Schirmer 2015). Thus, the ER, ONM, and INM constitute a continuous membrane system (Figure 1.1 A).

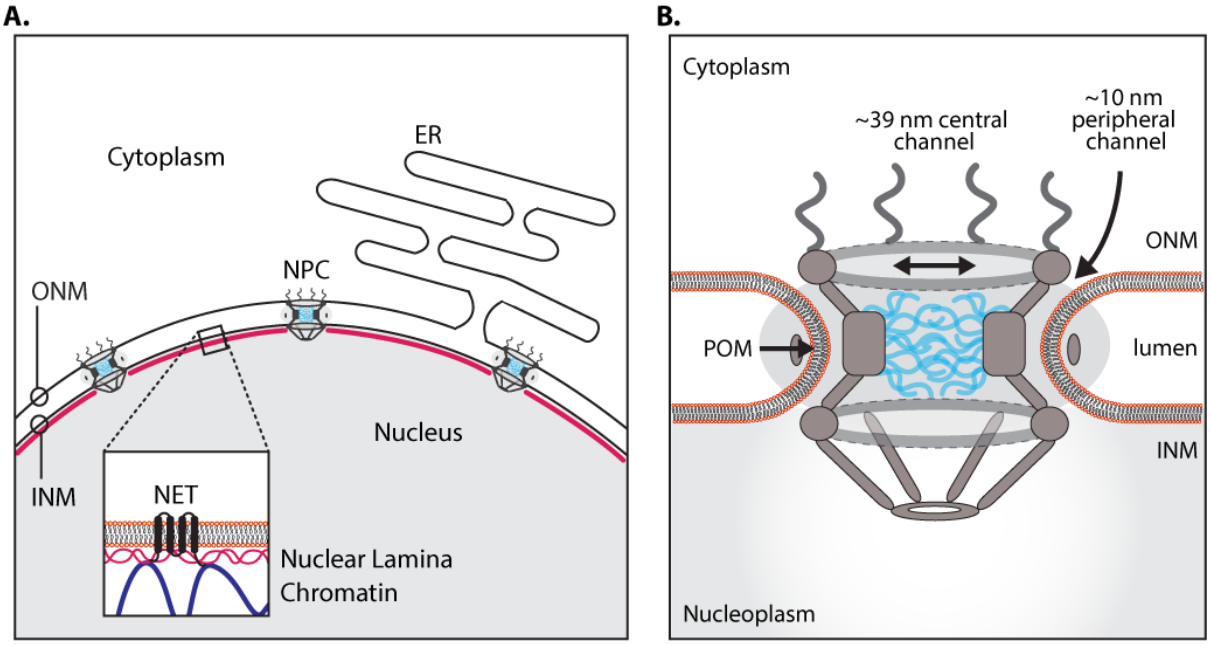

Figure 1.1 – The Nuclear Envelope and Nuclear Pore Complex (A) *Organization of the mammalian nuclear envelope (NE). The NE is a double-membrane system that encapsulates the genome, separating the nucleoplasm from the cytoplasm. The outer nuclear membrane (ONM) is contiguous with the endoplasmic reticulum (ER) and connects to the inner nuclear membrane (INM) at multiple locations, forming pores through the NE which are stabilized by nuclear pore complexes (NPCs). The INM is underlined by a meshwork of intermediate filament lamin proteins which make up the nuclear lamina (red). Some NE transmembrane proteins (NETs) present in the INM interact with lamins and/or chromatin (blue)* ***(B)*** *Structure of the nuclear pore complex (NPC). NPCs function as semipermeable channels in the NE for nucleocytoplasmic molecular exchange. Transmembrane nucleoporins (Nups) tether the NPC*

to the pore membrane (POM) which connects the ONM and INM with both convex and concave membrane curvature. In addition to the central channel of the NPC, which is lined with FG repeats (blue) thought to facilitate the translocation of cargoes up to ~39 nm in diameter across the NE, there exist ~10 nm diameter peripheral channels between the core scaffold of the NPC and pore membrane. Adapted from (Dixon and Schirmer 2018).

Although compartmentalisation of the genome likely arose to protect DNA from potentially damaging metabolic enzymes, conferring a major evolutionary benefit to the first eukaryotic cells, proteins that reside in the NE have been shown to be involved in numerous functions, greatly expanding the role of the NE. Such functions include: spatial genome organisation (Meaburn et al. 2007; Zuleger et al. 2013; Robson et al. 2016), compartmental epigenetic silencing (Ye and Worman 1996; Makatsori et al. 2004; Shaklai et al. 2007; Demmerle et al. 2012), DNA replication (Meier et al. 1991; Moir et al. 1994; Spann et al. 1997; Ellis et al. 1997; Kennedy et al. 2000), transcriptional regulation (Ivorra et al. 2006), mechano-transduction (Ho et al. 2013; Swift et al. 2013), mechanical stability (Lammerding et al. 2004; Broers et al. 2004; Lammerding et al. 2006; Lee et al. 2007), and cell migration (Lee et al. 2007; Willis et al. 2008). Furthermore, in the context of the innate immune response the NE functions to segregate DNA from cytosolically localised DNA sensors which would otherwise induce immune signalling against self-DNA (Motwani et al. 2019). NE localised proteins form the NE proteome, which despite the continuity of lipid membranes with the ER, is distinct from that of the ER with both INM and ONM having partially unique sets of transmembrane proteins, often termed NETs for **N**uclear **E**nvelope **T**ransmembrane proteins (Schirmer et al. 2003; Worman and Schirmer 2015). Moreover, the NE proteome has been shown to differ notably between tissues with many NETs showing tissue restricted expression and localisation at the NE which is evidence of tissue-specific functions for NETs and highlights that the NE is more than just a physical barrier between the nucleus and cytoplasm (Korfali et al. 2010; Wilkie et al. 2011; Korfali et al. 2012; de Las Heras et al. 2013).

1.2 - Protein transport to the inner nuclear membrane

The NPCs are the principal route into and out of the nucleus, because of this nearly all molecules travelling between the cytoplasm and nucleus must pass through these channels. Structurally the NPC consists of multiple copies of ~30 distinct protein subunits called nucleoporins (Nups) which form a semipermeable channel with pseudo-eightfold symmetry (Gall 1967). The core of the NPC is normally considered as a three-stacked ring structure

surrounding a central channel, with cytoplasmic and nuclear rings sandwiching an inner spoke ring which anchors the NPC to the pore membrane (where ONM and INM meet) through transmembrane Nups (Frenkiel-Krispin et al. 2010). In addition to the core structure of the NPC, eight cytoplasmic filaments protrude into the cytoplasm from the cytoplasmic ring, while from the nuclear ring emanates the nuclear basket (Beck and Hurt 2016; von Appen and Beck 2016). As well as the central channel, structural analysis using electron microscopy revealed the presence of smaller peripheral channels around the central channel adjacent to the pore membrane (Hinshaw et al. 1992; Beck et al. 2007) (Figure 1.1 B).

While small molecules, including metabolites and ions, are able to diffuse freely through NPCs, soluble molecules larger than ~40 kDa or 5 nm, such as proteins and RNA are unable to pass through freely. Instead these molecules require energy-dependent mechanisms to traverse the NPC based on the recognition of nuclear localization signals (NLS) or nuclear export signals (NES) present on cargo molecules by nuclear transport receptor proteins, importins and exportins (Güttler and Görlich 2011; Grossman et al. 2012). These nuclear transport receptors mediate cargo transport across the NPC by means of hydrophobic interactions with phenylalanine-glycine-rich nucleoporin repeat domains (FG-repeat domains) present on the Nups which line the central channel. Receptor-cargo binding and release are dictated by a gradient of the GTPase, Ran, across the NPC. For import, cargos are bound in the cytoplasm by importins which translocate through the central channel of the NPC into the nucleus. In the nucleus, Ran bound to GTP (Ran-GTP) binds to the importin-cargo complex causing dissociation of the importin from its cargo. The importin-Ran-GTP complex then translocates to the cytoplasm where it is dissociated by action of the Ran binding proteins (RanBP1/2) and Ran-GTP is bound by the Ran GTPase activating protein (Ran-GAP) that induces hydrolysis of GTP to GDP. Ran-GDP is subsequently trafficked to the nucleus by the transport protein, NUTF2, and once in the nucleus Ran-GDP interacts with RCC1, a Ran guanine nucleotide exchange factor (GEF) which replaces GDP for GTP forming Ran-GTP. Conversely, for export an exportin protein binds to its cargo in the nucleus and must associate with Ran-GTP to form a stable export complex allowing for transport across the NPC. Once in the cytoplasm this complex is disassembled by RanBP1/2 and Ran-GAP resulting in the formation of Ran-GDP. The directionality of transport is thus dictated by differential localisation of Ran-GTP, with a high concentration of Ran-GTP in the nucleus maintained by

the chromatin-associated Ran-GEF, RCC1, and a low concentration in the cytoplasm due to the action of Ran-GAP (Fried and Kutay 2003; Cook et al. 2007).

The translocation of INM bound transmembrane proteins into the nucleus appears more complex than that of soluble proteins, with evidence to support multiple different mechanisms for different proteins (Ohba et al. 2004; Saksena et al. 2004; King et al. 2006; Braunagel et al. 2007; Zuleger et al. 2011; Meinema et al. 2011; Ungricht et al. 2015; Dixon and Schirmer 2018). Since NETs are primarily thought to be co-translationally inserted into the ER membrane (Laba et al. 2014) they should be able to diffuse freely through the ER to the ONM. However, negotiating the NPC to reach the nucleus presents a greater obstacle for transmembrane proteins than soluble proteins. Following the route taken through the central channel of the NPC by soluble proteins (Fiserova et al. 2010; Yang 2013) would seem incompatible for a transmembrane protein as it would either require a mechanism to prevent co-translational insertion into the ER membrane, or a mechanism to extract them from the ER membrane post-translationally. Instead, transmembrane proteins are thought to transit through the NPC while remaining embedded in the lipid bilayer of the pore membrane. Given the existence of ~10 nm wide peripheral channels in the NPC adjacent to the pore membrane (Hinshaw et al. 1992; Beck et al. 2007; Maimon et al. 2012; Bui et al. 2013; von Appen et al. 2015), it is thought that the nucleoplasmic mass of NETs passes through these openings while their transmembrane domains diffuse through the pore membrane. Indeed, it has been demonstrated experimentally that provided the nucleoplasmic mass of an INM targeted NET does not exceed ~60kDa it can still traffic from the ER to the INM (Soullam and Worman 1995; Ohba et al. 2004; Turgay et al. 2010; Zuleger et al. 2011; Ungricht et al. 2015). No such size restriction exists for soluble proteins and this would indicate that transmembrane and soluble proteins take different routes through the NPC.

A number of different mechanisms for trafficking and enrichment of NETs at the INM have been proposed (Dixon and Schirmer 2018). The best described of which include lateral diffusion in the membranes of the ER and NE followed by retention at the INM, ATP-dependent transport, and NLS-dependent receptor-mediated transport. In the lateral diffusion-retention model of transmembrane protein targeting to the INM, NETs diffuse laterally in the membranes of the ER and NE and pass through the peripheral channels of the NPC by undirected passive diffusion while remaining embedded in the pore membrane. NETs

are able to accumulate in the INM through binding to nuclear localised partners (Powell and Burke 1990; Smith and Blobel 1993; Soullam and Worman 1993). This model is supported by the observed ~60 kDa size restriction limit of the nucleoplasmic domains of INM proteins (Soullam and Worman 1995; Ohba et al. 2004; Turgay et al. 2010; Zuleger et al. 2011; Ungricht et al. 2015) and the identification of nuclear binding partners for several NETs. A major binding partner of INM proteins is the nuclear lamina underlying the INM which binds NETs including LBR (Worman et al. 1988; Ye and Worman 1994), LAP1 and LAP2 (Senior and Gerace 1988; Foisner and Gerace 1993), emerin (Clements et al. 2000), SUN2 (Hodzic et al. 2004), and most of the NETs identified by proteomics (Schirmer et al. 2003) tested thus far (Malik et al. 2010). As well as binding to the nuclear lamina, several NETs also bind to chromatin or chromatin-associated proteins, for example, LBR binds to heterochromatin protein 1 (HP1) (Ye and Worman 1996) and the LEM domain family of proteins (LAP2, emerin, Man1) bind to the chromatin-associated protein barrier to autointegration factor (BAF) (Brachner and Foisner 2011). Moreover, several NETs direct particular patterns of genome organization indicative of chromatin binding (Zuleger et al. 2013; Robson et al. 2016). Although, recent studies suggest that lateral diffusion and retention are the major determinants of protein targeting to the INM (Boni et al. 2015; Ungricht et al. 2015) several proteins have been described which require additional factors for INM localization (Zuleger et al. 2011; Katta et al. 2014). For example targeting of SUN2 and emerin to the INM appears to be an energy-dependent process requiring ATP (Ohba et al. 2004; Zuleger et al. 2011; Dixon and Schirmer 2018). Another well-described mechanism of protein transport to the INM that is used by a few NETs is the NLS-dependent facilitated transport mechanism. The yeast orthologues of human Man1 and LEM2 proteins, Heh1 and Heh2, were found to contain NLSs and accumulate at the INM in yeast via a receptor-mediated transport pathway (King et al. 2006; Lusk et al. 2007). These NLSs are separated from the transmembrane domain by an intrinsically disordered (ID) linker region and both NLS and ID linker are required and sufficient to accumulate a membrane protein at the INM in yeast (Meinema et al. 2011). Subsequently, the NLS and linker region of Heh2 was shown to target a membrane-embedded reporter to the INM in human cells suggesting that this transport mechanism could function in higher eukaryotes (Kralt et al. 2015). What is perhaps most striking about this receptor mediated transport mechanism is that importins required for translocation through the NPC are larger than the ~60 kDa limit for translocation through the peripheral channels of the NPC. This

suggests that transport must occur simultaneously through the central channel and peripheral channels with the NET maintained in the nuclear pore membrane. Work in yeast showed that a ID linker region of at least 120 amino acid residues between transmembrane domain and NLS is required for this transport mechanism (Meinema et al. 2011; Meinema et al. 2013; Laba et al. 2015). The team behind these studies proposed that this ID linker effectively slices through the core NPC scaffold allowing the NLS bound by importins to translocate through the central channel while the transmembrane domains of the NET remain embedded in the pore membrane. In support of this mechanism, human LBR and Lap2β, which contain ID-linkers and NLSs, were recently shown to simultaneously transit through the central channel as well as the peripheral channels of the NPC (Mudumbi et al. 2020).

1.3 - The innate immune system and pattern recognition

The mammalian immune system consists of two arms, innate and adaptive, the combined action of which drives the clearance of pathogen infection. While the innate immune system provides the first line of defence against invading pathogens with a fast-acting, generalised response to infection, the adaptive immune response is highly specific, relying on specialised immune cells, and often results in immunological memory.

Innate immune responses to pathogen infection are initiated through the recognition of distinct 'non-self' components of microorganisms (pathogen associated molecular patterns (PAMPs)) by germline-encoded host cell sensors, known as pattern recognition receptors (PRRs) (Janeway, C.A. 1989; Medzhitov 2009). PAMPs are usually essential to the invading pathogen and evolutionarily conserved so they cannot be readily mutated to enable evasion of PRRs. An increasingly large number of PRRs have been identified which detect signatures of pathogen infection in different subcellular locations (Palm and Medzhitov 2009; Unterholzner 2013; Chow et al. 2015; Sparrer and Gack 2015). Toll-like receptors (TLRs) (Kawai and Akira 2011) and C-type lectin receptors (CLRs) (Dambuza and Brown 2015) detect extracellular PAMPs at the plasma membrane and in endosomal compartments and are predominantly expressed by specialised cells of the immune system (Dambuza and Brown 2015). Conversely, receptors that detect intracellular PAMPs are localised in the cytoplasm and/or nucleus and include: the viral RNA sensing RIG-I-like receptors (RLRs) (Yoneyama et al. 2015), cytosolic DNA sensors including cyclic GMP-AMP synthase (cGAS) (Sun et al. 2013) and the AIM2-like receptors (ALRs) (Unterholzner et al. 2010; Caneparo et al. 2018), and NOD-like

receptors (NLRs) which primarily sense intracellular bacteria (Kersse et al. 2011). In contrast to TLRs and CLRs these sensors are more widely expressed enabling the detection of intracellular infection by virtually all cell types.

1.3.1 - Innate immune responses to viral infection

In response to viral infection, a key mechanism of host cell antiviral defence is the induction of the interferon (IFN) response, following the recognition of viral PAMPs, which upregulates the expression of antiviral genes and pro-inflammatory cytokines to recruit specialised cells of the immune system to clear infection. The major PAMPs recognised by host PRRs during viral infection are the nucleic acids of actively replicating viruses (Sparrer and Gack 2015; Ma et al. 2018). Once these are detected by PRRs, signalling cascades are initiated through the activation of PRR family-specific adaptor proteins, which converge on a group of well characterized kinases. Through a series of phosphorylation events these kinases activate immune transcription factors, culminating in the expression of IFNs and pro-inflammatory cytokines and chemokines (Goubau et al. 2013; Liu et al. 2015a). In turn, secreted IFN binds to the surface interferon-α/β receptor (IFNAR) in an autocrine and paracrine manner leading to the activation of JAK-STAT signalling cascades. Activated STAT proteins dimerize and translocate to the nucleus where they induce the expression of IFN-stimulated genes (ISGs) whose products antagonize viral replication through mechanisms including viral RNA cleavage and the induction of apoptosis. Among ISGs are some PRRs and proteins involved in immune signalling cascades, resulting in a positive feedback loop and sensitising neighbouring cells for detection of viral infection. At the same time, secreted cytokines and chemokines regulate the recruitment and activation of cells of the adaptive immune system to clear viral infection (Schneider et al. 2014). In addition to IFN induction, some PRRs activate inflammasome complexes leading to activation of caspases, in particular caspase-1, and maturation of pro-forms of IL-1β and IL-18 pro-inflammatory cytokines (Chen and Ichinohe 2015). Caspase-1 also cleaves the cytosolic protein gasdermin D into an N-terminal domain (GSDMD-N) and C-terminal domain (GSDMD-C), GSDMD-N oligomerises on the cell membrane forming transmembrane pores resulting in cell membrane rupture and release of pro-inflammatory intracellular contents in a specialised form of inflammatory cell death termed pyroptosis (Bergsbaken et al. 2009).

The large array of PRRs and web of signalling cascades they initiate upon recognition of pathogen invasion require tight regulation, adding another layer of complexity to the innate immune response. Left unchecked, the excessive production of IFNs and pro-inflammatory cytokines can have deleterious effects on the host resulting in autoimmune disease (Kato and Fujita 2014; Crowl et al. 2017), while insufficient innate immune responses can result in higher disease severity and lethality. Key proteins involved in innate immune responses triggered following cytosolic RNA and DNA recognition will be discussed below.

1.3.2 - Detection of cytosolic viral RNA

Detection of cytosolic viral RNA occurs primarily through the RLR family of DExD/H-box helicases, which consists of retinoic acid-inducible gene-I (RIG-I) (Yoneyama et al. 2004), melanoma differentiation-associated gene 5 (MDA5) (Kang et al. 2002), and laboratory of genetics and physiology 2 (LGP2). All three are able to bind directly to RNA through their helicase and C-terminal domains, although only RIG-I and MDA-5 possess N-terminal caspase activation and recruitment domains (CARDs) which enable association with the CARD of the downstream adaptor protein MAVS (IPS-1/VISA/Cardif) located at the mitochondrial outer membrane (Seth et al. 2005; Kawai et al. 2005; Meylan et al. 2005). Although unable to activate MAVS itself, LGP2 appears to contribute to the regulation of immune responses by inhibiting RIG-I and supporting MDA5 signalling (Ahmad and Hur 2015). Both RIG-I and MDA5 recognise distinct viral RNA structural features which are absent from mature host RNAs, preventing aberrant activation in the absence of viral infection (Schlee and Hartmann 2016). RIG-I primarily recognises uncapped 5’-triphosphate double-stranded RNA (dsRNA) that lacks overhangs (Marques et al. 2006; Hornung et al. 2006; Schlee et al. 2009), while MDA-5 is potently activated by very long dsRNA (>300bp) independently of any structure on the ends of the RNA (Gitlin et al. 2006; Kato et al. 2006; Kato et al. 2008). Upon RNA ligand binding, RIG-I undergoes a conformational switch from an inactive to active form, exposing its CARDs and forming a tetramer (Kowalinski et al. 2011; Wu et al. 2014; Zheng et al. 2015). MDA5 on the other hand is thought to adopt a ring-like conformation around dsRNA with monomers of MDA5 stacking along the dsRNA to form MDA5 filaments, with the CARDs decorating the outer surface of this structure and forming oligomers capable of activating MAVS (Wu et al. 2013a). The exposed CARDs of RNA bound RIG-I/MDA5 bind the CARD of MAVS inducing the formation of prion-like MAVS aggregates (Hou et al. 2011) which serve as scaffolding

complexes for the recruitment and activation of downstream signalling components. These include TNF receptor-associated factors (TRAFs), TANK-binding kinase 1 (TBK1), and IκB kinase (IKK) complexes. TRAFs activate TBK1 and IκB kinase epsilon (IKKε) kinases which phosphorylate interferon regulatory factor 3 (IRF3) and IRF7 transcription factors. MAVS signalling complexes also recruit and activate the IKKα/β/γ complex. The IKKα/β/γ complex consists of three subunits, the regulatory IKKγ subunit (also known as NF-κB essential modulator, NEMO) and catalytic subunits IKKα and IKKβ. TRAFs mediate ubiquitination at MAVS signalling complexes and the K63-linked ubiquitin chains are bound by IKKγ which in turn recruits IKKα/β subunits which phosphorylate and activate one another. Activated IKKα/β/γ phosphorylates IκB, the inhibitor of NF-κB, which is subsequently ubiquitinated and targeted for proteasomal degradation. In unstimulated cells NF-κB dimers are bound by IκB which masks an NLS on NF-κB proteins, sequestering them in the cytoplasm and so IKKα/β/γ mediated phosphorylation of IκB releases NF-κB dimers. Active IRF3/7 and NF-κB transcription factors are then able to translocate to the nucleus where they induce the expression of type-I IFNs and pro-inflammatory cytokines (Chiang et al. 2014; Kato and Fujita 2014; Sparrer and Gack 2015) (Figure 1.2). In addition to RLRs, a number of other sensors of cytosolic viral RNA exist many of which directly inhibit viral propagation upon recognition of RNA (Sparrer and Gack 2015; Schlee and Hartmann 2016). These include protein kinase R (PKR) which inhibits cellular translation and activates the inflammasome, and may act with RLRs to induce IFN-mediated immune responses (Levin and London 1978; Pfaller et al. 2011), and 2',5'-oligoadenylate synthetase (OAS) which upon dsRNA binding synthesises 2'5'-linked oligoadenylate that acts as a second messenger to activate RNase L, which then degrades RNA in the cytoplasm (Hornung et al. 2014). RNA fragments generated by RNase L may then serve as ligands of the RIG-I-MAVS pathway, amplifying antiviral signalling (Malathi et al. 2007).

1.3.3 - Cytosolic DNA sensing and the cGAS-STING pathway

It has long been known that the introduction of DNA into cells is able to stimulate a protective immune response against viral infection (Rotem et al. 1963). Cytosolic DNA can arise from a number of sources including infection with DNA viruses or intracellular bacteria, artificial introduction by transfection, or host-cell DNA 'leakage' into the cytosol as a result of cellular stress or damage. However, it has only been within the last fifteen years that the molecular mechanisms for sensing and responding to cytosolic DNA have been uncovered, following the

discovery in 2006 that cytosolic DNA potently stimulates an IRF3-dependent IFN response independently of the endosomal DNA sensor, TLR9 (Ishii et al. 2006; Stetson and Medzhitov 2006).

The detection of DNA in the cytosol principally activates two immune signalling pathways, the cGAS-STING pathway which drives the induction of type-I IFN and the caspase-1 inflammasome pathway. The absent in melanoma 2 (AIM2) protein is the primary cytosolic DNA receptor that activates the inflammasome pathway, forming an inflammasome complex with ASC and caspase-1 after binding DNA. The active AIM2 inflammasome controls the proteolytic maturation of the proinflammatory cytokines IL-1β and IL-18 and induces cell death through pyroptosis, a highly inflammatory form of lytic programmed cell death (Bürckstümmer et al. 2009; Fernandes-Alnemri et al. 2009; Hornung et al. 2009; Roberts et al. 2010). Conversely, cGAS is the principal and best described cytosolic DNA sensor for activation of the cGAS-STING pathway and subsequent induction of type-I IFN (Sun et al. 2013; Ablasser and Chen 2019; Ahn and Barber 2019; Motwani et al. 2019).

cGAS binds to dsDNA independently of sequence so it can be activated by dsDNA ligands indiscriminately of their origin, although DNA length is important with longer dsDNAs >45 bp allowing the formation of ladder-like networks of cGAS dimers and enabling stronger signalling (Luecke et al. 2017; Andreeva et al. 2017; Zhou et al. 2018). Following binding to dsDNA, cGAS catalyses the synthesis of a cyclic-dinucleotide (CDN) second messenger, 2’3’-cyclic GMP-AMP (cGAMP), from ATP and GTP (Civril et al. 2013; Diner et al. 2013; Gao et al. 2013b; Li et al. 2013c; Sun et al. 2013; Wu et al. 2013b; Ablasser et al. 2013a). Binding of dsDNA by cGAS results in the formation of liquid-liquid phase separated droplets, in which increased local concentration of cGAS and reactants result in enhanced cGAMP production (Du and Chen 2018). cGAMP then binds directly to STING dimers localised at the ER (Diner et al. 2013; Gao et al. 2013b; Ablasser et al. 2013a; Zhang et al. 2013). STING was previously shown to bind bacterial CDNs (Burdette et al. 2011) but binds to endogenous cGAMP with higher affinity (Zhang et al. 2013) and so cGAMP is a more potent ligand for stimulating STING activation. Binding of cGAMP or bacterial CDNs induces a conformational change in inactive STING dimers (Shang et al. 2012; Gao et al. 2013b; Zhang et al. 2013) leading to the formation of active STING dimers, which are able to pack side-by-side to form tetramers and higher-order oligomers (Shang et al. 2019). The activation of STING through CDN binding results in

its translocation out of the ER, where it is retained in its resting state by the Ca^{2+} sensor STIM1 (Srikanth et al. 2019). STING is transported through COPII mediated vesicular transport, via the ER-Golgi intermediate compartment (ERGIC), to the Golgi apparatus and eventually to post-Golgi vesicles and lysosomes where it is degraded (Ishikawa et al. 2009; Saitoh et al. 2009; Dobbs et al. 2015; Gonugunta et al. 2017). This redistribution event is characteristic of STING activation and can be visualised clearly using fluorescence microscopy as the accumulation of STING in the Golgi and perinuclear foci in cells post-DNA stimulation (Ishikawa et al. 2009; Saitoh et al. 2009; Dobbs et al. 2015; Gonugunta et al. 2017; Franz et al. 2018). In addition to activating STING in the cell in which it is produced, cGAMP can be transferred to nearby cells through gap junctions (Ablasser et al. 2013b) and packaged into progeny virions during viral infection to initiate STING signalling (Bridgeman et al. 2015; Gentili et al. 2015).

Following activation and translocation out of the ER, STING recruits TBK1 which phosphorylates STING at the critical serine residues S366 and S358 (Zhong et al. 2008; Tanaka and Chen 2012; Liu et al. 2015a; Zhang et al. 2019). TBK1 binds to STING via its C-terminal tail (CTT) and phosphorylates the STING dimer adjacent to the one it is bound by virtue of STING dimer oligomerisation upon cGAMP binding (Tanaka and Chen 2012; Zhang et al. 2019). Phosphorylation of STING at S366 and S358 by TBK1 allows the recruitment of IRF3 which is subsequently phosphorylated by TBK1 resulting IRF3 homo-dimerization and dissociation from STING (Zhong et al. 2008; Tanaka and Chen 2012; Liu et al. 2015a; Zhang et al. 2019). This occurs via a shared mechanism between the immune adaptor proteins STING, MAVS, and TRIF, all of which contain a conserved *p*LX*I*S (where *p* is a hydrophilic residue and *x* is any residue) motif that is phosphorylated by TBK1 and subsequently bound by the positively charged surface of IRF3 (Liu et al. 2015a). The phosphorylation and dimerization of IRF3 exposes a masked NLS leading to accumulation of IRF3 in the nucleus where it forms a complex with the transcriptional coactivators CBP/p300 and induces the expression of type-I IFNs and pro-inflammatory cytokines in concert with NF-κB and AP1 (ATF2/c-Jun) transcription factors (Lin et al. 1998; Yoneyama et al. 1998; Kumar et al. 2000; Servant et al. 2002; Zhu et al. 2015). In addition to the recruitment and activation of IRF3, STING also directs the activation of NF-κB and MAPK signalling pathways, albeit to a lesser extent than IRF3 (de Oliveira Mann et al. 2019) (Figure 1.2). However, the mechanism through which STING

activates NF-κB signalling is less well understood compared to IRF3 activation through TBK1, and the mechanism of STING-dependent MAPK activation is not yet known. For NF-κB activation conflicting models have been proposed, in one TBK1 is required and functions upstream of NF-κB activation where it is required for full phosphorylation and activation of IKKα/β/γ (Abe and Barber 2014; Fang et al. 2017). TRIM32, TRIM56, and TRAF6 have been proposed to mediate the ubiquitination required for IKKα/β/γ recruitment and activation (Abe and Barber 2014; Fang et al. 2017). In the other model TBK1 is not required for NF-κB activation because reports have shown that the CTT of STING, which is required for TBK1 binding and IRF3 activation, is dispensable for NF-κB activation in humans (de Oliveira Mann et al. 2019). Interestingly, ray-finned fish exhibit a much stronger NF-κB response following immune stimulation with dsDNA compared to mammals and this is explained by the finding that the CTT of zebrafish STING is extended compared to mammalian STING species and contains a domain that directly recruits TRAF6 which in turn serves to activate NF-κB (de Oliveira Mann et al. 2019). STING also activates the STAT6 transcription factor which interacts with STING upon immune stimulation and is phosphorylated by TBK1, resulting in STAT6 dimerization and translocation to the nucleus where it induces a specific set of chemokines (CCL2, CCL20, and CCL26) which attract specialised immune cells to the site of infection (Chen et al. 2011).

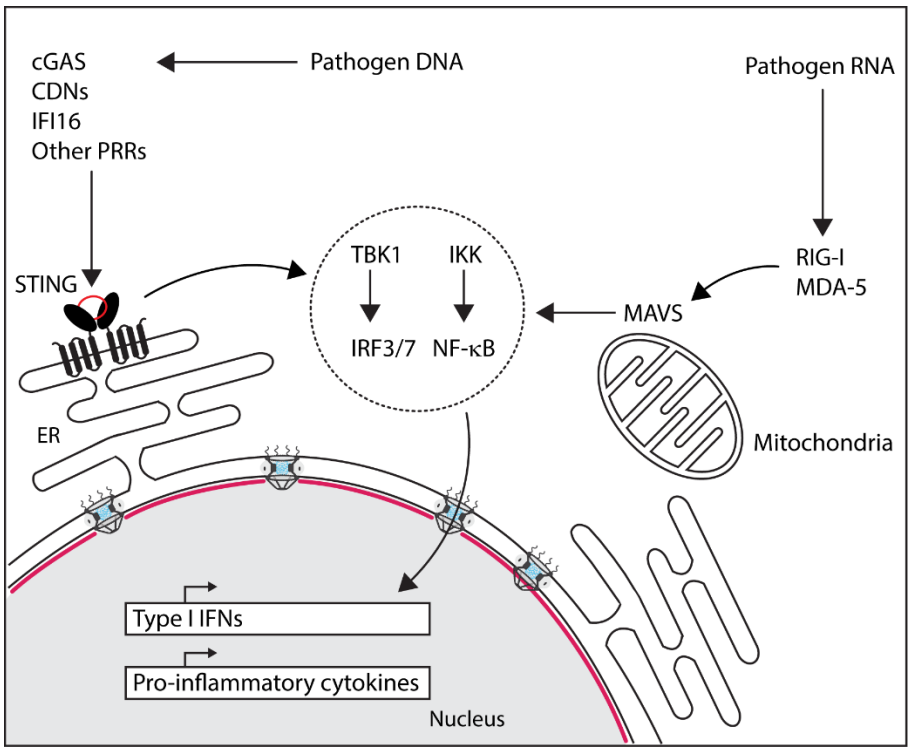

Figure 1.2 - Cytosolic DNA and RNA sensing pathways. *Pathogen DNA in the cytosol is detected by a number of host cell pattern recognition receptors (PRRs). STING homodimers at the endoplasmic reticulum are activated principally through binding cyclic dinucleotides such as the secondary messenger cGAMP produced by cGAS upon dsDNA binding. Upon activation STING traffics to perinuclear puncta where it becomes associated with downstream TBK1 and IKK kinases. These kinases in turn activate IRF3/7 and NF-κB transcription factors which translocate to the nucleus and induce expression of type I interferons (IFNs) and pro-inflammatory cytokines. Viral RNA in the cytosol is detected principally by RIG-I and MDA-5 PRRs, which in turn interact with and activate the critical adaptor protein, MAVS, at the mitochondrial membrane. Active MAVS polymers recruit TBK1 and IKK kinases, leading to IRF3/7 and NF-κB activation.*

Intriguingly, despite recognising DNA in the cytoplasm and initially being described as localising to the cytoplasm, it has been shown that at least a pool of cGAS and perhaps even the majority in some cells resides in the nucleus (Orzalli et al. 2015; Gentili et al. 2019; Volkman et al. 2019). A nuclear localisation of cGAS would help to explain how cGAS is able to function in the detection of DNA viruses nearly all of which replicate their DNA exclusively in the nucleus and were previously proposed to 'leak' DNA into the cytoplasm allowing for host cell detection. However, this would mean that in its resting state only a proportion of cGAS is present in the cytosol and able to detect cytosolic DNA. cGAS requires intact chromatin for nuclear localisation and is tethered to chromatin independently of DNA binding. Moreover, cGAS is not 'inert' in its tethered state but competent to detect foreign DNA since mutations in the cGAS tethering surface render cGAS constitutively active against self-DNA (Volkman et al. 2019). Thus, it has been proposed that there must be a regulatory step of cGAS untethering prior to assembly of cGAS onto DNA and subsequent cGAS activation (Volkman et al. 2019). Recent cryo-EM structures of cGAS have revealed that it is tightly tethered to nucleosomes via the acidic patch of H2A-H2B histone dimers which prevents it from binding to free DNA (Cao et al. 2020; Kujirai et al. 2020; Michalski et al. 2020). However, the mechanism by which cGAS is able to become untethered in order to detect DNA remains to be investigated, highlighting that the cGAS-STING pathway is yet to be fully elucidated.

Since the cGAS-STING pathway is critical for the induction of type-I IFNs and pro-inflammatory cytokines in response to cytosolic DNA, it must be strictly regulated to enable the clearance of pathogen infection and to prevent aberrant or sustained activation which would result in immune pathology. A number of positive and negative regulators of cGAS and STING have been identified which ensure sufficient and prevent excessive stimulation of this pathway, respectively (Motwani et al. 2019). Positive regulation of the cGAS-STING pathway includes

the ubiquitination of STING by TRIM32 (Zhang et al. 2012) and TRIM56 (Tsuchida et al. 2010; Yang et al. 2018) which enhances STING's interaction with TBK, and palmitoylation of STING at residues C88 and C91 in the Golgi which is required for type-I IFN induction (Mukai et al. 2016). Conversely, in terms of negative regulation cGAS is cleaved by caspase 1 resulting in its degradation (Wang et al. 2017b) while STING is degraded, via autophagy, following activation of downstream signalling components in order to attenuate signalling (Saitoh et al. 2009; Prabakaran et al. 2018). In addition to the direct regulation of cGAS and STING, a number of host cell nucleases antagonise DNA sensing through degradation of potentially immune stimulatory DNA that accumulates as a result of normal cellular function. These include the cytosolic 3'-5' exonuclease, TREX1 (Stetson et al. 2008), and lysosomal endonuclease DNase II (Lan et al. 2014).

1.3.4 - Additional DNA sensors

In addition to cGAS several other cytosolic DNA sensors have been described which may induce the activation of the STING signalling pathway (Ma et al. 2018). Firstly, STING itself should be considered a PRR since it is able to directly bind to bacterial CDNs produced by bacteria during intracellular infection (Woodward et al. 2010; Burdette et al. 2011). STING is also able to bind directly to DNA, although whether it is able to elicit an immune response through binding DNA on its own remains unclear (Abe et al. 2013).

Secondly, Interferon-γ-inducible protein 16 (IFI16), a member of the ALR family, is one such protein that has a role in DNA sensing and STING activation. IFI16 binds DNA in a sequence independent manner (Unterholzner et al. 2010; Jin et al. 2013; Morrone et al. 2014) and associates with STING following immune stimulation with dsDNA or herpes simplex virus (HSV1) infection to activate antiviral gene expression (Unterholzner et al. 2010; Horan et al. 2013). IFI16 is localised predominantly to the nucleus but has been reported to sense pathogenic DNA in both the cytoplasm and nucleus (Kerur et al. 2011; Orzalli et al. 2012; Orzalli et al. 2013); shuttling between the two compartments depending on the acetylation status of its nuclear localisation sequence (NLS) (Li et al. 2012). *In vitro*, IFI16 oligomerises along naked dsDNA with optimal polymerisation requiring ~150bp of dsDNA (Morrone et al. 2014). This may explain how IFI16 activates immune responses to viral DNA, which is 'naked', without auto-immune activation against host DNA in the nucleus, which is wrapped around nucleosomes separated by short DNA linker regions, 38-53 bp long. While most early studies

into IFI16 function used RNA interference to reduce protein expression, a study using *ALR*$^{-/-}$ mice, which lack all 13 ALR family members, demonstrated that ALRs are dispensable for IFNβ induction in response to transfected DNA in mice, and that human primary fibroblasts which lack IFI16 still mount normal IFN responses against HCMV infection (Gray et al. 2016). This calls into question how widespread the requirement for IFI16 is in inducing IFN expression in response to immune stimulation by cytosolic DNA and DNA viruses. However, two recent studies have indicated that, at least in a subset of human cells, cGAS and IFI16 act cooperatively to induce immune responses to cytosolic DNA and DNA viruses, with both proteins required for full STING activation and induction of IFN (Almine et al. 2017; Jønsson et al. 2017). IFI16 promotes dimerization and phosphorylation of STING following immune stimulation with DNA or cGAMP (Almine et al. 2017; Jønsson et al. 2017), and also acts as a co-factor to cGAS augmenting cGAMP production in human monocytes (Jønsson et al. 2017). In addition to its role in the type-I IFN response, IFI16 sensing of viral DNA in the nucleus also activates the inflammasome pathway via recruitment of ASC and caspase-1 (Diner et al. 2015).

DEAD-box helicase 41 (DDX41) is another putative DNA sensor required for type-I IFN induction in mouse myeloid dendritic cells (mDCs) stimulated with dsDNA (Zhang et al. 2011). DDX41 was identified as a DNA sensor in an siRNA screen of all DExD/H-box family members in which knockdown of DDX41 impaired the type-I IFN and pro-inflammatory cytokine responses to DNA and DNA viruses (Zhang et al. 2011). DDX41 is ubiquitously expressed and able to bind directly to dsDNA and CDNs (Zhang et al. 2011; Parvatiyar et al. 2012; Omura et al. 2016) after phosphorylation by Bruton's tyrosine kinase (BTK) (Lee et al. 2015). Following ligand binding, DDX41 is proposed to bind to STING at the ER and activate downstream signalling (Zhang et al. 2011; Parvatiyar et al. 2012). However, DDX41's role as a PRR in innate immune responses to cytosolic DNA is less clear than that of cGAS or STING. Other groups have reported that overexpression of DDX41 has little effect on IFNβ production (Sun et al. 2013), that knockdown of DDX41 has little effect on STING trafficking or IRF3 nuclear accumulation following immune stimulation with dsDNA or HSV1 (Abe et al. 2013), and that the crystallised DEAD domain of DDX41, which was proposed to mediate DNA/CDN binding, could not bind dsDNA or cyclic-di-GMP *in vitro* (Jiang et al. 2017). Therefore, more work will be required to fully explain the role of DDX41 in cytosolic DNA triggered immune responses.

RNA polymerase III may also function as a cytosolic DNA sensor since it is able to induce IFNβ production upon binding to the synthetic dsDNA mimetic, poly(dA-dT), through synthesis of dsRNA with a 5' triphosphate moiety from the DNA template which serves as a ligand for the RIG-I-MAVS pathway (Ablasser et al. 2009; Chiu et al. 2009). Additionally, DNA damage response proteins, DNA-dependent protein kinase (DNA-PK, a heterotrimeric complex of DNA-PKcs, Ku70, and Ku80) and meiotic recombination 11 homolog A (Mre11) have also been reported to activate the STING pathway upon recognition of cytosolic DNA (Ferguson et al. 2012; Kondo et al. 2013; Morchikh et al. 2017; Wang et al. 2017a).

Finally, TLR9 which is the only TLR of the 10 identified in humans that can bind DNA also acts as a DNA sensor; recognising unmethylated CpG motifs in dsDNA (Hemmi et al. 2000) which are rarely present in mammalian genomes but found commonly in those of bacteria and DNA viruses. However, unlike cGAS which is widely expressed, TLR9 is expressed predominantly in plasmacytoid dendritic cells of the innate immune system and detects DNA in endosomal compartments as opposed to cytoplasm (Latz et al. 2004; Kim et al. 2008). Upon activation TLR9 signals through the MyD88 adaptor protein to induce expression of type-I IFNs and pro-inflammatory cytokines (Kawai and Akira 2011).

The abundance of DNA sensors raises the question of why so many? Although it is clear that cGAS functions as the ubiquitous, essential cytosolic DNA sensor upstream of STING, additional sensors may reflect cell specific adaptations or redundancy given that the immune system is frequently targeted by the invading pathogens it seeks to destroy. Furthermore, additional sensors may act to fine tune cGAS-STING signalling based on the localisation and type of immune stimulus (Ma et al. 2018; Motwani et al. 2019). Thus, it is possible that additional DNA sensors or modulators of cGAS-STING signalling remain to be identified.

1.4 - Activation of the cGAS-STING pathway by self-DNA

Since cGAS binds dsDNA irrespective of sequence the cGAS-STING pathway can be activated by the presence of self-DNA in the cytoplasm as well as foreign DNA from invading pathogens. This is normally avoided by compartmentalisation of host DNA in the nucleus and mitochondria and through negative regulation of the pathway to prevent accumulation of DNA in the cytoplasm. However, self-DNA can accumulate in the cytoplasm as a result of DNA damage, cell stress, or during a number of autoinflammatory diseases, leading to cGAS-STING

activation. Such DNA serves as a so-called danger associated molecular pattern (DAMP) which triggers innate immune responses. Self-DNA also gains access to the cytoplasm during physiological processes such as mitosis and apoptosis but in these cases does not activate the cGAS-STING pathway, suggesting that mechanisms must exist to transiently impair activation of cGAS and/or STING (Ablasser and Chen 2019). Indeed, during apoptosis, pro-apoptotic caspases prevent activation of immune signalling to ensure an immunologically silent cell death (Rongvaux et al. 2014; White et al. 2014), while in the case of mitosis cGAS is rendered inactive by phosphorylation and through chromatin binding which prevents cGAS oligomerisation and activation (Zhong et al. 2020; Li et al. 2021). Moreover, cells may dampen activation of the cGAS-STING pathway against transient exposure to self-DNA through repair processes. For example, during cell migration nuclear envelope rupture often occurs leading to detection of nuclear DNA by cGAS, but downstream signalling can be mitigated by rapidly repairing NE breaks through the ESCRT machinery (Denais et al. 2016; Raab et al. 2016). Activation of the cGAS-STING pathway through detection of self-DNA when such tempering mechanisms are insufficient or do not exist are discussed below.

1.4.1 - Activation of the cGAS-STING pathway by nuclear DNA damage

The cGAS-STING pathway is activated in response to prolonged exposure of nuclear DNA to the cytosol as a result of DNA damage. DNA damage in the nucleus often results in the formation of cytoplasmic micronuclei, small DNA containing organelles encapsulated by NE derived membranes, produced as a result of genotoxic stress and chromosome mis-segregation during cell division (Fenech et al. 2011). The membranes of micronuclei are prone to rupture, likely due to a compromised nuclear lamina and/or reduced membrane repair capacity compared to the NE, leading to the release of self-DNA into the cytosol (Hatch et al. 2013). cGAS is recruited to micronuclei after membrane rupture and catalyses the synthesis of cGAMP which in turn binds to STING triggering the induction of type-I IFN and pro-inflammatory cytokines (Bartsch et al. 2017; Mackenzie et al. 2017; Yang et al. 2017; Harding et al. 2017). DNA damage also appears to activate the cGAS-STING pathway in the absence of micronuclei through the accumulation of cytoplasmic DNA ‘speckles’ which lack nuclear membranes (Lan et al. 2014; Härtlova et al. 2015; Shen et al. 2015; Erdal et al. 2017). Interestingly, cGAS has also been shown to be recruited to sites of DNA damage in the nucleus

and to suppress repair of DNA double-strand breaks through homologous recombination, a function that is independent of STING and cGAS catalytic activity (Liu et al. 2018).

Recently, STING has also been shown to respond to nuclear DNA damage independently of cGAS (Dunphy et al. 2018). Nuclear DNA damage caused as a result of treatment with the topoisomerase inhibitor, etoposide, is detected by ATM and PARP1 proteins and results in the formation of a non-canonical STING signalling complex consisting of TRAF6, IFI16, p53, and STING. This complex drives an NF-κB-dominated transcriptional response as opposed to cGAS-dependent detection of cytosolic DNA and downstream STING signalling which predominantly activates IRF3 signalling. Interestingly, NF-κB dependent signalling does not require STING phosphorylation, STING redistribution to perinuclear foci, or TBK1 activity. However, etoposide treatment also induced IFNβ expression, which involves IRF3 activity as well as NF-κB, and this does require STING redistribution and TBK1 activity but is also independent of cGAS. Thus, nuclear DNA damage appears to elicit a cGAS-independent STING signalling pathway that is distinct from the detection of cytoplasmic DNA released from micronuclei which activates canonical cGAS-STING signalling (Dunphy et al. 2018).

1.4.2 - Activation of the cGAS-STING pathway by mitochondrial DNA

As well as being activated as a consequence of nuclear DNA damage, the cGAS-STING pathway can be activated due to the release of mitochondrial DNA (mtDNA), a symptom of cell stress. Since mtDNA is immunostimulatory, the cell possesses mechanisms to prevent aberrant immune signalling triggered by mtDNA as a result of normal physiological processes (Rongvaux 2018). For example, programmed cell death induced through the mitochondrial pathway of apoptosis leads to the release of mtDNA into the cytosol but is usually immunogenically silent due to the concomitant activation of caspases which inhibit the type-I IFN response (Rongvaux et al. 2014). Similarly, mitophagy of senescent mitochondria clears a source of potential immune stimulatory mtDNA which is degraded in the autophagasome by the DNAse II nuclease (Rongvaux 2018).

On the other hand, during pathogen infection mtDNA can be released into the cytosol and trigger cGAS-STING signalling providing the cell with another mechanism of instigating an immune response. During a study to investigate the effect of mtDNA instability on cells, elicited by partial deficiency of the abundant mtDNA binding protein TFAM (transcription factor A, mitochondrial), it was found that mtDNA binds to and activates cGAS inducing innate

immune signalling (West et al. 2015). Moreover, the same study demonstrated that infection of murine embryonic fibroblasts (MEFs) with herpesviruses similarly resulted in TFAM depletion, mtDNA leakage, and activation of the cGAS-STING pathway indicating that mtDNA serves as a ligand for activation of immune responses during herpesvirus infection (West et al. 2015). Although this study found no such effect on mitochondria during infection with a number of RNA viruses, other studies have found that infection with Dengue virus (DENV), an RNA virus, causes mitochondrial damage and mtDNA leakage which is similarly detected by cGAS (Aguirre et al. 2017; Sun et al. 2017). Moreover, DENV encodes viral proteins which antagonise the host immune response through degradation of cGAS (Aguirre et al. 2017) and STING (Aguirre et al. 2012). Furthermore, it has recently been shown that influenza A virus (IAV) or encephalomyocarditis virus (EMCV) infection triggers the release of mtDNA stimulating the cGAS-STING pathway in human cell lines (Moriyama et al. 2019). As well as being released into the cytoplasm during viral infection, mtDNA is also released during infection by certain strains of *Mycobacterium tuberculosis*, triggering induction of the type-I IFN response through the cGAS-STING pathway (Wiens and Ernst 2016).

1.4.3 - The cGAS-STING pathway and auto-inflammatory disease

Although the DNA of eukaryotes is largely prevented from accessing the cytoplasm through compartmentalisation in the nucleus and mitochondria, a small amount appears to become exposed to the cytosol as a result of normal cellular processes. However, this basal level of DNA leakage to the cytoplasm does not normally accumulate to levels sufficient to induce an immune response due to the actions of proteins which degrade DNA (Stetson et al. 2008; Lan et al. 2014). A growing number of autoinflammatory diseases characterised by mutations in several DNases which result in the accumulation of immune stimulatory DNA in the cytosol have been identified. These include Aicardi-Goutieres syndrome (AGS) in which high levels of circulating type-I IFN, a result of chronic cGAS-STING activation, cause neuronal inflammation (Crow and Manel 2015). AGS can be caused by mutations in a number of proteins including the 3'-5' exonuclease TREX1 which degrades endogenous ssDNA and dsDNA in the cytoplasm (Crow et al. 2006; Stetson et al. 2008), and all components of the RNase H2 endonuclease complex (Crow and Manel 2015), which is responsible for removing ribonucleotides that become mis-incorporated into genomic DNA. Failure to remove these ribonucleotides results in genomic instability and the formation of micronuclei leading to cGAS-STING activation

(Mackenzie et al. 2016; Mackenzie et al. 2017). A similar disease has been found to be caused by mutations in the lysosomal endonuclease, DNase II which as well as degrading phagocytosed DNA in professional phagocytes also degrades DNA that results from damaged host cell nuclear DNA (Lan et al. 2014; Rodero 2017). As a result of DNase II mutations, DNA accumulates in the cytoplasm activating the cGAS-STING pathway and resulting in constitutive type-I IFN induction (Lan et al. 2014; Rodero 2017). The cGAS-STING pathway is also constitutively active in the autoinflammatory disease STING-associated vasculopathy with onset in infancy (SAVI) (Jeremiah et al. 2014; Liu et al. 2014; Munoz et al. 2015). SAVI is caused by gain-of-function mutations in STING which lead to its spontaneous activation and translocation out of the ER in the absence of cGAMP (Jeremiah et al. 2014; Liu et al. 2014; Dobbs et al. 2015).

The cGAS-STING pathway is also implicated in several other self-DNA-driven inflammatory diseases beyond those caused by mutations in nucleases responsible for clearance of self-DNA (AGS) or mutations in STING itself (SAVI). This includes myocardial infarction in which the cGAS-STING pathway is involved in the activation of a deleterious inflammatory response which occurs as a result of tissue damage and DNA leakage from dying cells (King et al. 2017). STING is also required for the activation of inflammatory responses in Parkinson's disease mouse models through cGAS-mediated detection of mtDNA which accumulates in the cytoplasm due to impaired mitophagy resulting from the loss of PINK1 and parkin proteins which are mutated in Parkinson's disease (Sliter et al. 2018). Additionally, the cGAS-STING pathway is activated in the premature aging disease, Hutchinson-Gilford progeria syndrome (HGPS), a laminopathy caused by mutations in the *LMNA* gene resulting in the production of a truncated lamin A protein called progerin. Cells expressing progerin show increased levels of DNA damage and replication stress caused by replication fork stalling and nuclease mediated DNA degradation; this combined with a compromised NE integrity as a result of progerin in the nuclear lamina results in the leakage of DNA into the cytoplasm. Cytoplasmic DNA is recognised by the cGAS-STING pathway resulting in the upregulation of innate immune response genes (Graziano et al. 2018; Kreienkamp et al. 2018; Gonzalo and Coll-Bonfill 2019). Interestingly this appears to be a cell intrinsic response mediated by STAT1 independently of IFN since HGPS fibroblasts do not express IFN.

1.4.4 - The cGAS-STING pathway in senescence and cancer

As mitotic cells proliferate, they eventually reach a state of replicative senescence characterised by the cessation of cell division. Cellular senescence is typified by a number of distinctive phenotypic alterations including chromatin changes, an altered secretome, and an increase in cell size. Functionally cellular senescence serves as a safeguard against tumorigenesis since cells accumulate DNA damage and mutations over time and senescence prevents the continued replication of these damaged cells. More recently cellular senescence has also been shown to play a role in development, tissue repair, and organismal aging (Van Deursen 2014). The onset of senescence can be caused by cell damage or stresses that induce DNA damage including telomere attrition, DNA damaging agents, reactive oxygen species, oncogene activation, and laminopathies such as HGPS. DNA damage results in the formation of micronuclei and cytoplasmic chromatin fragments which are detected by the cGAS-STING signalling pathway initiating a type-I IFN response. cGAS-STING signalling leads to the senescence-associated secretory phenotype (SASP), which is characterised by the secretion of pro-inflammatory cytokines, growth factors, and proteases that promote the recruitment of immune cells to clear the pre-malignant senescent cell which harbours damaged DNA and could potentially develop into a cancer (Yang et al. 2017; Yum et al. 2019). In support of the cGAS-STING pathway playing a role in preventing tumorigenesis through inducing SASP, low levels of cGAS and STING expression in tumours of lung adenocarcinoma patients, hepatocellular carcinoma patients, and in patients with gastric cancer is linked with poor prognosis and decreased survival (Bu et al. 2016; Song et al. 2017; Yang et al. 2017). Moreover, STING and/or cGAS expression is lost in many tumour cells lines further suggesting that the cGAS-STING pathway is antagonistic to tumorigenesis (Sun et al. 2013; Wu et al. 2013b; Bhatelia et al. 2014; Xia et al. 2016a; Xia et al. 2016b; Chen et al. 2017).

When normal cells overcome cell cycle checkpoints and senescence, they become cancer cells which can proliferate uncontrollably. Despite originating from endogenous tissue, cancer cells can be recognised by the adaptive immune system and targeted for destruction. This so called 'anti-tumour immunity' is dependent on cross-priming of tumour cell-specific cytotoxic $CD8^+$ T cells. Activation of $CD8^+$ T cells requires two signals from an interaction with an antigen presenting cell (APC) such as a dendritic cell: firstly, the cross-presentation of a tumour-derived antigen in the context of MHC class I molecules by the APC, and secondly a co-

stimulatory signal such as an interaction between CD86 and CD28 signalling molecules on the APC and $CD8^+$ T cell, respectively. Dead tumour cells can be phagocytosed by dendritic cells which then present tumour-derived antigen on their cell surface in the context of MHC class I providing the first signal (Yum et al. 2019). At the same time, phagocytosed tumour cell DNA or cGAMP which escapes into the cytoplasm of dendritic cells activates the cGAS-STING pathway resulting in the production of type-I IFN (Woo et al. 2014) which is essential for activation of anti-tumour $CD8^+$ T cells (Diamond et al. 2011; Fuertes et al. 2011) since it upregulates the expression of co-stimulatory signalling molecules (Marckmann et al. 2004). Thus, the cGAS-STING pathway in dendritic cells promotes anti-tumour immunity through the recognition of tumour DNA and/or tumour produced cGAMP and the production of type-I IFN to activate cancer killing $CD8^+$ T cells.

While cGAS and STING may inhibit tumorigenesis through DNA damage sensing with the induction of SASP and through cross-presentation of $CD8^+$ T cells by dendritic cells which phagocytose dead cancer cells, prolonged inflammation induced by the cGAS-STING pathway can promote tumorigenesis and metastasis (Grivennikov et al. 2010). In an epithelial cancer model, DNA damage sensed by the cGAS-STING pathway promoted inflammation and carcinogenesis with *STING*$^{-/-}$ mice resistant to this skin cancer (Ahn et al. 2014). Additionally, in a brain metastatic cancer model cGAMP produced by brain metastatic cancer cells was transferred to astrocytes through gap junctions, activating STING in neighbouring astrocytes and inducing the production of inflammatory cytokines which in turn supported tumour growth (Chen et al. 2016). Therefore, the cGAS-STING pathway can also have protumour functions through promoting inflammation-driven tumorigenesis and metastasis.

However, acute activation of immune responses has been shown to have a strong anti-cancer effect and activation of the cGAS-STING pathway is now being targeted for development of cancer immunotherapy (Yum et al. 2019; Yum et al. 2020). Interestingly, classic cancer therapies that were designed to directly target cancer cells including ionising radiation and chemotherapy have now been shown to indirectly activate the cGAS-STING pathway resulting in antitumour immunity. Local treatment of tumours with ionising radiation has long been known to not only reduce the size of the targeted tumour but to also reduce the size of distant tumours, a phenomenon known as the abscopal effect (Mole 1953). This was later shown to be dependent on the activation of $CD8^+$ T cells (Lee et al. 2009) and activation of the cGAS-

STING pathway (Deng et al. 2014; Harding et al. 2017). Radiation induces DNA damage and micronuclei in cancer cells which activates cGAS-STING signalling resulting in the induction of IFNβ promoting the cross-priming of anti-tumour $CD8^+$ T cells. Similarly, chemotherapy which interferes with cell proliferation thus inhibiting tumour growth has also been found to directly stimulate cGAS-STING signalling resulting in activation of dendritic cells and anti-tumour $CD8^+$ T cells. For example, the PARP inhibitor, Olaparib induces DNA damage and the formation of micronuclei resulting in the activation of cGAS-STING signalling in tumour cells and paracrine activation of dendritic cells (Pantelidou et al. 2019). More recently several cyclic dinucleotide STING agonists have been tested in tumour models in order to stimulate STING signalling and hence upregulate cancer immunity with promising effects. Several clinical trials are currently ongoing using STING agonists alone or in combination with other cancer treatments (Yum et al. 2019).

1.5 - Additional functions of STING

Beyond its role as the central adaptor protein in innate immune signalling cascades triggered by cytosolic DNA which induce type-I IFN and proinflammatory cytokine expression, it has become clear that STING has additional functions. These include the induction of autophagy upon trafficking to the ERGIC after binding cGAMP, a function which is independent of the activation of the type-I IFN pathway (Gui et al. 2019). In addition, as well as restricting the proliferation of DNA viruses through type-I IFN induction, STING also restricts the proliferation of some RNA viruses (Maringer and Fernandez-Sesma 2014; Ma and Damania 2016), although the mechanisms through which it does so remain to be fully elucidated.

1.5.1 - Autophagy

Induction of autophagy following cGAMP binding appears to be a primordial function of STING, pre-dating the evolution of interferons. The cGAS-STING pathway is evolutionarily ancient with homologs of cGAS and STING found in the anemone species, *Nematostella vectensis*, which diverged from the human ancestor >500 million years ago (Kranzusch et al. 2015). Interestingly, *N. vectensis* STING lacks the C-terminal residues present in vertebrate STING that are required for the activation of the type-I IFN pathway, and when expressed in HEK293T cells is unable to induce TBK1 activation after immune stimulation with cGAMP (Gui et al. 2019). However, both *N. vectensis* and human STING lacking the C-terminal activation

domain, $STING_{1-340}$, are able to induce the conversion of microtubule-associated protein 1A/1B-light chain 3 (LC3) into a lipidated form LC3-II, a key step in the formation of autophagosomes, following immune stimulation by DNA transfection or cGAMP delivery. Upon cGAMP binding, STING translocates to the ERGIC which serves as the membrane source for LC3 lipidation. LC3 lipidation following cGAMP stimulation requires WD repeat domain phosphoinositide-interacting protein 2 (WIPI2) and autophagy protein 5 (ATG5) (Gui et al. 2019). Autophagy induced by STING activation is proposed to provide a mechanism of cytosolic DNA and pathogen clearance through delivery of DNA/pathogen containing autophagosomes to lysosomes for degradation and by doing so provides the cell with an additional means of pathogen defence (Gui et al. 2019). Moreover, it has been shown that the cGAS-STING pathway activates autophagy in response to infection of macrophages with *Mycobacterium tuberculosis* (Watson et al. 2012; Watson et al. 2015) and Gram-positive bacteria (Moretti et al. 2017).

1.5.2 - STING in the restriction of RNA viruses

As has already been noted, the cGAS-STING pathway can function in the restriction of RNA viruses despite these viruses containing no DNA of their own, in the case of DENV through detection of mtDNA leakage as a result of viral infection (Aguirre et al. 2017; Sun et al. 2017). Furthermore, retroviruses, including HIV, can activate the cGAS-STING pathway through detection or viral cDNA after reverse-transcription (Gao et al. 2013a; Lahaye et al. 2013; Rasaiyaah et al. 2013; Jakobsen et al. 2013), provided cDNA escapes the viral capsid in the cytoplasm. However, normally the HIV viral capsid shields cDNA from the host cell cytoplasm and delivers cDNA directly into the nucleus upon binding NPCs (Jacques et al. 2016; Sumner et al. 2017). Such cases of STING antagonism of RNA viruses involve the canonical activation of the cGAS-STING pathway and the induction of type-I IFN.

Further evidence of antiviral STING functions during RNA virus infection comes from studies which have shown that the replication of multiple positive- and negative-sense RNA viruses is enhanced in the absence of STING (Ishikawa and Barber 2008; Zhong et al. 2008; Ishikawa et al. 2009; Sun et al. 2009; Nazmi et al. 2012; Aguirre et al. 2012; Nitta et al. 2013; Yi et al. 2015; Holm et al. 2016; Ding et al. 2018; Franz et al. 2018). These include the negative-sense viruses: Vesicular stomatitis virus (VSV) (Ishikawa and Barber 2008; Zhong et al. 2008; Ishikawa et al. 2009; Holm et al. 2016; Franz et al. 2018), Sendai virus (SeV) (Zhong et al. 2008),

Newcastle disease virus (NDV) (Sun et al. 2009), Japanese encephalitis virus (JEV) (Nazmi et al. 2012), and Influenza A virus (IAV) (Franz et al. 2018) and the positive-sense viruses: DENV (Yu et al. 2012; Aguirre et al. 2012), Hepatitis C Virus (HCV) (Nitta et al. 2013; Yi et al. 2015), Sindbis Virus (SINV) (Franz et al. 2018), and Zika virus (ZIKV) (Ding et al. 2018). Moreover, several studies have reported that STING is activated during RNA virus infection and required for full induction of type-I IFN responses, indicating a role for STING in antagonising RNA viruses (Ishikawa and Barber 2008; Zhong et al. 2008; Sun et al. 2009; Sun et al. 2012; Yu et al. 2012; Aguirre et al. 2012; Holm et al. 2016). Although, others have argued that STING is not required for type-IFN induction in response to RNA virus infection (Ishikawa et al. 2009; Li et al. 2013b; Franz et al. 2018). Furthermore, it has been shown that the 3' UTR RNA of HCV can trigger a STING-dependent response in hepatocytes (Ding et al. 2013). However, STING does not bind directly to the dsRNA mimic poly(I:C) *in vitro* (Abe et al. 2013), nor does it dimerise and undergo translocation to perinuclear foci after RNA virus infection or poly(I:C) stimulation (Franz et al. 2018). Therefore, how STING functions in immune responses against RNA viruses remains less clear than its counteraction of DNA viruses through the cGAS-STING pathway induction of type-I IFN.

In support of STING contributing to antiviral responses against RNA viruses, several RNA viruses antagonise STING implying that STING function restricts viral proliferation (Ishikawa et al. 2009; Sun et al. 2012; Yu et al. 2012; Aguirre et al. 2012; Ding et al. 2013; Nitta et al. 2013; Xing et al. 2013; Chen et al. 2014; Yi et al. 2015; Holm et al. 2016; Ding et al. 2018). Several members of the *Flaviviridae* family of viruses have been shown to target STING. Intriguingly, human STING amino acids 125-222 were found to exhibit significant homology to flavivirus non-structural protein NS4B and NS4B of yellow fever virus (YFV) has been shown to bind STING and block RIG-I and STING-dependent signalling (Ishikawa et al. 2009), while HCV NS4B also binds to STING and prevents its interaction with MAVS (Nitta et al. 2013) or TBK1 (Ding et al. 2013) inhibiting IFN induction. Although the DENV-2 NS4B protein has not been found to inhibit IFN induction (Rodriguez-Madoz et al. 2010), the DENV viral protease complex NS2B3 has been shown to inhibit IFN induction through binding and cleaving human STING (but not murine STING) (Yu et al. 2012; Aguirre et al. 2012; Stabell et al. 2018). Zika virus (ZIKV) is another flavivirus which antagonises STING in human cells (Ding et al. 2018). This study found that human, but not mouse, STING is cleaved by NS2B3 proteases encoded

by a number of flaviviruses, including DENV, WNV, JEV, and ZIKV, but not YFV (Ding et al. 2018). This is due to the amino acid differences between human and mouse STING at the identified cleavage site, which in humans consists of RG residues at amino acids 78/79 compared to QG in mouse (Ding et al. 2018; Stabell et al. 2018).

The *Coronaviridae* family of RNA viruses also target STING to inhibit IFN responses. Several coronaviruses have been shown to inhibit STING-dependent type-I IFN production through a conserved mechanism. The human coronavirus HCoV-NL63 and SARS-CoV papain-like proteases PLP2-TM and PLpro-TM, respectively, interact with STING, inhibiting STING dimerization and K63-linked polyubiquitination, the formation of STING signalling complexes and induction of type-I IFN (Clementz et al. 2010; Sun et al. 2012; Chen et al. 2014). Similarly, the PLP2 protein of the coronavirus porcine epidemic diarrhoea virus (PEDV) also interacts with STING and disrupts K63-linked polyubiquitination of STING antagonising IFN expression (Xing et al. 2013).

Finally, IAV is the only negative-sense RNA virus which has so far been shown to antagonise STING activation and type-I IFN induction. The IAV fusion peptide, which constitutes the N-terminal region of IAV hemagglutinin (HA) and is required for viral membrane fusion in host cell endosomes, binds STING directly and this appears to inhibit STING dimerization and activation selectively in response to viral membrane fusion (Holm et al. 2016).

1.5.3 - STING's mechanisms of defence in RNA virus infection

Several mechanisms have been proposed to explain STING's role during RNA virus infection. Firstly, STING interacts with the RNA sensor RIG-I and downstream adaptor MAVS, but not the RNA sensor MDA-5, and interaction with RIG-I increases with RNA virus infection (Ishikawa and Barber 2008; Zhong et al. 2008). Since MAVS is localised to the mitochondria, a separate cellular pool of STING located at the mitochondria or mitochondria-associated ER membranes (MAM) may be involved in RNA virus sensing (Zhong et al. 2008; Ishikawa et al. 2009; Ran et al. 2014). Thus, STING contributes to immune responses against RNA viruses sensed by RIG-I, such as VSV, SeV, NDV, JEV, and HCV, but not those sensed exclusively by MDA5, such as encephalomyocarditis virus (ECMV), likely through recruitment of TBK1 and IRF3 following activation via interaction with RIG-I and MAVS complexes localised at the MAM or mitochondria (Ishikawa and Barber 2008; Zhong et al. 2008; Ishikawa et al. 2009; Maringer and Fernandez-Sesma 2014; Ran et al. 2014).

cGAS may also be involved in sensing RNA virus infection as it appears to be a potent restriction factor of several positive-sense single-stranded RNA viruses (SINV, YFV, VEEV, CHIKV, WNV), plausibly through regulating the basal expression level of some antiviral genes due to continuous low-level activation of the cGAS-STING pathway through endogenous ligands (Schoggins et al. 2011; Schoggins et al. 2014). Alternatively, cGAS may sense viral RNA ligands directly triggering activation of STING; cGAS has been shown to bind a synthetic 50mer dsRNA, although this did not result in the generation of cGAMP (Civril et al. 2013) and cGAS does not bind polyI:C *in vitro* (Sun et al. 2013). Therefore, whether cGAS contributes to cytosolic RNA sensing directly seems unlikely.

A further STING-dependent but cGAS-independent RNA virus sensing pathway has been proposed in which STING is stimulated through sensing fusion of viral and host cell membranes (Holm et al. 2012; Holm et al. 2016). Knockout of STING but not cGAS was found to impair the production of type-I IFN in cells infected with SeV, NDV, or IAV, and in STING deficient mice led to elevated VSV replication (Holm et al. 2016). Intriguingly, infection of cells deficient for MAVS with these viruses still led to increased STING dimer formation indicative of STING activation. Moreover, MAVS-deficient cells still produced a significant residual IFNβ response when infected with SeV, NDV, or IAV compared to control cells and this residual response was lost when STING was knocked down by shRNA and cells were infected with IAV (Holm et al. 2016). This suggests that STING is able to evoke some level of immune response against RNA viruses independently of pathways dependent on cGAS or MAVS. The authors of the study also found that type-I IFN induction can be triggered by fusogenic liposomes in a STING-dependent but cGAS-independent manner (Holm et al. 2012; Holm et al. 2016). Such liposomes fuse with cell membranes, mimicking membrane fusion events such as those that occur during enveloped viral infection. Intriguingly, this membrane fusion triggered STING activation and type-I IFN induction is selectively antagonised by the IAV fusion peptide, likely through direct interaction with STING and inhibition of STING dimerization, while DNA induced IFN responses are unaffected by IAV fusion peptide (Holm et al. 2016). The exact mechanism through which membrane fusion is sensed and how those signals are transduced to activate STING remains poorly understood but appears to involve phospholipase C-γ (PLC-γ) and phosphatidylinositol-3-OH kinase (PI(3)K) (Holm et al. 2012).

Another recent study has suggested that STING inhibits translation in response to RNA virus infection, and in this way antagonises viral proliferation (Franz et al. 2018). Franz et al. found that type-I IFN induction or ISG expression as a result of RNA virus infection did not depend on STING, however, in agreement with other studies, the absence of STING results in higher viral titres with RNA virus infection indicating that STING antagonises RNA viral infection. They found that translation of exogenous and viral mRNAs is more efficient in the absence of STING and that STING restricts translation globally in response to poly(I:C) transfection or VSV infection. This STING-dependent restriction of translation was found to require RIG-I but not MAVS leading to a model whereby RLRs have two antiviral effector functions during RNA virus infection. Firstly, RLRs upon ligand detection activate MAVS to induce type-I IFN and secondly, through STING a response is initiated to restrict translation. The mechanism through which STING influences translation is not yet known but appears to be distinct from PKR mediated translational suppression and the translocon (Franz et al. 2018).

It is clear then that STING functions in the restriction of RNA viruses. Although, there is good evidence that STING contributes to immune responses triggered by RNA viruses through interacting with RIG-I and MAVS (Ishikawa and Barber 2008; Zhong et al. 2008; Ishikawa et al. 2009; Maringer and Fernandez-Sesma 2014; Ran et al. 2014), and that STING restricts viral translation in a manner dependent on RIG-I (Franz et al. 2018), mechanistic details remain to be fully elucidated. Furthermore, how STING is activated in response to viral membrane fusion is unknown (Holm et al. 2016) and whether STING contributes to IFN induction in response to RNA virus infection remains contentious. Finally, it remains to be clarified whether such mechanisms act in combination and whether other, as-yet undescribed mechanisms of RNA virus detection resulting in STING activation exist (Maringer and Fernandez-Sesma 2014; Ma and Damania 2016).

1.6 - A role for STING at the nuclear envelope

Although, STING clearly localises to the peripheral ER, it also localises at the NE as seen by immunofluorescence (Ishikawa and Barber 2008; Ishikawa et al. 2009; Sun et al. 2009; Chen et al. 2011). While a NE localisation could indicate the presence of STING in either the ONM or INM (or indeed both), there is reason to believe that STING could function as an integral INM protein especially when considering the localisation of other well-known INM proteins (Batrakou et al. 2009). For example, lamin B receptor (LBR) is one of the earliest described

NETs (Worman et al. 1988; Ye and Worman 1994) with several NE specific functions: binding Lamin B, binding chromatin, HP1 binding, and regulating NE structure (Olins et al. 2010). However, LBR also localises to the ER where it acts as a sterol reductase (Clayton et al. 2010). Similarly, the INM protein, emerin, which functions in mechanotransduction, cellular polarity organisation, chromatin tethering, cell signalling, and gene expression also localises to the ONM and peripheral ER where it interacts with the cytoskeleton (Salpingidou et al. 2007). Thus, it is not inconceivable that STING could have multiple localisations and different functions specific to those localisations. Indeed, as well as localising to the ER where it functions in immune response signalling triggered by cytosolic DNA, STING is also reported to associate with mitochondria-associated ER membranes and the mitochondria where it is thought to regulate IFN responses triggered by viral RNA through interacting with RIG-I and MAVS (Zhong et al. 2008; Ishikawa et al. 2009; Ran et al. 2014).

STING's identification in NE preparations isolated from rat liver (as NET23) occurred prior to the discovery of its critical role in the cytosolic dsDNA-triggered IFN response and its reported localisation in the ER (Schirmer et al. 2003). However, work in the Schirmer lab on potential NE-specific roles for STING did not begin until after this discovery. In an initial study to determine the localisation of NETs within the NE, a STING-RFP construct was shown to target to the NE and to resist detergent extraction from the NE in contrast to the ER protein, calreticulin (Figure 1.3 A). Since the nuclear lamina is resistant to such pre-fixation extraction with detergent, a similar biochemical resistance to extraction of a NET typically indicates an INM association (Malik et al. 2010). One caveat of this method is that some NETs present only in the ONM can also resist detergent extraction due to interactions with cytoskeletal filaments such as the Nesprin family of proteins (Rajgor and Shanahan 2013) and so resistance to detergent extraction alone does not necessarily indicate INM localisation. In the same study STING-RFP did not localise at the NE in Lamin A/C knockout (*LMNA*$^{-/-}$) murine embryonic fibroblasts (MEFs) whereas in *LMNA*$^{+/+}$ MEFs STING-RFP was clearly present in the NE by fluorescence microscopy again suggesting an INM localisation and interaction with the nuclear lamina (Figure 1.3 B). Together this data suggests that as well as accessing the ONM by virtue of being an ER-localised protein, STING may also be targeted to the INM in a manner dependent on Lamin A/C expression. However, another experiment in the same study indicated that STING-RFP was present only in the ONM and not the INM. Using 3D structured

illumination microscopy (3D-SIM) which can distinguish INM localisation of a NET from ONM localisation (Schermelleh et al. 2008), based on whether fluorescent signal is in the same plane of the NE with either the nucleoplasmic facing, Nup153, or cytoplasmic facing Nup358, STING-RFP expressed in HT1080 cells appeared to localise exclusively to the ONM in the same plane as Nup358. Therefore, the localisation of STING within the NE remained ambiguous. Later in another study by the lab which set out to identify NETs that might be involved in organising chromatin, the overexpression of STING in HeLa or HT1080 cells was found to promote chromatin compaction (Malik et al. 2014). Moreover, endogenous levels of STING expression were found to correlate with degree of chromatin compaction in different cell types and overexpression of STING altered the epigenetic state of chromatin with an increase in repressive histone modifications and a decrease in histone modifications associated with active chromatin. This was the first study to indicate a NE function for STING, with histone modifications and chromatin compaction radiating from the nuclear periphery over the time-course of STING expression.

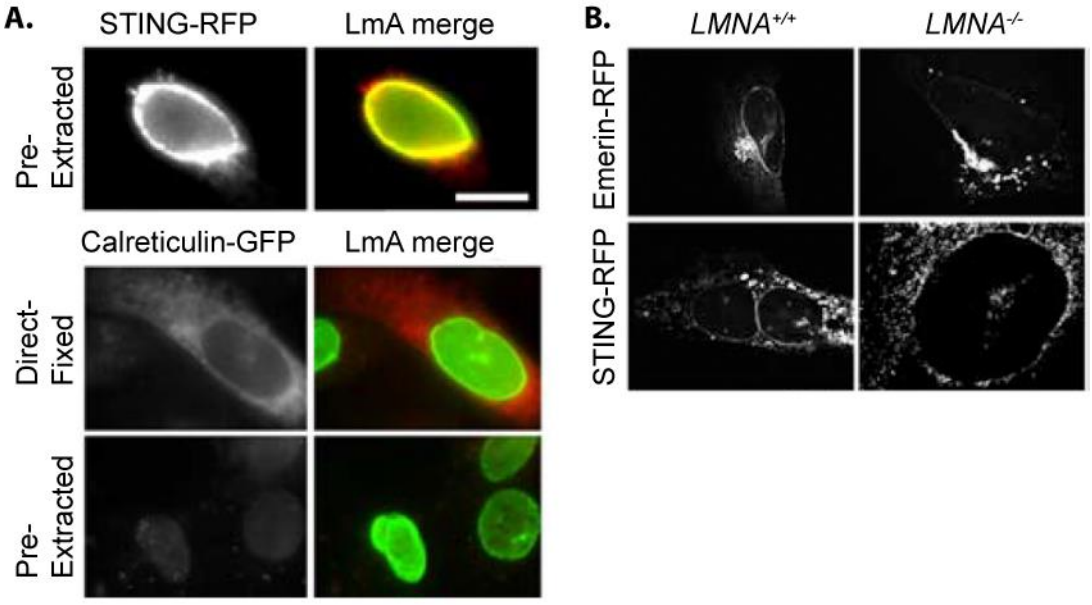

Figure 1.3 – STING-RFP resists detergent extraction and fails to target to the NE in Lamin A/C knockout MEFs (A) *STING-RFP (red) transiently expressed in HT1080 cells stably expressing Lamin A-GFP (green) (LmA) resists detergent pre-extraction in the NE. Calreticulin-GFP (coloured red) transiently expressed in HT1080 cells expressing Lamin A-RFP (green) (LmA) shows complete loss of staining in detergent pre-extracted cells compared to direct formaldehyde fixed cells* ***(B)*** *STING-RFP fails to target to the NE in Lamin A/C knockout MEFs similar to the known inner nuclear membrane protein Emerin. Figure adapted from Malik et al. 2010.*

A subsequent repetition of the 3D-SIM experiment using a STING-GFP construct expressed in HT1080 cells and examining a larger number of cells revealed that in some cells STING localised to the INM (in the same plane as Nup153) while in other cells STING localised to the ONM (in the same plane as Nup358) (Figure 1.4). This prompted the hypothesis that STING may change localisation within the NE based on innate immune response induction triggered by plasmid DNA used for transient expression of the STING-GFP construct. However, whether an immune response was induced was not investigated. Separately, STING-GFP mobility within the NE was found to increase during HSV1 infection or after transfection of the dsRNA mimic, poly(I:C), as measured by fluorescence recovery after photobleaching (FRAP). This experiment used an HT1080 cell line stably expressing an inducible STING-GFP construct to avoid immune stimulation caused by transient transfection of plasmid DNA. (Figure 1.5). This further implies that STING localisation within the NE might change during an immune response. However, again whether cells were infected was not confirmed (i.e. by staining against a viral protein) and similarly HSV1 infection would be expected to induce redistribution of STING to perinuclear foci, although it is possible that this is antagonised by HSV1 infection or not seen at two hours post infection.

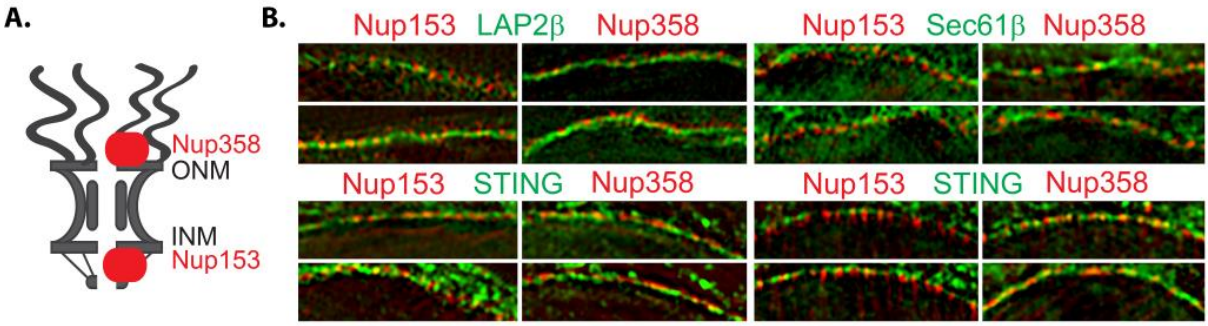

Figure 1.4 - 3D-Structured illumination microscopy (SIM) of STING in the NE. (A) *Schematic showing Nup153 and Nup358 localization in the NPC, Nup153 is in the nuclear pore basket on the nucleoplasmic face of the NPC while Nup358 is in the cytoplasmic filaments of the NPC on the cytoplasmic side of the NPC.* ***(B)*** *STING-GFP (green) transiently expressed in HT1080 cells localizes at the inner nuclear membrane (INM) with Nup153 (red) in some cells and at the outer nuclear membrane (ONM) with Nup358 (red) in other cells. Upper panel controls: LAP2β-GFP is in the INM and Sec61β-GFP in the ONM. Lower panels: STING is in the inner nuclear membrane in some cells and the outer in others when HT1080 cells are transiently transfected with a STING-GFP construct. Figure adapted from Dixon et al. 2020. Experiment performed by Poonam Malik.*

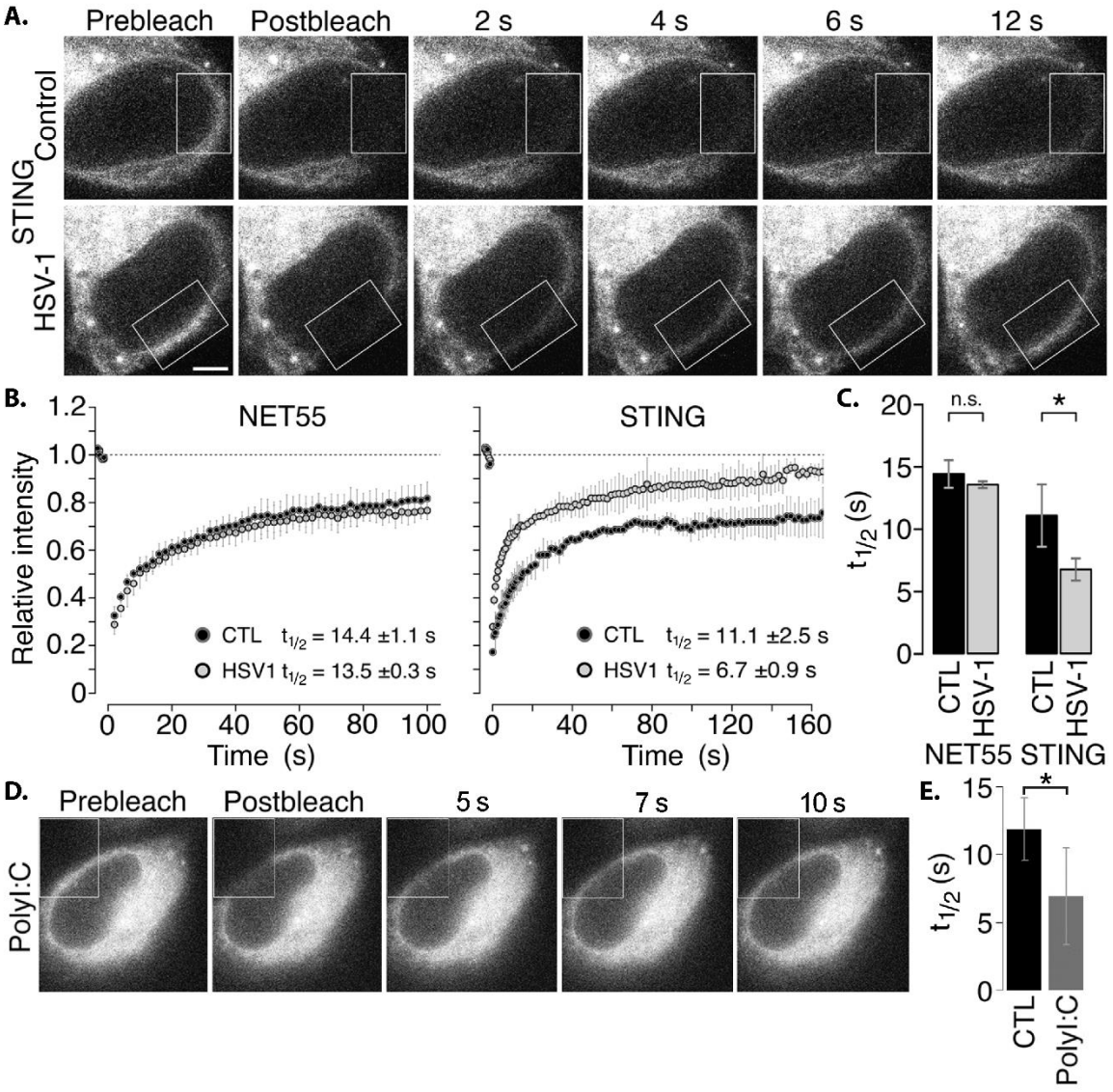

Figure 1.5 – Fluorescence Recovery After Photobleaching (FRAP) of STING in the NE shows STING increases mobility during HSV-1 infection or poly(I:C) transfection. (A) *FRAP of STING-GFP in control (mock-infected) and HSV-1 infected cells (2 hpi) showing redistribution of STING-GFP into photobleached area (marked by white box). Scale bar, 5 µM.* ***(B)*** *Fluorescence recovery curves from three replicate experiments as in a. Another NE protein, NET55, is shown as a control that does not change its dynamics with HSV-1 infection. CTL, control; HSV1, HSV-1 infected.* ***(C)*** *Bar plot comparing the average half recovery times ($t_{1/2}$) between the control and HSV-1 infected cells. Error bars show +/- standard deviation (student's T test, * $p \leq 0.05$).* ***(D)*** *FRAP of STING-GFP in cells 2 h after poly(I:C)-treatment, photobleaching an area within the white outlined box. Scale bar = 5 µm.* ***(E)*** *Bar plot comparing the average half recovery times ($t_{1/2}$) between the untreated control and the poly(I:C) treated cells. Error bars show +/- standard deviation (student's T test, * $p \leq 0.05$). Figure adapted from Dixon et al. 2020. Experiment performed by Natalia Saiz-Ros and analyzed by Jose de las Heras.*

To investigate potential NE-specific functions of STING, a proteomics approach was chosen to identify candidate partner proteins and generate a dataset on which my thesis is founded. Putative interaction partners were identified by immunoprecipitation of C-terminally tagged STING-GFP from NE preparations isolated from HEK293T cells transiently expressing a STING-GFP construct. It was hypothesised that such NE STING interactors may have been missed in previous STING proteomics analyses using whole cell lysates due to the difficulty in removing transmembrane proteins from the INM, which requires stringent extraction conditions in order to disrupt protein interactions with the nuclear lamina (Malik et al. 2010). Therefore, a reversible cross-linking approach was employed, whereby isolated NEs were cross-linked prior to immunoprecipitation using an anti-GFP antibody, which allowed for more rigorous extraction conditions while preserving protein-protein interactions (Figure 1.6 A). In parallel, mock transfected HEK293T cells were subject to the same procedure as a control dataset. After immunoprecipitation, cross-linking was reversed (Figure 1.6 B), and samples were sent for identification of STING interactors by mass spectrometry (see Appendix Table 1).

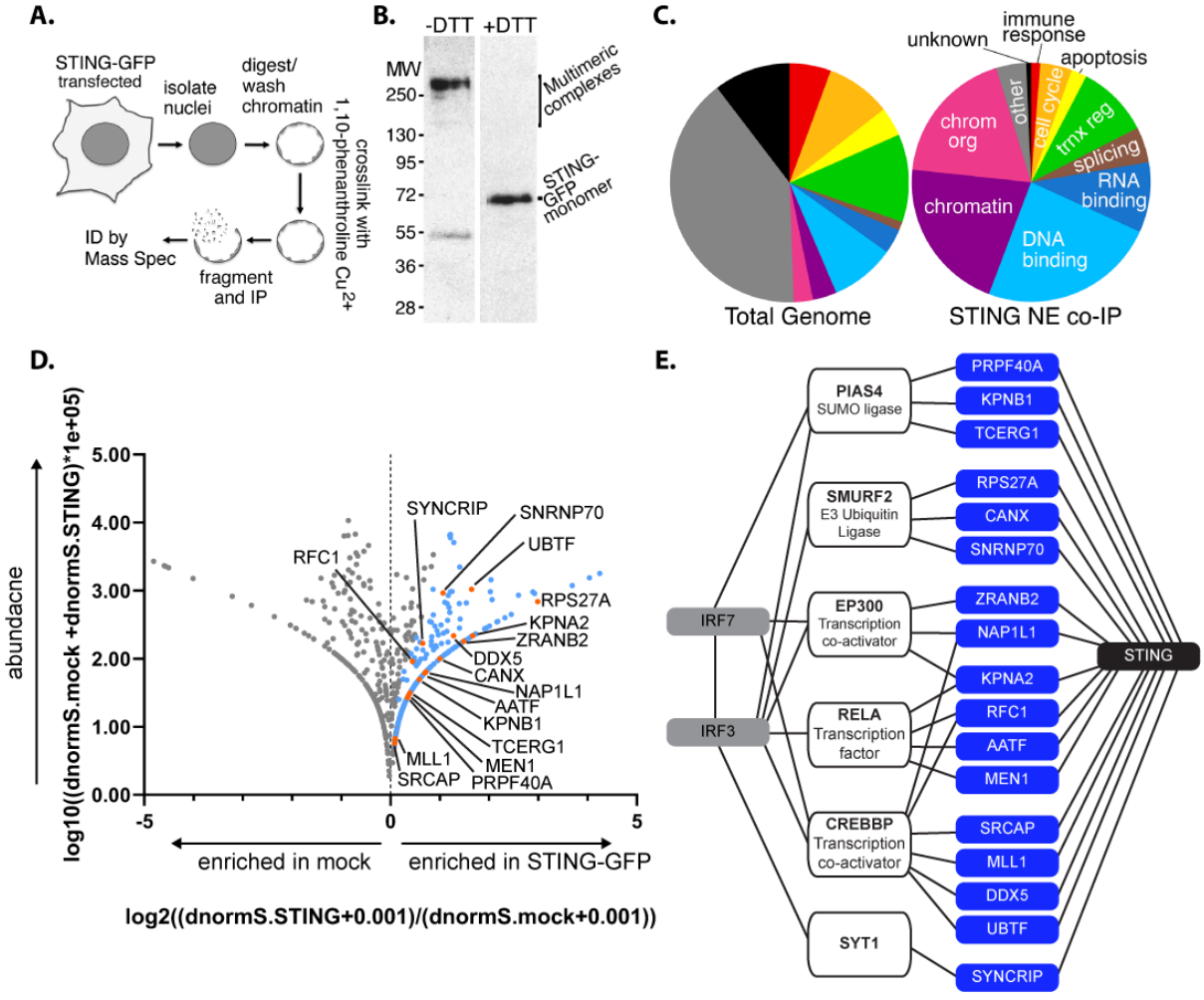

Figure 1.6 – The NE-STING proteome is enriched for chromatin organizing and RNA/DNA binding proteins. (A) *Schematic showing NE isolation and cross-linking approach for co-immunoprecipitation experiment. NEs were isolated from HEK293T cells expressing STING-GFP or mock transfected cells. The NEs were crosslinked with orthophenanthroline copper, fragmented by sonication and STING-GFP crosslinked proteins recovered by immunoprecipitation with GFP antibodies. The crosslinking was reversed to release these other proteins and their identity determined by mass spectrometry*. ***(B)*** *Cross-linking of NEs with orthophenanthroline copper chases most STING-GFP to multimeric species >200 kDa while a smaller portion appears at 55 kDa presumably due to intramolecular crosslinks. DTT-induced reversal of crosslinking restores all STING-GFP to its expected molecular weight at ~69 kDa.* ***(C)*** *Gene ontology (GO) biological process classification for STING-GFP enriched NE partners. The representation of the GO-terms by number of genes in the total human genome is shown on the left while on the right are the terms as represented in the most enriched proteins of the STING-GFP sample (as determined by two-fold enriched normalised spectral counts in the STING-GFP sample over the mock sample, ad further restricted to include only proteins detected by at least two peptides or by one peptide but at least two spectra).* ***(D)*** *Volcano plot showing all proteins identified in the mass spectrometry experiment plotted by degree of enrichment in each sample (log2((dnormS.STING+0.001)/(dnormS.mock+0.001))) against overall abundance (log10((dnormS.mock+dnormS.STING)*1e+05)). The strongest STING-GFP interactors are highlighted in blue and include 17 proteins which interact with six known interactors of the IRF3/7 transcription factors (highlighted in orange and labelled).* ***(E)*** *Whether any of the* putative *STING NE partners identified from the reversibly crosslinked NEs were known to interact with IRF3/7 was searched for using the HPRD interactome database. 17 of the putative STING NE partners (blue) had reported interactions with 6 proteins (white boxes) reported to bind IRF3/7 transcription factors (grey) central to IIR activation. Figure adapted from Dixon et al. 2020. Experiment performed by Poonam Malik, analyzed by Jose de las Heras, volcano plot and STING-partner-IRF3/7 interaction plot created by me.*

To determine the most likely STING-GFP interactors from this dataset, reliably identified spectra were normalised according to protein mass to obtain the relative abundance of proteins in each sample (dnormS). Spectra that were two-fold enriched in the STING-GFP sample compared to the mock sample were then identified and this set of proteins was further restricted to include only proteins detected by at least two peptides in the STING-GFP sample yielding 198 proteins. To this set of proteins an additional 22 proteins were added that were detected by only one peptide but had at least two spectra giving a final set of 220 proteins (see Appendix Table 1). The Gene Ontology (GO)-biological process terms associated with this set of proteins was compared to the GO terms associated with the proteins of the total human genome revealing an enrichment of proteins with GO-terms for chromatin/chromosome organisation and RNA/DNA binding (Figure 1.6 C). The mass spectrometry dataset plotted by enrichment in either STING-GFP or mock samples and

relative abundance with the top 220 proteins enriched in the STING-GFP sample highlighted in blue/orange is shown (Figure 1.6 D). Due to STING's known role as an adaptor protein in cytosolic dsDNA stimulated immune responses, whether any of the proteins identified in the mass spectrometry were known to interact with IRF3/7 immune transcription factors was investigated by searching the Human Protein Reference Database (HPRD, Johns Hopkins University) and visualised using Cytoscape. This revealed that 17 proteins identified as interactors of STING in the NE had indirect interactions with IRF3/7 through six known IRF3/7 interactors (Figure 1.6 E). All of these STING interactors have gene ontology (GO) terms associated with either DNA or RNA binding and we hypothesised that they could be involved in the sensing of nucleic acids during an innate immune response.

Although STING is typically considered an ER protein, immunofluorescence published by other groups and the Schirmer lab clearly shows that a pool of STING localises to the NE and proteomics from the Schirmer identified STING as a NE protein. However, the exact localisation of STING within the NE, INM compared to ONM remains to be determined.

1.7 Aims

Data discussed above show that STING is present in the NE and indicate that it may access the INM and that STING mobility in the NE increases following immune stimulation, therefore the first aim of this project was: ***(1) To determine STING's localisation within the NE and assess whether this changes in response to different immune stimuli.*** An INM localisation of STING could explain STING's restriction of nuclear replicating herpesviruses (Ishikawa et al. 2009; Orzalli et al. 2012; West et al. 2015; Reinert et al. 2016), and STING's involvement in the sensing of host cell nuclear DNA damage (Dunphy et al. 2018), since such mechanisms would not require transmission of a signal outside of the nucleus but could instead activate STING at the INM.

Having identified a set of putative NE STING interactors and found that 17 of these proteins have links to IRF3/7 transcription factors the second aim was: ***(2) To test whether any of these STING partners are involved in innate immune responses.*** Putative partner proteins of NE STING with known links to IRF3/7 transcription factors could be involved in activation of STING signalling from within the nucleus, and NE partners with GO-terms for RNA binding could be

involved in STING's restriction of RNA viruses, the mechanisms of which remain incompletely explained (Maringer and Fernandez-Sesma 2014; Holm et al. 2016; Franz et al. 2018).

Chapter 2

Materials and Methods

2.1 – Materials

2.1.1 Bacterial strains and genotypes

DH5alpha: F- endA1 glnV44 thi-1 recA1 relA1 gyrA96 deoR nupG Φ80dlacZΔM15 Δ(lacZYA-argF) U169 hsdR17(rK- mK+) λ–

StrataClone Solopack: F- endA1 glnV44 thi-1 recA1 relA1 gyrA96 deoR nupG Φ80dlacZΔM15 Δ(lacZYA-argF) U169 hsdR17(rK- mK+) λ–. (Stratagene, 240207)

2.1.2 - Buffers and solutions

Table 2.1 – Buffers used

Buffer/Solution name	Composition
Lysogeny broth (LB)	1 % tryptone 0.5 % yeast extract 10 mM NaCl pH 7.4
Phosphate Buffered Saline (PBS)	65 mM $Na2PO_4$ 8.8 mM $KH2PO_4$ 137 mM NaCl 2.7 mM KCl pH 7.4
Tris Buffer Saline (TBS)	20 mM Tris 137 mM NaCl pH 7.6
TAE	40 mM Tris 20 mM acetic acid 1 mM EDTA
DMEM	Dulbecco's Modified Eagle Medium (Sigma-Aldrich, D5796)
Opti-MEM	Opti-MEM® I Reduced Serum Medium (Gibco, 31985062)
MEM (2X)	Modified Eagle Medium (2X) (Gibco, 11935046)
SDS-PAGE running buffer	25 mM Tris pH 8.3 192 mM glycine 0.1 % SDS
2X Laemmli buffer	100 mM Tris pH 6.8 4 % SDS 20 % glycerol

	10 % 2-mercaptoethanol 0.05 % bromophenol blue
Alkaline Lysis Buffer I	50 mM Tris pH 8.0 10 mM EDTA
Alkaline Lysis Buffer II	200 mM NaOH 1 % SDS
Alkaline Lysis Buffer III	3 M KOAc pH 5.5
Co-immunoprecipitation Lysis Buffer	150 mM NaCl 5 mM EDTA pH 8.0 50 mM Tris pH 8.0 1 % IGEPAL® CA630 (NP40 alternative)
IAV growth medium (VGM)	DMEM 0.14 % BSA 1-10 µg/mL TPCK trypsin (Worthington Biochemical Corporation) 100 units/mL penicillin 100 µg/mL streptomycin
IAV overlay medium	1.2 % Avicell 0.5X DMEM 0.14% BSA 1nµg/mL TPCK trypsin 100 units/mL penicillin 100 µg/mL streptomycin
Serum free medium (SFM)	DMEM 100 units/mL penicillin 100 µg/mL streptomycin
2X MEM growth medium	MEM (2X) 4 % FBS 200 units/mL penicillin 200 µg/mL streptomycin
2 % Crystal Violet solution	2 g Crystal violet (Sigma-Aldrich) dissolved in 25 % methanol
0.1M PHEM Buffer	120 mM PIPES, 20 mM EGTA, 50 mM HEPES, 4 mM $MgCl_2$, pH 6.9

2.1.3 - Primary Antibodies

Table 2.2 – Primary antibodies used in this study

Antigen	Host	IF dilution	WB dilution	Band size (kDa)	Source
SNRNP70	Rabbit	1:1000	1:2000	48, 62	Abcam (ab51266)
DDX5	Goat	1:1000	1:2000	65	Abcam (ab10261)
RPS27A	Rabbit	-	1:250	18	Abcam (ab172293)
SYNCRIP (7A11.2)	Mouse	1:500	1:1000	59-70	Merck Millipore (#MAB11004)
SYNCRIP (18E4)	Mouse	1:500	1:1000	59-70	Merck Millipore (#05-1517)
MEN1	Rabbit	1:500	1:1000	68	Abcam (ab2605)
AATF	Rabbit	-	1:500	70	Abcam (ab39631)
Nup153	Mouse	1:250	1:1000	154	Abcam (ab24700)
STING (AF6516)	Sheep	1:200	1:1000	37	R&D Systems (AF6516)
STING (D2P2F)	Rabbit	1:500	1:1000	37	Cell Signaling Technology (#13647)
cGAS	Rabbit	-	1:500	62	Atlas Antibodies (HPA031700)
cGAS (D1D3G)	Rabbit	-	1:1000	62	Cell Signaling Technology (#15102)
IRF3 (FL-425)	Rabbit	1:50	1:250	50	Santa Cruz Biotechnology
IRF3 (phospho S386)	Rabbit	-	1:500	50	Abcam (ab76493)
Lamin B2	Guinea Pig	1:200	-	-	(Schirmer et al. 2001)
Lamin A/C (3262)	Rabbit	-	1:1000	69/62	(Schirmer et al. 2001)
α-tubulin	Sheep	-	1:1000	50	Cytoskeleton Inc. (#ATN02)
γ-tubulin	Mouse	-	1:5000	48	Sigma-Aldrich (T6557)
Histone H3	Mouse	-	1:2000	17	Abcam (ab10799)
NF-κB p65 (L8F6)	Mouse	1:500	-	-	Cell Signaling Technology (#6956)
MAVS	Rabbit	1:50	-	-	Cell Signaling Technology (#3993)
NP	Rabbit	1:1000	1:1000	55	Paul Digard (A2915)
NS1	Rabbit	1:250	1:500	25	Paul Digard (NS1-RBD)
FLAG	Mouse	-	1:500	-	Sigma-Aldrich (F1804)
GFP	Rabbit	-	1:1000	-	Life Technologies (A-11122)
GFP	Rabbit	-	-	-	Abcam (ab6556)

2.1.4 - Secondary Antibodies

Table 2.3 – Secondary antibodies used in this study

Antigen	Host	Dye/conjugate	Dilution	Source
Anti-mouse	Donkey	Alexa Fluor 488	1:1000	Invitrogen #A21202
Anti-mouse	Donkey	Alexa Fluor 568	1:1000	Invitrogen #A10037
Anti-mouse	Donkey	Alexa Fluor 647	1:1000	Invitrogen #A31571
Anti-rabbit	Donkey	Alexa Fluor 488	1:1000	Invitrogen #A21206
Anti-rabbit	Donkey	Alexa Fluor 568	1:1000	Invitrogen #A10042
Anti-rabbit	Donkey	Alexa Fluor 647	1:1000	Invitrogen #A31573
Anti-goat	Donkey	Alexa Fluor 488	1:1000	Invitrogen #A11055
Anti-goat	Donkey	Alexa Fluor 594	1:1000	Invitrogen #A11058
Anti-guinea pig	Goat	Alexa Fluor 647	1:1000	Invitrogen #A21450
Anti-mouse	Donkey	IRDye®680RD	1:1000	Licor #926-68072
Anti-mouse	Donkey	IRDye®800CW	1:1000	Licor #926-32212
Anti-rabbit	Donkey	IRDye®680RD	1:1000	Licor #926-68073
Anti-rabbit	Donkey	IRDye®800CW	1:1000	Licor #926-32213
Anti-goat	Donkey	IRDye®680RD	1:1000	Licor #925-68074
Anti-goat	Donkey	IRDye®800CW	1:1000	Licor #926-32214
Anti-sheep	Donkey	6 nm gold	1:50	Aurion #806.344
Anti-rabbit	Goat	5 nm gold	1:50	Aurion #806.011
Anti-rabbit	Donkey	PLA® Probe PLUS	1:5	Sigma-Aldrich #DUO92002
Anti-mouse	Donkey	PLA® Probe PLUS	1:5	Sigma-Aldrich #DUO92001
Anti-goat	Donkey	PLA® Probe MINUS	1:5	Sigma-Aldrich #DUO92006

2.1.5 - Virus stocks

The wild-type strain of herpes simplex virus-1 (HSV-1) used in this study was 17+. Wild-type strains of influenza A virus used in this study were A/PR8/34(H1N1) and A/Udorn/72(H3N2). Viral stocks of A/PR8/34(H1N1) were generated using a reverse genetics system as described in (De Wit et al. 2004) with plasmids and HEK293T and MCDK cells used for viral growth a gift from Professor Paul Digard (Roslin Institute, Edinburgh). Viral stocks of A/Udorn/72(H3N2) were a gift from Eleanor Gaunt (Paul Digard, Roslin Institute, Edinburgh). A/PR8/34(H1N1) NS1 mutant strains R38K41A and N81 were also generated using a reverse genetics system and swapping the plasmid encoding wild type NS1 for respective mutant NS1, these plasmids were a gift from Professor Paul Digard (Roslin Institute, Edinburgh).

2.1.6 - Mammalian cells

HT1080 fibroblasts, BHK-21 cells, and U2OS cells were obtained from ATCC. HEK293FT cells were a gift from Justina Cholewa-Waclaw (Adrian Bird, WCCB), these cells are derived from a fast-growing clone of HEK293T cells stably expressing the SV40 large T antigen from the pCMVSPORT6Tag.neo plasmid. HEK293T cells, A549 cells, and MDCK cells were a gift from Professor Paul Digard (Roslin Institute, Edinburgh). An HT1080 cell line stably expressing a doxycycline inducible STING-GFP construct was created by Mike Robson (Eric Schirmer, WCCB) using a lentiviral vector system (pLVX-TRE3G backbone, Clontech).

2.2 - Mammalian cell culture

2.2.1 – Cell maintenance

All cells were cultured at 37 °C in a humid atmosphere with 5 % CO_2. HT1080, HEK293T, A549, Vero, and MDCK cells were grown in DMEM supplemented with 10 % fetal bovine serum (FBS), 100 units/mL penicillin and 100 µg/mL streptomycin. HT1080, HEK293T, A549, and Vero cells were passaged when they reached ~70-80 % confluency, typically every 2-3 days, in a 1:10 dilution by trypsinisation. MDCK cells were passaged upon reaching 100 % confluency.

HEK293FT cells and HT1080 cells stably expressing a doxycycline inducible STING-GFP construct were grown in DMEM supplemented with 10 % FBS, 100 units/mL penicillin, 100 µg streptomycin, and 0.5 mg/mL geneticin (G418) to maintain selection of pCMVSPORT6Tag.neo and STING-GFP integrated cells, respectively. These cells lines were passaged when they reached ~70-80 % confluency by 1:10 dilution using trypsinisation. STING-GFP HT1080 cells were treated with 0.05 µg/mL doxycycline for 20 h prior to use in experiments in order to induce STING expression before use in experiments. This concentration of doxycycline and length of treatment enriched for HT1080 cells expressing low levels of STING-GFP and prolonged treatment with doxycycline or the use of higher concentrations resulted in higher levels of STING-GFP expression and the formation of aggregates in the ER (Figure 2.1 A). Recently it was revealed that such STING aggregates are a form of phase-separation and prevent overactivation of innate immune responses (Yu et al. 2021) (Figure 2.1 B and C).

BHK-21 cells were maintained in Glasgow Modified Eagle's Medium (GMEM, Invitrogen), supplemented with 2 mM L-glutamine, 10 % new-born calf serum, 10 % tryptose phosphate broth, 100 units/mL penicillin, and 100 µg/mL streptomycin.

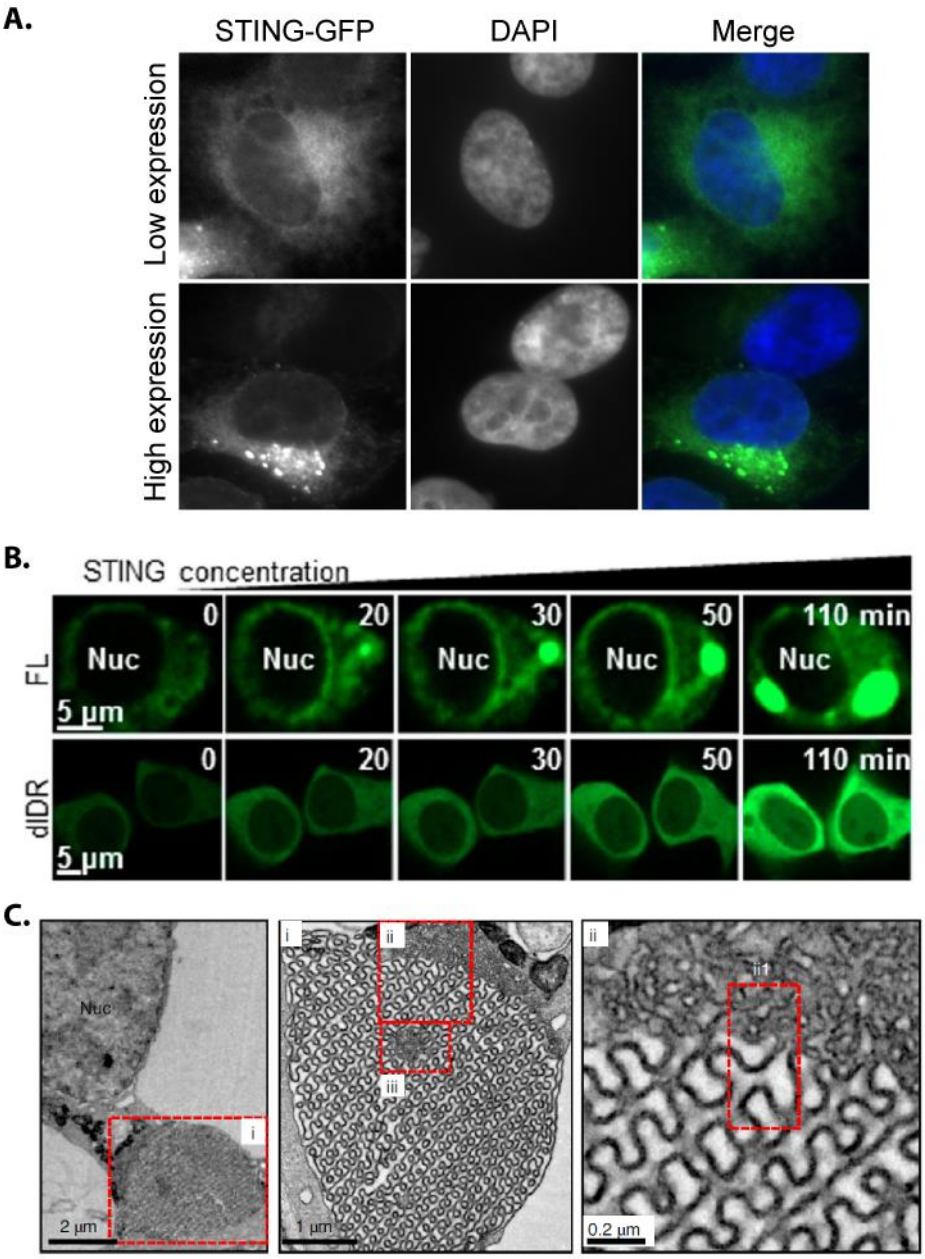

Figure 2.1 – Doxycycline inducible STING-GFP expression. (A) *HT1080 cells stably expressing a doxycycline inducible STING-GFP construct were treated with low levels of doxycycline (0.05 µg/mL) to induce STING-GFP expression. Prolonged exposure with doxycycline or induction using higher concentrations increased the formation of STING-GFP ER aggregates which presumably represent phase condensates of STING in the ER.* ***(B)*** *STING condensates grow larger with increasing STING expression. HEK293T cells transfected with full-length STING-GFP (FL) or STING$^{d309-379}$-GFP (dIDR), after 12 h live cell imaging was performed with micrographs showing the indicated timepoints starting 12 h post-transfection. STING condensates form and grow larger in cells transfected with STING-GFP (FL) but do not form in cells transfected with STING$^{d309-379}$-GFP (dIDR) which lacks the intrinsically disordered region of STING required for the formation of condensates.* ***(C)*** *Electron microscopy of STING condensates reveals a puzzle-like membrane structure in the ER, formed by STING aggregation. (B) and (C) adapted from* (Yu et al. 2021).

2.2.2 – Plasmid transfection

For FRET-FLIM experiments HEK293T cells were transfected with plasmids containing STING-RFP, Lamin A-GFP, or an RFP-GFP tandem construct using Lipofectamine® 2000 (Invitrogen) according to the manufacturer's instructions. Briefly, 70,000 cells were seeded on 13 mm glass coverslips (VWR International) per well of a 24-well plate in a volume of 1 mL growth medium the day before transfection in order to be at ~50 % confluency at the time of transfection. The next day 0.5 µg of plasmid DNA and 1 µL of Lipofectamine® 2000 reagent were diluted separately in 25 µL of Opti-MEM for each well of a 24-well plate that was to be transfected, vortexed briefly, and incubated for 5 minutes at room temperature. After 5 minutes DNA and Lipofectamine® 2000 reagent were combined, mixed, and incubated at room temperature for a further 20 minutes. During this time, the volume of growth medium in each well of the 24-well plate was adjusted to 0.5 mL. After 20 minutes the DNA-lipovesicle mixture was added to cells in a drop-wise manner so as not to disturb adherent cells. For co-immunoprecipitation experiments using SYNCRIP Q1/Q3-FLAG and STING-GFP constructs HEK293T cells were similarly transfected using Lipofectamine® 2000 but in a 10 cm tissue culture dish with volumes scaled accordingly.

2.2.3 – siRNA transient transfection

HT1080 cells were seeded at 300,000 cells/well of a 6-well plate on the day before knockdown. The next day knockdown was performed using the siRNA duplexes listed in Table 2.4 and jetPRIME transfection reagent (POLYPLUS) according to the manufacturer's instructions, for a final concentration of 50 nM siRNA, 4 µL jetPRIME, 200 µL jetPRIME buffer per well. For STING knockdown a mixture of siRNA#1 and siRNA#2 were used for a final concentration of 50 nM. siRNA was added to jetPRIME buffer and vortexed to mix before the addition of jetPRIME reagent. The mixture was then vortexed again and incubated for 15 minutes at room temperature before addition to cells in a drop-wise manner. 24 hours after knockdown cells were trypsinised and re-seeded 1:2 in 6-well plates for Western blotting and qPCR experiments, or at 50,000 cells/well of a 24-well plate on 13 mm glass coverslips for immunofluorescence, or without coverslips for virus infection experiments. Cells were used in experiments 48 hours after siRNA treatment. HEK293FT cells were treated similarly except they were seeded at 400,000 cells/well of a 6-well plate and for luciferase assays 24 hours

after initial siRNA treatment cells were replated at 50,000 cells/well of a 48-well plate for subsequent co-transfection of luciferase assay plasmids and a repetition of siRNA treatment.

Table 2.4 – siRNA duplexes used in this study

Protein	Sequence (5'-3')	Source
Non-target control (siCTL)	Sense – AAUUCUCCGAACGUGUCACGU[dT][dT] Antisense - ACGUGACACGUUCGGAGAAUU[dT][dT]	Sigma Aldrich (UK)
SYNCRIP	Sense - CUAUCGUGGUGGAUAUGAAGA[dT][dT] Antisense - UCUUCAUAUCCACCACGAUAG[dT][dT]	Sigma Aldrich (UK)
MEN1	Sense - GAUCAUGCCUGGGUAGUGUU[dU][dG] Antisense - AACACAUACCCAGGCAUGAUC[dC][dU]	Sigma Aldrich (UK)
DDX5	Sense – CCCAAUAAGACUUUAGAAGUA[dT][dT] Antisense - UACUUCUAAAGUCUUAUUGGG [dT][dT]	Sigma Aldrich (UK)
SNRNP70	Sense – GGUCUACAGUAAGCGGUCA[dT][dT] Antisense - UGACCGCUUACUGUAGACC [dT][dT]	Sigma Aldrich (UK)
RPS27A	Sense – UUAGUCGCCUUCGUCGAGA[dT][dT] Antisense - UCUCGACGAAGGCGACUAA [dT][dT]	Sigma Aldrich (UK)
TCERG1	Sense – GGAGUUGCACAAGAUAGUU[dT][dT] Antisense – AACUAUCUUGUGCAACUCC[dT][dT]	Sigma Aldrich (UK)
AATF	Sense – AAGCGCUCUGCCUACCGAGUU[dT][dT} Antisense – AACUCGGUAGGCAGAGCGCUU[dT][dT]	Sigma Aldrich (UK)
STING	Sense#1 – GCACCUGUGUCCUGGAGUA[dT][dT] Antisense#1 – UACUCCAGGACACAGGUGC[dT][dT] Sense#2 – GCAUCAAGGAUCGGGUUUA[dT][dT] Antisense#2 – UAAACCCGAUCCUUGAUGC[dT][dT]	Sigma Aldrich (UK)

2.2.4 – Innate immune response induction

To stimulate innate immune responses for Western blotting and qPCR experiments, cells seeded at 300,000 cells/well in a 6 well-plate the day before immune stimulation. 24 hours later cells were transfected with 10 µg poly(I:C) (Sigma), 5 µg pcDNA3.1, or transfection reagent alone (mock) using 4 µL Lipofectamine® 2000 transfection reagent in 200 µL Opti-MEM added to cells in 2 mL culture medium to stimulate an innate immune response. For immunofluorescence experiments cells were seeded at 50,000 cells/well of a 24-well plate the day before immune stimulation and 24 hours later were transfected with 2 µg poly(I:C) (Sigma), 1 µg pcDNA3.1, or transfection reagent alone (mock) using 1 µL Lipofectamine® 2000 transfection reagent in 50 µL Opti-MEM added to cells in 0.5 mL culture medium. Transfection of cGAMP was also performed using Lipofectamine® 2000 for a final concentration of 2 µg/mL

for HT1080 cells and up to 10 µg/mL for HEK293T cells. Cells were then processed for experiments after the time indicated in figure legends.

2.2.5 – Dual-Luciferase Reporter Assay

24 hours after an initial siRNA knockdown transfection of HEK293FT cells seeded in 6-well plates, 50,000 cells were seeded per well of a 48-well plate. After another 24 hours, cells were co-transfected with plasmids expressing luciferase reporter constructs (IFNβ promoter- *P. pyralis* luciferase or NF-κB/AP1- *P. pyralis* luciferase at 30 ng and HSV-thymidine kinase promoter- *R. reniformis* luciferase (pRL-TK) at 5 ng) and either cGAS and STING (20 ng each) or empty vector DNA (pcDNA3.1 at 40ng). Luciferase plasmids were a gift from Professor Greg Towers (Division of Infection and Immunity, UCL, London). For each well, 1 µL of Fugene6 transfection reagent (Promega) was incubated with 25 µL of Opti-MEM for 5 minutes at room temperature, separately plasmid constructs and 280 ng of the required siRNA oligos (second knockdown) were also diluted in 25 µL of Opti-MEM for 5 minutes at room temperature. After 5 minutes, the transfection reagent Opti-MEM mixture and plasmid/siRNA Opti-MEM mixture were combined, and this final mixture was incubated for a further 20 minutes at room temperature. After 20 minutes, the transfection reagent-plasmid/siRNA Opti-MEM mixture was added to cells with each well containing 150 µL fresh growth medium. After 24 hours growth medium was exchanged for 300 µL fresh growth medium.

To measure luminescence produced by luciferase activity, cells were harvested 96 hours after the initial siRNA knockdown transfection (48 hours after plasmid transfection). Media was removed and cells were washed in PBS before re-suspension in 75 µL 1X Passive Lysis Buffer (PLB; Dual-Luciferase Reporter Kit, Promega). Cells were incubated in PLB for 15 minutes at room temperature and further homogenised by pipetting. 25 µL of the homogenised lysate was transferred to a well on a 96-well plate and luminescence signal was detected using a Modulus Microplate Multimode Reader (Turner Biosystems). The plate reader was programmed to inject 40 µl of Luciferase Assay Substrate re-suspended in Luciferase Assay Buffer II and 35 µl of 1X Stop&Glo Reagent (Dual-Luciferase Reporter Kit, Promega) per well, with a 2 second delay between injections and 10 second measurement period after each injection. Luminescence signal produced by IFNβ/NF-κB- *P. pyralis* luciferase was divided by pRL-TK- *R. reniformis* luciferase luminescence signal to control for variation in transfection efficiency and cell number. Relative fold induction was calculated by dividing the *P. pyralis*/*R.*

reniformis luminescence ratio of reporter constructs in cells transfected with STING and cGAS plasmids by the *P. pyralis*/*R. reniformis* luminescence ratio in control cells transfected with empty vector DNA instead of STING and cGAS and so lacking a functional cGAS-STING pathway.

2.2.6 – Generation of HT1080 SYNCRIP knockout cell lines by CRISPR/Cas9 gene editing

Two guide RNAs (gRNA) targeting exons 3 and 6 of the *SYNCRIP* gene in the human genome were selected using the Synthego CRISPR Design Tool (Synthego, USA). gRNA#1 (5'-CACCGCAGTGATCTCTCTCATGTTC-3') and gRNA#2 (5'-CACCGTTGTACAAAAGAAGCAGCTC-3') were cloned into individual pX458 plasmids according to the Zhang lab method (Ran et al. 2013). HT1080 cells were transfected with plasmids encoding gRNA#1 or gRNA#2 using Lipofectamine® 2000 and fluorescence activated cell sorting (FACS) was used 24 hours after transfection to select for GFP-positive single cells. Single cells were sorted into wells of a 96-well plate containing 100 µL FBS. After sorting, 100 µL cell growth medium was added to wells and single cell colonies were grown up and screened for SYNCRIP knockout by Western blotting and sequencing of the *SYNCRIP* gene.

2.3 – Virology methods

2.3.1 – Influenza A virus production

Influenza A virus (IAV) A/PR8/34(H1N1) stocks were generated using a pDUAL 8 plasmid reverse genetics system, as described previously (De Wit et al. 2004), in which each of the 8 genome segments of IAV are encoded by a separate plasmid. A/PR8/34(H1N1) NS1 mutant strains R38K41A and N81 were also generated using the same reverse genetics system but swapping the plasmid encoding wild type segment 8 (NS) for a plasmid encoding mutant NS1 (R38K41A or N81, which consists of only the first 81 amino acid residues of NS1). To prepare a p0 stock, 250 ng of each of the 8 pDUAL plasmids (0.5 µL of a 500 ng/µL stock encoding IAV genome segments 1-8) was added to 100 µL Opti-MEM and separately 4 µL of Lipofectamine® 2000 was diluted in 100 µL Opti-MEM. Both tubes were mixed gently and incubated separately for 5 minutes at room temperature, the Lipofectamine® 2000/Opti-MEM mixture was then added to the DNA/Opti-MEM mixture, gently mixed by pipetting and incubated for 20 minutes at room temperature. At the same time as preparing p0 stock, a mock virus negative control stock was prepared by omitting the pDUAL plasmid encoding segment 1.

During this incubation, 1 mL of HEK293T cells at a concentration of 1,000,000 cells/mL was added per well of a 6 well-plate. Transfection mixes were then added to HEK293T cells in suspension in a drop-wise manner. The next day medium on HEK293T cells was changed to 2 mL of virus growth medium (VGM) (serum free DMEM, supplemented with 0.14 % BSA (1:50 from a 7 % BSA stock prepared in sterile distilled water), and 1 µg/mL of TPCK trypsin (Worthington Biochemical Corporation) (1:1000 from a 1 mg/mL stock diluted in PBS), 100 units/mL penicillin and 100 µg/mL streptomycin). After 48-72 hours supernatants were harvested and 1 mL aliquots prepared in 2 mL screw capped tubes, these were centrifuged for 1 minute at 13,000 xg to pellet any cells and stored at -80 °C.

To make a p1 working virus stock, p0 stocks prepared in HEK293T cells were used to infect MDCK cells in a T-25 flask. MDCK cells were seeded the day before at 5,000,000 cells/flask in 10 mL growth medium. Cell monolayers were washed 2X with 10 mL serum free DMEM supplemented with 100 units/mL penicillin and 100 µg/mL streptomycin. After removing the last wash 1 mL of 100 µL p0 stock diluted in 1 mL VGM was added to cells, the flask gently washed to ensure even coverage and cells incubate for 1 hour at 37 °C. After this incubation, 5 mL of VGM was added to flasks and cells were incubate for 48 hours. After 48 hours, provided there was significant cytopathic effect (CPE), supernatants were harvested into a 15 mL tube, centrifuged at 3,000 xg for 5 minutes, aliquoted into screw capped tubes, and stored at -80 °C.

2.3.2 – Influenza A virus titration by plaque assay

In order to determine influenza A virus stock concentrations plaque assays were used. Two days before titration MDCK cells were seeded in 6-well plates at ~750,000 cells/well (typically 1X confluent T-150 flask could be used to seed 8X 6-well plates). After two days, confluent monolayers of MDCK cells were infected with serially diluted virus stocks. Assuming that wild-type A/PR8/34(H1N1) grows to a titre of 1 x10^8 plaque forming units (PFU)/mL stocks were serially diluted to 1:1 x10^8 and serial 1 in 10 dilutions of 1:1000-1:1 x10^8 were used for the 6 wells of a 6-well plate. MDCK cells were washed 2X with 1 mL/well serum free DMEM, after the last wash was removed 800 µL of virus dilution was added per well and plates were incubated for 1 hour at 37 °C. After this incubation cells were overlaid with 2 mL overlay medium (1:1 mixture of DMEM and 2.4 % Avicell ((RC-591 NF) diluted in distilled water and autoclaved), supplemented with 0.14 % BSA, 1 µg/mL TPCK trypsin, 100 units/mL penicillin,

and 100 µg/mL streptomycin). Cells were then incubated for 48 hours at 37 °C, ensuring that plates were not disturbed in this time. After 48 hours, overlay medium was removed and cell monolayers were fixed with 2 mL/well 3.7 % formaldehyde (diluted in PBS) for 30 minutes. Fixative was then removed, and cells were stained with 0.01 % toluidine blue for 1 hour at room temperature. Stain was then removed, and cells monolayers were rinsed with water and left to dry. Quantification of viral titres was determined by counting the number of plaques in a well with a dilution that gave between 10 and 100 plaques (Figure 2.2). PFU/mL was determined by multiplying the number of plaques by the dilution factor and correcting for the volume of virus added.

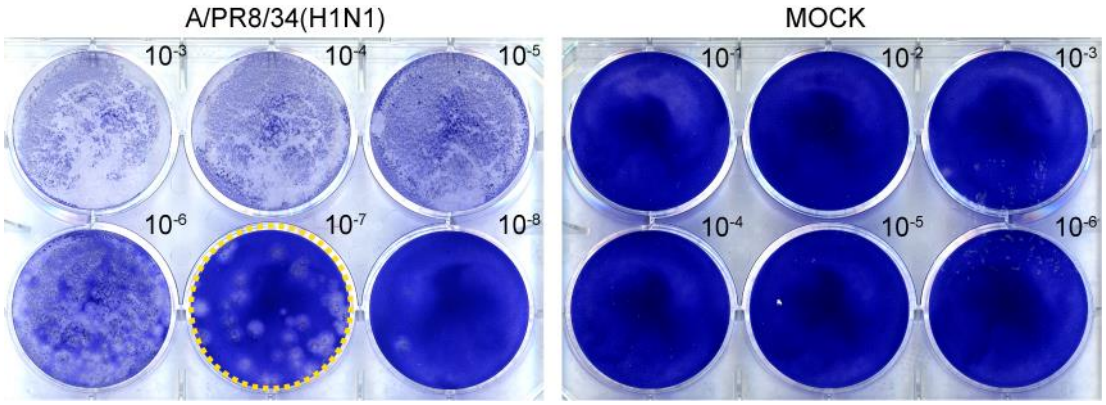

Figure 2.2 – Example plaque assay of A/PR8/34(H1N1) virus stock and mock infected MDCK cell monolayers. *Plaques formed on MDCK cells were counted for the well corresponding to a 10^{-7} dilution of p1 virus stock (yellow circle). No plaques formed in mock infected wells since no virus is produced in the absence of one of the IAV genome segments. To determine an accurate titre, virus stocks were titrated in triplicate.*

2.3.3 – Infection of cells with Influenza A virus

For determination of IAV proliferation in cells and immunofluorescence experiments, 100,000 HT1080 cells were seeded per well of a 24-well plate the day before infection (on 13 mm glass coverslips for immunofluorescence experiments). For time-course experiments, a separate well was required per time-point being analysed. On the day of infection cells were washed 2X with 0.5 mL SFM and cells in one well of a 24-well plate per condition (e.g. siRNA treatment) was counted to determine the number of cells. SFM was removed and IAV was added at the specified multiplicity of infection (MOI = (stock virus titre (PFU/mL)*volume of titre to use)/number of cells) in a final volume of 200 µL SFM. Cells were incubated for 1 hour at 37 °C to allow for viral particles to adsorb to cells. After 1 hour, cells were washed with 0.5 mL SFM to remove free virus and then overlaid with 0.5 mL VGM. Supernatants were collected

at indicated timepoints (with 0 hours post infection beginning after overlay of VGM) and stored at -80 °C until virus titration by plaque assays to determine viral proliferation. For immunofluorescence experiments, after the adsorption incubation cells and washing cells were overlaid with VGM -TPCK Trypsin since this tended to result in cells detaching from coverslips. Cells were then fixed in 3.7 % formaldehyde (in PBS) for 15 minutes before proceeding with immunofluorescence. For Western blotting and co-immunoprecipitation experiments cells were seeded the day before infection at 500,000 cells/well of a 6-well plate and 3,000,000 cells in a 10 cm dish, respectively. On the day of infection cells were washed with SFM, counted, and infected with MOI indicated in figure legends, for 6-well plates virus was adsorbed to cells in a final volume of 800 µL SFM while for 10 cm dishes virus was adsorbed to cells in a final volume of 3 mL SFM. After 1 hour incubation to allow virus to adsorb to cells, cell monolayers were washed with SFM and overlaid with VGM – TPCK Trypsin (2 mL/well of a 6-well plate and 10 mL in a 10 cm dish). At desired time points post-infection cells for Western blotting were washed with PBS and lysed directly in 200 µL 2X Laemlli buffer. For co-immunoprecipitation experiments cells were washed with ice-cold PBS and lysed in 1 mL Co-immunoprecipitation lysis buffer with freshly added protease inhibitors.

2.3.4 – Herpes simplex virus-1 production

HSV-1 wild type strain 17+ viral stocks were generated in BHK-21 cells. The day before infection 1,500,000 cells were seeded in a 60 mm plate. The next day cells were infected with HSV-1 stocks at an MOI of 0.005, cell growth medium was removed, and virus was added in a final volume of 0.7 mL cell growth medium. To generate a mock virus stock, cells were ‘inoculated’ in parallel with 0.7 mL cell growth medium. Cells were incubated at 37 °C for 1 hour to allow virus to adsorb to cells, plates were gently rocked every 15 minutes to ensure an even coverage of the cell monolayer, before adding an additionally 3 mL growth medium and incubating cells for a further 2-3 days at 37 °C (until extensive CPE is observed). Cells were then scraped into the cell medium with a cell scraper and transferred into a 15 mL screw-cap tube and sonicated for 30 seconds in a water bath sonicator at 4 °C to release cell bound virus. Virus suspension was then centrifuged for 12 minutes at 5,000 xg to pellet cell debris and supernatant was aliquoted into 0.5 mL aliquots in 2 mL screw cap tubes and stored at -80 °C.

2.3.5 – Herpes simplex virus-1 titration by plaque assay

In order to determine HSV-1 stock concentrations plaque assays were used to determine viral titre (PFU/mL). The day before infection 200,000 Vero cells were seeded per well of 12-well plate, after 24 hours or when cells reached 90 % confluence cells were infected with 10-fold serial dilutions of HSV-1 diluted in SFM (10^{-1} to 10^{-8}). Cell growth medium was removed from wells and 100 µL of virus dilution was added per well, with each virus dilution used to infect cells in duplicate. Plates were then incubated for 1 hour at 37 °C, gently rocking the plate every 15 minutes. After 1 hour, virus inoculum was removed, and cells were overlaid with 2 mL of overlay medium (1:1 mix of 2X MEM growth medium and 1.2 % Avicell (RC-591 NF) (diluted in distilled water and autoclaved)). Plates were then incubated for 3 days at 37 °C before fixation and staining. Overlay medium was removed and cells were fixed for 30 minutes in 3.7 % formaldehyde (diluted in PBS). Fixative was then removed, and cells were stained with 2 % crystal violet solution for 1 hour at room temperature. Stain was then removed, and cells monolayers were rinsed with water and left to dry. Quantification of viral titres was determined by counting the number of plaques in a well with a dilution that gave between 10 and 100 plaques (Figure 2.3). PFU/mL was determined by multiplying the number of plaques by the dilution factor and correcting for the volume of virus added.

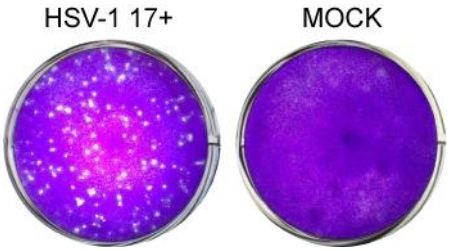

Figure 2.3 – Example plaque assay of HSV-1 17+ virus stock and mock infected Vero cell monolayers. *Plaques formed on Vero cells. No plaques formed in mock infected wells. To determine an accurate titre, virus stocks were titrated in triplicate.*

2.3.6 – Infection of cells with Herpes simplex virus-1 (HSV-1)

The day before infection 100,000 cells were seeded per well of a 24-well plate. The next day one well of cells for each siRNA knockdown condition was counted and cell monolayers were infected at an MOI of 5 with virus stocks or mocks diluted in SFM for a final volume of 200 µL per well. After 1 hour of adsorption, cells were wash 2X with PBS to remove free virus and 0.5 mL of cell culture medium was added to wells. At the desired timepoints cells were

scraped into cell medium, suspensions were transferred into 1.5 mL tubes, and stored at -80 °C. In order to determine viral titres in each sample plaque assays were used, virus/cell suspensions were subject to 3X freeze thaw-cycles with samples vortexed after each sample prior to use in plaque assays.

2.4 – Nucleic acid methods

2.4.1 – Sequencing plasmid DNA

Plasmids SYNCRIP (Q1)-FLAG (RC228458) and SYNCRIP (Q3)-FLAG (RC217902) (OriGene Technologies) were verified before use in experiments by sequencing. BigDye™ Terminator v3.1 Cycle Sequencing kit (Applied Biosystems #4337455) was used, and reactions were sent for sequencing by Edinburgh Genomics (University of Edinburgh). Provided chromatograms were analysed using SnapGene® 4.3.11 software (SnapGene).

2.4.2 – RNA extraction

RNA extraction was performed using TRIzol™ reagent (Invitrogen, #15596026). Cell culture medium was removed, and cells were lysed directly in 0.5 mL TRIzol™ per well of a 6-well plate, cells were scraped, and the lysate homogenised by pipetting and transferred to a 1.5 mL tube. After incubation at room temperature for 5 minutes, 0.1 mL of chloroform was added, the mixture was shaken vigorously for 30 seconds, and incubation continued for a further 5 minutes at room temperature. Samples were then centrifuged at 12,000 xg for 15 minutes at 4 °C, after which the upper aqueous phase was transferred to a new tube and mixed with 0.25 mL isopropanol. After a 10-minute incubation at room temperature the mixture was centrifuged 12,000 xg for 10 minutes at 4 °C. The supernatant was discarded, and pelleted RNA was washed with 70 % ethanol. After air drying at room temperature for 5 minutes pellets were resuspended in 20 µL RNase-free water. Alternatively, RNA extraction was achieved using RNeasy Mini Kit (Qiagen) according to the manufacturer's instructions. RNA yield was determined using a NanoDrop 2000c spectrophotometer and RNA integrity assessed by agarose gel electrophoresis.

2.4.3 – Quantitative PCR (qPCR)

cDNA was generated using SuperScript™ II Reverse Transcriptase (Invitrogen #18064022) First-Strand cDNA Synthesis protocol. Oligo$(dT)_{18}$, dNTPs, and 2 µg total RNA were incubated at 65 °C for 5 minutes before the addition of 5X First-Strand Buffer, 10 mM DTT, and 40 U

RNaseOUT™. After a brief mix and incubation at 42 °C for 2 minutes, 200 U SuperScript™ II Reverse Transcriptase was added, mixed, and incubated at 42 °C for 3 hours, before a 15-minute heat inactivation step at 70 °C. cDNA was diluted with 180 µL of nuclease-free water to give a final volume of 200 µL and then stored at -20 °C until use.

For qPCR reactions, 20 µL reactions containing 8.4 µL of diluted cDNA, 400 nM each of forward and reverse primers (see Table 2.5) and 1X LightCycler® 480 SYBR Green I Master (Roche) were prepared in a 96-well LightCycler® 480 Multiwell Plate. Polymerase chain reactions were carried out in a LightCyler® 480 using the program detailed in Table 2.6 and expression data was analysed using LightCycler® 480 Software v1.5.0.39 (Roche). Ct values were exported to Microsoft Excel and ΔCt expression values calculated ($2^{-(\text{Ct target-Ct reference})}$).

Table 2.5 – Primers used for qPCR

Gene	Forward Primer (5'-3')	Reverse Primer (5'-3')
IFNβ	CCTGAAGGCCAAGGAGTACA	AGCAATTGTCCAGTCCCAGA
CCL5/RANTES	GCTGTCATCCTCATTGCTACTG	TGGTGTAGAAATACTCCTTGATGTG
GAPDH	GTGAAGGTCGGAGTCAACG	ATGACAAGCTTCCCGTTCTC

Table 2.6 – Thermocycling conditions for qPCR

Target (°C)	Acquisition mode	Hold (mm:ss)	Ramp rate (°C/s)	Acquisition (per °C)
Preincubation, 1 cycle				
95		05:00		
Amplification, 45 cycles				
95		00:10		
51		00:15		
72	Single	00:20		1
Melting Curve, 1 cycle				
95		00:05		
65		01:00	2.2	

97	Continuous			5
Cooling, 1 cycle				
22		00:30	2.2	

2.5 – Microscopy methods

2.5.1 – Immunofluorescence

Adherent cells were grown on 13 mm coverslips No. 1.5 (VWR International) and washed with PBS to remove cell debris and cell growth medium prior to fixation with 3.7 % formaldehyde, 1X PBS for 15 minutes at room temperature. Alternatively, where indicated, cells were fixed with ice-cold 100 % methanol at -20 °C for 15 minutes. After fixation cells were washed twice with PBS and permeabilised for 7 minutes with 0.2 % Triton-X-100 in PBS and then washed 3 times in PBS. Coverslips were blocked with 4 % bovine serum albumin (BSA), 1X PBS for 30 minutes at room temperature and subsequently incubated with primary antibody (dilutions listed in Table 2.2) overnight at 4 °C or for 1 hour at room temperature. Coverslips were washed 3 times in PBS and incubated with appropriate secondary antibodies conjugated to Alexa Fluor® dyes (listed in Table 2.3) and 4,6-diamidino-2 phenylindole, dihydrochloride (DAPI) at a final concentration of 2 µg/mL, for 30 minutes at room temperature. Coverslips were washed 3 times in PBS and mounted on slides with Fluoromount-G® (SouthernBiotech) or VECTASHIELD® (Vector Labs). Alternatively, for immunofluorescence experiments using anti-STING (D2P2F) antibody (Cell Signaling Technology) staining was performed according to (Almine et al. 2017), with cells fixed in methanol at -20 °C, permeabilised for 12 minutes in 0.5 % Triton-X-100 in PBS and blocked with 5 % FBS, 0.2 % Tween-20 in PBS. Cells were stained with primary antibodies overnight at room temperature and incubated with secondary antibodies for 3 hours at room temperature.

2.5.2 – Pre-fixation detergent extraction assay

Adherent cells grown on 13 mm coverslips No 1.5 (VWR International) were washed with PBS and then extracted prior to fixation with 0.1 % Triton-X-100 for 1 minute at room temperature, washed with PBS, and then incubated with 0.1 % Triton-X-100 again for 1 minute. Cells were then washed with PBS and fixed in 100 % methanol at -20 °C for 15 minutes. In parallel cells were directly fixed without extraction. Downstream

immunofluorescence was performed as described for anti-STING (D2P2F) antibody (Cell Signaling Technology)

2.5.3 – Proximity Ligation Assay (PLA)

Proximity Ligation Assays were performed using Duolink® PLA reagents following the manufacturer's instructions (Duolink® In Situ Red Starter Kit, DUO92103, and Duolink® In Situ PLA® Probe Anti-Rabbit PLUS, DUO92002, Sigma-Aldrich). Adherent cells grown on 13 mm coverslips No 1.5 (VWR International) were fixed and permeabilised as for immunofluorescence staining. Cells were then blocked in Duolink® Blocking Solution (Sigma-Aldrich) for 1 hour at 37 °C in a humidity chamber. Coverslips were then incubated with indicated primary antibodies diluted in Duolink® Antibody Diluent (Sigma-Aldrich) overnight at 4 °C in a humidity chamber. The next day coverslips were washed in Duolink® Wash Buffer A (Sigma-Aldrich) and incubated with Duolink® PLA Probes (PLUS and MINUS for specific antibody pair used for primary antibody incubation) for 1 hour at 37 °C in a humidity chamber. Coverslips were washed with Duolink® Wash Buffer A and incubated with Duolink® Ligase in Ligation buffer for 30 minutes at 37 °C in a humidity chamber. Coverslips were washed with Duolink® Wash Buffer A and then incubated with Duolink® Polymerase in Amplification buffer for 100 minutes at 37 °C in a humidity chamber. Finally, coverslips were washed with Duolink® Wash Buffer B and mounted on slides with Fluoromount-G® with DAPI (SouthernBiotech).

2.5.4 – Fluorescence Microscopy and analysis

Images were acquired on a Zeiss Axio Imager equipped with alpha-Plan ApoChromat 1.46 NA 100x objective, Marzhauser 8 slide motorised stage, Hamamatsu Flash sCMOS camera, and CooLED pE-300 Lightsource, using MicroManager image acquisition software. Image analysis was performed in ImageJ (FIJI) (Schindelin et al. 2012). For nuclear/cytoplasmic distribution analysis mean nuclear localised signal was determined using a DAPI mask to select ROI, mean cytoplasmic signal was determined using a mask based on auto-thresholding of signal with DAPI mask subtracted to select ROI. To calculate PLA foci per cell, PLA foci were counted by thresholding based on signal intensity followed by the 'analyse particles' function of ImageJ and this number was divided by the number of DAPI stained nuclei per field of view.

2.5.5 – Förster-Resonance Energy Transfer (FRET) with fluorescence lifetime imaging (FLIM) microscopy

HEK293T cells were seeded at 70,000 cells on 13 mm glass coverslips No. 1.5 in a well of a 24-well plate. The next day cells were transiently transfected with plasmids encoding Lamin A-GFP, an RFP-GFP tandem construct, or Lamin A-GFP and STING-RFP (Malik et al. 2010). After 24 hours cells were fixed for 15 minutes in 3.7 % formaldehyde before washing in PBS and mounting in Vectashield®. Imaging was performed on a Leica SP5 SMD confocal laser scanning microscope equipped with PicoHarp 300 (TCSPC module and picosecond event timer) and single photon avalanche detectors (SPAD). Leica application suite with FLIM wizard software and integrated Symphotime software were used for single photon counting acquisition and FLIM measurements were carried out for 5 minutes per field of view. FLIM data was analysed using FLIMfit 5.1.1 software (Imperial College London) with an instrument response function (IRF) calculated from a AlexaFluor 488 fluorescent reference slide.

2.5.6 – Single molecule Fluorescence Recovery After Photobleaching (smFRAP) microscopy

Imaging was performed on an Olympus IX81 microscope equipped with a 1.4-NA 100x oil-immersion apochromatic objective (UPLSAPO 100XO, Olympus). An Obis™ solid state 488-nm (Coherent Inc) was passed through dichroic filters (Di01- R405/488/561/635-25x36, Semrock) and emission filters (NF01- 405/488/561/635-25X5.0, Semrock) as well as a circular variable metallic neutral density filter (Newport) and directed into the microscope using a micrometer stage (Newport). HT1080 cells stably expressing doxycycline inducible STING-GFP were plated on No. 0 cover glass 35-mm dishes with 14 mm Microwell (MatTek). After overnight induction of STING-GFP expression with 0.05 µg/mL doxycycline, 2 hours before imaging cells were transfected via lipofection agent Transit-X2 (Mirus Bio LLC) with plasmid DNA, poly(I:C), or transfection reagent alone (mock). Growth media was replaced with Transport Buffer (20 mM HEPES, 110 mM KOAc, 5 mM NaOAc, 2 mM MgOAc, and 1 mM EGTA, pH 7.3) 30 minutes prior to imaging to slow membrane movements and reduce autofluorescence. Imaging was performed on the Nuclear Envelope region opposite the bulk of the peripheral ER. The region was photobleached for 1 minute at 5 mW and then imaged for 30 seconds at 50 µW. An optical chopper rotating at 2-Hz was utilized during capture to allow for fluorescence recovery. Images were captured using the Slidebook software package (Intelligent Imaging Innovation). Data were analyzed using the ImageJ (FIJI) plugin GDSC SMLM (Single Molecule

Light Microscopy ImageJ Plugins, University of Sussex) (Herbert 2014) and OriginPro 2019 (OriginLab). smFRAP microscopy was performed by collaborator Mark Tingey (Weidong Yang, Temple University)

2.5.7 – Immunogold Electron Microscopy

HT1080 cells or HT1080 cells stably expressing inducible STING-GFP induced overnight with doxycycline were fixed for 2 minutes by the addition of a 2X fixation buffer (8 % formaldehyde, 0.2 M PHEM buffer) to culture medium (1:1), this was then replaced with 1X fixation buffer (4 % formaldehyde, 0.1 M PHEM buffer, 0.05 % glutaraldehyde) and fixation continued for 2 hours. Cells were then scraped into the fixation buffer and transferred to microfuge tubes, before pelleting and washing with PBS. Cell pellets were stored in PBS prior to sectioning and immunostaining. Cell pellets were embedded in 10 % gelatin in 0.1 M phosphate buffer, pH 7.4 before being infused overnight with 15 % polyvinylpyrrolidone (PVP), 1.7 M sucrose in 0.1 M phosphate buffer, pH 7.4. Liquid nitrogen frozen pellets were sectioned on a cryo-ultramicrotome (UC7 with FC7 cryo-attachment; Leica). Immunoelectron microscopy was performed using the Tokuyasu method (Tokuyasu 1973). Cryosections were thawed, rinsed with 1 % glycine in PBS, and blocked with 1 % BSA in PBS. For endogenous STING staining, grids were incubated with anti-STING antibody at 1:7 dilution (AF6516, R&D Systems), rinsed in PBS, then incubated with a 6 nm donkey anti–sheep IgG antibody conjugated to 6 nm colloidal gold (Aurion). For STING-GFP expressing cells grids were incubated with a rabbit anti-GFP antibody at 1:20 dilution (Abcam), rinsed in PBS, then incubated with a 5 nm goat anti–rabbit IgG antibody conjugated to 5 nm colloidal gold (Aurion). Grids were then rinsed in PBS, transferred to 1 % glutaraldehyde (Agar Scientific) in PBS, washed in water, and embedded in 2 % methyl cellulose containing 0.4 % uranyl acetate (Agar Scientific). Imaging was performed at 100 kV with a Hitachi H7600 TEM and Xarosa 20 Megapixel camera.

2.6 – Protein methods

2.6.1 – Protein Extraction and Western Blotting

For Western blotting, cell monolayers were washed with PBS and cells were lysed directly in 2X Laemmli buffer (with the addition of NA_3VO_4 and NaF for detection of phosphorylated proteins). Samples were sonicated using a probe sonicator (Ultrasonic Atomizer VCX ATFT 1

second on/1 second off amplitude 20 %) to shear DNA and then boiled for 5 minutes at 95 °C before separation by SDS-PAGE. Proteins were transferred onto nitrocellulose membranes by wet-transfer and subsequently membranes were blocked in blocking buffer (5 % milk powder (w/v) in TBS with 0.05% Tween-20) for 1 hour at room temperature. For detection of phosphorylated proteins, 5 % BSA (w/v) was used in place of milk powder. Membranes were incubated with primary antibodies diluted in blocking buffer at the dilutions indicated in Table 2.2 overnight at 4 °C. The next day membranes were washed 3 times in TBS, 0.05 % Tween-20 and incubated with secondary antibodies diluted in blocking buffer at the dilutions indicated in Table 2.2 for 1 hour at room temperature. Membranes were washed 3 times in TBS, 0.05% Tween-20, and antibody labelling detected using a Li-Cor Odyssey Quantitative Fluorescence Imager. Image Studio 5.2 software (Li-Cor) was used for Western blot analysis and normalisation of protein levels detected in samples.

2.6.2 – Co-immunoprecipitation

For co-immunoprecipitation experiments HT1080 or HEK293FT cells were treated as indicated in figure legends with regard to innate immune stimulation or infection and transient expression of plasmid constructs. Cells were seeded in 10 cm dishes to be ~80 % confluent at the time of immune stimulation or viral infection. At the indicated time points post-immune stimulation/viral infection cells were washed with ice-cold PBS and then lysed directly in 1 mL ice-cold Co-immunoprecipitation Lysis Buffer (150 mM NaCl, 5 mM EDTA pH 8.0, 50 mM Tris pH 8.0, 1 % IGEPAL® CA630, supplemented with 2 µg/mL Aprotinin, 10 µg/mL Leupeptin, 1 µg/mL Pepstatin A, and 1 mM PMSF). Lysis buffer was supplemented with RNase inhibitors when analysing immunoprecipitation of influenza A virus RNA. Cells were scraped into lysis buffer, transferred to a 1.5 mL tube, and incubated on ice for 10 minutes. Lysates were passed through a 25 G needle 5 times using a syringe to shear DNA, and incubation continued on ice for a further 10 minutes. Lysates were centrifuged at 13,000 xg for 10 minutes at 4 °C and supernatant transferred to a new tube. 250 µL of cell lysate was made up to 1 mL with lysis buffer and incubated with 2 µg of primary antibody overnight at 4 °C with gentle rocking on a nutator. The next day, 30 µL of protein A/G Dynabeads™ 50 % bead slurry was added to cell lysate-antibody mix as appropriate (Protein A, for rabbit IgG, Protein G, for goat, sheep, or mouse IgG) and incubated at 4 °C for 30 minutes with gentle rocking on a nutator. Pellets were washed 5 times with 0.5 mL cell lysis buffer and resuspended in 20 µL 2X Laemmli buffer,

vortexed, and then centrifuged. Samples were boiled at 95 °C for 5 minutes and analysed by SDS-PAGE with Western blotting. Alternatively, for analysis of RNA bound by immunoprecipitated protein, pellets were resuspended in TRIzol™ and RNA extraction performed. Isolated RNA was reverse transcribed as described for qPCR and PCR performed to produce amplicons detailed in figure legends, which were detected by agarose gel electrophoresis.

Chapter 3

Localisation and Dynamics of STING at the Nuclear Envelope

3.1 – Introduction

Although STING was first reported as a nuclear envelope (NE) protein in a proteomics study (Schirmer et al. 2003), nearly all studies have focused on its role in the ER since it was identified as the critical adaptor protein in innate immune signalling induced by the presence of cytoplasmic dsDNA (Ishikawa and Barber 2008; Ishikawa et al. 2009; Almine et al. 2017; Jønsson et al. 2017; Dunphy et al. 2018; Yang et al. 2018; Srikanth et al. 2019). Thus, I considered that before engaging studies on a nuclear envelope role, I should first establish its localization and dynamics in the nuclear envelope. Proteomics identified STING in the NE (Schirmer et al. 2003; Korfali et al. 2010), however, it could be limited to the outer nuclear membrane (ONM), which is continuous with the ER, and not access the inner nuclear membrane (INM). The lumen separating the INM and ONM is only ~50 nm and so it is difficult to distinguish INM from ONM localisation by fluorescence microscopy approaches as this is below the resolution limit of most fluorescence microscopy. Previous attempts to determine if STING is present in the ONM or INM proved inconclusive with some data arguing STING was in the INM but other data suggesting it exclusively resides in the ONM (Malik et al. 2010). In order to investigate STING's localisation within the NE, this study used a combination of different assays to assess whether STING was present in the inner (INM) or outer nuclear membrane (ONM), in parallel with other candidate NETs (Malik et al. 2010). One method commonly used to determine whether a protein is present in the INM is the use of detergent extraction to remove ER and ONM proteins prior to fixation. INM proteins that interact with the intermediate filament lamin network underlying the INM are typically retained by detergent extraction because nuclear lamin polymers resist even harsh extraction conditions with as much as 1 M NaCl and 1M urea. In *Malik et al. 2010* pre-extraction of cells with Triton X-100 to remove membranes and soluble proteins prior to fixation showed that in HT1080 cells stably expressing lamin A-GFP and transiently expressing a STING-RFP construct, STING remained at the nuclear envelope in contrast to the ER protein calreticulin (Figure 1.3). Since the nuclear lamina is resistant to such pre-extraction with detergent, a similar biochemical resistance to extraction of a nuclear envelope transmembrane protein (NET) typically

indicates an INM association. One caveat of this method is that some NETs present only in the ONM can also resist detergent extraction due to interactions with cytoskeletal filaments such as the Nesprin family of proteins (Rajgor and Shanahan 2013). According to the diffusion-retention hypothesis, binding to the nuclear lamina is thought to be the mechanism by which NETs accumulate at the INM (Soullam and Worman 1995). Therefore, whether STING localised to the NE in a Lamin A dependent manner was also tested. In Lamin A/C knockout (*LMNA*$^{-/-}$) murine embryonic fibroblasts (MEFs) STING-RFP did not localise to the NE whereas in *LMNA*$^{+/+}$ *MEFs* STING-RFP was clearly present in the NE by fluorescence microscopy further suggesting an INM localisation and interaction with the nuclear lamina (Figure 1.3).

The same study also used a super resolution fluorescence microscopy technique, 3D structured illumination microscopy (3D SIM), which can distinguish INM from ONM localisation (Schermelleh et al. 2008), to determine STING and other NET proteins localisation withing the NE. Whether proteins localise to the INM or ONM can be determined based on whether fluorescent signal in the same plane of the NE with either the nucleoplasmic facing, Nup153, or cytoplasmic facing Nup358. Surprisingly, although STING-RFP resisted detergent extraction and did not localise to the NE in *LMNA*$^{-/-}$ MEFs, by 3D-SIM it localised predominantly in the same plane as Nup358 indicating ONM localisation. However, subsequent repetition of this experiment using a STING-GFP construct and examining a larger number of cells revealed that in some cells STING localised to the INM while in other cells STING localised to the ONM (Figure 1.4) This prompted the hypothesis that STING localisation in the NE may be altered by immune stimulation since in these experiments cells were transiently transfected with plasmid DNA which might induce activation of cGAS-STING signalling. A potential criticism of these experiments is that they all used STING constructs tagged with RFP/GFP and overexpressed in cells, so it is possible that both tagging, and overexpression alter the localisation of STING.

Given the ambiguity surrounding STING localisation within the NE, in this chapter I set out to ***determine the localisation of STING within the NE and to investigate whether this changes during the course of an innate immune response to a variety of stimuli.*** This chapter will describe several approaches which demonstrate that STING resides in both the INM and ONM, and moreover that STING in the INM redistributes to the ONM following immune stimulation with either dsDNA or the dsRNA mimic poly(I:C).

3.2 – HT1080 cells and HT1080 cells expressing inducible STING-GFP are suitable for studying STING localisation in the nuclear envelope

In order to study STING localisation and dynamics within the NE, it was first necessary to determine a suitable cell line to use. Given STING's critical function in the innate immune response to cytosolic DNA and its role in the response to host cell DNA damage (Dunphy et al. 2018), it is unsurprisingly found expressed in a wide variety of tissues (Ishikawa and Barber 2008), because almost any cell can suffer genomic damage or be vulnerable to pathogen infection. However, many immortalised and tumour cell lines have defective cytosolic DNA triggered innate immune signalling pathways compared to primary cells which are able to mount full DNA-activated antiviral responses. This in part is due to the nature by which cell lines gained their immortality. For example, it has been shown that cell lines immortalised by 'DNA tumour viruses', including HeLa cells and human embryonic kidney 293 (HEK 293) cells, express viral oncoproteins which antagonize the cGAS-STING pathway (Lau et al. 2015). In the case of HeLa cells, which were derived from a cervical carcinoma caused by infection with human papillomavirus 18 (HPV18) (Boshart et al. 1984), expression of the viral oncogene E7 inhibits the cGAS-STING pathway, while for HEK293 cells, immortalised by transformation with human adenovirus 5 (hAd5) DNA (Graham et al. 1977), the hAd5 E1A protein blocks cGAS-STING pathway activation. Intriguingly this occurs through a common mechanism of binding STING via the conserved (LXCXE) protein motif of these oncoproteins, which is also essential for binding and inhibition of the retinoblastoma (Rb) tumour suppressor protein (Lau et al. 2015). In addition, expression of STING and cGAS is reduced or lost in many cell lines resulting in variable levels of responsiveness to immune stimulation by cytosolic DNA (Sun et al. 2009; Sun et al. 2013; Malik et al. 2014; Xia et al. 2016a; Deschamps and Kalamvoki 2017a).

Therefore, I first sought to determine a suitable cell line to use for studying STING dynamics at the NE. Western blotting for endogenous STING and cGAS expression in HT1080, A549, HEK293FT, and HEK293T cell lines was used to assess protein levels and revealed that only HT1080 cells expressed detectable levels of both STING and cGAS (Figure 3.1 A). This agrees with previous reports that cGAS and STING expression are low in HEK293T cells and that STING is expressed in HT1080 cells (Sun et al. 2009; Sun et al. 2013; Orzalli et al. 2015). To confirm that HT1080 cells express a functional endogenous cGAS-STING pathway, HT1080 cells were transfected with empty vector DNA (pcDNA3.1) or the synthetic RNA mimetic poly(I:C) to induce an innate immune response. Two hallmarks of STING activation in response to dsDNA

immune stimulation were measured: the redistribution of STING to perinuclear foci and the accumulation of the transcription factor IRF3 in the nucleus. As expected, in response to the presence of cytosolic dsDNA STING accumulated in perinuclear foci, while in response to transfection with poly(I:C) no redistribution of STING was evident when compared to unstimulated cells (Ishikawa et al. 2009; Franz et al. 2018) (Figure 3.1 B and C). IRF3 also accumulated in the nuclei of cells stimulated with dsDNA indicating that signalling downstream of STING activation is intact. This data supports a previous report showing that HT1080 cells induce IFNβ expression in response to immune stimulation with cGAMP suggesting that the STING pathway if functional in HT1080 cells (Wang et al. 2016). The accumulation of IRF3 in the nucleus of poly(I:C) stimulated cells suggests that the cytosolic dsRNA sensing pathway consisting of RIG-I/MDA-5 and MAVS is also intact in HT1080 cells because this pathway also activates IRF3 (Figure 3.1 B). To confirm specificity of STING antibody staining, two different STING antibodies were used for immunofluorescence, one a monoclonal antibody raised in sheep which is compatible with formaldehyde fixed cells only (Figure 3.1 B) while the other, a monoclonal raised in rabbit, is compatible with methanol fixed cells only (Figure 3.1 C). Both antibodies showed the same pattern of STING staining, although the antibody requiring methanol fixed cells tended to stain more strongly. Co-staining of cells with an anti-Nup153 antibody to label the NE highlights the presence of a NE-pool of STING in addition to its distribution throughout the ER (Figure 3.1 B and C), which is present in both sets of fixed cells. In order to be able to follow STING dynamics in real-time, without the need to transiently introduce plasmid DNA for expression of fluorescently labelled proteins, which would induce an innate immune response against the cytoplasmic plasmid DNA, a stable doxycycline-inducible STING-GFP HT1080 cell line was used. STING-GFP behaved similarly to endogenous STING, accumulating in perinuclear foci after immune stimulation with plasmid DNA but not with poly(I:C), while IRF3 accumulates in the nucleus of both dsDNA and poly(I:C) stimulated cells (Figure 3.1 D). Finally, to check the specificity of the STING antibodies used for immunofluorescence, western blotting was performed with both antibodies on lysates of cells treated with siRNAs against STING or a non-target control siRNA. Both antibodies recognise a single protein band, of a molecular weight close to the predicted ~42 kDa of STING, which is depleted in cells treated with siRNAs against STING (Figure 3.1 E). Therefore, this experiment shows that HT1080 cells and HT1080 cells stably expressing STING-

GFP under the control of an inducible promoter are both suitable cell lines for studying STING NE localisation and dynamics.

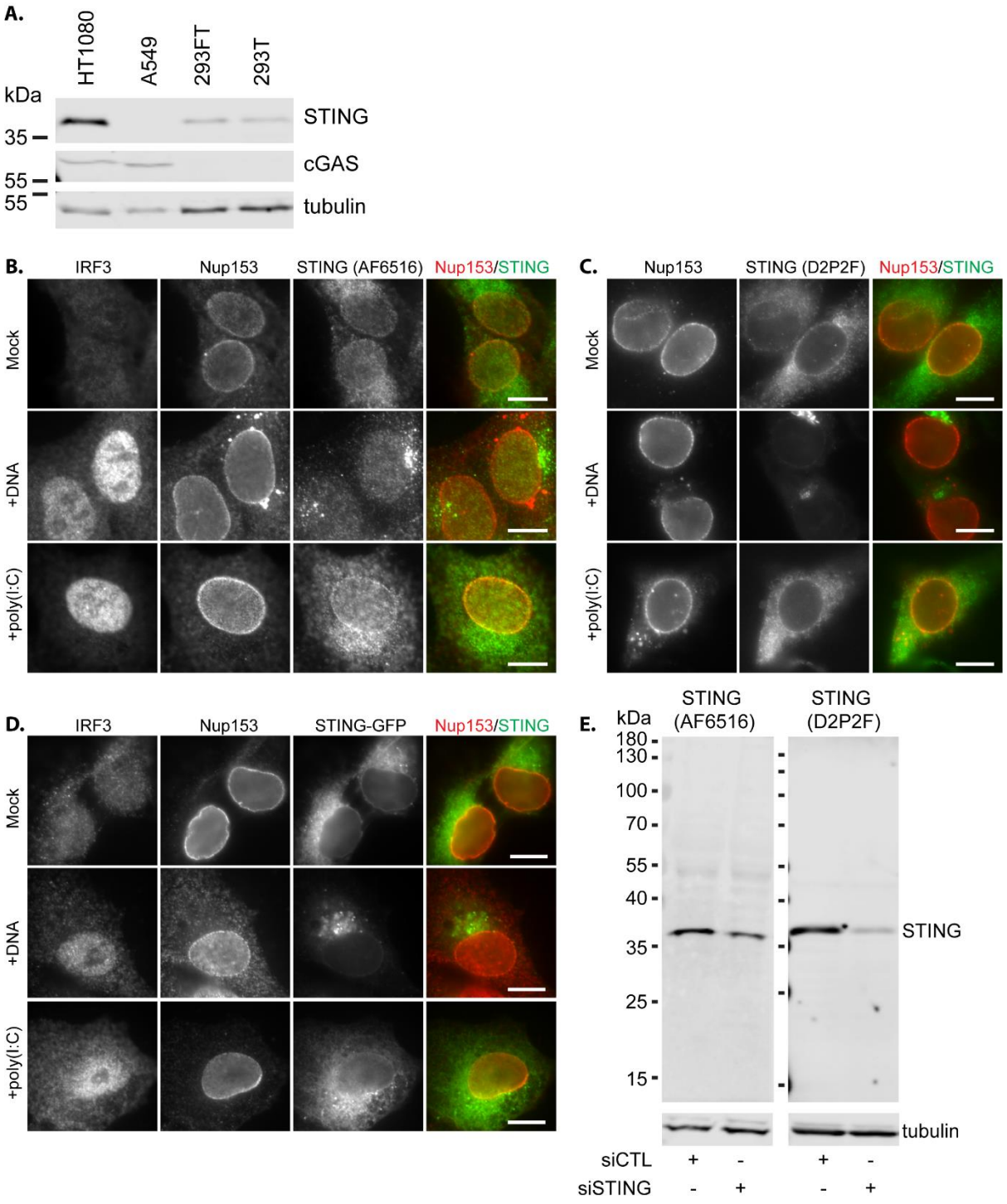

Figure 3.1 – HT1080 cells and STING-GFP inducible HT1080 cells are suitable for studying STING localisation in the nuclear envelope. (A) *HT1080 cells express detectable levels of STING and cGAS by western blot. A549 cells do not express detectable levels of STING while HEK293T and HEK293FT cells do not express detectable levels of cGAS and have lower levels of STING.* ***(B)*** *Immunofluorescence using STING antibody AF6516, compatible only with formaldehyde fixation, shows that STING redistributes to perinuclear foci 2 h post-transfection*

of plasmid DNA (dsDNA) but not dsRNA (poly(I:C)). IRF3 accumulates in the nucleus of cells stimulated by transfection of dsDNA or poly(I:C) indicating the initiation of an innate immune response. Co-staining with anti-Nup153 antibody highlights partial NE localisation of STING. ***(C)*** *Immunofluorescence using STING antibody D2P2F, compatible only with methanol fixation, confirms that STING redistributes to peri-nuclear foci 2 h post-transfection of dsDNA but not poly(I:C) and that a pool of STING is present in the NE, marked by Nup153 staining.* ***(D)*** *A doxycyline-inducible STING-GFP construct expressed in HT1080 cells behaves similarly to endogenous STING, accumulating in perinuclear foci after dsDNA stimulation and partially localising to the NE. dsDNA and RNA sensing pathways remain functional in this cell line as shown by the accumulation of IRF3 in the nucleus after dsDNA/poly(I:C) transfection.* ***(E)*** *Western blotting confirms that STING AF6516 and D2P2F antibodies are specific for STING, detecting a single band which is depleted by STING specific siRNAs. Scale bars = 10 µm.*

3.3 – Endogenous STING resists detergent extraction in HT1080 cells

Although previous evidence indicated that STING was present in the INM due to its ability to resist detergent extraction prior to fixation (Malik et al. 2010), these experiments were carried out using overexpression constructs of STING-RFP and Lamin A-GFP and so it is possible the overexpression or protein tagging affected STING's normal localisation in the NE. Therefore, the same detergent extraction assay was employed to test if endogenous STING also resisted detergent extraction and whether this was affected by immune stimulation. If STING is present in the INM and interacts with the nuclear lamina it should resist detergent extraction while if STING is present only in the ONM it should be removed by detergent extraction unless it interacts with detergent extraction resistant cytoskeletal components or nesprin proteins in the ONM which also resist detergent extraction. HT1080 cells were mock transfected of transfected with dsDNA or poly(I:C) in order to stimulate an innate immune response and after 2 h either fixed directly or first extracted with 0.1% Triton-X 100 detergent to remove cell membranes and then fixed. STING in the NE resisted detergent extraction as shown by the presence of a nuclear rim stain for STING and loss of STING ER staining in detergent extracted cells compared to directly fixed cells (Figure 3.2). In cells stimulated with dsDNA such NE staining was lost, as was expected given that STING accumulates in peri-nuclear foci after dsDNA stimulation. These foci also tended to resist detergent extraction likely as a consequence of a more stable STING structure formed by STING aggregation through side-to-side packing at these foci (Ergun et al. 2019; Shang et al. 2019). Finally, in cells stimulated with poly(I:C) STING NE staining was still detectable in detergent extracted cells, indicating that the nuclear pool persists during immune stimulation.

As a complementary approach to determining INM vs ONM localisation a digitonin permeabilization assay was considered. This assay takes advantage of the fact that digitonin preferentially permeabilises cholesterol-rich cell membranes such as the plasma membrane but not ER and NE membranes which contain little cholesterol and remain intact (Ginsbach and Fahimi 1987). Therefore, antibody labelling in digitonin permeabilised cells cannot access the nucleus so only protein residing in the ER and ONM will be stained (Adam et al. 1990). Conversely Triton-X 100 shows no such preference and permeabilises all cell membranes, thus antibody staining in Triton-X 100 permeabilised cells can label proteins in the INM as well as ER and ONM. By comparing antibody staining in fixed cells permeabilised with digitonin to fixed cells permeabilised with Triton-X 100 an increase staining in Triton-X 100 permeabilised cells implies a pool of protein in the INM. However, the STING (D2P2F) antibody used in the pre-fixation detergent extraction assay requires methanol fixation which disrupts cell membrane integrity. While this is fine if detergent permeabilization is performed before fixation such as in the pre-fixation detergent extraction assay this antibody could not be used with a digitonin permeabilization assay since this requires detergent permeabilization after fixation. The STING (AF6516) antibody which is compatible with formaldehyde fixed cells only could have been used in a digitonin permeabilization assay. However, since this antibody stained less strongly than the D2P2F antibody, I did not think it likely that a difference in antibody staining in digitonin or Triton-X 100 permeabilised cells would easily be discerned, and this assay was not performed.

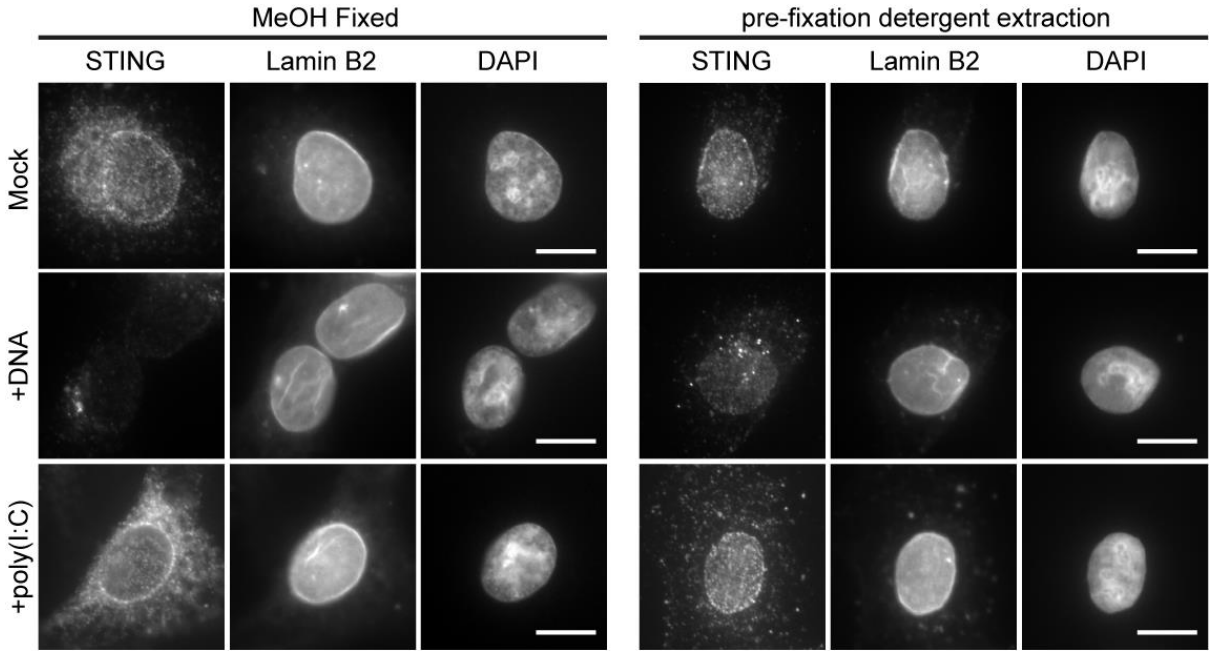

Figure 3.2 – STING at the NE resists detergent extraction. *Left panels, HT1080 cells fixed directly in methanol (MeOH fixed) show STING and Lamin B2 localisation by immunofluorescence in cells 2 h post mock, DNA, or poly(I:C) transfection. Right panels, HT1080 cells extracted with 0.1% Triton X-100 prior to methanol fixation show that STING at the NE resists detergent extraction similarly to Lamin B2. Scale bar = 10 µm.*

3.4 – Immunogold-EM of STING shows distribution at nuclear envelope in unstimulated and immune stimulated cells

Since all evidence of STING's presence in the INM up to this point has been indirect, electron microscopy (EM) coupled with immunogold labelling of endogenous STING was employed to directly determine STING localisation in the NE. Immunogold-EM is widely considered the gold-standard for determining localisation of a protein within the NE since the high resolution of EM allows for determination of protein residence in either INM or ONM. In immunogold-EM, cells are stained with primary antibody and a secondary antibody conjugated to a gold nanoparticle. Gold particle density is much greater than organic material and so gold particles appear as the strongest signal, a dark spot in electron micrographs. HT1080 cells were fixed directly in 4 % formaldehyde plus 0.05 % glutaraldehyde in 0.1 M PHEM buffer, to allow for preservation of cell membranes, before sectioning and labelling with anti-STING antibody (AF6516), followed by a secondary antibody conjugated to 6 nm gold particles. Example micrographs show labelling of endogenous STING close to both INM and ONM, as well as localising throughout the cytoplasm in close proximity to ER membranes as would be expected for STING localisation in resting cells (Figure 3.3 A, yellow arrows). Gold particles up to 50 nm away from the NE were counted since this distance accounts for the size of the C-terminus of STING (~4.3 nm) (Ouyang et al. 2012), antibody length (~16 nm x2)(Harris et al. 1997), and gold particle size (6 nm diameter). Immunogold labelling shows a 0.79:1 distribution of endogenous STING between ONM (122 particles) and INM (142 particles) (Figure 3.3 E). In addition to gold particles clearly associated with either INM or ONM a number of gold particles appeared either in transit through NPCs (18 particles) or to be in the lumen between INM and ONM (16 particles). Given that the C-terminus of STING, against which the anti-STING antibody is targeted, is cytoplasmic/nucleoplasmic such 'luminal' particles are likely either on the INM or ONM side of the NE but due to sectioning artefacts falsely appear to be luminal and so cannot be ascribed clearly to one or the other. Although labelling of endogenous STING for immunogold-EM was successful, particle counts were quite low indicating that either STING abundance is low in HT1080s or that epitopes were masked

by the fixation process. Indeed, immunofluorescence of cells fixed with glutaraldehyde and formaldehyde in parallel to those for immunogold EM shows variable staining against STING with some cells staining more strongly than others (Figure 3.3 B top panels). Staining using another antibody against STING (D2P2F) in HT1080 cells fixed with methanol suggests that this is likely due to an issue of epitope masking resulting from the extended fixation in formaldehyde and glutaraldehyde required for EM, since all cells fixed with methanol and stained with STING (D2P2F) show robust labelling (Figure 3.3 B bottom panels). Since particle counts for endogenous STING labelling were low, the distribution of STING in an inducible STING-GFP HT1080 cell line was also determined by immunogold EM. Example micrographs show that like endogenous STING, STING-GFP localises to both the INM and ONM as well as ER (Figure 3.3 C). Staining of samples prepared for immunogold-EM with gold-conjugated secondary antibodies only, yielded very few detectable gold particles, indicating that there is little background staining caused by the secondary antibodies (Figure 3.3 D). Intriguingly, STING-GFP accumulated more in the ONM than INM compared to endogenous STING with a ratio of roughly 1.46:1 (ONM:INM) (Figure 3.3 E); however, a much greater number of gold particles were classed as 'luminal' compared to the endogenous labelling which could also account for this difference. Regardless, it is clear that the presence of STING in the INM is not an artefact of overexpression since overexpression increases the ONM pool. Finally, I wanted to test whether STING distribution in the NE changed during an innate immune response. Therefore, samples fixed 2 h post-immune stimulation with transfected DNA were also analysed for distribution of STING-GFP in the NE. Despite a generally lower abundance of STING-GFP in the NE in DNA stimulated samples, likely due to translocation of STING to perinuclear foci (see Figure 3.1), the ratio of STING-GFP in the INM compared to the ONM was the same as in unstimulated cells (Figure 3.3 F). The overall drop in STING NE levels with DNA stimulation might indicate that NE localised STING (both INM and ONM) also functions in the innate immune response to cytosolic DNA since it must redistribute from the INM in the same proportion as STING in the ONM to maintain the ratio.

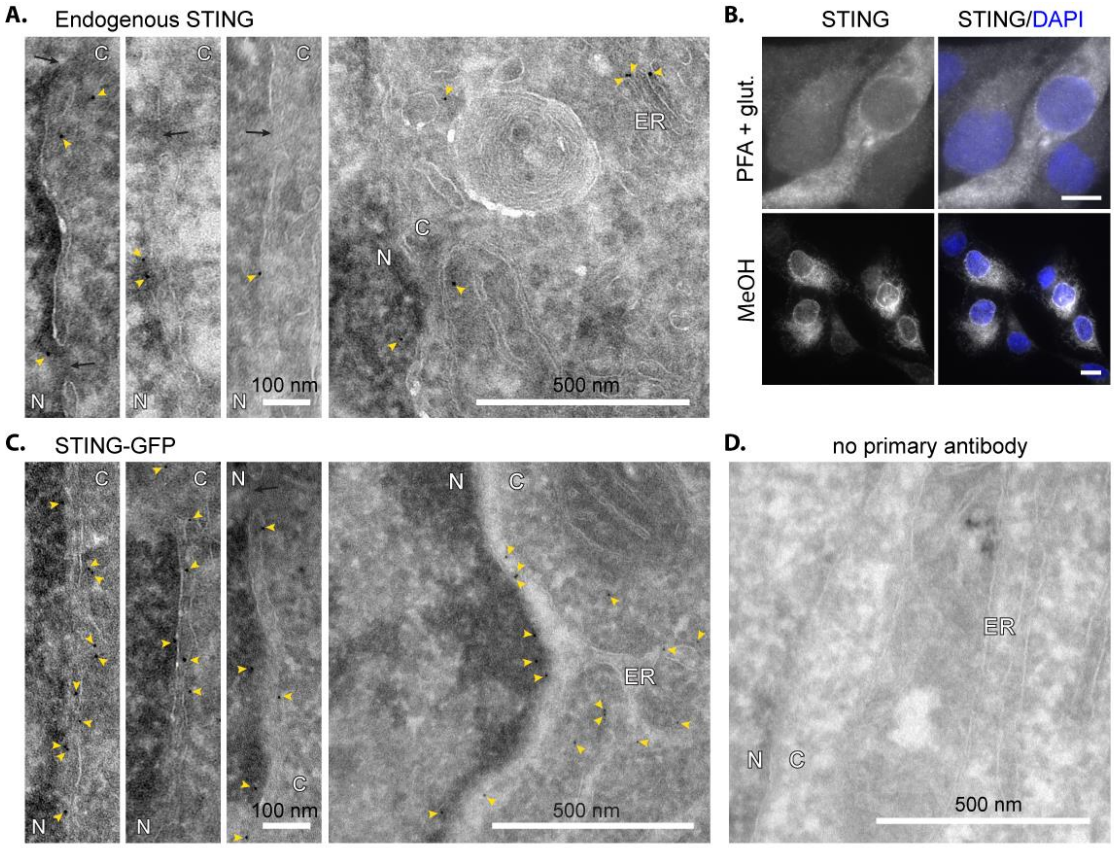

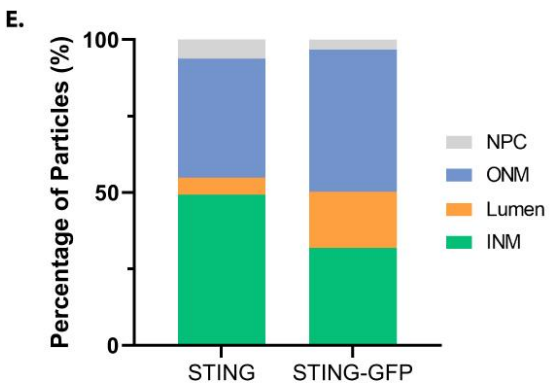

# Particles	INM	Lumen	ONM	NPC	Total
Endogenous STING	142	16	112	18	288
STING-GFP	232	134	338	24	728

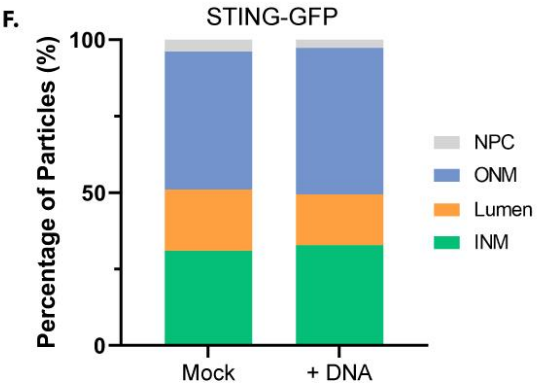

# Particles	INM	Lumen	ONM	NPC	Total
Mock	121	78	176	15	390
+ DNA	111	56	162	9	338

Figure 3.3 – STING is present in INM and ONM by immunogold-EM. (A) *Example micrographs of HT1080 cells stained with STING (AF6516) antibody and gold-conjugated secondary antibody show that endogenous STING localises to both inner and outer membranes of the nuclear envelope (NE), as well as to the endoplasmic reticulum (ER). Yellow arrows highlight gold particles corresponding to STING labelling. Black arrows indicate nuclear pore complexes (NPC). N = nucleus, C = cytoplasm.* ***(B)*** *Example images of immunofluorescence staining against STING on samples fixed in parallel to samples for EM (top panels, PFA + 0.05 % glutaraldehyde) or cells fixed with methanol and stained with STING (D2P2F) antibody. Scale bars = 10 µm.* ***(C)*** *Example micrographs of HT1080 cells expressing STING-GFP stained with anti-GFP antibody and gold-conjugated secondary antibody, show that STING-GFP localises to INM, ONM, and ER. N = nucleus, C = cytoplasm.* ***(D)*** *Example micrograph of cells prepared for*

immunogold-EM stained with only gold-conjugated secondary antibody. ***(E)*** *Quantification of gold particles within 50 nm of the NE from endogenous STING and STING-GFP samples, lumen particles in between INM and ONM, NPC particles in close proximity to nuclear pore.* ***(F)*** *Quantification of gold particles as in (E) but for STING-GFP samples that were mock stimulated or fixed 2 h after stimulation with DNA. Sectioning and immunogold labelling performed by Christine Richardson and image acquisition and analysis by me.*

3.5 – FRET with FLIM confirms that STING is in the INM but is inadequate to measure changes in STING distribution in response to immune stimulation

While the pre-fixation detergent extraction assay and immunogold-EM establish a pool of STING at the INM, the detergent extraction assay is not quantitative and with the immunogold-EM it is not practical to image enough cells to accurately establish the distribution of STING in the NE with various immune stimuli. Therefore, I proposed to use Förster-resonance energy transfer (FRET) with fluorescence lifetime imaging (FLIM) in order to track STING localisation at the NE during innate immune responses against different immune stimuli. FRET is a physical phenomenon in which an excited 'donor' fluorophore can transfer energy in a non-radiative fashion to a nearby 'acceptor' fluorophore resulting in the emission of energy (fluorescence) by the acceptor. FRET can occur provided the emission spectrum of the donor overlaps sufficiently with the excitation spectrum of the acceptor (>30%) and that the two proteins are within the 1-10 nM distance of each other required for FRET to occur and is characterised by the FRET efficiency (E) (Bajar et al. 2016). Given the requirement for fluorophores to be within 10 nM of each other for FRET to occur, FRET between two tagged proteins infers a protein-protein interaction. In FLIM-FRET, the fluorescence lifetime (τ), defined as the average time that a fluorophore remains in its excited state, is measured by detecting individual photons using a fast single-photon detector. Following excitation, a fluorophore will return to the ground state through both radiative (photon emission) and nonradiative decay. By measuring the τ of donor fluorophore alone (τ_D) or donor fluorophore in the presence of a suitable acceptor fluorophore (τ_{DA}), whether or not FRET occurs can be determined since donor emission will be quenched by FRET interaction decreasing the donor lifetime. The FRET E is described by the equation: $E = 1 - (\tau_{DA}/\tau_D)$(Bajar et al. 2016). FLIM yields images with pixel intensity values given by τ and so also gives information about where interactions occur.

I proposed that measuring FRET E could provide a measure of changes in INM/ONM distribution of STING by using HEK293T cells transiently co-transfected with an acceptor

STING-RFP construct and Lamin A-GFP donor construct. Since STING does not target to the NE in cells lacking Lamin A (Malik et al. 2010), and resists detergent extraction indicating an interaction with the nuclear lamina, and is in close proximity to the INM by immunogold-EM, I reasoned it likely that STING interacts with Lamin A and that FRET between them would be possible. If STING is in the ONM and unable to interact with Lamin A then no FRET should occur and the fluorescence lifetime of excited GFP molecules should be unaffected (Figure 3.4 A1), on the other hand if STING is in the INM it should be close enough to Lamin A-GFP for it to transfer energy to the STING-RFP, thus reducing the fluorescence lifetime of GFP (Figure 3.4 A2). Lamin A-GFP and STING-RFP were confirmed to localise to the NE and ER/NE respectively (Figure 3.4 B) and fluorescence lifetimes were measured for Lamin A-GFP alone, Lamin A-GFP in the presence of STING-RFP, and for a tandem GFP-RFP construct (positive control). Example images of GFP donor construct localisation, regions of interest (ROI) used for measurement of fluorescence lifetime values, and fluorescent lifetime intensity values are shown (Figure 3.4 C) and the average fluorescence lifetime values for each cell are plotted (Figure 3.4 D) showing a significant reduction in mean fluorescence lifetime for both GFP-RFP tandem construct and Lamin A-GFP in the presence of STING-RFP compared to Lamin A-GFP alone. A mean fluorescence lifetime of 2.281 ns for Lamin A-GFP fits well within the range of fluorescence lifetimes reported for GFP expressed alone in HeLa cells of between 2.2 and 2.4 ns at pH values ranging between 6.5 and 7.5 (Nakabayashi et al. 2008). Mean FRET E for the GFP-RFP tandem construct is 0.141 (E = 1 - (1959/2281)) and for Lamin A-GFP + STING-RFP is 0.061 (E = 1 - (2142/2281)) or 14.1 % and 6.1 % respectively. Using the reported Förster radius (r_0), which is the distance at which 50 % FRET occurs, for an EGFP-mCherry pair of 5.4 nm the distance between the GFP and RFP can be calculated using the following equation(Bajar et al. 2016):

$$\text{Distance (r)} = r_0 \sqrt[6]{\frac{1-E}{E}}$$

which gives a mean distance of 7.3 nm and 8.5 nm between the GFP and RFP fluorophores of the GFP-RFP tandem sample and Lamin A-GFP + STING-RFP sample, respectively.

Having confirmed that STING-RFP is in close enough proximity to Lamin A-GFP for FRET to occur, confirming localisation of STING-RFP to the INM, I next wanted to test whether the fluorescence lifetime of Lamin A-GFP in the presence of STING-RFP was affected by the

induction of an innate immune response to dsDNA or poly(I:C), as a proxy for STING-RFP localisation in the NE. HEK293T cells were chosen specifically for this assay since they do not express detectable levels of cGAS (Figure 3.1) and are thus defective in sensing cytoplasmic dsDNA. Therefore, plasmid DNA could be transiently transfected into HEK293T cells without initiating an innate immune response. After expression of STING-RFP, an innate immune response could then be induced by transfecting cGAMP to activate STING and subsequent downstream signalling or by transfecting poly(I:C) to induce an immune response to dsRNA. cGAMP transfection was confirmed to activate endogenous STING in HT1080 cells, as shown by the redistribution of STING to perinuclear foci and the accumulation of IRF3 in the nucleus of cells transfected with cGAMP (Figure 3.4 E). However, STING-RFP did not accumulate in perinuclear foci following stimulation with cGAMP (Figure 3.4 F) and so this assay was not pursued further.

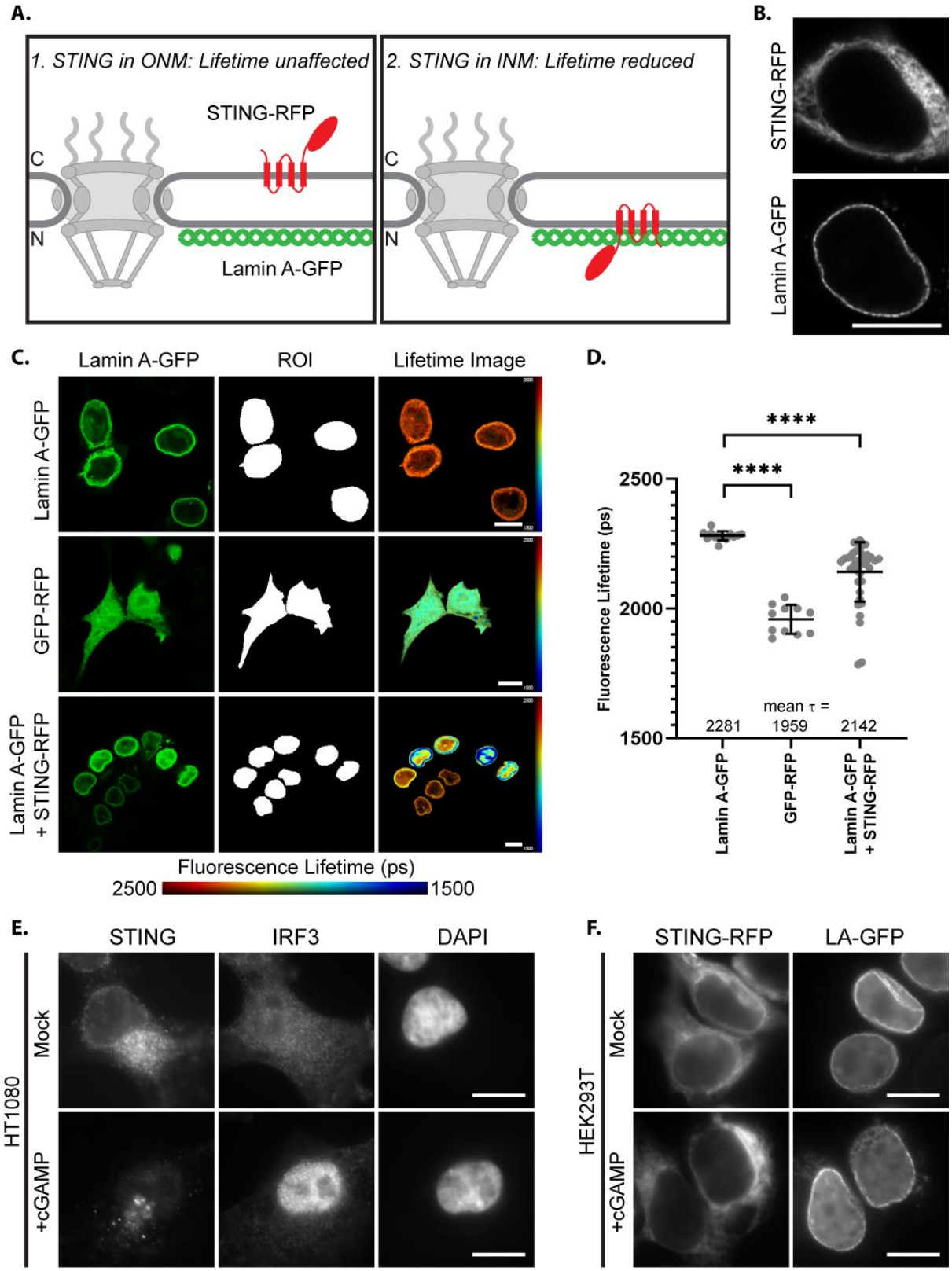

Figure 3.4 – FLIM-FRET shows STING-RFP interacts with Lamin A-GFP. (A) *Schematic showing (1) effect on Lamin A-GFP fluorescence lifetime if STING-RFP is only present in the outer nuclear membrane (ONM), or (2) reduction of fluorescence lifetime if STING-RFP is present in the inner nuclear membrane (INM) and interacts with Lamin A-GFP.* ***(B)*** *Targeting of STING-RFP and Lamin A-GFP in HEK293T cells.* ***(C)*** *Example micrographs of HEK293T cells transfected with*

Lamin A-GFP (negative control), GFP-RFP (positive control), and Lamin A-GFP + STING-RFP constructs used for FLIM-FRET measurements. Left panels = confocal image of donor localisation, middle panels = region of interest (ROI) for FLIM measurements, right panels = fluorescence lifetime intensity image, heatmap: red (high) – blue (low) fluorescence lifetime. ***(D)*** *Mean fluorescence lifetimes (τ) values generated from ROIs (whole nucleus for Lamin A-GFP, whole cell for GFP-RFP), each point is a single ROI. Ordinary one-way ANOVA with Dunnett's multiple comparison test, **** $p \leq 0.0001$. Error bars show standard deviation.* ***(E)*** *Transfection of cGAMP activates STING in HT1080 cells, causing STING to redistribute to perinuclear foci and IRF3 to accumulate in the nucleus.* ***(F)*** *cGAMP transfection in HEK293T cells does not result in STING-RFP accumulation in perinuclear foci. Scale bars = 10 µm.*

3.6 - smFRAP microscopy shows that STING redistributes from INM to ONM upon immune stimulation by DNA or poly(I:C)

As an alternative approach to measure STING distribution in the NE following immune stimulation, a fluorescence recovery after photobleaching (FRAP) assay was employed. A specialised form of FRAP which can track single molecules (smFRAP) and determine the distribution of nuclear envelope transmembrane proteins in the NE (INM vs ONM) was recently developed by the Yang Lab (Mudumbi et al. 2016). In smFRAP a single point of 0.5 µm diameter on the nuclear envelope is photobleached to ablate GFP fluorescence of a GFP-tagged nuclear envelope transmembrane (NET) protein of interest. Individual GFP-NETs that diffuse into this area from outside the photobleached region are then tracked using a regulated on-off laser excitation. By tracking hundreds of FRAP events the distribution of GFP-NET between INM and ONM can then be determined (Mudumbi et al. 2016). In collaboration with a student in the Yang lab, Mark Tingey, this technique was employed to measure the distribution of STING-GFP in our inducible STING-GFP HT1080 cell line in mock, poly(I:C), and dsDNA stimulated cells (Figure 3.5 A). The ratio of STING-GFP in the ONM:INM was found to be 1.39:1 in mock stimulated cells (Figure 3.5 A and C) which very closely matches the ONM:INM ratio of STING-GFP in mock stimulated cells determined by immunogold-EM (Figure 3.3 F) of 1.45:1 (176:121 particles). Post-stimulation with poly(I:C) or dsDNA, there is a significant increase in the ONM:INM ratio of STING-GFP, 4.44:1 and 4.07:1 respectively (Figure 3.5 A). Given that STING is known to redistribute from the ER and accumulate in perinuclear foci post-DNA stimulation the increased ONM:INM ratio after dsDNA transfection is unsurprising and likely reflects a redistribution of STING from the INM to the ONM and subsequent loss of STING from the ONM as it translocates out of the ER (Figure 3.5 D). Indeed, there is also a significant increase in the diffusion coefficient for STING-GFP in cells stimulated with DNA compared to mock stimulated cells, which means there is an increase in mobility of

STING-GFP in the NE (Figure 3.5 B and C). More surprising is the increased ONM:INM ratio for STING-GFP in cells stimulated with poly(I:C) because no changes in STING distribution are seen by conventional fluorescence microscopy in cells stimulated with poly(I:C) (see (Franz et al. 2018) and Figure 3.1). STING-GFP mobility in the NE also increased after immune stimulation with poly(I:C) as seen by the increased diffusion coefficient (Figure 3.5 B and C). Since there is no apparent loss of STING at the NE in cells stimulated with poly(I:C) by immunofluorescence this increased ONM:INM ratio and mobility is interpreted as a redistribution of STING-GFP from the INM to the ONM (Figure 3.5 D).

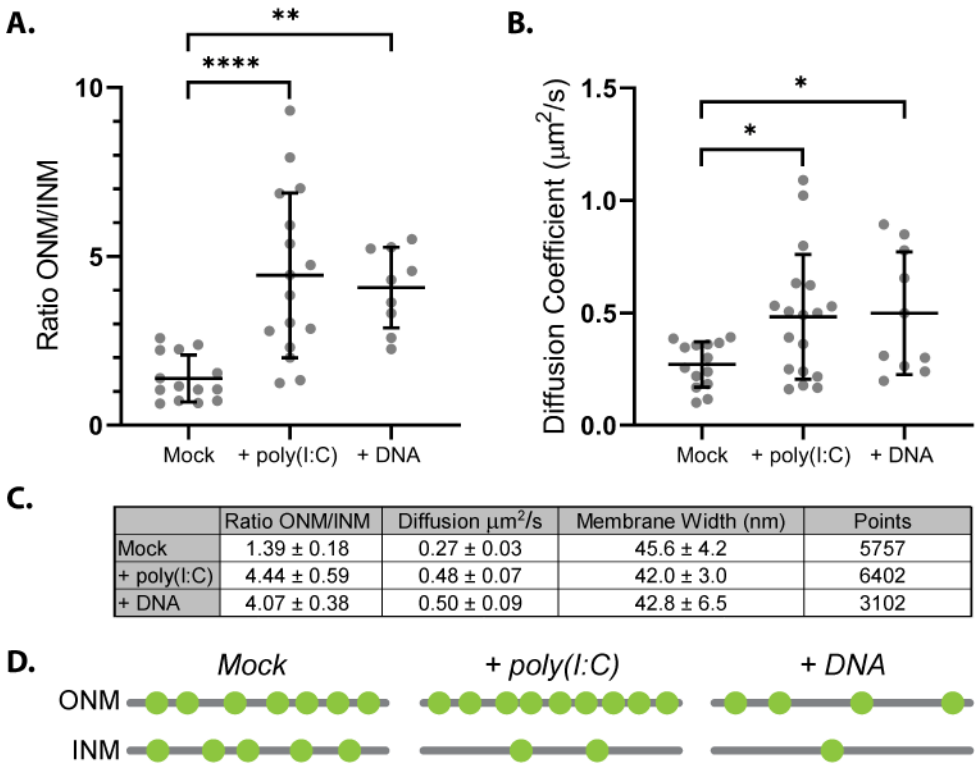

C.

	Ratio ONM/INM	Diffusion µm²/s	Membrane Width (nm)	Points
Mock	1.39 ± 0.18	0.27 ± 0.03	45.6 ± 4.2	5757
+ poly(I:C)	4.44 ± 0.59	0.48 ± 0.07	42.0 ± 3.0	6402
+ DNA	4.07 ± 0.38	0.50 ± 0.09	42.8 ± 6.5	3102

Figure 3.5 – smFRAP shows STING-GFP redistributes from inner (INM) to outer nuclear membrane (ONM) during innate immune stimulation with DNA or poly(I:C). (A) *ONM:INM ratio of STING-GFP in the nuclear envelope in cells 2 h after mock, poly(I:C), or dsDNA transfection. Each point represents the distribution at a single point in a cell with hundreds of individual STING-GFP molecules measured to determine ONM:INM distribution. Ordinary one-way ANOVA with Dunnett's multiple comparison test, **** $p \leq 0.0001$, ** $p \leq 0.01$. Mean ratio value shown by line, error bars show standard deviation.* ***(B)*** *Mobility of STING-GFP in nuclear envelope of the same samples and measurement points from (A). Ordinary one-way ANOVA with Dunnett's multiple comparison test, * $p \leq 0.05$. Mean diffusion coefficient shown by line, error bars show standard deviation.* ***(C)*** *Summary of data plotted in (A) and (B), mean values +/- standard error. Distance between INM and ONM (membrane width) based on individual STING-GFP molecules measured and number of STING-GFP molecules (points) measured is also given.* ***(D)*** *Schematic showing interpretation of distribution of STING-GFP molecules*

(green spots) in the nuclear envelopes of conditions tested. smFRAP microscopy performed by Mark Tingey (Weidong Yang, Temple University), graphing and statistical analysis by me.

3.7 – Chapter Summary

In this chapter I have shown that HT1080 cells retain a functional cGAS-STING cytoplasmic dsDNA sensing pathway and that both these and HT1080 cells stably expressing an inducible STING-GFP construct are suitable for studying STING localisation in unstimulated and DNA/polyI:C stimulated cells. Using immunogold-EM, I have shown that STING is present in both the inner and outer membranes of the NE with an ONM:INM ratio of 0.79:1 for endogenous STING in unstimulated cells, a result supported by the finding that endogenous STING in the NE resists detergent extraction. Moreover, I have shown that STING-GFP similarly targets to INM and ONM by immunogold-EM and that STING-RFP is able to FRET with Lamin A-GFP when co-expressed in HEK293T cells, confirming Lamin A as a STING interaction partner identified in a previous co-immunoprecipitation experiment coupled with mass spectrometry. Although, this FLIM-FRET set-up proved not to be suitable for measuring STING redistribution during an immune response, a separate microscopy technique, smFRAP, showed that in response to DNA and RNA stimuli STING-GFP redistributes from the INM to ONM. That STING redistributes from INM to ONM in response to immune stimulate with poly(I:C) is a surprising finding given that STING shows no general change in localisation following poly(I:C) stimulation by conventional immunofluorescence microscopy. Given that STING has been shown to restrict multiple RNA viruses (Ishikawa and Barber 2008; Zhong et al. 2008; Ishikawa et al. 2009; Maringer and Fernandez-Sesma 2014; Ran et al. 2014) and to inhibit cellular translation in response to VSV infection or poly(I:C) transfection (Franz et al. 2018) this finding could provide insight about the mechanism through which STING exerts these effects.

One of the outstanding questions raised by these experiments is how does STING in the INM respond to cytoplasmic immune stimuli? In the case of dsDNA immune stimulation, it is likely that cGAMP produced by cGAS upon dsDNA binding in the cytoplasm, can freely diffuse through the NPC due to its small size and bind to STING located at the INM. In the case of poly(I:C) which is a dsRNA-like complex consisting of synthetic polymers of a range of lengths, how the sensing of the poly(I:C) stimulus results in a redistribution of STING from the INM is unknown. STING does not bind directly to poly(I:C) *in vitro* (Abe et al. 2013), nor does it dimerise and undergo translocation to perinuclear foci after poly(I:C) stimulation (Franz et al. 2018). Transfection of poly(I:C) stimulates multiple dsRNA sensing pathways because it

delivers poly(I:C) into the endosomal compartments where it is sensed by TLR3 and eventually cytoplasm where it is sensed by RIG-I and MDA-5 cytoplasmic dsRNA sensors(Palchetti et al. 2015). How this sensing can then be transferred to STING is not clear, however, STING interacts with the RIG-I and the downstream adaptor protein MAVS, and STING interaction with RIG-I increases with RNA virus infection (Ishikawa and Barber 2008; Zhong et al. 2008). Since MAVS is localised to the mitochondria, a separate cellular pool of STING located at the mitochondria or mitochondria-associated ER membranes could be involved in sensing poly(I:C) in the cytoplasm (Zhong et al. 2008; Ishikawa et al. 2009; Ran et al. 2014). How such sensing is propagated to STING at the INM, however, is not obvious. Interestingly, sensing of poly(I:C) by TLR-3 in endosomal compartments has been shown to stimulate apoptosis while binding of poly(I:C) by RIG-I and MDA-5 triggers IRF3-mediated signalling and upregulation of IFNβ. It is possible that activation of one or both of these signalling pathways activate STING at the INM resulting in a redistribution to the ONM. Future experiments should look at whether poly(I:C) mediated redistribution of STING at the NE requires TLR3, RIG-I, and MDA-5 dsRNA sensors as well as TRIF and MAVS adaptor proteins. Another important question raised is how is STING retained at the INM? One of the mechanisms thought to retain NET proteins at the INM is binding to the nuclear lamina or chromatin proteins such as LBR binding to HP1 or LEM-domain proteins binding to BAF (Burke and Stewart 2013). Whether STING is retained in the INM by direct interaction with a specific nuclear localised partner should be investigated further. STING targeting to the NE was lost in *LMNA*$^{-/-}$ MEFs (Malik et al. 2010) and in my experiments STING-RFP was able to FRET with Lamin A-GFP suggesting an interaction with Lamin A. Whether STING also forms interactions with specific chromatin proteins such as BAF or HP1 and the nature of the STING-Lamin A interaction should be investigated, for example by investigating STING NE localisation in Lamin A mutant cell lines. Additionally, STING mutants could be tested for NE targeting.

While immunogold EM shows unequivocally that endogenous STING is present in the INM and ONM of HT1080 cells, this data could be strengthened by looking at STING NE localisation in additional cell lines such as the monocytic THP-1 cell line which has been shown to have high levels of STING expression (Sun et al. 2009). Finally, the use of a CRISPR/Cas9 engineered HT1080 cell line in which STING is tagged with GFP could be used to confirm smFRAP results which used an inducible STING-GFP HT1080 cell line.

Chapter 4

Nuclear Envelope STING partners function in innate immune responses

4.1 – Introduction

Having confirmed that STING is present in both inner and outer nuclear membranes in the previous chapter, I next set out to test whether putative NE partners of STING that were identified previously in a reversible crosslinking proteomics study in the Schirmer lab (Figure 1.6 and Figure 4.1 A) and found to have known indirect links to IRF3/7 transcription factors, could be involved in innate immune responses (IIR). Whether these proteins are directly or indirectly interacting with STING cannot be stated for certain since crosslinking and immunoprecipitation will preserve both direct and indirect interactions. All of these proteins referred to from now on as 'NE STING partners' are known RNA or DNA binding proteins, which prompted the hypothesis that they could function as direct sensors of pathogen RNA or DNA in the nucleus and form part of a signalling network with STING at the NE. Interestingly, many of these partners have only been reported to bind RNA, which suggests that they could support a mechanism for STING in mediating IIR against RNA ligands. This finding is particularly provocative considering that STING functions in the restriction of RNA viruses (Ishikawa and Barber 2008; Zhong et al. 2008; Ishikawa et al. 2009; Maringer and Fernandez-Sesma 2014; Ran et al. 2014) and is targeted during RNA virus infection (Ishikawa et al. 2009; Sun et al. 2012; Yu et al. 2012; Aguirre et al. 2012; Ding et al. 2013; Nitta et al. 2013; Xing et al. 2013; Chen et al. 2014; Yi et al. 2015; Holm et al. 2016; Ding et al. 2018), but the exact mechanisms through which STING antagonises RNA viruses remain to be elucidated (Holm et al. 2016; Franz et al. 2018). Therefore, it was hypothesised that ***RNA-binding partners of STING in the NE may provide a mechanism through which STING antagonises RNA viruses.*** For example, by recognising viral RNA and subsequently activating STING. Similarly, ***DNA-binding partners of STING in the NE could have a role in STING mediated immune signalling stimulated by dsDNA ligands or infection with DNA viruses.***

Since the majority of the NE STING partner proteins are encoded by essential genes, according to a CRISPR mediated knockout screen to characterise essential genes in the human genome (Wang et al. 2015) (Figure 4.1 B), siRNA knockdown was proposed in order to screen partner

proteins for a role in IIR since short-term knockdown of a protein is likely to be less lethal than a knockout and generation of knockout cell lines would not be possible for essential genes. In order to prioritise the list of partners to test, a literature search was conducted to see if any of the proteins had previously been reported to be involved in immune responses. KPNB1 and KPNA2 were not chosen since they encode Importin β1 and Importin α2 respectively, which are required for transport of proteins containing a nuclear localisation signal (NLS) (Grossman et al. 2012), such as IRF3/7 (Kumar et al. 2000; Zhu et al. 2015), and so their knockdown would impair the type-I IFN response indirectly. Meanwhile, several of the NE STING partners appeared to be particularly promising candidates because they were already reported to have some function relating to viral infection or host cell immune responses. The involvement of several of these proteins in viral infection or immune responses is described below. SYNCRIP, also known as hnRNP Q, has been shown to facilitate hepatitis C virus (HCV) replication and associate with viral RNA(Kim et al. 2004; Liu et al. 2009), as well as being involved in the replication of the coronavirus, murine hepatitis virus (MHV) (Choi et al. 2004). SYNCRIP is also a member of the GAIT complex which is involved in transcript-specific translational inhibition in myeloid cells stimulated with IFNγ (Mukhopadhyay et al. 2009; Arif et al. 2012; Arif et al. 2018). Menin/MEN1, the protein encoded by the *MEN1* gene, is a tumour suppressor and regulates multiple signalling pathways including inhibiting the activity of NF-κB (Heppner et al. 2001) and AP1 (JunD) transcription factors (Agarwal et al. 1999). It has also been found to play a role in maintaining T cell function (Suzuki et al. 2018) and regulating the immune response of $CD8^+$ T cells to infection(Yamada et al. 2016). DDX5 is a DEAD-box RNA helicase and a positive regulator of the replication of multiple RNA viruses including HCV, Japanese encephalitis virus (JEV) and human immunodeficiency virus 1 (HIV-1) (Goh et al. 2004; Li et al. 2013a; Zhou et al. 2013; Cheng et al. 2018). Conversely, DDX5 appears to be a negative regulator of DNA viruses and restricts Myxoma virus (MYXV) replication in human cell lines (Rahman et al. 2017), as well as Hepatitis B virus (HBV) replication in human cancer cells (HeLa and A549) (Zhang et al. 2016). RPS27A expression increases significantly during HBV infection potentially suggesting a role in IIR (Fatima et al. 2012). TCERG1 facilitates HIV-1 transcription and viral replication (Coiras et al. 2013). AATF, also known as CHE-1, is a central regulator of p53 in the DNA damage response where it prevents p53-mediated apoptosis (Bruno et al. 2006; Iezzi and Fanciulli 2015; Welcker et al. 2018).

A.

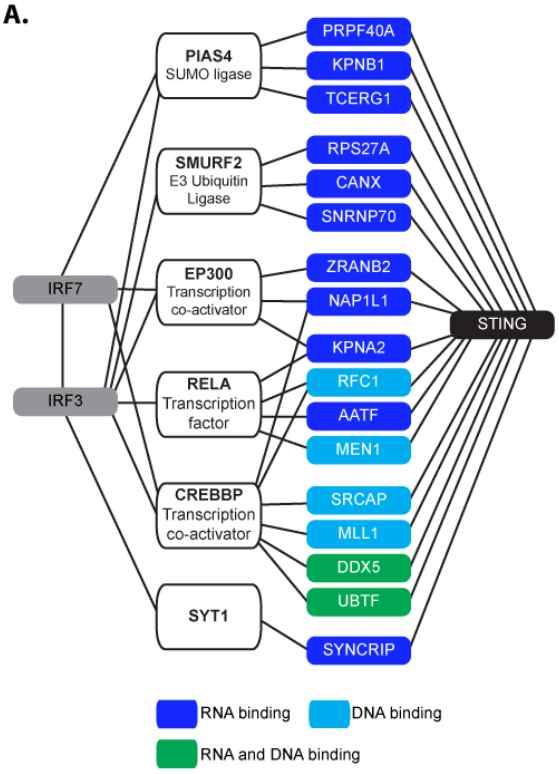

B.

GENE	PROTEIN	CS score	ESSENTIAL
KPNB1	Importin β	-2.842	Y
RPS27A	Ubiquitin-40S ribosomal protein 27a	-2.337	Y
RFC1	Replication factor C subunit 1	-2.237	Y
MLL1	MLL1/KMT2A	-1.584	Y
SRCAP	Helicase SRCAP	-1.554	Y
SNRNP70	snRNP70	-1.385	Y
UBTF	Nucleolar transcription factor 1	-1.351	Y
AATF	AATF	-1.343	Y
MEN1	Menin	-1.193	Y
DDX5	DEAD box protein 5	-0.643	N
KPNA2	Importin α	-0.625	N
PRPF40A	Pre-mRNA-processing factor 40 homolog A	-0.555	N
TCERG1	Transcription elongation regulator 1	-0.475	N
SYNCRIP	Syncrip/hnRNP Q	-0.426	N
CANX	Calnexin	-0.282	N
NAP1L1	Nucleosome assembly protein 1-like 1	-0.179	N
ZRANB2	Zinc finger Ran-binding domain-containing protein 2	-0.132	N

GENE	PROTEIN	CS score	ESSENTIAL
CREBBP	CREB-binding protein	-2.13	Y
EP300	Histone acetyltransferase p300	-1.151	Y
RELA	NFκB subunit p65	-0.418	N
PIAS4	PIAS4	-0.353	N
SMURF2	SMURF2	0.022	N
SYT1	Synaptotagmin-1	0.025	N

**Essential according to Wang et al,. 2015 CRISPR screen*

Figure 4.1 – STING nuclear envelope partners with connections to IRF3/7 transcription factors. (A) *Network of interactions between STING nuclear envelope partners identified by mass spectrometry (blue) and known IRF3/7 interactors (white) according to the Human Protein Reference Database. Partner proteins reported to bind RNA only (dark blue), DNA only (light blue), or RNA and DNA (green).* ***(B)*** *STING interactors and IRF3/7 interactors ranked as essential genes (Y – yes or N – no) according to a CRISPR knockout screen of the human genome*(Wang et al. 2015).

In this chapter I describe several assays I have used to test whether the novel STING partners identified by coimmunoprecipitation of cross-linked material from isolated NEs, with an indirect link to IRF3/7 transcription factors, contribute to dsDNA and dsRNA triggered immune responses. I also describe whether their knockdown has an impact on proliferation of the DNA virus, herpes simplex virus 1 (HSV-1). Next, I will show co-immunoprecipitation experiments and proximity ligation assays using endogenous proteins in order to confirm STING-partner interactions. Finally, I present data to show that some of these partner proteins, found to contribute to dsDNA/dsRNA triggered IIR, change localisation in response to immune stimulation similarly to the behaviour shown for STING in the previous chapter.

4.2 – Knockdown of some NE-STING partners inhibits IFNβ promoter and NF-κB driven luciferase reporter activation

Since interactome data from the HPRD showed an indirect link between STING partners and IRF3/7 transcription factors, I hypothesised that these partners could, as a result of being RNA

and/or DNA binding proteins, through an interaction with STING activate IRF3/7 to stimulate interferon production and activate IIR. Therefore, I screened several STING partners for a role in activating an IFNβ promoter driven luciferase reporter or an NF-κB/AP1 transcription factor activated luciferase reporter. The induction of IFNβ is one of the primary responses fibroblast cells have in response to cytosolic dsDNA/dsRNA detection, with secreted IFNβ signalling in an autocrine and paracrine manner resulting in the upregulation of antiviral genes. The IFNβ promoter requires the cooperative assembly of IRF3/7, NF-κB, and AP1 transcription factors for gene expression to be induced (Honda et al. 2006). The NF-κB luciferase reporter meanwhile consists of the chicken ovotransferrin gene minimal promoter downstream of κB sites which can be bound and activated by either NF-κB or AP1 transcription factor binding. HEK293FT cells, which lack a functional cGAS-STING response to cytosolic dsDNA due to undetectable levels of cGAS expression and low levels of STING expression (Zhang et al. 2013; Malik et al. 2014) (Figure 3.1 A), were used in this assay so that only cells co-transfected with cGAS and STING plasmids have a functional cGAS-STING pathway.

In this assay cells are transfected with either a luciferase reporter construct consisting of the *Phonitus pyralis* luciferase gene under the control of the IFNβ promoter or a promoter activated by NF-κB/AP1 transcription factor binding, as well as plasmids for cGAS and STING expression. The expression of cGAS and STING reconstitutes the innate immune signalling pathway against cytosolic dsDNA, resulting in an immune response induced by the same plasmids used for protein expression, and the activation of luciferase reporters. Co-transfection of a *Renilla reniformis* luciferase reporter under the control of the HSV-thymidine kinase promoter, which provides constitutive weak expression, allows for normalisation of *P. pyralis* luciferase signal to *R. reniformis* luciferase signal and controls for reporter plasmid transfection efficiency (Figure 4.2 A). The fold induction of the firefly luciferase reporter in cells transfected with STING and cGAS plasmids compared to control cells transfected with empty vector DNA instead of STING and cGAS and so lacking a functional cGAS-STING pathway for IIR against cytosolic dsDNA is then calculated. Thus, the assay system also effectively tests the STING dependence of the effects of its partners as luciferase levels in the absence of transfected cGAS-STING are also measured as a control.

Prior to transfection of luciferase assay plasmids, cells were treated with siRNAs against the STING partners. Knockdowns were confirmed by Western blotting with treatment resulting in

robust knockdown of most partners (Figure 4.2 B). Several of the antibodies recognised multiple bands on the Western blots. SYNCRIP has multiple isoforms in mammalian cells (Liu et al. 2009; Vu et al. 2017) (UniProtKB, O60506 human SYNCRIP/hnRNP Q) and immunoblotting against SYNCRIP in HEK293FT cell lysates identified multiple distinct bands. The predicted molecular weights of the most abundant SYNCRIP isoforms are 69 kDa (Q3), 65 kDa (Q2), and 62 kDa (Q1) and siRNA treatment mostly reduced the abundance of the lowest molecular weight band detected. The highest molecular weight band detected is likely the closely related protein, hnRNP R, which shares considerable homology (81.2 %) with SYNCRIP, and the antibody used for detection of SYNCRIP is also known to detect hnRNP R (detected as ~80 kDa band) (Mizutani et al. 2000; Mourelatos et al. 2001; Choi et al. 2004; Vu et al. 2017; Cappelli et al. 2018). The middle band is likely isoforms Q3 and Q2, while the lower band isoform Q1. Two bands were detected for MEN1, the major isoform of which is 68 kDa (UniProtKB, O00255 human MEN1), and both were depleted by siRNA treatment. A single band was detected for DDX5 at the expected molecular weight of ~60 kDa (UniProtKB, P17844 human DDX5), and was significantly depleted by siRNA treatment. Blotting against SNRNP70 detected two major bands, the larger of which likely corresponds to the biggest isoform of SNRNP70 (predicted molecular weight ~52 kDa, UniProtKB, P08621 human SNRNP70) since this was depleted by siRNA treatment. Immunoblotting against RPS27A detected a single band at the predicted molecular weight of ~18 kDa (UniProtKB – P62979 human RPS27A) which was successfully depleted by siRNA treatment. Two bands were detected when staining for AATF, the lower band of which matches the predicted molecular weight of ~63 kDa (UniProtKB – Q9NY61 human AATF): both bands showed a partial depletion with siRNA treatment.

In agreement with previous reports (Ishikawa and Barber 2008; Zhong et al. 2008; Fang et al. 2017), cGAS and STING expression resulted in robust activation of the IFNβ luciferase reporter and comparatively weaker activation of the NF-κB luciferase reporter, ~60-fold and ~35-fold respectively in control siRNA treated cells. siRNA mediated knockdowns of MEN1, DDX5, SNRNP70, or RPS27A were found to significantly reduce IFNβ promoter driven luciferase expression compared to siRNA control treated cells (siCTL), indicating that these proteins may contribute to induction of IFNβ following immune stimulation by cytoplasmic dsDNA (Figure 4.2 C). Knockdown of the same proteins was also tested for an effect on induction of a

luciferase reporter activated by binding of NF-κB. In addition to knockdown of MEN1, DDX5, SNRNP70, and RPS27A, siRNA mediated knockdown of SYNCRIP and AATF was found to significantly reduce NF-κB activated reporter induction compared to siCTL treated cells (Figure 4.2 D). This suggests that these proteins might affect different aspects of immune signalling cascades with SYNCRIP and AATF exerting a greater effect on the NF-κB and AP1 signalling pathways than on the IRF3/7 signalling pathway. Knockdown of TCERG1 did not have a significant effect on activation of either luciferase reporters and so was not investigated further.

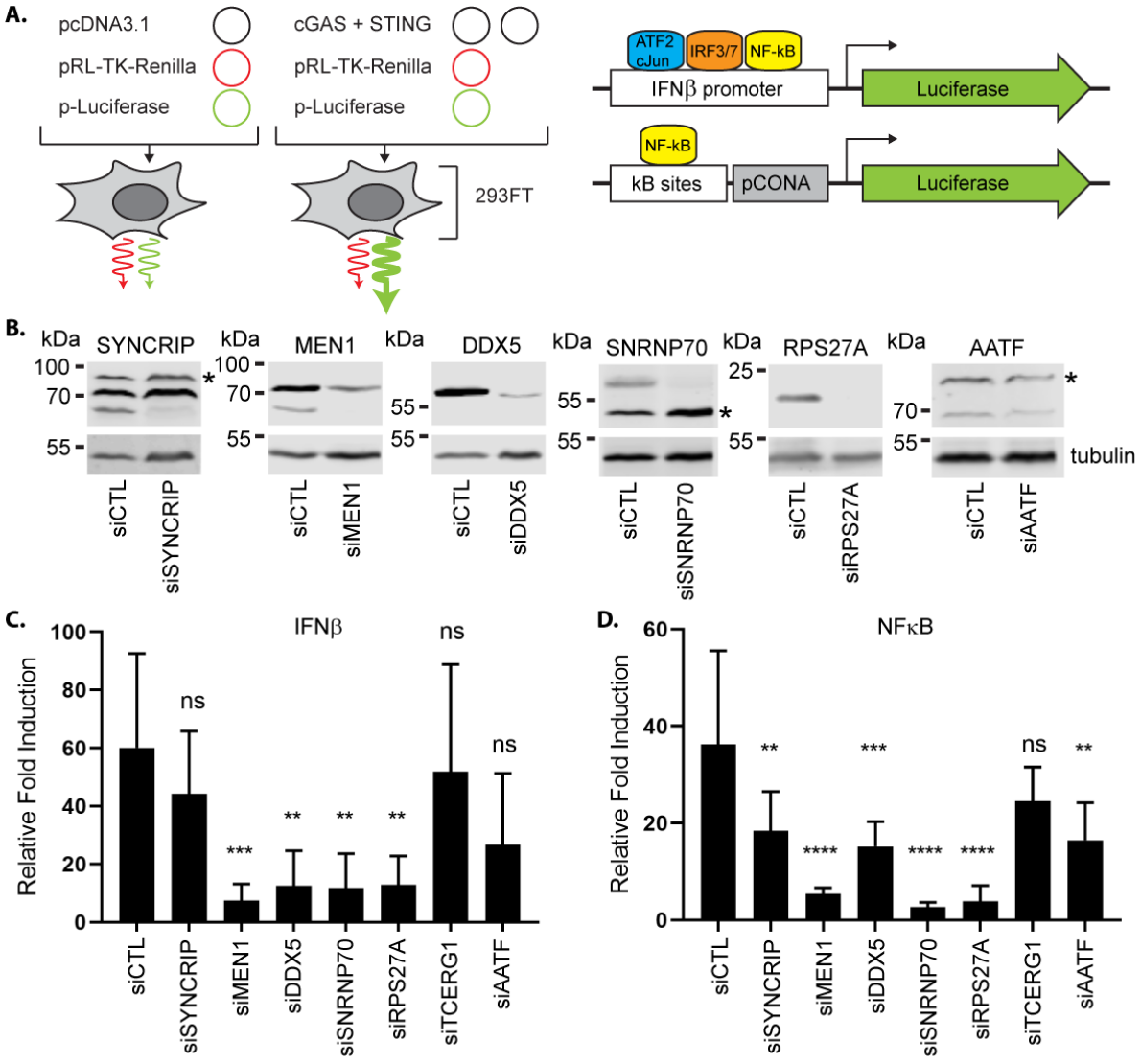

Figure 4.2 – Knockdown of STING partners impairs innate immune response stimulated luciferase reporter activation. (A) *Schematic of dual luciferase reporter assay showing plasmids transfected into HEK293FT cells. pcDNA3.1 =empty vector DNA, cGAS and STING = plasmids expressing cGAS and STING in pcDNA3.1 vectors, pRL-TK-Renilla = Renilla reniformis luciferase gene under the control of thymidine kinase promoter, p-Luciferase = Phonitus pyralis*

*luciferase gene under the control of IFN*β *promoter or a promoter activated by NFκB and AP1 transcription factor binding (pCONA = minimal promoter from chicken conalbumin gene).* ***(B)*** *Western blotting confirms knockdown of STING partners in HEK293FT cells by siRNA treatment, siCTL = non-target control siRNA, * = non-specific protein band. Blots representative of three independent experiments.* ***(C)*** *Relative fold induction of IFN*β *promoter driven luciferase gene in cells transfected with cGAS and STING plasmids normalised to pcDNA3.1 empty vector transfected in cells treated with control siRNA (siCTL) or siRNAs against STING partners. Ordinary one-way ANOVA with Dunnett's multiple comparisons, ** p < 0.01, *** p < 0.001, ns = not significant p > 0.05. n = 3. Error bars show standard deviation.* ***(D)*** *Relative fold induction of NFκB/AP1 transcription factor driven luciferase gene in cells transfected with cGAS and STING plasmids normalised to pcDNA3.1 empty vector transfected in cells treated with control siRNA (siCTL) or siRNAs against STING partners. Ordinary one-way ANOVA with Dunnett's multiple comparisons, ** p < 0.01, *** p < 0.001, **** p < 0.0001, ns = not significant p > 0.05. n = 3. Error bars show standard deviation.*

4.3 – STING partners are similarly knocked down in HT1080 cells so activation of endogenous IFNβ expression can be tested

The luciferase assay relied on reconstitution of cGAS and STING expression in HEK293FT cells as well as the co-transfection of luciferase expression plasmids. The advantage of this was the ability to test STING dependence of effects; however, a drawback of this approach is that there could be variability in STING and cGAS expression as a consequence of variation in transfection efficiency or indirect effects of partner knockdown prior to plasmid transfection. For example, the ribosomal protein RPS27A is required for ribosome biogenesis and has extra-ribosomal functions in promoting cellular proliferation, cell-cycle progression, and inhibition of apoptosis (Wang et al. 2014a). Thus, its knockdown could impair production of cGAS and STING proteins. Additionally, the timing of immune stimulation was not tightly controlled in this experiment because luciferase activity was measured 48 h after plasmid transfection. This means that the cGAS-STING pathway would be activated at some point between expression of cGAS and STING proteins and the detection of the plasmid DNA from which they were expressed. Thus, whether STING partner proteins affect earlier, or later steps of immune signalling pathways cannot be determined from this assay.

Therefore, I wanted to support the results of the luciferase assay by measuring endogenous IFN production in response to immune stimulation in STING expressing cells treated with siRNAs against the STING partners. Since HT1080 cells have a functional cGAS-STING pathway and produce IFNβ (Krishnamurthy et al. 2006) I chose to use this cell line to measure IFNβ production in response to immune stimulation. As a control to compare the effects of STING

partner knockdowns on IFNβ production to, cells were also treated with siRNAs against STING to inhibit IFNβ production.

First, a robust reduction of STING or STING partners following siRNA treatment in HT1080 cells was confirmed by Western blotting (Figure 4.3 A, quantified in B), with the same antibodies largely detecting the same bands in HT1080 cells as seen in HEK293FT cells. There are at least 5 known isoforms of SYNCRIP produced by alternative splicing and Western blotting detected 3 or 4 immunoreactive bands for SYNCRIP in HEK293T cell lysates and HT1080 cells lysates (Figure 4.2 B and Figure 4.3 A). Note that 3 or 4 bands were resolved for both cell lysates and it was not the case that one cell line expressed only 3 immunoreactive bands and the other 4. Instead, 4 immunoreactive bands were not always resolved because two of the bands ran very close together on 10 % SDS-PAGE. The second highest molecular weight band ~70 kDa likely represent the 69 kDa (Q3) isoform, with the lowest molecular weight band the 62 kDa (Q1) isoform, and the middle band which is not depleted by siRNA treatment the 65 kDa (Q2) isoform (the highest molecular weight band detected at ~80 kDa is probably hnRNP R(Mizutani et al. 2000; Mourelatos et al. 2001; Choi et al. 2004; Vu et al. 2017; Cappelli et al. 2018)). Quantification of protein knockdown measured by western blot shows a significant depletion of 60-80 % for all partner proteins and >80 % for STING (Figure 4.3 B). Note that for protein bands detected by SYNCRIP antibody, presumed Q3 and Q2 isoform signal was quantified together as bands were not always well enough resolved to quantify separately. It is therefore difficult to say the exact extent to which isoform Q3 is depleted, however, it is clear that the cytoplasmic Q1 isoform is almost completely reduced by siRNA treatment. Immunofluorescence staining for STING and partner proteins in cells treated with partner specific siRNAs or a control siRNA was next performed to confirm protein depletion seen in Western blots. Since we had hypothesised that partners could function as nuclear sensors of viral RNA or DNA, immunofluorescence was also used to determine that these STING partners identified from a NE fraction localised at least partially at the NE/nucleus (Figure 4.3 C). MEN1, DDX5, and SNRNP70 localised predominantly to the nucleus in agreement with previous reports (La et al. 2004; Wang et al. 2009; Stejskalova and Stane 2014) and siRNA knockdown greatly depleted any nuclear staining. The different isoforms of SYNCRIP are reported to localise to different cellular compartments, with the Q1 isoform predominantly cytoplasmic while Q2 and Q3 are mostly nuclear, while the highly homologous

hnRNP R is also a nuclear protein (Chen et al. 2008; Cappelli et al. 2018). In agreement with western blotting, siRNA treatment against SYNCRIP primarily depleted the cytoplasmic signal, suggesting that is the Q1 isoform that is mostly being targeted by siRNA treatment.

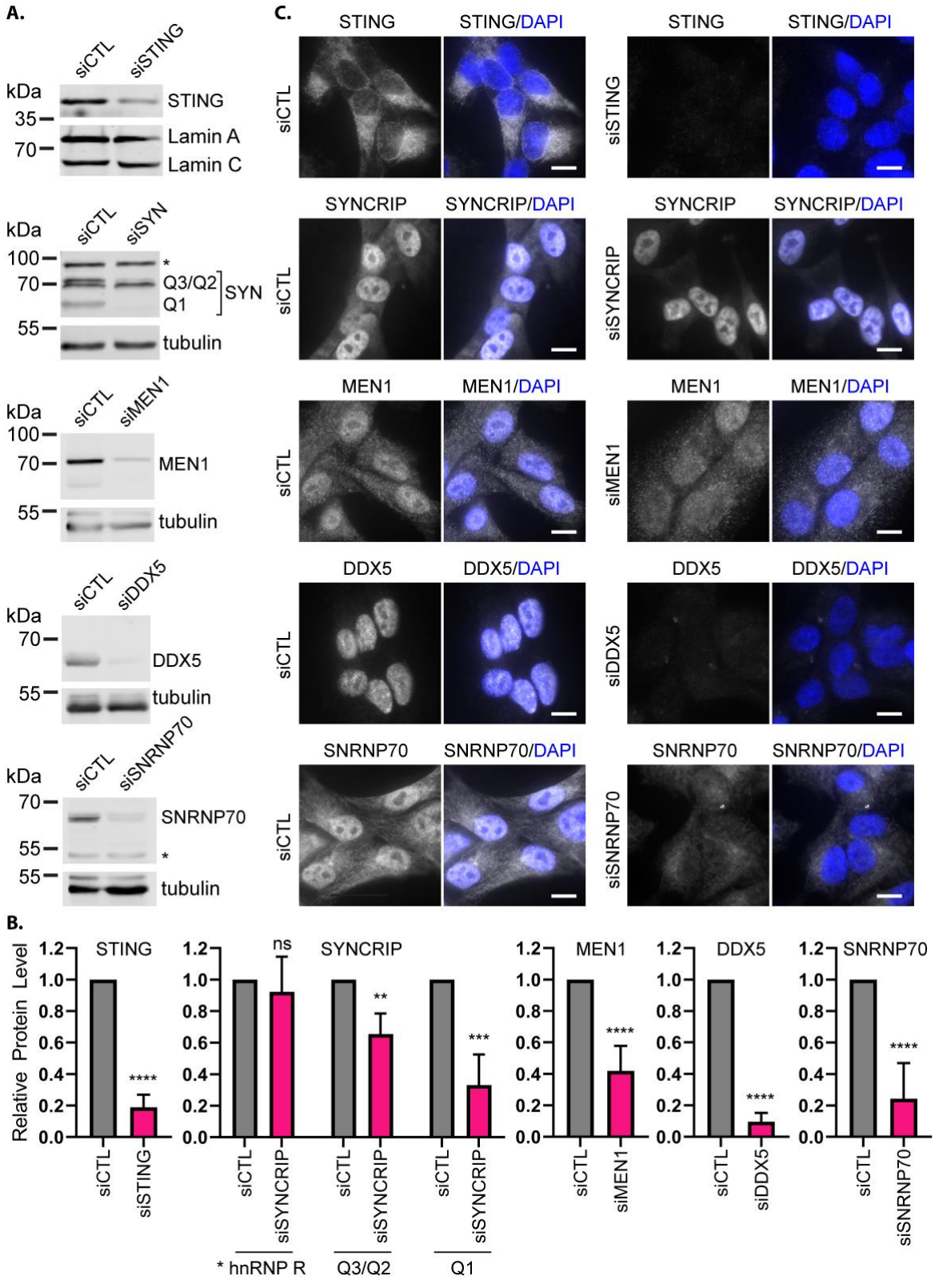

Figure 4.3 – Knockdown of STING and partner proteins in HT1080 cells. (A) *Western blotting of HT1080 cells treated with non-target control siRNA (siCTL) or siRNAs against STING and STING partners. Blots representative of three independent experiments. * = non-specific protein band.* ***(B)*** *Quantification of STING and partner protein levels from Western blotting in cells treated with target siRNAs normalised to cells treated with siCTL. SYN = SYNCRIP. Q1/Q2/Q3 = major SYNCRIP isoforms. Two-tailed unpaired t-tests. ** p < 0.01, *** p < 0.001, **** p < 0.0001, ns = not significant p > 0.05. n = 3. Error bars show standard deviation.* ***(C)*** *Immunofluorescence of STING and STING partners in HT1080 cells treated with STING and STING partner specific siRNAs or siCTL, shows protein localisation and confirms siRNA mediated knockdown. Scale = 10 µM.*

4.4 – Knockdown of SYNCRIP and SNRNP70 significantly reduces induction of endogenous IFNβ mRNA as a result of immune stimulation by dsDNA but not dsRNA

Having confirmed siRNA mediated knockdown of proteins in HT1080 cells, I next measured endogenous IFNβ expression by qPCR following IIR stimulation. Induction of IFNβ expression is one of the central response's fibroblasts have following detection of cytosolic DNA or viral RNA and thus provides a good assay to measure perturbation of innate immune signalling pathways. I tested the effect of knockdown of individual STING partners (SYNCRIP, MEN1, DDX5, and SNRNP70) or STING on IFNβ expression in HT1080 cells by measuring IFNβ mRNA levels 4 h after immune stimulation with dsDNA or the dsRNA mimic poly(I:C) (Figure 4.4). The effect of TCERG1 knockdown was not tested since it did not have an effect in the luciferase assays. The effect of knocking down RPS27A was also not tested since RPS27A knockdown caused high levels of cell death likely because it encodes a fusion protein of ubiquitin and the ribosomal subunit S27a which are essential to cell functioning.

Knockdown of STING by siRNA treatment significantly reduced the expression of IFNβ, ~80 %, following immune stimulation with DNA but not RNA compared to control siRNA treated cells measured 4 h after transfection of dsDNA/poly(I:C) (Figure 4.4A and B) in agreement with previous studies showing that STING is essential for IFNβ induction in response to cytosolic dsDNA (Ishikawa and Barber 2008; Ishikawa et al. 2009; Holm et al. 2016; Franz et al. 2018). A 4 h post-immune stimulation timepoint was chosen because STING activation, as marked by phosphorylation and accumulation in perinuclear foci, occurs rapidly (within 1 h) of dsDNA transfection (Ishikawa and Barber 2008; Ishikawa et al. 2009; Holm et al. 2016; Franz et al. 2018). Also, I wanted to test whether STING partners had an effect early on in the innate immune response since we were predicting that they could function as sensors of dsDNA/dsRNA. Knockdown of SNRNP70, similarly to STING, reduced expression of IFNβ

triggered by DNA immune stimulation, albeit ~50 % compared to ~80 % reduction in STING knockdown cells. This suggests that SNRNP70 is involved in innate immune responses to cytosolic dsDNA in agreement with luciferase assay results. Knockdown of SYNCRIP also significantly reduced expression of IFNβ triggered by DNA immune stimulation, ~50 %. This was slightly surprising because SYNCRIP knockdown did not have a significant effect on activation of the IFNβ promoter driven luciferase reporter and only had a significant effect on induction on the NF-κB/AP1 activated luciferase reporter in HEK293T cells. However, IFNβ promoter driven luciferase reporter activation was slightly lower in SYNCRIP knockdown cells compared to control knockdown cells and it is possible that this effect was not detected as significant due to a large variance between biological repeats. Alternatively, it might be that SYNCRIP exerts its function on IFNβ induction earlier on after stimulation with dsDNA and this is compensated for in its absence later on and so was not detected in the luciferase assay. Knockdown of MEN1 and DDX5 had no effect of endogenous IFNβ expression following immune stimulation with DNA. These differences could be a result of the different cell lines used (HEK293FT and HT1080) or may indicate that any effect on IFNβ induction may occur at a later timepoint since endogenous levels were measured 4 h after immune stimulation in HT1080 cells compared with 48 h after transfection of cGAS and STING plasmids in HEK293FT cells.

A reduction in IFNβ expression was only seen for SYNCRIP and SNRNP70 knockdown cells following immune stimulation with DNA but not poly(I:C), as was the case with STING knockdown cells (Figure 4.4 A and B). This suggests that SYNCRIP and SNRNP70, similarly to STING, modulate the IFN response to cytosolic dsDNA but not dsRNA. Knockdown of MEN1 also had no effect on IFNβ expression triggered by poly(I:C), however, knockdown of DDX5 significantly increased expression of IFNβ induced by poly(I:C) transfection which would suggest that DDX5 is inhibitory to innate immune responses stimulated by dsRNA.

Finally, it should be noted that siRNA treatment alone did not induce IFNβ expression (see Mock stimulated columns) indicating that the siRNAs used in this study are not themselves immune stimulatory (Figure 4.4 A and B). To ensure mRNA used to generate cDNA for qPCR experiments was not degraded during the extraction process, RNA was run on agarose gels to check integrity before reverse transcription to generate cDNA (Figure 4.4 C). The efficiency of primers used for qPCR (IFNβ, target gene and GAPDH, housekeeping gene for

normalisation) was also checked prior to use with both confirmed to have high efficiency, 97.28 % (slope – 3.389, amplification factor 1.97) and 94.88 % (slope – 3.451, amplification factor 1.95) respectively (Figure 4.4 D).

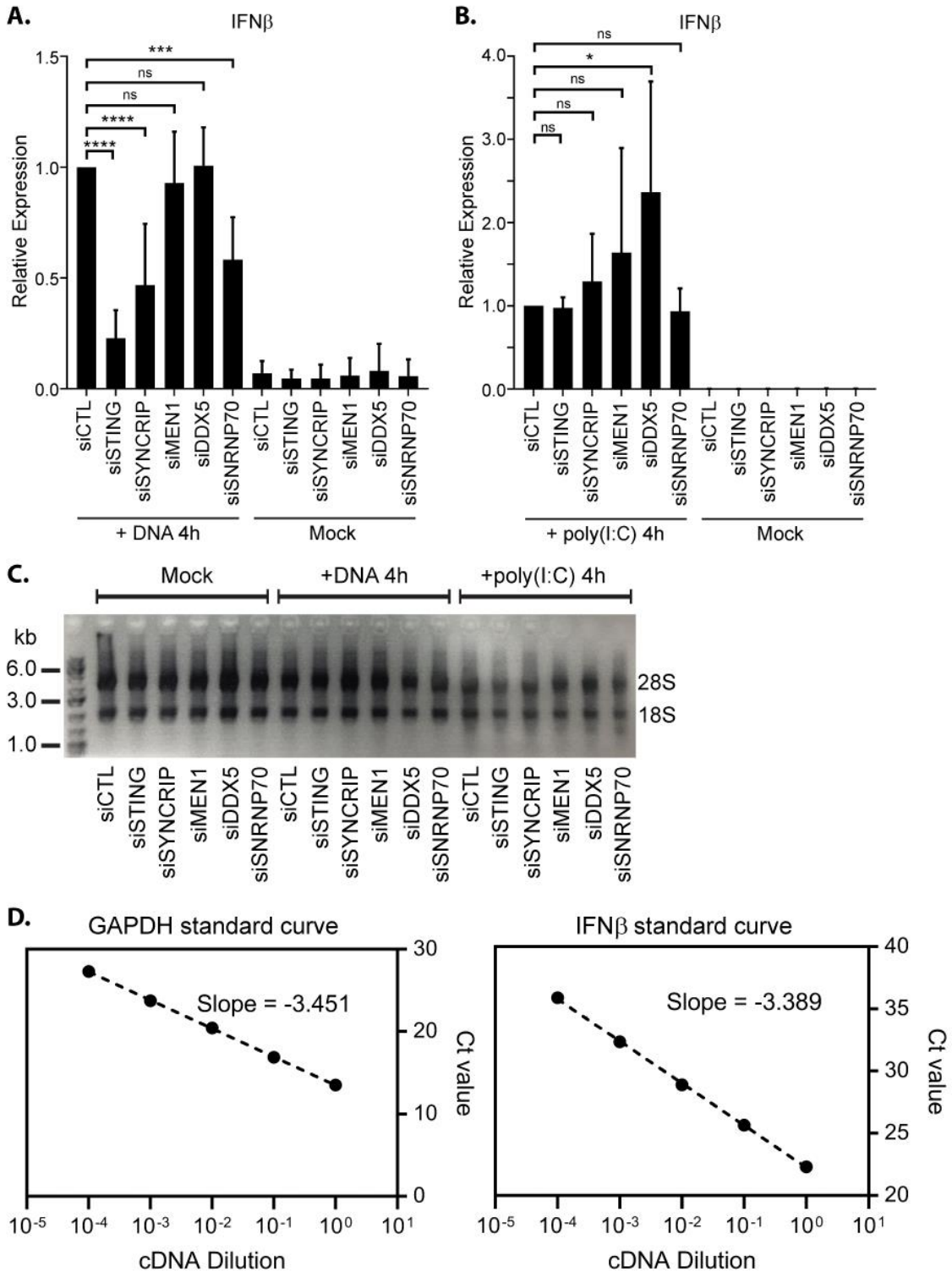

Figure 4.4 – Knockdown of SYNCRIP and SNRNP70 reduces IFNβ expression after immune stimulation with dsDNA. *IFNβ mRNA levels in HT1080 cells transfected with dsDNA* ***(A)*** *or poly(I:C)* ***(B)*** *(RNA isolated 4 h post-transfection) after treatment with siRNAs against STING and partners or non-target control siRNA (siCTL). Mean IFNβ mRNA expression normalised to GAPDH and shown relative to expression in siCTL cells stimulated with dsDNA* ***(A)*** *or poly(I:C)* ***(B)****. Ordinary one-way ANOVAs with Dunnett's multiple comparisons, * p < 0.05, *** p < 0.001, **** p < 0.0001, ns = not significant p > 0.05. n = 3. Error bars show standard deviation.* ***(C)*** *Representative RNA gel showing integrity of total RNA isolated from mock, dsDNA, and poly(I:C) stimulated cells. 28S and 18S rRNA bands indicate RNA integrity.* ***(D)*** *Standard curves for GAPDH and IFNβ primers used in qPCR experiments shown in (A) and (B), calculated using serial dilutions of cDNA from siCTL + DNA sample. Slope value allows calculation of primer efficiency (efficiency = (10^(-1/slope value)-1)*100 and amplification factor = 10^(-1/slope value).*

4.5 – At a later time point post-immune stimulation with dsDNA, knockdown of MEN1 also significantly reduces expression of endogenous IFNβ

In the luciferase assay in HEK293FT cells knockdown of MEN1 and DDX5 strongly reduced induction of the IFNβ promoter driven luciferase reporter. However, 4 h after immune stimulation with dsDNA no effect was seen on endogenous IFNβ mRNA levels by qPCR for MEN1 and DDX5 in HT1080 cells. Since in the luciferase assay, reporter induction was measured 48 h post-transfection of luciferase assay plasmids, it is possible that an effect of MEN1 or DDX5 knockdown is only seen at a later timepoint post-immune stimulation. Therefore, endogenous IFNβ mRNA levels were measure by qPCR 8 h after immune stimulation with dsDNA in STING partner knockdown cells. 8 h was chosen because STING activation and subsequent degradation has been reported to occur within 12 h of stimulation with dsDNA (Konno et al. 2013; Prabakaran et al. 2018), with IFNβ mRNA levels similarly peaking within 12 h (Shirota et al. 2006). As was the case 4 h post-transfection of dsDNA, knockdown of STING, SYNCRIP, and SNRNP70 caused a significant reduction in IFNβ expression (Figure 4.5 A). At this timepoint cells treated with siRNA against MEN1 also showed a significant reduction, ~50 %, in IFNβ expression compared to control cells, in agreement with luciferase assay data. Knockdown of DDX5 caused the opposite effect with a significant increase in IFNβ expression compared to control siRNA treated cells, suggesting that DDX5 is an inhibitor of dsDNA (Figure 4.5 A) and dsRNA (Figure 4.4 B) triggered IFN responses. Since a change in mRNA level doesn't necessarily translate into a difference in protein level, I also attempted to measure IFNβ protein levels in culture medium 12 h after dsDNA stimulation using an ELISA kit. However, no IFNβ protein was detected, and I did not have reagents to

repeat this experiment. It is possible that I should have measured IFNβ protein levels at a later timepoint since HT1080 cells have been shown to secrete IFNβ (Krishnamurthy et al. 2006). To confirm that knockdown of STING partners affects IIR to dsDNA I also measured mRNA levels of the pro-inflammatory cytokine, CCL5/RANTES, following immune stimulation with dsDNA in STING or STING partner knockdown cells. CCL5 is a chemotactic cytokine secreted by cells to recruit specialised cells of the immune system and similarly to IFNβ its expression is induced by IRF and NF-κB transcription factors (Gürtler et al. 2014). In agreement with IFNβ data, knockdown of STING, SYNCRIP, MEN1, or SNRNP70 caused a significant reduction in CCL5 expression compared to siRNA control treated cells, > 80 % for STING knockdown and ~50–60 % for partner knockdown, while no significant difference was seen in cells treated with siRNA against DDX5 (Figure 4.5 B). Primers used for CCL5 amplification showed high efficiency, 90.53 % (slope – 3.572, amplification factor 1.91) (Figure 4.5 C).

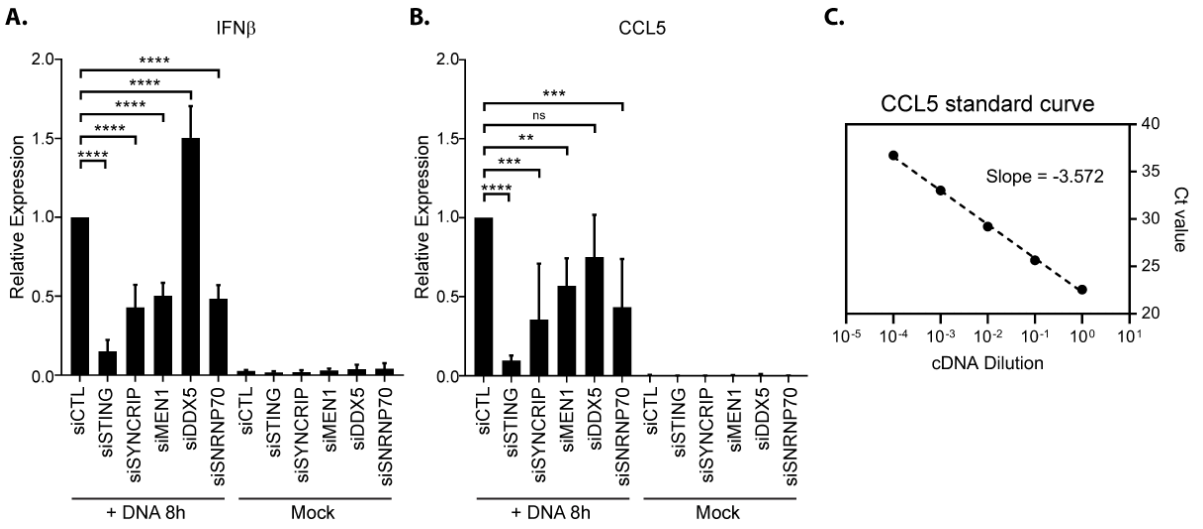

Figure 4.5 – Knockdown of SYNCRIP, MEN1 and SNRNP70 reduces IFNβ and CCL5 expression 8 h after immune stimulation with dsDNA. (A) *IFNβ or* ***(B)*** *CCL5 mRNA levels in HT1080 cells transfected with dsDNA (RNA isolated 8 h post-transfection) after treatment with siRNAs against STING and partners or non-target control siRNA (siCTL). Mean mRNA expression normalised to GAPDH and shown relative to expression in siCTL cells stimulated with dsDNA. Ordinary one-way ANOVAs with Dunnett's multiple comparisons, ** p < 0.01, *** p < 0.001, **** p < 0.0001, ns = not significant p > 0.05. n = 3. Error bars show standard deviation.* ***(C)*** *Standard curves for CCL5 primers used in qPCR experiments shown (B), calculated using serial dilutions of cDNA from siCTL + DNA sample. Slope value allows calculation of primer efficiency (efficiency = (10^(-1/slope value)-1)*100 and amplification factor = 10^(-1/slope value).*

siRNA treatment of cells can result in off-target effects whereby in addition to targeting the desired mRNA for depletion, an unrelated mRNA is also silenced due to some

complementarity between the siRNA 'guide' strand and mRNA other than desired target (Bartoszewski and Sikorski 2019). Therefore, to rule out the possibility that siRNAs against STING partner proteins affected expression of STING and cGAS, Western blotting was performed to quantitate protein abundance of STING and cGAS. As expected, siRNA treatment against STING significantly reduced STING protein levels without affecting cGAS when compared to siRNA control treated cells. Knockdown of STING partners did not significantly affect STING or cGAS protein levels when compared to control treated cells (Figure 4.6 A and B). However, the siRNA against DDX5 caused a partial reduction in STING protein levels compared to the control, but not at a level that was statistically significant or indeed as much as siRNA treatment specific to STING (Figure 4.6 A). An alternative explanation for the reduction in STING protein levels seen in DDX5 knockdown cells could be that DDX5 is involved in promoting STING protein stability or gene expression. While this was not pursued further here it could be worth investigating in the future since STING and cGAS are known to be downregulated in many immortalised cell lines through ill-defined mechanisms (Sun et al. 2009; Sun et al. 2013; Malik et al. 2014; Xia et al. 2016a; Deschamps and Kalamvoki 2017a) and so DDX5 could conceivably be involved in such processes.

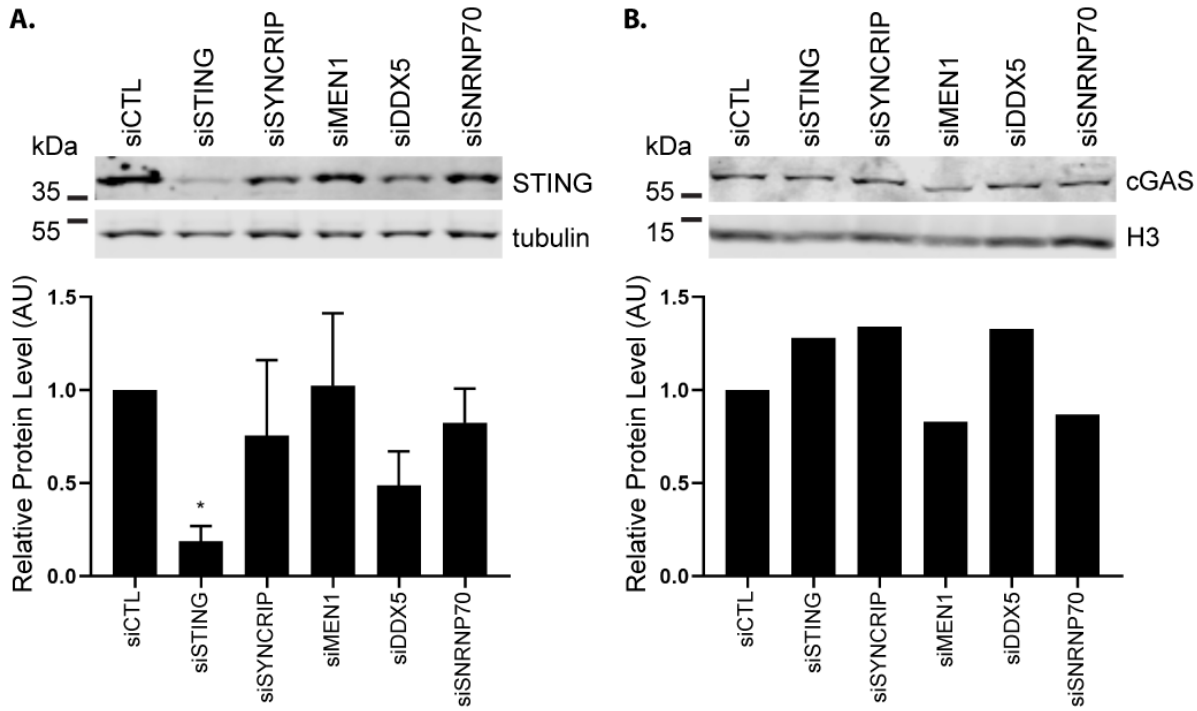

Figure 4.6 – Knockdown of STING partners does not significantly affect levels of STING and cGAS in HT1080 cells. *Representative western blost showing STING* ***(A)*** *or cGAS* ***(B)*** *protein levels in HT1080 cells treated with siRNAs against STING and partners or non-target control*

*siRNA (siCTL). Quantification showing mean STING protein levels relative to siCTL cells normalised according to tubulin loading control. Ordinary one-way ANOVA with Dunnett's multiple comparisons, * p < 0.05. n = 3 (A) n = 1 (B). Error bars show standard deviation.*

4.6 – Knockdown of STING partners reduces activation of IRF3 in response to DNA but not poly(I:C)

Having found that STING partners contributed to the induction of IFNβ and CCL5 in response to cytosolic DNA, I wanted to examine which parts of the immune signalling pathway triggered by cytosolic dsDNA were being affected. To do this I first looked at the activation of immune transcription factor IRF3, since STING partners were proposed to have indirect links to IRF3/7 and because IRF3 is one of the transcription factors which induces CCL5 (Lin et al. 1998) and IFNβ expression (Honda et al. 2006). IRF3 normally resides in the cytoplasm as a monomeric protein but following activation of cGAS-STING, RIG-I/MDA-5-MAVS, or TLR3/4-TRIF pathways it is recruited to active STING, MAVS, or TRIF signalling complexes and phosphorylated by TBK1 (Liu et al. 2015a). Subsequently phosphorylated IRF3 (pIRF3) dissociates from adaptor proteins and forms homodimers which translocate to the nucleus and activate type-I IFN and pro-inflammatory cytokine expression (Yoneyama et al. 1998; Liu et al. 2015a). Western blotting with an antibody specific to phosphorylated-IRF3 (S386) allowed for determination of IRF3 activation following immune stimulation with dsDNA or poly(I:C) (Figure 4.7 A, B, and D). As expected, knockdown of STING significantly reduced IRF3 phosphorylation at 4 h after DNA triggered immune stimulation compared to control cells, but had no effect on IRF3 phosphorylation in cells stimulated with poly(I:C) (Figure 4.7 B - E). Knockdown of SYNCRIP, MEN1, and SNRNP70 also reduced levels of phosphorylated-IRF3 in cells stimulated with dsDNA (Figure 4.7 B and C). Interestingly, knockdown of DDX5 also reduced levels of phosphorylated-IRF3 in dsDNA stimulated cells despite DDX5 knockdown increasing levels of IFNβ mRNA in dsDNA stimulated cells (Figure 4.5 A). This suggests that DDX5's effect on IFNβ induction is not through IRF3 activation. Knockdown of SYNCRIP and MEN1 had no effect on activation of IRF3 in poly(I:C) stimulated cells in agreement with qPCR data, suggesting that SYNCRIP and MEN1 knockdown effects are specific to dsDNA stimulated IIR (Figure 4.7 D and E). Meanwhile, knockdown of both DDX5 and SNRNP70 significantly increased levels of phosphorylated-IRF3 in cells stimulated with poly(I:C). This is consistent with IFNβ qPCR data for DDX5 but not SNRNP70 which saw no difference in IFNβ expression at 4 h after stimulation with poly(I:C). This difference could be due to the timepoint at which IFNβ expression was analysed and may require analysis at a later timepoint to see a difference.

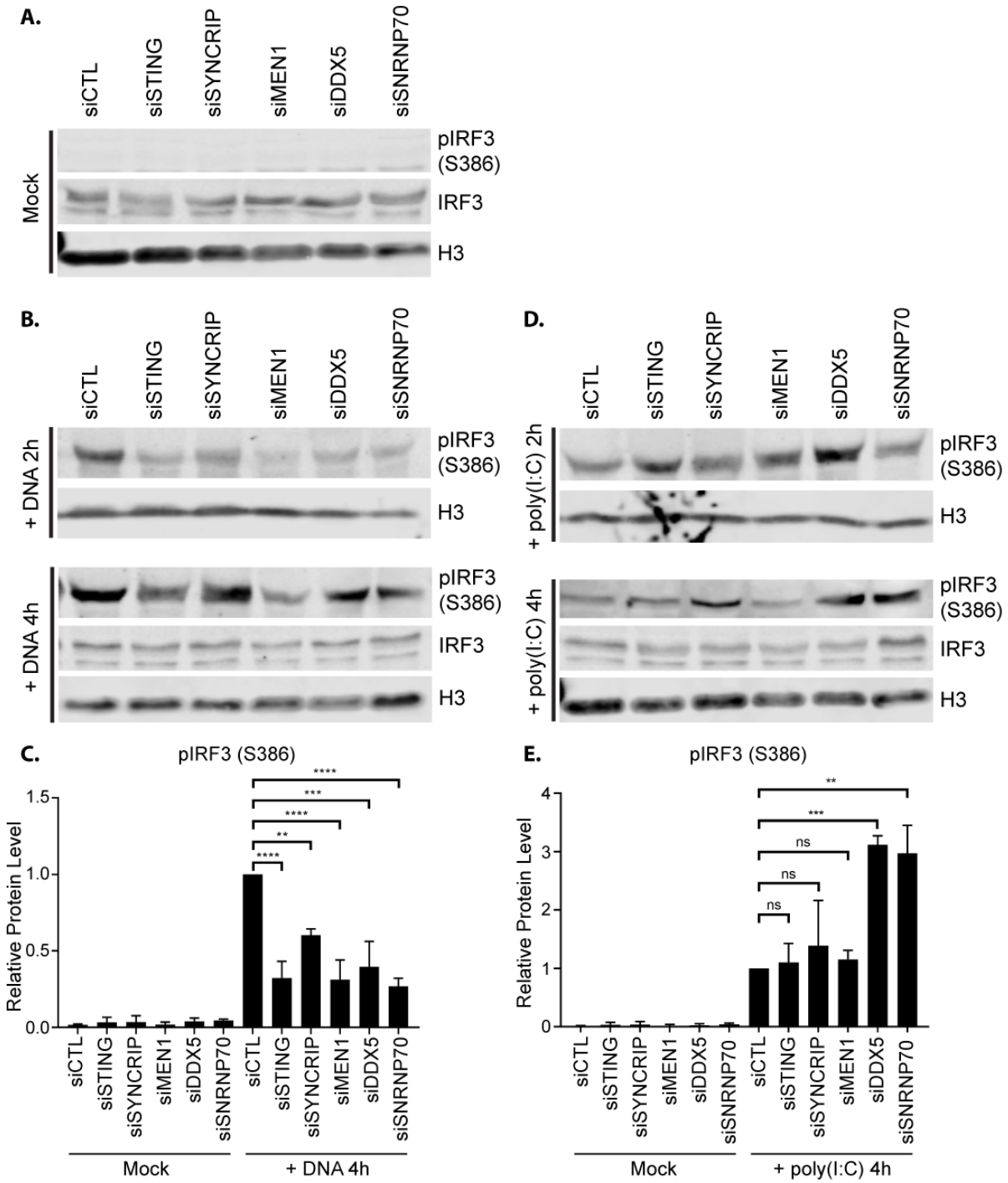

Figure 4.7 – Knockdown of STING partners significantly reduces activation of IRF3 in cells stimulated with dsDNA and significantly increases activation in cells stimulated with poly(I:C). (A) *Representative western blot showing levels of activated IRF3 (phosphorylated IRF3, pIRF3 (S386)), total IRF3, and histone H3 in mock stimulated cells treated with siRNAs against STING and partners.* ***(B)*** *Representative western blot showing levels of activated IRF3 (phosphorylated IRF3, pIRF3 (S386)), total IRF3, and histone H3 in cells treated with siRNAs against STING and partners and stimulated with dsDNA.* ***(C)*** *Quantification of activated IRF3 (pIRF3(S386)) in mock and cells stimulated with DNA for 4 h, protein levels relative to control siRNA (siCTL) cells stimulated with DNA. pIRF3 levels normalised to H3. Ordinary one-way ANOVA with Dunnett's multiple comparisons, ** p < 0.01, *** p < 0.001, **** p < 0.0001. n =*

3. Mean values are plotted and error bars show standard deviation. ***(D)*** *Representative western blot showing levels of activated IRF3 (phosphorylated IRF3, pIRF3 (S386)), total IRF3, and histone H3 in cells treated with siRNAs against STING and partners and stimulated with poly(I:C).* ***(E)*** *Quantification of activated IRF3 (pIRF3(S386)) in mock and cells stimulated with poly(I:C) for 4 h. Protein levels are shown relative to control siRNA (siCTL) cells stimulated with poly(I:C). pIRF3 levels normalised to H3. Ordinary one-way ANOVA with Dunnett's multiple comparisons, ** p < 0.01, *** p < 0.001, ns = not significant p > 0.05. n = 3. Mean values are plotted and error bars show standard deviation.*

4.7 – Knockdown of STING partners reduces accumulation of IRF3 in the nucleus following stimulation with dsDNA

As another means of measuring the activation of IRF3 and to look at activation of NF-κB in cells treated with siRNAs against STING and partners following immune stimulation with DNA, I also measured accumulation of IRF3 and NF-κB in the nucleus of cells by immunofluorescence. In unstimulated cells IRF3 exists as an unphosphorylated monomer dispersed throughout the cytoplasm. Following immune stimulation with dsDNA or poly(I:C) IRF3 is phosphorylated, dimerises, and translocated to the nucleus (Kato and Fujita 2014; Liu et al. 2015a; Sparrer and Gack 2015). Similarly, in unstimulated cells NF-κB is inactive and resides in the cytoplasm, following immune stimulation with dsDNA or poly(I:C) NF-κB is activated and translocated to the nucleus (Abe et al. 2013; Kato and Fujita 2014; Sparrer and Gack 2015). Transfection of dsDNA or poly(I:C) activates cytosolic DNA/RNA sensing pathways, inducing the activation of IRF3 and NF-κB and resulting in their accumulation in the nucleus where they induce expression of target genes (Figure 4.8 A). In cells stimulated with poly(I:C) both IRF3 and NF-κB accumulated in the nucleus, while in DNA stimulated cells most only accumulated IRF3 in the nucleus, in agreement with findings that the cGAS-STING pathway predominantly activates IRF3 (Abe and Barber 2014; Liu et al. 2015b; Dobbs et al. 2015; Dunphy et al. 2018). Accordingly, I quantified the percentage of cells with nuclear accumulation of IRF3 and NF-κB in cells treated with siRNAs against STING and partner proteins following immune stimulation with dsDNA (Figure 4.8 B and C). Knockdown of STING drastically inhibited the nuclear accumulation of IRF3 while knockdown of all STING partners tested similarly reduced accumulation of IRF3 in the nucleus compared to siRNA control treated cells, although to a lesser extent (Figure 4.8 B and D). Knockdown of STING and partners largely had no effect on accumulation of NF-κB in the nucleus following immune stimulation with dsDNA, barring knockdown of DDX5 which caused a slight increase in nuclear

accumulation of NF-κB (Figure 4.8 C). This could explain the increase in IFNβ expression in cells knocked down for DDX5 despite a reduction in levels of activated IRF3 since both NF-κB and IRF3 are required to induce IFNβ expression.

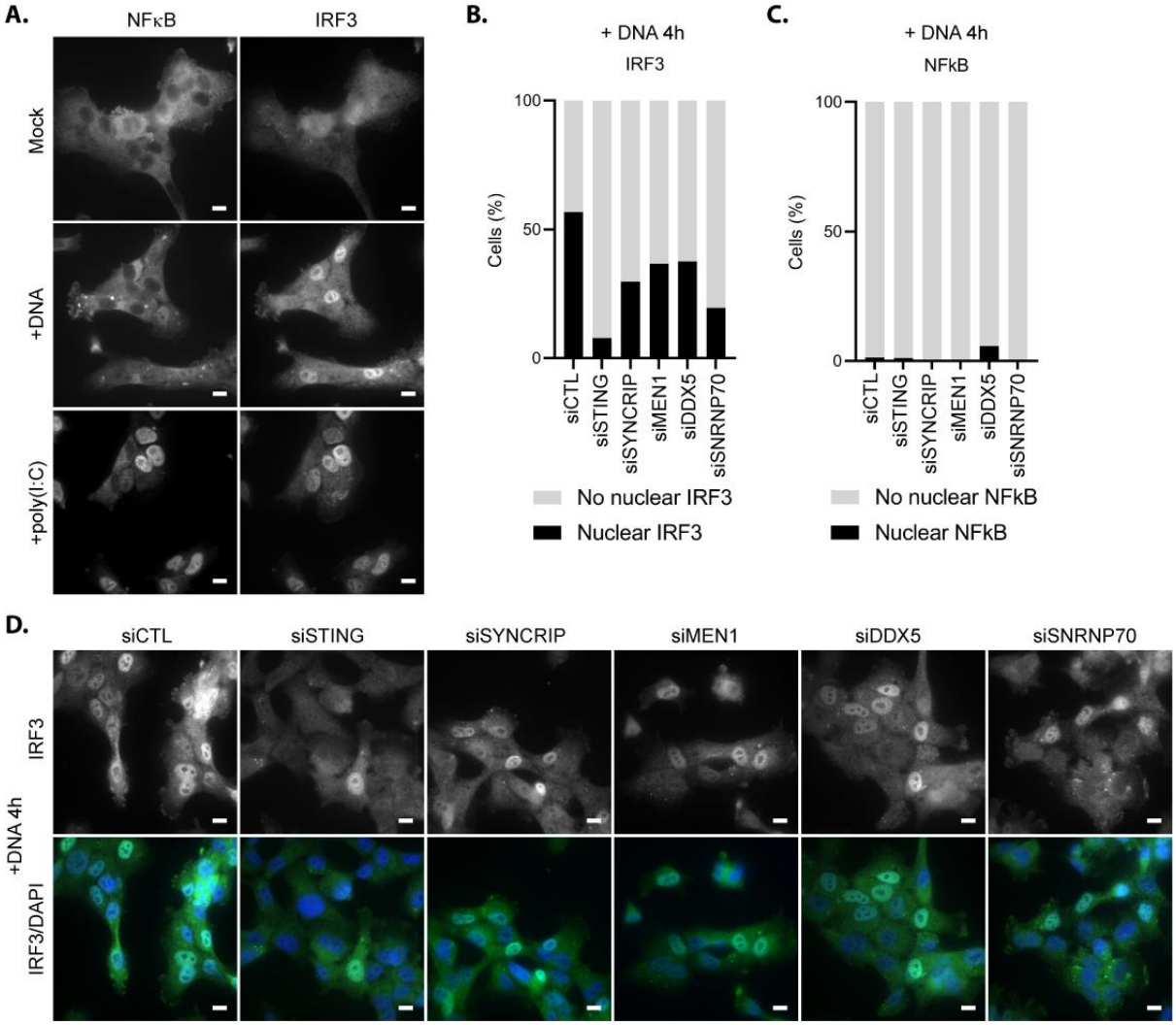

Figure 4.8 – Knockdown of STING partners significantly reduces nuclear accumulation of IRF3 in cells stimulated with dsDNA. (A) *Localisation of NF-κB (p65) and IRF3 transcription factors in mock, dsDNA, and poly(I:C) stimulated cells. Quantification of cells with nuclear accumulation of IRF3* ***(B)*** *or NF-κB (p65)* ***(C)*** *in cells treated with siRNAs against STING and partners following immune stimulation with dsDNA. > 100 cells and 10 fields of view quantified for each condition.* ***(D)*** *Example micrographs showing accumulation of IRF3 in the nucleus of cells treated with siRNAs against STING and partners or control siRNAs (siCTL) and stimulated with dsDNA. Scale = 10 μM.*

4.8 – Knockdown of STING partners and effects on proliferation of the DNA virus, HSV-1

Having confirmed that knockdown of STING partners has an effect on dsDNA triggered IIR as shown by an alteration in IRF3 activation, IFNβ transcript levels, and CCL5 transcript levels, I wanted to test whether any of the STING partners affect the proliferation of a virus with a

DNA genome. For this I used herpes simplex virus (HSV-1), which has a dsDNA genome, because it has already been shown to be restricted by the cGAS-STING pathway (Ishikawa et al. 2009; Gao et al. 2013a; Sun et al. 2013) with *STING*$^{-/-}$ mice susceptible to lethal infection with HSV-1 (Ishikawa et al. 2009). HT1080 cells treated with siRNAs against STING or partners were infected with HSV-1 and viral titres measured by plaque assay at various timepoints post-infection (Figure 4.9 A). Surprisingly, STING knockdown did not have an impact on HSV-1 viral titres compared to control siRNA treated cells with titres almost identical at 12 hours post infection (hpi) and siCTL titres modestly higher at 18 hpi (Figure 4.9 B).

This finding may be explained by recent work which shows that the dependence on STING for restriction of HSV-1 in mice and murine cell lines is not shared in the HT1080 human cell line I used in this experiment (Latif et al. 2020). In this study, *Latif et al.* dissected the relative contributions of TLR3-TRIF and cGAS-STING signalling pathways in the restriction of HSV-1 in human and murine cell lines. This work built on a previous report from the same group which uncovered a requirement for the adaptor protein, TRIF, in the cGAS-STING signalling pathway (Wang et al. 2016). TRIF is the essential adaptor protein for the endosomal dsRNA sensor, TLR3, and is also required for the endosomal branch of TLR4 signalling, which recognise lipopolysaccharide (LPS) (Yamamoto et al. 2002; Fitzgerald et al. 2003). Similarly to STING, activation of TRIF leads to IFNβ expression through TBK1 and IRF3 (Liu et al. 2015a). In their previous work, TRIF was found to be required for STING mediated IIR with TRIF interacting directly with STING to promote its dimerization and translocation to perinuclear foci following immune stimulation with cyclic dinucleotide STING ligands. Moreover, HSV-1 grew to higher titres in *TRIF*$^{-/-}$ MEFs and *TRIF*$^{-/-}$ mice were susceptible to lethal infection (Wang et al. 2016). Viral infection is a far more complex immune stimulus than transfected DNA or RNA and triggers multiple signalling pathways culminating in the induction of type-I IFNs and pro-inflammatory cytokines. Infection with HSV-1 is sensed by both the dsDNA sensing cGAS-STING pathway and the dsRNA sensing TLR-3 pathway. As a dsDNA virus, the genome of HSV-1 serves as a ligand to stimulate cGAS-STING signalling as does the leakage of mitochondrial or nuclear DNA as a consequence of viral infection (West et al. 2015; Roers et al. 2016). While, like most if not all viruses, HSV-1 produces dsRNA during replication and this, as well as cellular dsRNA released from dead infected cells, can be endocytosed activating TLR3 in neighbouring cells (Nguyen et al. 2017; Sato et al. 2018; Dauber et al. 2019). Now in their

recent report *Latif et al.* show that in L929 and NB41A3 mouse cell lines, HSV-1 is primarily attenuated by cGAS-STING pathway, while in HT1080 and HeLa-M human cells lines HSV-1 is primarily attenuated by the TL3-TRIF pathway. Thus, this work could explain why STING knockdown did not affect HSV-1 viral titres compared to control knockdown in HT1080 cells in my experiments.

HSV-1 has been shown to antagonise the cGAS-STING pathway through multiple mechanisms with several viral proteins found to inhibit STING signalling (Zheng 2018). For example, the viral protein ICP27 has been reported to bind activated STING-TBK1 complexes thereby preventing activation of IRF3 (Christensen et al. 2016). Additionally, the tegument protein UL46 (VP11/12) has also been reported bind both STING and TBK1 and inhibit downstream immune responses (Deschamps and Kalamvoki 2017b). Furthermore, HSV-1 is also able to antagonise STING activation through the viral protein $y_1$34.5 which binds STING and inhibits its translocation to perinuclear foci and thus activation of IRF3 and IFNβ expression (Pan et al. 2018). Another example is the HSV-1 tegument protein UL41, an endoribonuclease also known as the virion host shut off protein (vhs), which also targets the cGAS-STING pathway with UL41 causing a reduction in cGAS mRNA levels possibly through selective degradation of cGAS mRNA via its RNase activity (Su and Zheng 2017). Thus, it is possible that HSV-1 is so effectively able to inhibit STING-mediated signalling that whether or not STING is present does not affect viral proliferation in HT1080 cells.

Knockdown of STING partners, MEN1 or SNRNP70, similarly had little to no effect on HSV-1 viral titres compared to control treated cells, while knockdown of SYNCRIP or DDX5 caused a slight reduction in viral titres compared to control treated cells (Figure 4.9). In the case of SYNCRIP knockdown, titres were ~4x lower at 12 hpi and ~2x lower at 18 hpi, while for DDX5 knockdown titres were ~6x lower at 12 hpi and ~5x lower at 18 hpi. For DDX5, since knockdown increases levels on phosphorylated-IRF3 and IFNβ mRNA in DNA stimulated cells, this would explain an inhibition of HSV-1 viral titres. However, this experiment was only performed once because after realising that STING knockdown would not be a sufficient positive-control in HT1080 cells, likely due to the minimal contribution of the cGAS-STING pathway to restricting HSV-1 in this cell line (Latif et al. 2020), whether NE STING partners affect HSV-1 proliferation could not readily be determined. Therefore, the data should be interpreted cautiously. Nonetheless, I decided to include it here since knockdown of DDX5 in

particular reduced HSV-1 viral titres compared to control knockdown cells and this correlates well with DDX5 being a negative regulator of dsDNA triggered IIR.

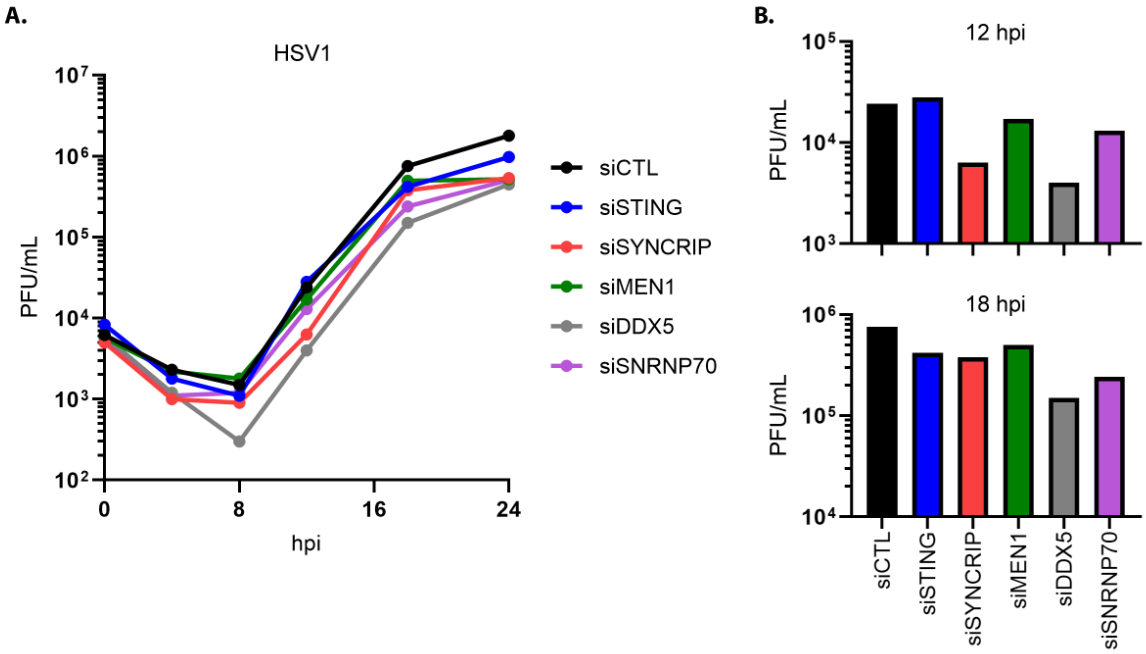

Figure 4.9 – Knockdown of STING partners and effect on herpes simplex virus (HSV-1) titres. ***(A)*** *Time-course experiment showing HSV-1 titres measured by plaque assay across 24 h in HT1080 cells treated with siRNAs against STING and partners and infected with HSV-1 at a multiplicity of infection (MOI) of 5.* ***(B)*** *Bar charts showing HSV-1 titres in cells from time-course shown in (A) at timepoints when virus is still in an exponential phase of growth at 12 h and 18 h post infection (hpi). PFU/mL = plaque forming units per mL. y-axis plotted using a log scale. n =1.*

4.9 – Attempts to co-immunoprecipitate STING with NE partners without cross-linking suggests they are not direct interactors

Since STING partners SYNCRIP, MEN1, DDX5, and SNRNP70 were all found to influence IIR, I next wanted to confirm STING-partner interactions from the NE co-immunoprecipitation experiment. In the original experiment an overexpressed STING-GFP construct was used because good STING antibodies were not yet available, and a reversible crosslinking approach was used because the conditions for extracting NETs from the NE are necessarily harsh due to both membrane insertion and association with the insoluble intermediate filament lamin polymer. Now that better commercial antibodies are available, I wanted to test if I could pulldown these partners without cross-linking and using endogenous STING. Additionally, I

wanted to test the hypothesis that STING-partner interactions increase following immune stimulation with dsDNA or poly(I:C).

Co-immunoprecipitation of STING and partners was performed using rabbit monoclonal or sheep polyclonal antibodies against endogenous STING or in the other direction with antibodies against several partners in HT1080 cells (mouse monoclonal anti-SYNCRIP, rabbit polyclonal anti-MEN1, goat polyclonal anti-DDX5, rabbit polyclonal anti-SNRNP70). I successfully immunoprecipitated STING, SYNCRIP, MEN1, and DDX5 from whole cell lysates (Figure 4.10 A - C), but the antibody against SNRNP70 proved unsuitable for immunoprecipitation (Figure 4.10 D). However, anti-STING antibody failed to co-immunoprecipitate partners SYNCRIP and DDX5 and only very weakly pulled-down MEN1, while none of SYNCRIP, MEN1, or DDX5 pulled-down STING (Figure 4.10 A – C). I postulated that since STING partners were found to influence IIRs stimulated by dsDNA or poly(I:C) an interaction with STING may only be seen by Western blot during IIR against dsDNA or poly(I:C) as this may enhance a weak interaction that was only seen by the mass spectrometry used in the original experiment. Therefore, co-immunoprecipitation was performed 2 h post-immune stimulation with dsDNA and/or poly(I:C) based on which immune stimuli partners were found to affect IIR. However, no co-immunoprecipitation was found in any immune stimulated conditions and in the case of MEN1 where there had been some co-immunoprecipitation of MEN1 with an anti-STING antibody in unstimulated cells this was lost in dsDNA stimulated cells (Figure 4.10 B). These results, while not supportive of the original pulldown experiment, may be due to be very transient interactions between STING and partners that were preserved by cross-linking used in the original experiment, but are disrupted by the buffers tested for co-immunoprecipitation (initially RIPA buffer: 150 mM NaCl, 50 mM Tris pH 8.0, 1% NP-40, 0.5 % sodium deoxycholate, 0.1 % SDS + protease inhibitors (data not shown) followed by NP-40 buffer: 150 mM NaCl, 50 mM Tris pH 8.0, 5mM EDTA, 1% NP-40 + protease inhibitors). Indeed, the original reasoning for using cross-linking when immunoprecipitating STING from NEs was that extraction from the NE often requires harsh conditions to disrupt interactions with the nuclear lamina and so extraction conditions that are too mild would maintain STING-partner interactions in the NE, but would not isolate STING and its partners from NE so that they would not be recovered in these experiments. Rather, the ER pool and the more minor NE pool that is not restricted by lamina interactions would be recovered. By

using reversible cross-linking STING in the NE could be extracted while preserving weaker interactions with partner proteins. Moreover, I performed co-immunoprecipitation experiments using whole cell lysates and since STING localises throughout the ER and only partially to the NE this could have inhibited detection of NE-STING interactions. Therefore, it would be appropriate to perform isolation of nuclei with and without cross-linking if repeating immunoprecipitation experiments using antibodies against endogenous proteins. A control experiment comparing the amount of STING extracted from nuclear and cytoplasmic fractions in buffers used for pulldown should be performed prior to this, since the percentage of STING extracted under these conditions could then be compared to the total amount of STING in the respective fractions solubilised directly in SDS-PAGE sample buffer. This might allow for optimisation of a pulldown buffer suitable for extracting STING from the NE but mild enough to preserve protein-protein interactions.

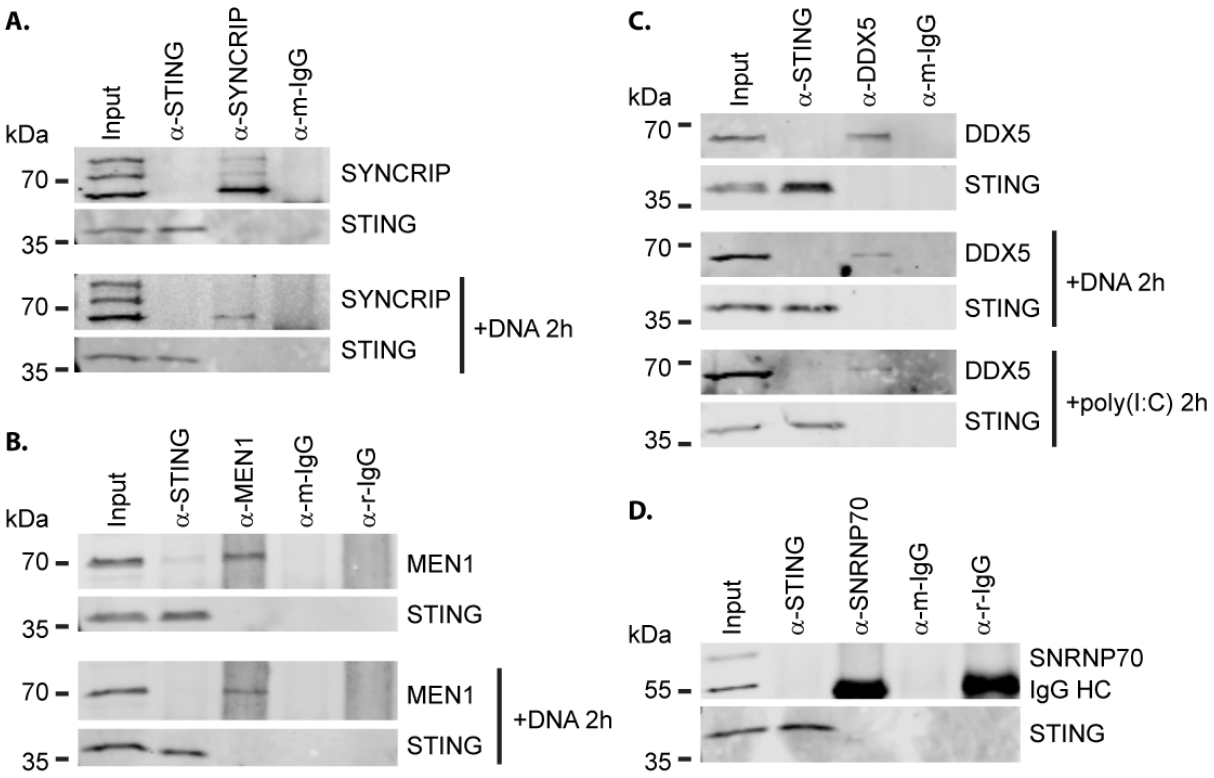

Figure 4.10 – Endogenous STING co-immunoprecipitates MEN1 but not SYNCRIP or DDX5 from whole cell lysates without crosslinking. (A) *Immunoprecipitation (IP) of endogenous STING or SYNCRIP from HT1080 whole cell lysates shows that antibodies are suitable for IP but does not confirm an interaction between SYNCRIP and STING.* ***(B)*** *IP of endogenous STING and MEN1 from HT1080 whole cell lysates shows that antibodies are suitable for IP and indicate that MEN1 interacts with STING (α-STING IP's MEN1 although α-MEN1 fails to IP STING) in unstimulated cells, but not cells stimulated with dsDNA.* ***(C)*** *IP of endogenous STING and DDX5 from HT1080 whole cell lysates shows that antibodies are suitable for IP but does not confirm*

an interaction between DDX5 and STING. ***(D)*** *Antibody against SNRNP70 is not suitable for IP. IgG HC, Immunoglobulin G heavy chain. m-IgG, mouse-IgG. r-IgG, rabbit-IgG. Immunoblots representative of ≥ 2 independent experiments.*

4.10 – Proximity Ligation Assay suggests STING and partners are in close proximity but requires further optimisation

Due to the many possible reasons for a negative result with co-immunoprecipitation experiments, I tried using a proximity ligation assay (PLA) as an alternative means of confirming STING-partner interactions. PLA relies on antibody staining against two target proteins; primary antibodies (raised in different species) against target proteins are first incubated with samples, these are then detected by secondary antibodies conjugated to complementary DNA oligos (PLA probes). DNA oligos can be hybridised providing they are within close proximity (~40 nm) to each other. Rolling circle amplification is used to generate an amplicon tethered to the PLA probes which can subsequently be detected by hybridisation of fluorescently labelled detection probes. These can be visualised by fluorescent microscopy as discreet foci where an interaction occurs (Bagchi et al. 2015). Since PLA does not require extraction of protein and instead detects interactions in situ, I postulated that it could be used overcome issues around suitability of buffers for confirming STING-partner interactions encountered using co-immunoprecipitation.

PLA was performed with secondary antibody staining alone as a negative control to quantitate background signal, with very few foci ~2 detected per cell (quantified by DAPI stain) (Figure 4.11 A, top panels). As a positive control for PLA, antibody staining was performed against MAVS and STING (AF6516 polyclonal sheep antibody) which are known to co-immunoprecipitate (Zhong et al. 2008), yielding ~25 PLA foci per cell. PLA performed for SYNCRIP and STING, MEN1 and STING, and SNRNP70 and STING all gave >30 PLA foci per cell (Figure 4.11 A). PLA could not be performed for DDX5 and STING because both primary antibodies were raised in sheep. Immunofluorescence staining performed in parallel to PLA using the same blocking and primary antibody staining steps shows that all STING partner and STING staining was as expected in cells, with MAVS staining labelling the mitochondria, STING staining labelling the ER and NE, and partner proteins localising to the nucleus and cytoplasm (Figure 4.11 B). PLA foci were quantified for all protein pairs in siRNA control treated cells and in cells treated with siRNAs against STING as a biological negative control, since knockdown of STING should prevent PLA foci from forming (Figure 4.11 C). Surprisingly, in cells treated

with STING specific siRNAs the average number of PLA foci for STING and partner proteins did not markedly decrease, with only STING + MEN1 and STING + SNRNP70 pairs showing a modest decrease in the number of foci per cell. This was also the case for MAVS + STING suggesting an issue with this assay. It is possible that this is due to non-specific staining of the STING antibody in cells treated with siRNAs against STING, although immunofluorescence staining against STING in these cells confirmed a loss of STING antibody staining (Figure 4.11 D). The assay therefore requires further optimisation with more stringent washing steps to remove non-specific staining or siRNA knockdown of STING partners as an alternative negative biological control to STING knockdown. Alternatively, the STING (D2P2F) monoclonal rabbit antibody which requires methanol fixation could be used. However, this would require finding antibodies against partner proteins that were compatible with methanol fixation since the ones used in this study are only compatible with formaldehyde fixation, hence the decision to use the sheep polyclonal STING (AF6516) antibody in this assay.

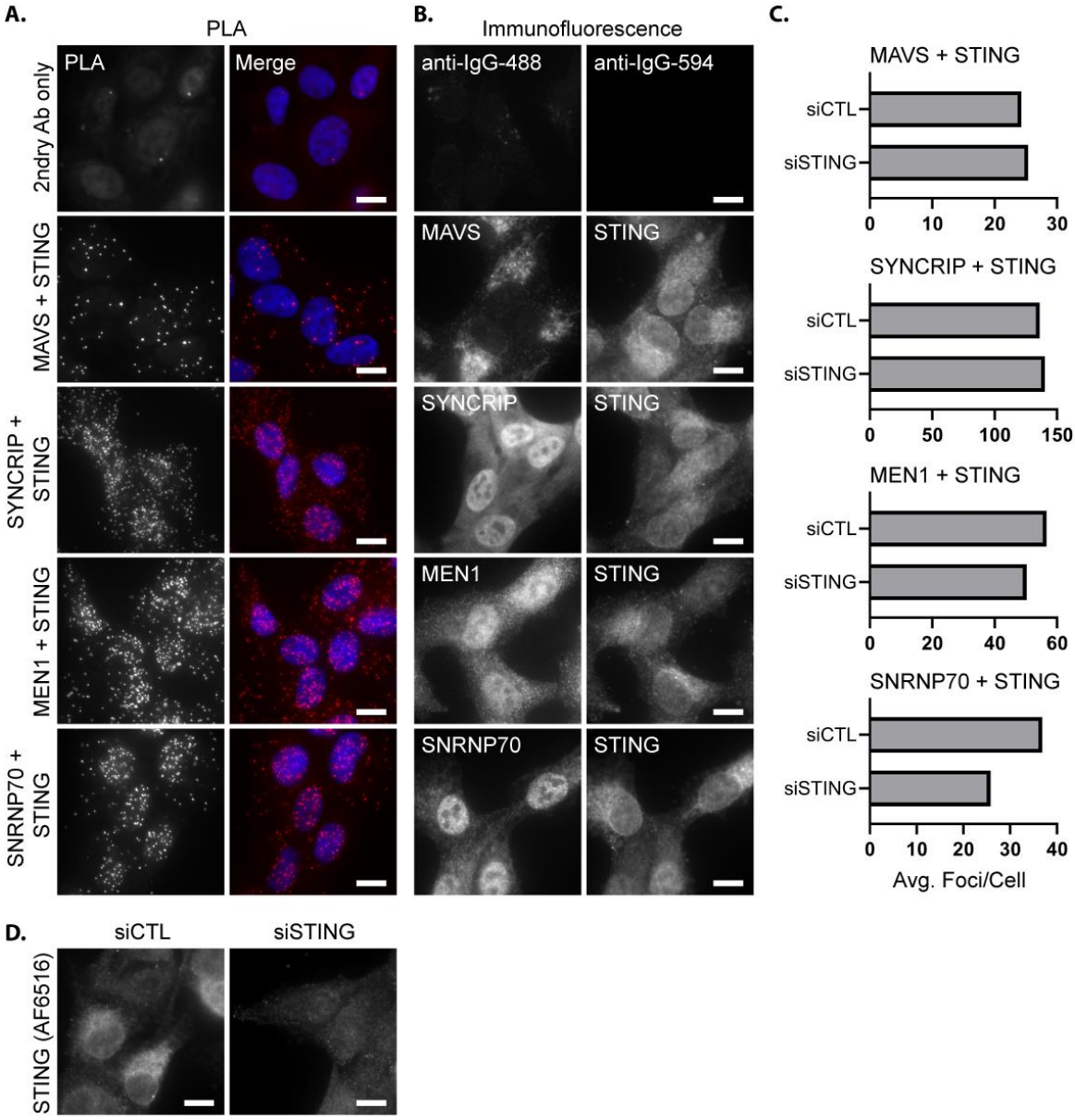

Figure 4.11 – Proximity ligation assay (PLA) suggests STING interacts with NE partners. (A) *Representative micrographs showing PLA foci in cells stained with antibodies against STING and MAVS (positive control) and in cells stained with antibodies against STING and SYNCRIP/MEN1/DDX5, but not in cells stained with secondary antibodies only (technical negative control).* ***(B)*** *Immunofluorescence staining showing expected localisation of STING and partner proteins and minimal background staining from secondary antibodies.* ***(C)*** *Quantification of PLA foci for STING and partners normalised to number of cells (based on DAPI stain) to give average number of PLA foci per cell in cells treated with control siRNA or depleted for STING with siRNAs against STING. > 100 cells and 10 fields of view counted per condition. Data representative of two independent experiments.* ***(D)*** *STING staining with antibody used for PLA confirms a loss of signal in cells treated with siRNAs against STING compared to control siRNA treated cells. Scale = 10 μM.*

4.11 – Redistribution of STING partners in response to stimulation with dsDNA and poly(I:C)

Preliminary work in the lab had suggested that SYNCRIP and MEN1 redistribute to the cytoplasm following immune stimulation with dsDNA or poly(I:C) (data not shown). Since I found that STING redistributes from the INM to ONM following immune stimulation with dsDNA or poly(I:C), it was speculated that STING could be involved in any such redistribution of partner proteins. Moreover, a redistribution of STING partners during an IIR may shed light on how they influence immune signalling. Interestingly, prior reports show that SYNCRIP redistributes from the nucleus to cytoplasm and accumulates in stress granules in response to treatment with phorbol 12-myristate 13-acetate (PMA) or heat shock (Quaresma et al. 2009). While, DDX5 has been shown to redistribute from the nucleus to the cytoplasm during HCV (Goh et al. 2004) and JEV infection (Li et al. 2013a). Therefore, I tested whether STING partners that were found to influence dsDNA or poly(I:C) stimulated IIR redistributed in response to immune stimulation. The nuclear/cytoplasmic distribution of SYNCRIP, MEN1, DDX5, and SNRNP70 was measured by immunofluorescence in mock, dsDNA, and poly(I:C) stimulated cells. The mean intensity values of nuclear localised signal, determined by a binary mask created from thresholding of DAPI signal, or mean intensity values of cytoplasmic signal, determined based on a binary mask created by thresholding partner protein signal minus DAPI binary mask, were measured using ImageJ (NIH). Co-staining with anti-IRF3 antibody was used where compatible with the STING partner antibody to confirm induction of IIR and allow for measurement of protein distribution in immune-stimulated cells only (Figure 4.12).

SYNCRIP was predominantly nuclear in all conditions tested (73.6 % nuclear in mock stimulated cells) but partially redistributed to the cytoplasm in cells stimulated with dsDNA, ~4.3 % more cytoplasmic compared to mock stimulated cells, although such redistribution was only modest, with most of the protein still present in the nucleus (69.3 % nuclear in dsDNA stimulated) (Figure 4.12 A). Since the SYNCRIP antibody recognises multiple SYNCRIP isoforms and the homologous hnRNP R protein, this assay does not show if a particular isoform of SYNCRIP changes distribution and moreover, changes in distribution could be masked by recognition of the nuclear localised hnRNP R. Similarly, MEN1 localised predominantly to the nucleus in all conditions but became slightly more cytoplasmic, ~3.5 %, in cells stimulated with poly(I:C) compared to mock stimulated cells (72.2 % nuclear in mock and 68.7% nuclear in poly(I:C) stimulated cells). No significant change in distribution was seen

in cells stimulated with dsDNA (70.2% nuclear), an unexpected finding given that MEN1 was found to influence IIR stimulated by dsDNA but not poly(I:C) (Figure 4.12 B). DDX5 localisation was not altered by immune stimulation with either dsDNA or poly(I:C), remaining almost entirely nuclear, >80 % nuclear in all conditions (Figure 4.12 C). SNRNP70 was also predominantly localised to the nucleus in all conditions, 66.8 % in mock and 66.3 % in dsDNA stimulated cells but became significantly more nuclear in cells stimulated with poly(I:C), 71.9%, although again this effect was quite modest, ~6.1 % more nuclear (Figure 4.12 D).

That these partners exhibited some redistribution could indicate a potential role of redistribution in IIR signalling as similarly small changes in phosphorylation state of proteins can have dramatic changes in a cellular phenotype. However, without further experimental evidence this remains speculative and the ~5 % shifts in distribution do not provide strong evidence that redistribution is associated with STING partner roles in innate immune signalling. As an alternative approach to measure the nuclear/cytoplasmic distribution of STING partner proteins in unstimulated and immune stimulated cells, nuclear and cytoplasmic fractions could be prepared, and Western blotting performed to determine localisation of partner proteins between nucleus and cytoplasm. This would be particularly informative in the case of SYNCRIP since the antibody used recognises multiple SYNCRIP isoforms which are reported to localise differently between nucleus and cytoplasm, the Q1 isoform is predominantly cytoplasmic while Q2 and Q3 are mostly nuclear, as well as the homologous hnRNP R which is also a nuclear localised protein (Chen et al. 2008; Cappelli et al. 2018).

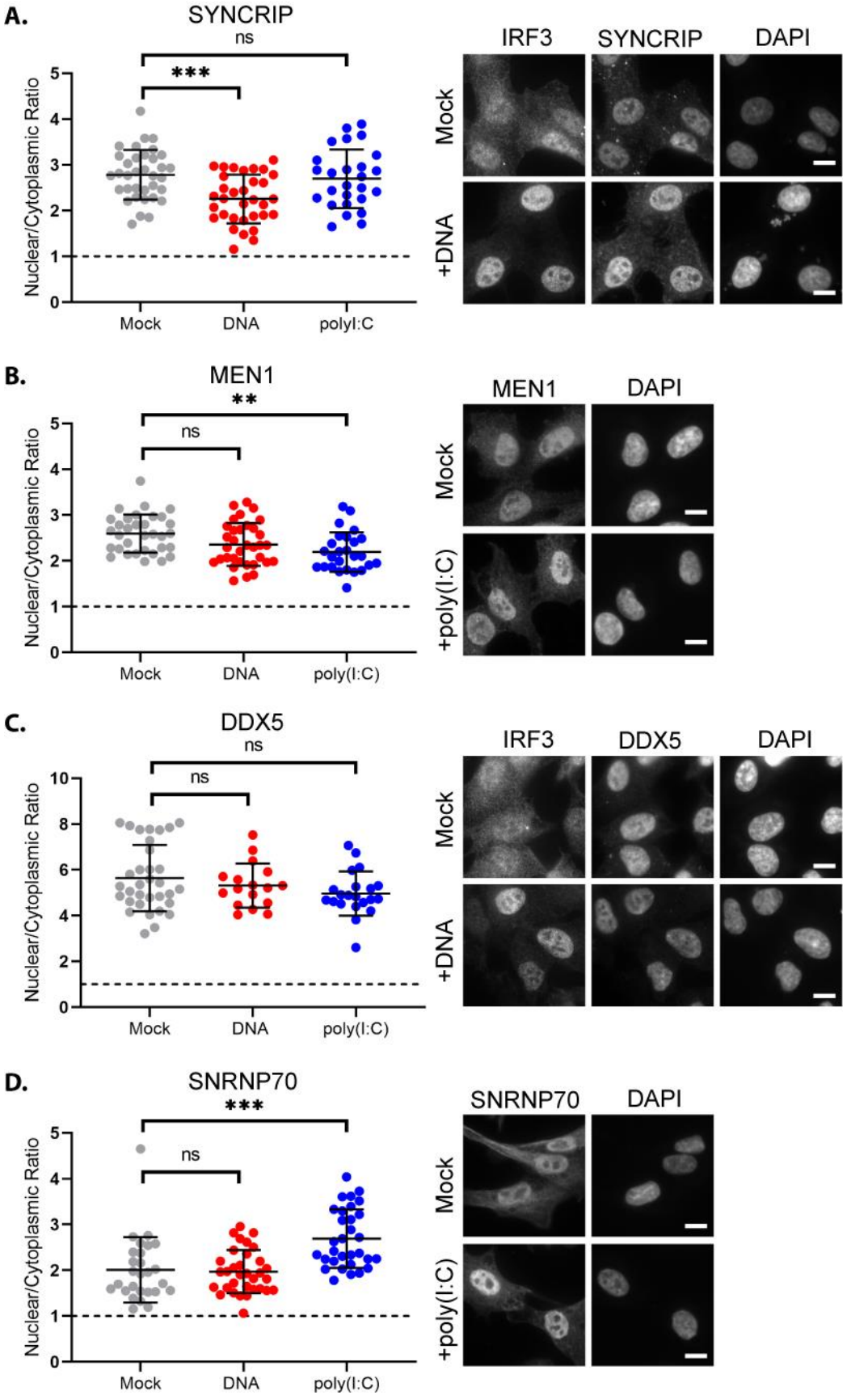
A.
SYNCRIP
ns
***
Nuclear/Cytoplasmic Ratio
Mock
DNA
polyI:C
IRF3
SYNCRIP
DAPI
Mock
+DNA
B.
MEN1
**
ns
Nuclear/Cytoplasmic Ratio
Mock
DNA
poly(I:C)
MEN1
DAPI
Mock
+poly(I:C)
C.
DDX5
ns
ns
Nuclear/Cytoplasmic Ratio
Mock
DNA
poly(I:C)
IRF3
DDX5
DAPI
Mock
+DNA
D.
SNRNP70
***
ns
Nuclear/Cytoplasmic Ratio
Mock
DNA
poly(I:C)
SNRNP70
DAPI
Mock
+poly(I:C)

Figure 4.12 – Nuclear/Cytoplasmic distribution of STING partners in mock and immune stimulated cells. (A) *Nuclear/Cytoplasmic ratio of mean intensity values from SYNCRIP antibody staining in mock, dsDNA, or poly(I:C) stimulated cells (cells fixed 2 h post transfection). Representative micrographs show IRF3 and SYNCRIP staining in mock and dsDNA stimulated cells (nuclear IRF3 staining confirms innate immune stimulation, cells without nuclear IRF3 staining in dsDNA/poly(I:C) transfected cells were not measured).* ***(B)*** *Nuclear/Cytoplasmic ratio of mean intensity values from MEN1 antibody staining in mock, dsDNA, or poly(I:C) stimulated cells (cells fixed 2 h post transfection). Representative micrographs show MEN1 staining.* ***(C)*** *Nuclear/Cytoplasmic ratio of mean intensity values from DDX5 antibody staining in mock, dsDNA, or poly(I:C) stimulated cells (cells fixed 2 h post transfection). Representative micrographs show IRF3 and DDX5 staining.* ***(D)*** *Nuclear/Cytoplasmic ratio of mean intensity values from SNRNP70 antibody staining in mock, dsDNA, or poly(I:C) stimulated cells (cells fixed 2 h post transfection). Representative micrographs show SNRNP70 staining. Ordinary one-way ANOVA with Dunnett's multiple comparisons test. ** $p < 0.01$, *** $p < 0.001$, ns = not significant $p > 0.05$. Error bars show standard deviation. Scale = 10 µM.*

4.12 – Chapter Summary

In this chapter I investigated the role in IIR of several STING partners with potential links to IRF3/7 transcription factors. The most congruent findings show that SYNCRIP is a positive regulator of IIR triggered by dsDNA with SYNCRIP knockdown reducing activation of an NF-κB/AP1 induced luciferase promoter, the activation of IRF3, and the expression of endogenous IFNβ and CCL5. The mechanism through which SYNCRIP mediates these effects remains unclear since an interaction between SYNCRIP and STING through coimmunoprecipitation could not be confirmed, although SYNCRIP and STING PLA indicates the proteins are in close proximity. SYNCRIP partially redistributed to the cytoplasm following immune stimulation with dsDNA but not poly(I:C), and because SYNCRIP effects were specific to dsDNA-stimulated IIR this data suggests that SYNCRIP could modulate the cGAS-STING DNA sensing pathway in the cytoplasm, upstream of IRF3 activation. MEN1 knockdown consistently impaired IIR signalling induced by dsDNA but not poly(I:C), with IRF3 activation and IFNβ and CCL5 expression reduced. That MEN1 knockdown reduced activation of the NF-κB/AP1 luciferase reporter is slightly surprising because MEN1 has been reported to interact directly with and inhibit NF-κB subunits(Heppner et al. 2001). It is possible that MEN1's function in activation of IRF3 is enough to counteract its repression of NF-κB explaining why I find it to be a positive factor for the induction of IFNβ. Since the cGAS-STING pathway primarily drives IRF3 activation over NF-κB activation in humans (de Oliveira Mann et al. 2019), MEN1 could play a role in promoting IRF3 activation while simultaneously depressing

NF-κB to promote this outcome. As for the reduction in NF-κB/AP1 luciferase reporter activation with MEN1 knockdown, it is difficult to explain why NF-κB activity is not higher since it should be derepressed in the absence of MEN1. However, it is possible that most of the activation of this reporter through cGAS-STING activation comes via the AP1 transcription factor family and MEN1 is required for optimal activation of this pathway. DDX5 on the other hand appears to be a negative regulator of IIR, since DDX5 knockdown increased the expression of IFNβ stimulated by both dsDNA and poly(I:C). However, not all assay results agree with DDX5 being a negative regulator in dsDNA stimulated IIR since DDX5 knockdown also impaired activation of IRF3 and both luciferase reporters. These findings could be explained by considering that DDX5 knockdown appeared to cause a partial reduction in STING protein levels and so negative effects of DDX5 knockdown could be an indirect effect of reduced STING levels and impaired cGAS-STING signalling. Knockdown of SNRNP70 consistently impaired IIR stimulated by dsDNA in all assays suggesting that SNRNP70 is a positive factor in the cGAS-STING pathway. Intriguingly SNRNP70 may function antagonistically in IIR triggered by dsRNA since IRF3 activation was increased in SNRNP70 knockdown cells following poly(I:C) stimulation as much as in DDX5 knockdown cells. However, no effect was seen on IFNβ expression in SNRNP70 knockdown cells stimulated with poly(I:C), this could be because the timepoint at which IFNβ expression was measured was too early (4 h) and a difference might be seen at a later timepoint. A function for SNRNP70 in IIR stimulated by dsRNA would be supported by the finding that SNRNP70 becomes significantly more nuclear in cells stimulated with poly(I:C). Evidence from PLA is also strongest for an SNRNP70-STING interaction because the biggest discrepancy in average PLA foci per cell was seen for this pairing between siRNA control and cells treated with siRNAs against STING. Although, co-immunoprecipitation and PLA do not strongly support the interaction between STING and the partner proteins identified by cross-linking immunoprecipitation and mass spectrometry, there is some indication that at least MEN1 and SNRNP70 interact with STING since some MEN1 was pulled down by anti-STING antibody and STING knockdown partially reduced the number of PLA foci for both MEN1-STING and SNRNP70-STING pairs.

While I have demonstrated that SYNCRIP, MEN1, and SNRNP70 are positive regulators of STING mediated IIR stimulated by dsDNA the mechanisms through which they effect IIR have

not been resolved. Likewise, I have shown that DDX5 is a negative regulator of IIR stimulated by dsDNA or poly(I:C) but have not resolved a mechanism through which DDX5 mediates these effects. Future experiments should investigate whether knockdown of these proteins affects levels of STING activation to determine whether they function upstream or downstream of STING. For example, levels of STING dimerization and phosphorylation, hallmarks of STING activation, following immune stimulation with dsDNA should be determined by Western blotting. Additionally, the percentage of cells with STING perinuclear foci, indicative of STING activation, in dsDNA stimulated cells knocked down for STING partners could be measured by immunofluorescence.

Interestingly, DDX5 has recently been reported to be a negative regulator of type-I IFN responses stimulated by infection with the RNA virus, vesicular stomatitis virus (VSV), or the DNA virus, HSV-1, with DDX5 knockdown resulting in significantly higher IFNβ protein levels in mouse peritoneal macrophages infected with these viruses (Zan et al. 2020). My data showing that DDX5 knockdown results in higher levels of IFNβ mRNA following immune stimulation with dsDNA or poly(I:C) and that DDX5 knockdown restricts HSV-1 proliferation agree with this study. Moreover, the authors of this study show that levels of IRF3 phosphorylation are elevated in VSV infected DDX5 knockdown cells in agreement with my data showing that levels of IRF3 phosphorylation are elevated in poly(I:C) stimulated DDX5 knockdown cells. Additionally, the authors identify the serine/threonine-protein phosphatase 2A catalytic subunit β (PP2A-Cβ) as an interactor of DDX5 and IRF3 and propose that DDX5 deactivates IRF3 by recruiting PP2A-Cβ to dephosphorylate IRF3 and thus inhibit type-I IFN responses (Zan et al. 2020). However, the exact molecular mechanism through which this occurs remains to be elucidated.

In order to reveal the direct mechanisms through which NE STING partners influence IIR, future studies should seek to identify interactors of STING partner proteins tested here through immunoprecipitation and mass spectrometry, comparing unstimulated cells to cells stimulated with dsDNA or poly(I:C). Furthermore, direct binding of dsDNA or poly(I:C) by partner proteins should be tested for example, by stimulating cells with biotin labelled dsDNA/poly(I:C) and performing co-immunoprecipitation experiments. Although only DDX5 was found to affect IFNβ induction following immune stimulation with poly(I:C), it is still possible that other STING partners are involved in IIR stimulated by dsRNA but are not

required for IFNβ induction following immune stimulation with poly(I:C) thus, whether they bind to poly(I:C) should be tested. Indeed, STING is required for restriction of many RNA viruses but is not necessary for induction of type-I IFN responses stimulated by poly(I:C). Although, whether STING is required for full induction of type-I IFN during RNA virus infection remains disputed (Ishikawa and Barber 2008; Zhong et al. 2008; Ishikawa et al. 2009; Sun et al. 2009; Sun et al. 2012; Yu et al. 2012; Aguirre et al. 2012; Li et al. 2013b; Holm et al. 2016; Franz et al. 2018). Therefore, it is possible that STING NE partners recognise dsRNA and through STING mediate antiviral effects that are distinct from IFNβ induction.

Poly(I:C) is commonly used as a synthetic analogue of viral dsRNA to stimulate IFN responses and has been shown to primarily stimulate three dsRNA sensors: TLR3, RIG-I, and MDA-5 (Kato et al. 2006; Kato et al. 2008; Dauletbaev et al. 2015; Palchetti et al. 2015). Interestingly, different lengths of poly(I:C) have been shown to principally stimulate different dsRNA sensors with MDA-5 primarily activated by longer poly(I:C) >~1 kb while RIG-I primarily senses shorter lengths of poly(I:C) ~0.3-1 kb (Kato et al. 2008). I tested several formulations of poly(I:C) from different manufacturers and found that all induced the accumulation of IRF3 in the nucleus following transfection (data not shown). When run on an agarose gel these poly(I:C) formulations showed a range of sizes that varied between manufacturers (Figure 4.13). In the end I opted to use a poly(I:C) formulation produced by Sigma-Aldrich which consisted of poly(I:C) of lengths ranging from ~0.5-1.5 kb since this length of poly(I:C) is principally recognised by RIG-I, and STING has been shown to interact with RIG-I but not MDA-5 and thus is proposed to restrict viruses sensed by RIG-I but not those sensed exclusively through MDA-5 (Ishikawa and Barber 2008; Zhong et al. 2008; Ishikawa et al. 2009; Maringer and Fernandez-Sesma 2014; Ran et al. 2014).

In addition to the activation of IRF3, poly(I:C) has also been shown to activate NF-κB driven inflammatory responses in airway epithelial cells (Dauletbaev et al. 2015) or to induce apoptosis in a TLR3 dependent manner in prostate cancer cell lines (Palchetti et al. 2015). Interestingly, the manner in which poly(I:C) is delivered to cells has been shown to effect which response dominates. *Palchetti et al.* found that poly(I:C) transfected using Lipofectamine 2000 or poly(I:C) added alone to cell culture medium is taken up through endocytosis where it sensed by TLR3, before being released into the cytoplasm where it activates RIG-I and MDA-5 sensors in the prostate cancer cell lines, PC3 and DU145. However,

transfected poly(I:C) localises more strongly in endosomes and drives more apoptosis through TLR3 than poly(I:C) delivered to cells without lipofectamine. Conversely, *Dauletbaev et al.* found that poly(I:C) delivered using liposome transfection more readily escaped endosomal compartments to stimulate RIG-I while poly(I:C) delivered without liposome transfection was retained in endosomes and signalled more through TLR3 to activate IRF3 and through an unidentified receptor to activate NF-κB. Thus, cell type used and mechanism of poly(I:C) delivery can activate different signalling pathways. In the future, both mechanisms of poly(I:C) delivery should be compared in the context of STING partner knockdown to determine whether this reveals a requirement of STING partners in signalling through a particular pathway in response to poly(I:C) stimulation. It is possible that differences in poly(I:C) used in experiments explain why I did not see redistribution of SYNCRIP to the cytoplasm following immune stimulation with poly(I:C) which had been described previously in the Schirmer lab (data not shown).

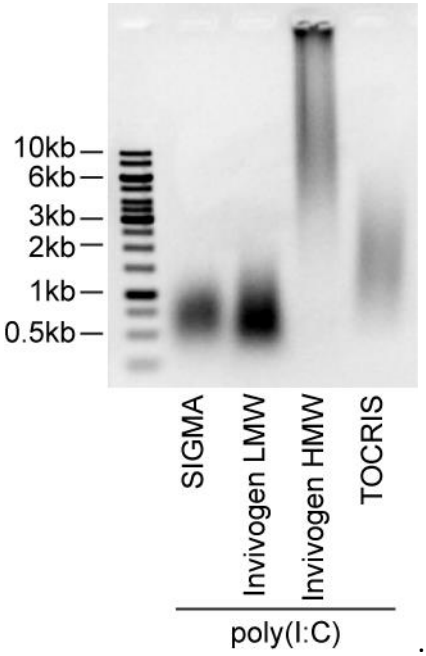

Figure 4.13 – Poly(I:C) displays a range of lengths that vary between manufacturers. (A) *Poly(I:C) purchased from Sigma-Aldrich (SIGMA), InvivoGen (LMW - low molecular weight, HMW - high molecular weight), and Tocris Bioscience was run on an agarose gel to determine the range of lengths of the different poly(I:C) formulations. Poly(I:C) from Sigma-Aldrich was chosen for use in experiments.*

In summary, I have shown that NE STING partners, SYNCRIP, MEN1, and SNRNP70 are novel positive regulators of IIR triggered by dsDNA transfection and that DDX5 is a negative regulator of IIR stimulated by dsDNA or poly(I:C). However, one of the hypotheses at the start

of this chapter was that ***RNA-binding partners of STING in the NE could provide a mechanism through which STING antagonises RNA viruses.*** Since initial results stimulating STING partner knockdown cells with poly(I:C) did not indicate a positive role in regulating IIR for STING partners while in cells stimulated with dsDNA STING partners do play a positive role in regulating IIR, dsDNA triggered immunity was the main focus of this chapter. However, as discussed above just because STING partners are not involved in promoting IFNβ responses stimulated by transfected poly(I:C) does not mean that they do not play a role in STING mediated restriction of RNA viruses, a function that will be explored in the next chapter.

Chapter 5

SYNCRIP is a novel antagonist of influenza A virus (IAV)

5.1 – Introduction

In the previous chapter I explored the role of several NE STING partners in innate immune responses, showing that SYNCRIP, MEN1, and SNRNP70 promote innate immune signalling stimulated by dsDNA and that DDX5 antagonises immune signalling stimulated by dsDNA or poly(I:C). However, none of the partner proteins tested appear to promote immune signalling stimulated by poly(I:C), a dsRNA mimic. This could be taken to refute my initial hypothesis that NE STING partners might be involved in STING's antagonism of RNA viruses since many of them are RNA binding proteins and so could be involved in sensing viral RNA. Nonetheless, it is possible that STING partners could still be involved in the antagonism of RNA viruses despite not being required for IFNβ induction in cells stimulated with poly(I:C) since STING appears to be involved in antagonising RNA viruses through mechanisms independent of IFNβ induction (Ishikawa et al. 2009; Li et al. 2013b; Franz et al. 2018). For example, it has been demonstrated that STING inhibits cellular translation in response to RNA virus infection or poly(I:C) transfection (Franz et al. 2018). Moreover, unlike transfection with poly(I:C), infection with an RNA virus presents the host cell with a more complex immune challenge which can activate STING-mediated signalling through different mechanisms. This includes through the detection of cytoplasmic dsDNA as a result of mitochondrial DNA leakage during infection with the RNA viruses, dengue virus (DENV), encephalomyocarditis virus (ECMV), or influenza A virus (IAV) (Aguirre et al. 2017; Sun et al. 2017; Moriyama et al. 2019), or through the recognition of virus-cell membrane fusion during IAV infection (Holm et al. 2016). Therefore, I proposed to test whether any of the STING partners found to be involved in innate immune signalling stimulated by either dsDNA or poly(I:C) played a role in antagonism of an RNA virus.

Initially, I had wanted to use positive-sense single-stranded (+ssRNA), negative-sense single-stranded (-ssRNA), and double-stranded RNA (dsRNA) viruses for infections, speculating that the different RNA genomes would provide a range of potential ligands to stimulate an innate immune response. However, it proved difficult to locally source multiple viruses and the expertise to work with them and so only IAV was used to test whether any of the STING

partners are involved in restricting RNA virus infection. Influenza viruses are -ssRNA viruses belonging to the *Orthomyxoviridae* family and are the causative agents of the respiratory disease influenza in birds and mammals. Three genera cause disease in humans, with the type A viruses the most virulent and causing the most severe disease. Influenza A viruses also infect birds and pigs, amongst other mammals, which cause them to be particularly dangerous since emergent viruses, which have novel surface glycoproteins against which human populations have little pre-existing immunity, have been known to arise from wild and farm animal reservoirs. The IAV genome is made up of eight -ssRNA segments packaged in viral ribonucleoprotein (vRNP) complexes which encode 10 major polypeptides but also several accessory gene products (Pinto et al. 2020). vRNPs consist of an individual viral RNA strand in an anti-parallel double helix structure bound by the viral polymerase at 5' and 3' ends and coated with nucleoprotein (NP) along its length (Fodor 2013; Te Velthuis and Fodor 2016). During infection, the IAV virion binds to sialic acid containing attachment factors on the cell surface through the viral glycoprotein, haemagglutinin (HA) (Sieben et al. 2020). The virion then enters the cell through endocytosis after engaging receptor-tyrosine kinases such as the epidermal growth factor receptor (EGRF) and is trafficked to the endosome. Within the endosome, the lowered pH causes a conformational change in HA that exposes the HA fusion peptide triggering fusion of viral and endosome membranes. vRNPs are consequently released into the host cell cytoplasm and trafficked to the nucleus where replication and transcription occur (Samji 2009; Dou et al. 2018). Replication within the nucleus is uncommon for an RNA virus but is part of what made using IAV to test whether NE STING partners restrict RNA viral proliferation more appealing, since a nuclear localisation of a viral RNA sensor could more readily allow for detection of IAV infection.

Like all viruses, influenza viruses seek to antagonise the host innate immune response to allow for more successful replication and spread. Thus, much work has already been done on how the virus targets host proteins to inhibit the innate immune response. The non-structural protein 1 (NS1) encoded by influenza viruses is the major antagonist of host cell immune responses, primarily through repression of the type-I/III IFN response (Ayllon and García-Sastre 2015). NS1 consists of two functionally distinct domains joined by a short linker region, an N-terminal dsRNA binding domain (amino acids 1-73) and a C-terminal effector domain required for multiple protein-protein interactions (amino acids 85-end). Research indicates

that NS1 exerts its antagonistic effects at multiple levels in the IFN response signalling pathway triggered by cytosolic dsRNA: through inhibition of RIG-I signalling preventing IRF3 and NF-κB activation; through binding CPSF30 to inhibit cellular mRNA polyadenylation and thereby the expression of cellular genes such as IFN; and by preventing activation of protein kinase R (PKR) and 2'-5'-oligo-adenylate synthetase (OAS) host immune response proteins (Ayllon and García-Sastre 2015).

RIG-I is a key PRR which recognises cytoplasmic dsRNAs with 5'-triphosphates and upon activation binds to the MAVS adaptor protein, leading to the activation of IRF3, NF-κB, and AP1 (c-Jun/ATF-2) transcription factors which are critical for the induction of IFN gene expression (Yoneyama and Fujita 2009). RIG-I activation requires ubiquitination by the E3 ubiquitin ligases TRIM25 (Gack et al. 2007) and RIPLET (Oshiumi et al. 2009) resulting in RIG-I oligomerisation and subsequent interaction with MAVS through the caspase activation and recruitment domains (CARDs) of both RIG-I and MAVS (Hou et al. 2011). IAV NS1 has been shown to bind TRIM25 (Gack et al. 2007) and RIPLET (Rajsbaum et al. 2012) thereby suppressing RIG-I ubiquitination and downstream signalling. However, not all IAV strains efficiently block RIG-I mediated signalling and IFNβ transcription. Specifically, NS1 proteins from seasonal H3N2 and H2N2 viruses do not block activation of IRF3 and IFNβ transcription, while the NS1 proteins from H5N1 viruses and some seasonal H1N1 viruses do block IRF3 activation and IFNβ transcription (Kuo et al. 2010). Intriguingly, TRIM25 binding activity is retained by NS1 proteins that do not suppress RIG-I signalling demonstrating that TRIM25 binding does not always lead to inhibition of IRF3 activation (Kuo et al. 2010)

As another means of suppressing the IFN response, the NS1 protein of several strains of IAV bind to the CPSF30 protein which is required for polyadenylation of host pre-mRNAs and production of mature mRNAs. In doing so NS1 blocks the production of IFNβ and other antiviral proteins since pre-mRNAs cannot be processed and therefore no translation can occur (Nemeroff et al. 1998; Noah et al. 2003). However, the NS1 proteins encoded by some H1N1 strains lack this ability and so rely on suppression of RIG-I signalling to inhibit IFN production (Kochs et al. 2007; Ayllon and García-Sastre 2015).

NS1 has also been shown to inhibit the activity of other antiviral proteins including PKR and OAS. PKR belongs to a family of eukaryotic translation initiation factor 2-alpha (eIF2α) kinases which phosphorylate eIF2α in response to a range of stimuli thereby inhibiting translation.

PKR is constitutively expressed in a latent form that is activated upon dsRNA binding leading to translational inhibition (Bevilacqua and Cech 1996). Moreover, PKR is also an interferon stimulated gene, so its expression is increased following stimulation with IFN. In addition to antagonising RNA virus infection through translational repression, PKR appears to be required for optimal IFNβ induction through RIG-I/MDA-5-MAVS signalling pathways (Pfaller et al. 2011; Hur 2019). NS1 binds PKR through an interaction that involves NS1 residues 123-127 which is thought to prevent the activating conformational change that occurs in PKR following dsRNA binding (Li et al. 2006; Min et al. 2007). OAS is another interferon stimulated gene which upon activation by dsRNA binding synthesises 2'-5'-oligoadenylate chains that activate latent RNase L. Active RNase L degrades ssRNA in the cytoplasm restricting viral proliferation (Hornung et al. 2014) and in turn RNA fragments generated by RNase L may serve as ligands of the RIG-I-MAVS pathway, amplifying antiviral signalling (Malathi et al. 2007). NS1 does not directly bind to OAS or RNase L but it is proposed that NS1 sequesters dsRNA ligands away from OAS preventing its activation, since the replication of an IAV encoding an NS1 RNA-binding mutant (R38A) is enhanced in the absence of RNase L (Min and Krug 2006).

In this chapter, I first tested if HT1080 cells are competent for IAV infection and proliferation since I had established that this cell line has a functional cGAS-STING pathway, and then used this to confirm findings from previous studies that STING restricts IAV. Subsequent screening of NE STING partners for an effect on IAV infection identified SYNCRIP as a novel restriction factor of IAV. Because SYNCRIP has multiple splice variants and it was difficult to be certain that all splice forms were knocked down by siRNA treatment, I further generated a *SYNCRIP*$^{-/-}$ HT1080 cell line by CRISPR/Cas9 gene editing that confirmed that SYNCRIP restricts IAV in HT1080 cells. I also tested STING and SYNCRIP for an interaction during infection with IAV by co-immunoprecipitation and tested by RNA-immunoprecipitation whether SYNCRIP or STING bind viral RNA. SYNCRIP levels and localisation were also measured over the course of infection as this could inform on SYNCRIP function during infection.

5.2 – IAV infects and replicates in HT1080 cells

Since HT1080 cells had been used for most assays assessing whether STING partners contribute to innate immune response and confirmed to have a functional cGAS-STING pathway it would be ideal to use them for IAV infection experiments. However, IAV typically infects cells of the respiratory system and most *in vitro* models use lung cell lines; so whether

IAV would infect HT1080 cells, a fibrosarcoma cell line, was not known. Therefore, I first tested whether the mouse-adapted strain of IAV, A/Puerto Rico/8/1934 H1N1 (referred to as PR8 from now on), would infect and proliferate in HT1080 cells (Figure 5.1 A). After 24 h cell supernatants contained significantly more virus as measured by an increase in the number of plaque-forming units (PFU) per mL, demonstrating that IAV replicated and produced progeny virus in HT1080 cells (Figure 5.1 A and B). IAV infection in HT1080 cells was also visualised by immunofluorescence using antibody against viral protein NP (Figure 5.1 C). Earlier during infection NP staining was mostly localised to the nucleus indicating vRNA replication and transcription are taking place, while at later timepoints during infection NP staining mostly localised to the cytoplasm indicative of assembly of progeny virions as would be expected with productive IAV infection. Western blotting against viral proteins, NP and NS1, in IAV infected lysates collected at the indicated timepoints during infection also shows that IAV replicates in HT1080 cells (Figure 5.1 D).

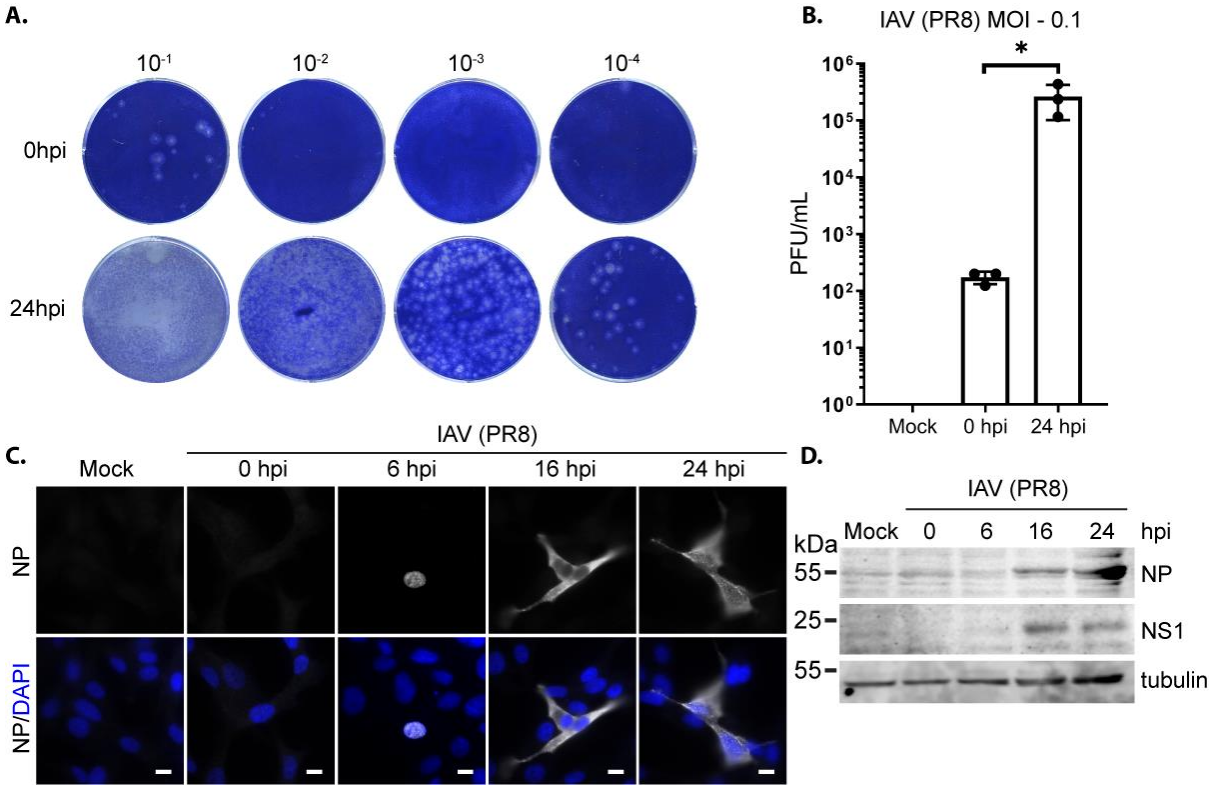

Figure 5.1 – Influenza A virus (IAV) infects and proliferates in HT1080 cells. (A) *Example plaque assay showing formation of viral plaques on a confluent monolayer of MDCK cells stained with toluidine blue. Serial dilution of supernatant from infected HT1080 cells collected at 0 and 24 hours post infection (hpi) shows that supernatants collected at 24 hpi contain > 1000x more infectious particles than at 0 hpi.* ***(B)*** *Quantitation of plaque forming units (PFU) per mL of supernatant calculated from plaque assays such as those shown in (A) shows that*

*PR8 infects and proliferates in HT1080 cells. PFU is calculated by counting the number of plaques at a dilution that yields between 10 and 100 plaques divided by the dilution factor, D, of that well multiplied by the volume, V, of diluted virus added to each well during the plaque assay (PFU/mL = no. of plaques/(D x V). MOI is multiplicity of infection, the number of PFU per cell used in initial infection. Unpaired t-test, * $p < 0.05$, $n = 3$.* ***(C)*** *Immunofluorescence micrographs showing infection of HT1080 cells with IAV (PR8) MOI – 1, NP is viral nucleoprotein expressed only in infected cells. Scale = 10 µM.* ***(D)*** *Western blotting of HT1080 cell lysates collected at multiple time points during infection show successful viral infection with infected cells expressing viral proteins NP and NS1, MOI – 1.*

5.3 – STING restricts IAV growth in HT1080 cells

STING knockdown enhances IAV replication in murine embryonic fibroblasts (MEFs) (Franz et al. 2018) and chicken DF-1 cells (Cheng et al. 2015), and IAV titres are significantly higher in the lungs of infected STING knockout mice compared to wild type mice (Moriyama et al. 2019). However, whether STING knockdown results in higher viral titres in IAV infected human cells has not been tested, although since IAV infection has been shown to activate STING dependent IFN induction in human cell lines (Holm et al. 2016; Moriyama et al. 2019) it is expected that STING knockdown would result in higher IAV titres compared to control siRNA treated cells. Indeed, in HT1080 cells treated with siRNAs against STING and infected with IAV (PR8) titres were significantly higher 16 hpi compared to control cells (Figure 5.2 A). Interestingly, this appears to be a strain specific effect since in cells infected with IAV strain, A/Udorn/1972 (H3N2) (referred to as Udorn from now on), no significant difference was seen in viral titres from infected cells treated with control or STING-specific siRNAs (Figure 5.2 B). This could be as a result of differences in how the NS1 proteins of PR8 and Udorn strains antagonise the IFN response. The NS1 of Udorn is able to bind to CPSF30 and therefore prevent translation of host mRNAs such as IFN whereas the NS1 of PR8 lacks this binding capability (Kochs et al. 2007; Ayllon and García-Sastre 2015). Instead PR8 NS1 primarily exerts it negative effects on IFN induction through inhibiting RIG-I signalling (Mibayashi et al. 2007; Opitz et al. 2007). Conversely, Udorn NS1 does not inhibit RIG-I signalling and IRF3 activation (Kuo et al. 2010; Krug 2015). In Udorn infected cells any STING-mediated antagonism of viral growth is presumably inhibited by NS1; so whether or not STING is present does not affect viral proliferation, whereas in PR8 infection STING is able to restrict viral growth through mechanisms which are not successfully overcome by PR8 NS1.

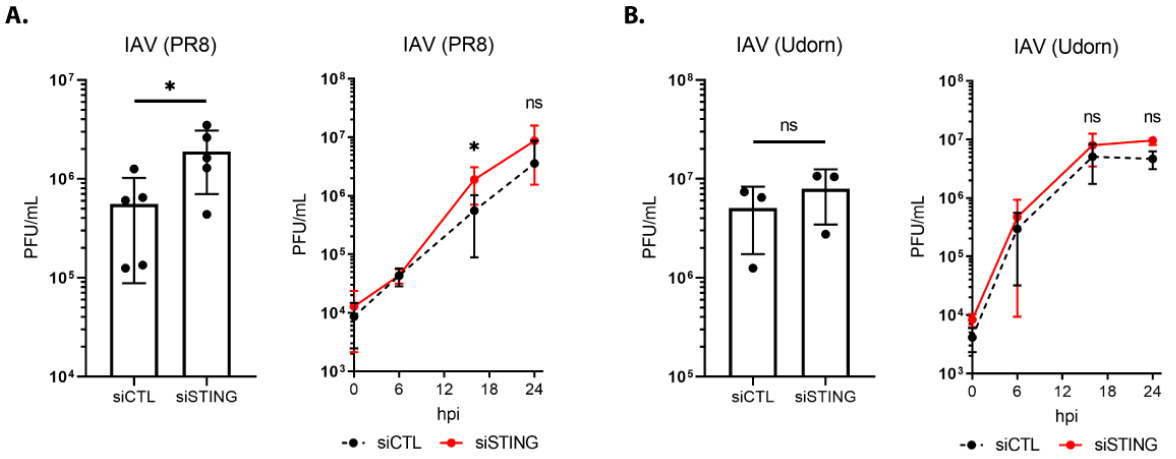

Figure 5.2 – STING restricts influenza A virus (IAV) strain PR8 but not Udorn. (A) *PR8 viral titres from infected control (siCTL) and STING knockdown (siSTING) HT1080 cells show that titres are significantly higher 16 hours post infection (hpi) in siSTING cells compared to siCTL cells (bar chart, left panel). Time course experiment shows viral growth in siCTL and siSTING cells (right panel). MOI – 3. Unpaired t-test, * $p < 0.05$, $n = 5$* ***(B)*** *Udorn viral titres from infected siCTL and siSTING cells show that titres are unaffected at 16 hpi in siSTING cells compared to siCTL cells (bar chart, left panel). Time course experiment shows viral growth in siCTL and siSTING cells (right panel). MOI – 3. Unpaired t-test, NS (not significant) $p > 0.05$, $n = 3$.*

5.4 – SYNCRIP restricts IAV growth in HT1080 cells

With IAV confirmed to proliferate in HT1080 cells and STING knockdown shown to increase IAV PR8 titres in infected cells, I next tested whether any NE STING partners, found to have a role in innate immune responses in the previous chapter, also had an effect of IAV proliferation. HT1080 cells treated with siRNAs against STING partners were infected with PR8 at an MOI of 0.01 and viral titres in cell culture supernatants measured at 24 hpi. Titres from cells treated with siRNA against SYNCRIP were significantly higher (~3.5x) than from cells treated with control siRNA (Figure 5.3 A). Infections were initially performed using a low MOI so that not all cells were infected allowing for multiple rounds of viral growth cycles and subsequent infections of uninfected cells in the culture. However, titres from HT1080 cells treated with siRNAs against STING partners and infected with IAV at low MOI were quite low (< 10,000 PFU/mL at 24 hpi). Therefore, the effect of SYNCRIP knockdown on IAV proliferation was separately confirmed in cells infected at a higher MOI of 3 in which all cells in the culture should be simultaneously infected. Titres from cells treated with siRNA against SYNCRIP were significantly higher (~3x) than from cells treated with control siRNA at 16 hpi in cells infected with PR8 at MOI of 3 (Figure 5.3 B).

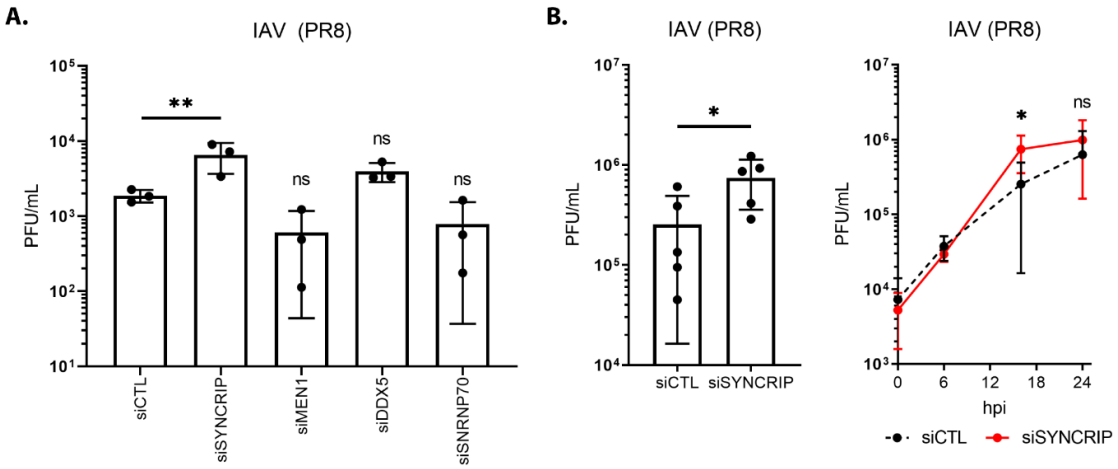

Figure 5.3 – STING partner SYNCRIP restricts influenza A virus (IAV) strain PR8. (A) *PR8 viral titres measured from infected control (siCTL) and STING partner knockdown HT1080 cells show that titres are significantly higher at 24 hours post infection (hpi) in SYNCRIP knockdown cells compared to siCTL cells. MOI – 0.1. Ordinary one-way ANOVA with Dunnett's multiple comparisons test. ** p < 0.01, ns (not significant) p > 0.05. n = 3.* ***(B)*** *PR8 viral titres measured from infected control (siCTL) and SYNCRIP knockdown (siSYNCRIP) HT1080 cells confirms that titres are significantly higher in SYNCRIP knockdown cells compared to siCTL cells in at 16 hpi in cells infected at a higher MOI of 3 (Bar chart, left panel). Time course experiment shows viral growth in siCTL and siSYNCRIP cells (right panel). MOI – 3. Unpaired t-test. * p < 0.05, ns (not significant) p > 0.05.*

5.5 – SYNCRIP knockdown effect on IAV titres is increased in cells infected with IAV (PR8) NS1 mutants

Since IAV is able to antagonise the host cell immune response it is possible that SYNCRIP antiviral effects are reduced by the virus. NS1 is the principal protein used by IAV to antagonise the host cell defences and so SYNCRIP knockdown cells were also infected with PR8 NS1 mutant viruses. Both a virus encoding a mutant NS1 in which the R38 and K41 residues are mutated to alanine (R38K41A) and a virus encoding an NS1 truncation mutant with only the first 81 amino acids (N81) grew to higher titres in SYNCRIP knockdown cells than control cells, when compared to cells infected with PR8 with wild type NS1, ~4x and ~6x higher for R38K41A and N81 mutants respectively (Figure 5.4). Although an unpaired t-test comparing mean titres in SYNCRIP and control knockdown cells infected with R38K41A gives a p value just above the 0.05 threshold of significance (Figure 5.4 A), a ratio-paired t-test gives a strongly significant difference (p = 0.0008). This difference in significance with different tests is due to a large variance in the titre values between biological repeats for both control and SYNCRIP knockdown samples. Since SYNCRIP knockdown titres are consistently ~4x higher than control titres for each biological repeat, the ratio-paired t-test is an appropriate

statistical test to perform and supports a significant difference between samples. Interestingly the difference in IAV titres between SYNCRIP and control knockdown samples was greatest for the N81 NS1 mutant (Figure 5.4 B). The R38K41A NS1 mutant lacks capability for dsRNA binding and is unable to interact with RIG-I, TRIM25 and RIPLET, greatly diminishing its ability to block IFN production (Wang et al. 1999; Rajsbaum et al. 2012; Ayllon and García-Sastre 2015). Conversely the N81 NS1 mutant is able to bind dsRNA but lacks the entire effector domain which is required for most protein-protein interactions including with TRIM25 and PKR, impairing its ability to restrict IFN production. That the difference in mutant virus titres between control and SYNCRIP knockdown cells (~4x higher R38K41A, ~6x higher N81) is increased relative to the difference in wild type PR8 titres between control and SYNCRIP knockdown cells (~3x higher) suggests that SYNCRIP could be partially involved in the RIG-I signalling pathway since both mutant viruses lack the ability to impair RIG-I signalling. The N81 virus is also impaired in its ability to antagonise PKR which may explain why the difference in N81 titres is even greater between control and SYNCRIP knockdown cells (Li et al. 2006; Min et al. 2007) and could suggest that SYNCRIP is also involved in PKR mediated viral antagonism.

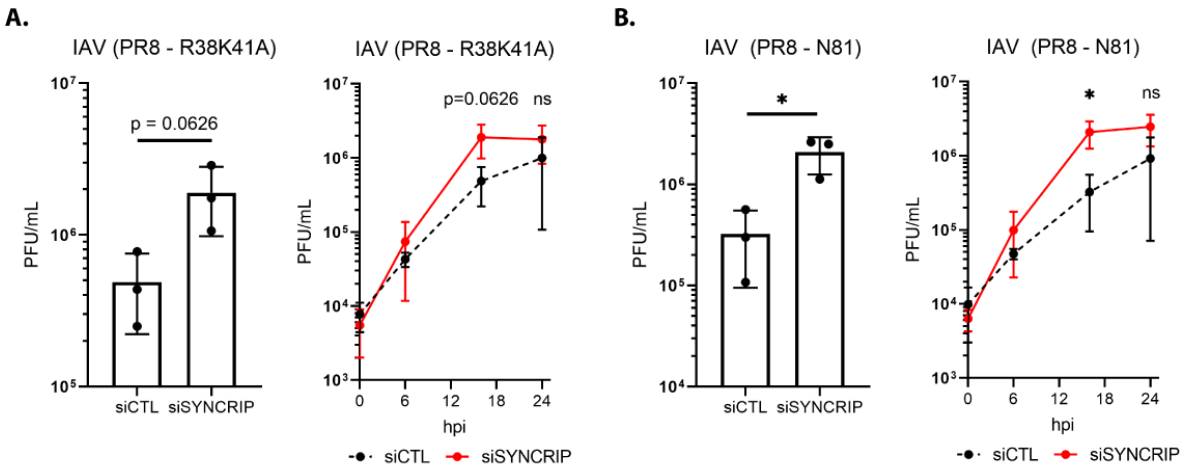

Figure 5.4 – Effect of SYNCRIP knockdown on influenza A virus (IAV) titres is increased in HT1080 cells infected with PR8 encoding NS1 mutants. *PR8 viruses encoding mutant NS1 proteins R38K41A* ***(A)*** *and N81* ***(B)*** *grow to significantly higher titres in SYNCRIP knockdown cells compared to control knockdown cells (siCTL) at 16 hpi (bar charts, left panels), ~4x higher for R38K41A and ~6x higher for N81 mutant viruses. Time course experiments shows viral growth in siCTL and siSYNCRIP cells (right panels). MOI – 3. Unpaired t-test. * $p < 0.05$, ns (not significant) $p > 0.05$. $n = 3$.*

5.6 – Simultaneous knockdown of SYNCRIP and STING increases IAV titres compared to knockdown of STING alone

Since knockdown of STING increased viral titres of PR8 but not Udorn infected cells, whether knockdown of SYNCRIP affects proliferation of the Udorn was also tested. Amongst other differences with PR8, Udorn expresses an NS1 protein capable of binding CPSF30 and in doing so inhibiting cellular translation. Similar to knockdown of STING, SYNCRIP knockdown did not have a significant effect on Udorn proliferation 16 hpi in in HT1080 cells infected with an MOI of 3 (Figure 5.5 A). This could suggest that STING and SYNCRIP restrict IAV through related mechanisms, although it is also possible that Udorn is able to overcome separate inhibitory effects of both proteins. To test whether SYNCRIP and STING restrict IAV through the same pathway, simultaneous knockdown of SYNCRIP and STING was tested for an effect on PR8 proliferation. In cells treated with siRNAs against SYNCRIP and STING PR8 grew to significantly higher titres (ratio-paired t-test) compared to cells treated with control and STING siRNAs (Figure 5.5 B). This suggests that SYNCRIP at least partially restricts IAV independently of STING. However, it is also possible that SYNCRIP exerts antiviral effects through multiple mechanisms only some of which are dependent on STING. Simultaneous knockdown of STING and SYNCRIP was confirmed by Western blotting (Figure 5.5 C). It should be noted that STING protein levels in SYNCRIP and STING double knockdown cells are slightly lower than in control siRNA and STING knockdown cells. Thus, another possible explanation for the increase in IAV titres seen in SYNCRIP and STING double knockdown cells compared to STING only knockdown cells could be a result of further STING protein reduction in the double knockdown cells.

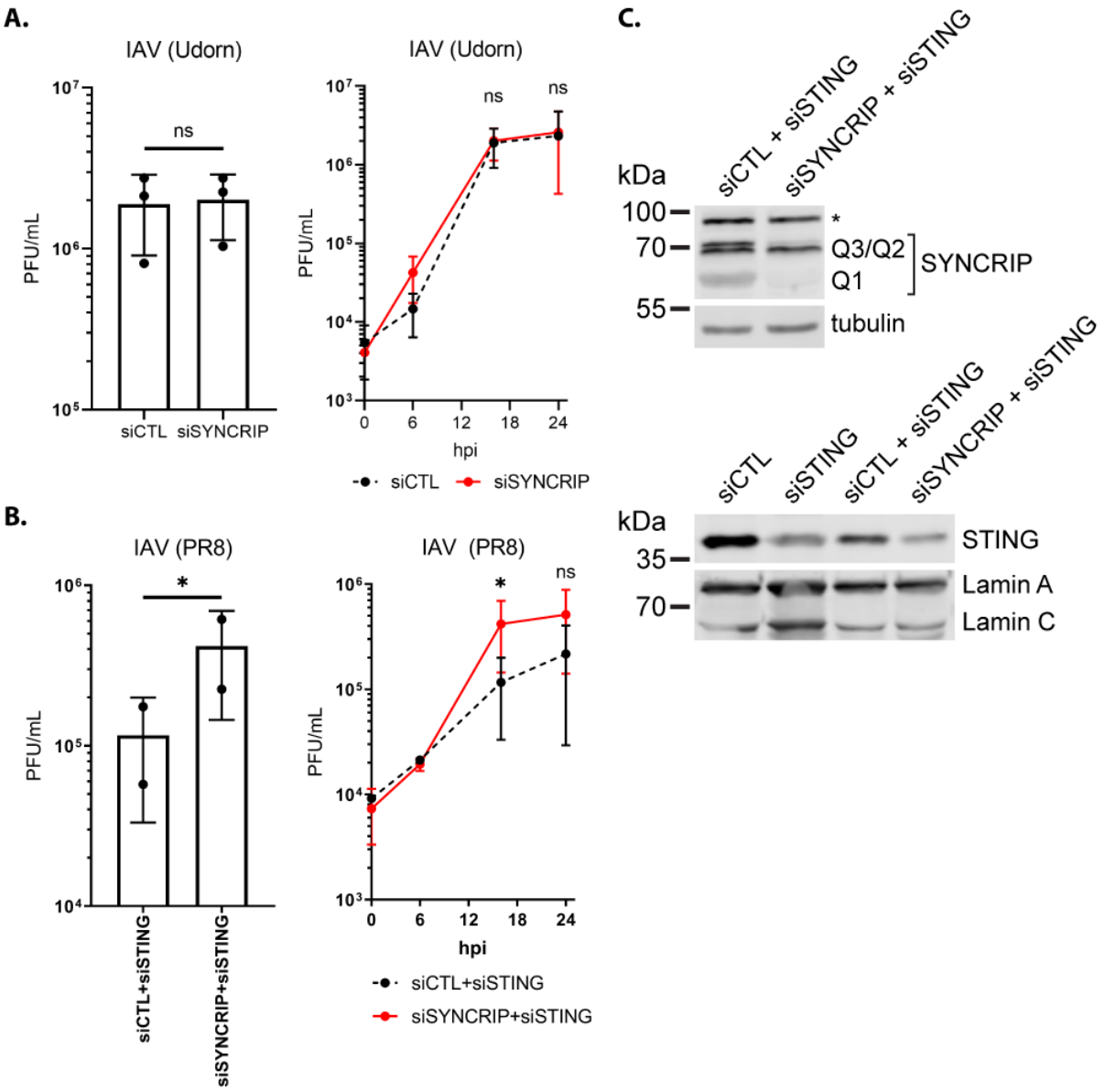

Figure 5.5 – Dual knockdown of SYNCRIP and STING results in higher viral titres compared to STING knockdown alone. (A) *Udorn titres are not significantly higher in SYNCRIP knockdown cells (siSYNCRIP) compared to control knockdown (siCTL) cells at 16 hpi (bar chart, left panel). Time course experiment shows viral growth in siCTL and siSYNCRIP cells (right panel). MOI – 3. Unpaired t-test. ns (not significant) p > 0.05. n = 3.* ***(B)*** *Simultaneous knockdown of STING and SYNCRIP result in higher viral titres (IAV PR8) compared to STING knockdown cells at 16 hpi (bar chart, left panel). Time course experiment shows viral growth in STING and SYNCRIP knockdown cells compared to STING only knockdown cells (right panel). MOI – 3. Ratio-paired t-test. * p < 0.05. n = 2.* ***(C)*** *Western blotting confirms knockdown of SYNCRIP (top) and STING (bottom) in dual knockdown cells, * indicates probable hnRNP R band.*

5.7 – An interaction between SYNCRIP and STING during IAV infection cannot be identified by immunoprecipitation

Although I was unable to see an interaction between SYNCRIP and STING by co-immunoprecipitation of endogenous proteins (Figure 4.10) this could reflect that the interaction identified in initial the mass spectrometry experiment used to identify NE STING partners was pushed by overexpression of STING and possible altered interactions of the STING-GFP. It is also possible that since a reverse cross-linking approach was used the interactions are quite indirect and this was only picked up because another protein that binds STING directly also binds another protein that binds SYNCRIP directly. However, it is also possible that a more direct interaction occurs that is just transient or happens under certain conditions such as virus infection. If this latter possibility was true, then infection with IAV might drive a STING-SYNCRIP interaction. Therefore, immunoprecipitation with STING or SYNCRIP antibodies was performed on whole cell lysates from mock or IAV (PR8) infected HT1080 cells 3 hpi. Endogenous STING and SYNCRIP did not co-immunoprecipitate one another even with IAV infection (Figure 5.6 A). It is possible that an interaction between SYNCRIP and STING cannot be seen by immunoprecipitation against endogenous proteins but might be seen with overexpressed proteins. Therefore, FLAG-tagged SYNCRIP constructs of isoforms Q1 and Q3, which were the isoforms most depleted by SYNCRIP siRNA treatment, were overexpressed in HEK293T cells along with a STING-GFP construct (in order to more closely follow the experimental set-up used in the mass spectrometry experiment) and whole cell lysates were used for immunoprecipitation. Western blotting using an anti-FLAG antibody confirmed that SYNCRIP-FLAG constructs were expressed and produced proteins of the expected molecular weight for both SYNCRIP Q1 and Q3 isofroms, ~66 kDa and ~73 kDa respectively (Lamin A expected molecular weight ~70 kDa) (Figure 5.6 B). Immunoprecipitation was then performed using anti-FLAG and anti-GFP antibody on HEK293T cell lysates from mock and IAV infected cells transiently overexpressing STING-GFP and SYNCRIP Q1-FLAG (Figure 5.6 C) or SYNCRIP Q3-FLAG (Figure 5.6 D). No co-immunoprecipitation was evident from cells overexpressing STING-GFP and either FLAG-tagged SYNCRIP isoforms. Immunoprecipitation and Western blotting in non-transfected cells confirmed specificity of antibodies used for immunoprecipitation (Figure 5.6 E).

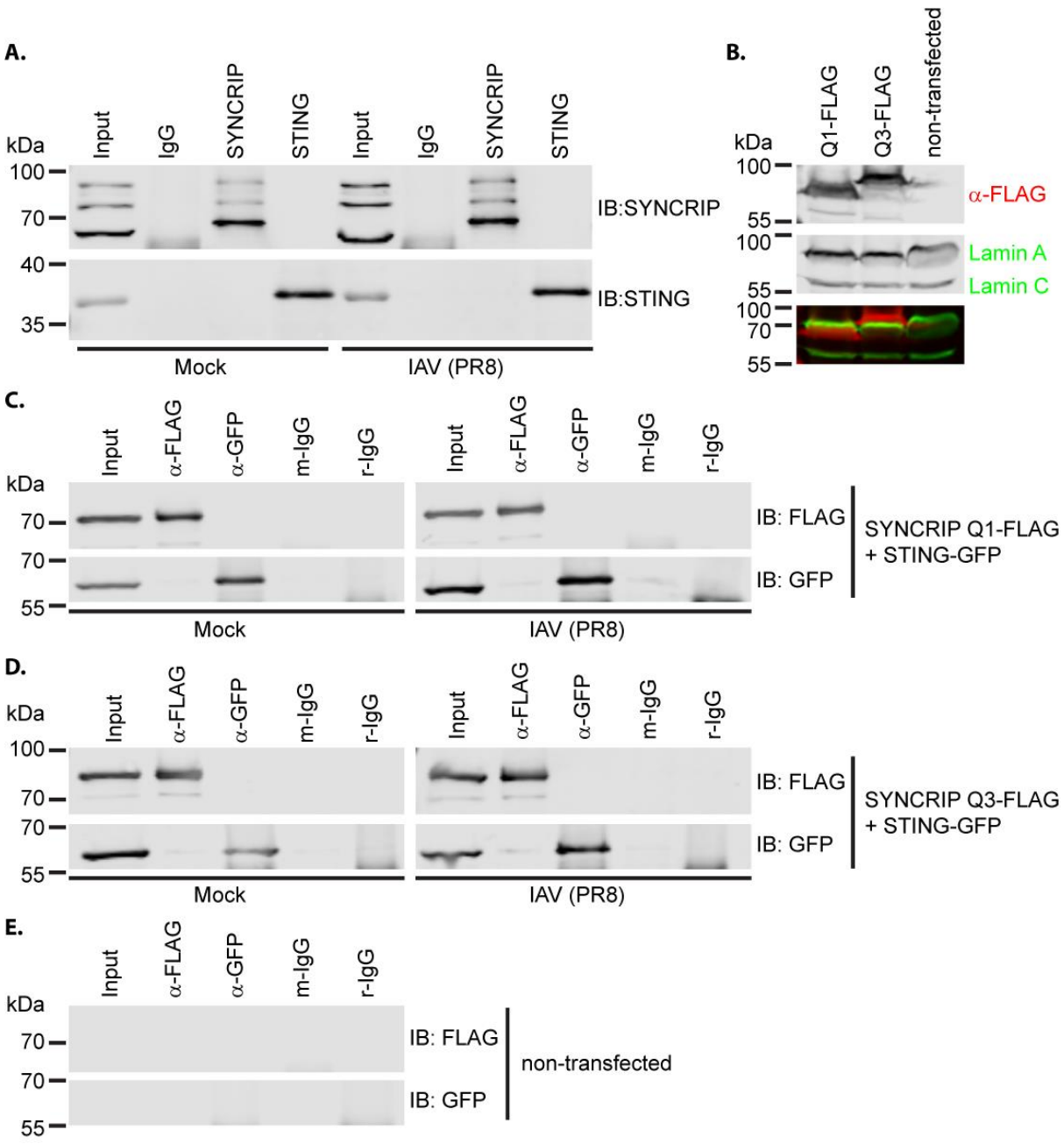

Figure 5.6 – Co-immunoprecipitation experiments do not show an interaction between SYNCRIP and STING during influenza A virus (PR8) infection. (A) *Endogenous SYNCRIP and STING do not co-immunoprecipitate in IAV (PR8) infected HT1080 whole cell lysates.* ***(B)*** *Western blotting confirms expression of FLAG-tagged SYNCRIP isoforms Q1 and Q3 in HEK293T cells.* ***(C)*** *SYNCRIP Q1-FLAG and STING-GFP do not co-immunoprecipitate in mock or IAV (PR8) infected HEK293T whole cell lysates.* ***(D)*** *SYNCRIP Q3-FLAG and STING-GFP do not co-immunoprecipitate in mock or IAV (PR8) infected HEK293T whole cell lysates. Cells infected with IAV (PR8) at MOI of 5 and whole cell lysates collected at 3 hours post infection. MOI of 5 was used to be confident that all cells in culture were infected with IAV* ***(E)*** *FLAG and GFP antibodies do not recognise proteins in non-transfected HEK293T whole cell lysates (same conditions used for fluorescence detection as (C and D) and brightness/contrast levels equally adjusted).*

5.8 – SYNCRIP and STING do not bind IAV mRNAs from segment 5 and 7

SYNCRIP is a conserved RNA-binding protein involved in a number of fundamental RNA processes including pre-mRNA splicing (Mourelatos et al. 2001; Chen et al. 2008), mRNA editing (Blanc et al. 2001), mRNA transport (Bannai et al. 2004; Kanai et al. 2004), translation (Kim et al. 2012), and mRNA degradation (Kuchler et al. 2014). Functionally, SYNCRIP binds to a diverse range of RNA sequences including, polyA sequences (Svitkin et al. 2013), UCUAUC-containing splicing regulatory elements (Kabat et al. 2009), and GGCU/A sequences present in a subset of miRNAs that are sorted into exosomes by a mechanism dependent on SYNCRIP (Santangelo et al. 2016; Hobor et al. 2018). More specifically in the context of RNA virus infection, SYNCRIP has been shown to bind to hepatitis C virus (HCV) (Kim et al. 2004; Liu et al. 2009) and murine hepatitis virus (MHV) RNA (Choi et al. 2004), although in these viruses it plays a pro-viral role promoting viral RNA translation (HCV) and replication (HCV and MHV). Therefore, I postulated that SYNCRIP may bind to IAV RNA and since SYNCRIP knockdown promotes IAV infection that SYNCRIP binding of IAV RNA could restrict viral infection, potentially through activating STING signalling. As a way to assess whether SYNCRIP or STING bind viral RNA during IAV infection, a native RNA immunoprecipitation (RIP) assay was performed. Since both SYNCRIP and STING antibodies successfully immunoprecipitate their target proteins (Figure 5.6 A), antibodies against endogenous proteins were used. STING has been reported not to bind the dsRNA mimic, poly(I:C), and so it was principally included as a negative control, however, whether STING binds IAV RNA has never been directly tested so it is possible STING could bind to specific viral RNA features or sequences. Cell lysates were collected from mock and IAV infected cells (3 hpi, MOI of 5) and immunoprecipitation performed in the presence of RNase inhibitors. Total RNA was isolated using TRIzol reagent and mRNA subject to reverse transcription to make cDNA. Primers were designed against two different IAV genome segments, segment 5 and segment 7 which encode NP and M1/M2 proteins respectively, and PCR performed to produce specific amplicons for segment 5 (1, 1.5, and 0.5 kb) and segment 7 (0.75 and 1 kb). Primers were designed against segment 5 and 7 RNAs specifically since NP and M1 proteins are particularly abundant during IAV infection with NP required for packaging of the viral genome and M1 protein forming the matrix underlying the viral envelope, thus segment 5 and 7 mRNAs were also predicted to be more abundant

(Dou et al. 2018). All primer pairs successfully produced amplicons of expected size for both segments 5 and 7 as shown by a discreet band identified in input lanes of IAV infected cell lysates but not mock infected cells (black arrowheads - Figure 5.7 A, segment 5 and Figure 5.7 B, segment 7). However, no amplicons were detected by PCR in either SYNCRIP or STING immunoprecipitation lanes indicating that neither SYNCRIP nor STING bind to IAV mRNAs produced from segment 5 or 7. To rule out the possibility that RNA had degraded during the immunoprecipitation steps, total RNA was also isolated from the first washes after antibodies were incubated with cell lysates. Assessment of RNA integrity shows that 28S and 18S rRNAs are intact in all wash samples as well as inputs (Figure 5.7 C) and this indicates that IAV segment 5 and 7 mRNAs should also be intact. Although this assay would suggest neither SYNCRIP nor STING bind to viral RNA there are several caveats of this method. Firstly, native RIP was performed using endogenous proteins and if there are transient or weak RNA-SYNCRIP/STING interactions these might be better identified if cross-linking was performed prior to cell lysis or if SYNCRIP and STING were overexpressed as tagged proteins. Secondly, it is possible that SYNCRIP or STING bind IAV RNAs other than mRNAs produced from segment 5 or 7, since only mRNA was reverse transcribed to make cDNA from total extracted RNA and only primers to produce amplicons from these segments were used for PCR. Thus, if SYNCRIP or STING bound other viral RNA species/segments this experiment would not identify them. Thirdly, it is possible that binding of viral RNA by SYNCRIP or STING alters the epitope recognised by the antibodies used for immunoprecipitation preventing the pulldown of proteins bound to RNAs, the use of tagged proteins for RNA pulldowns would alleviate this problem. However, since this assessment of vRNA binding by SYNCRIP did not yield positive results and due to time constraints, such experiments were not pursued further.

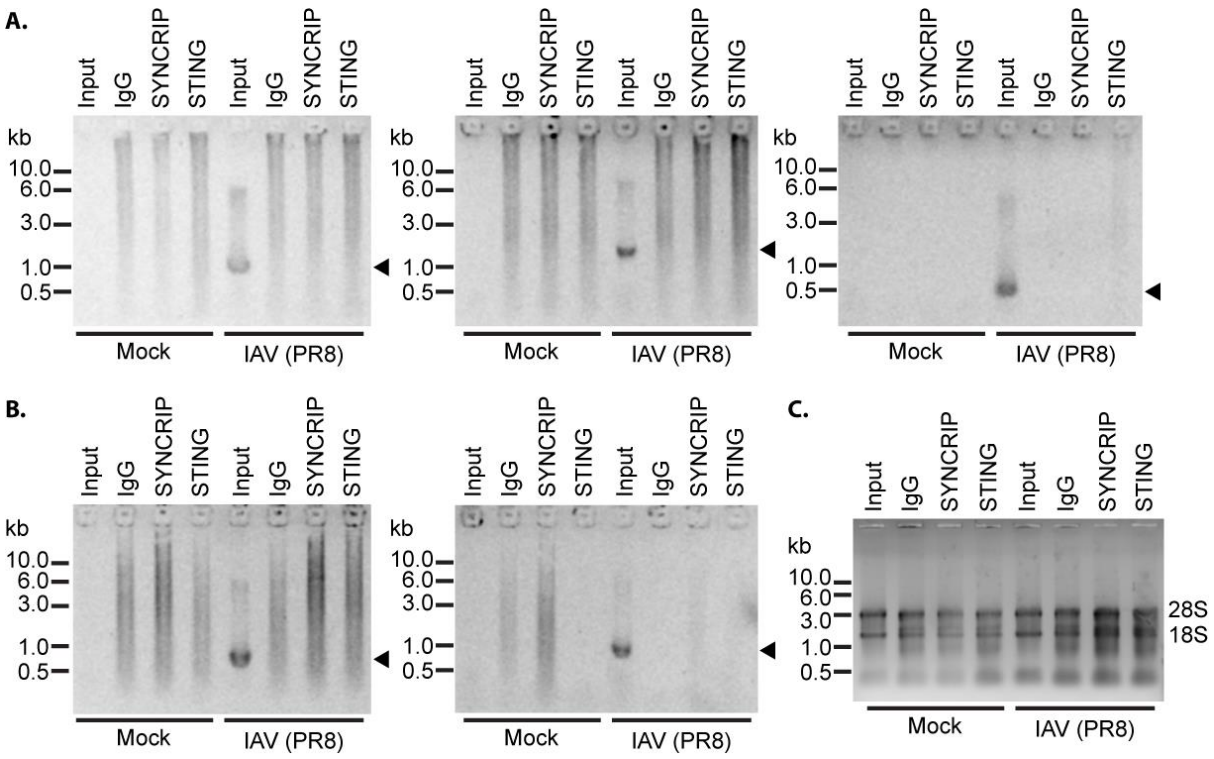

Figure 5.7 – RNA-immunoprecipitation experiments do not show an interaction between SYNCRIP or STING with tested segments of influenza A virus (PR8) mRNA. *Endogenous SYNCRIP and STING were immunoprecipitated from mock or IAV (PR8) infected whole cell lysates 3 hpi. Total RNA associated with pulled down proteins was isolated using TRIzol reagent and mRNA reverse transcribed to make cDNA. PCR using primers against viral mRNAs from segment 5* ***(A)*** *or segment 7* ***(B)*** *identify viral mRNA in infected whole cell lysates used as inputs for immunoprecipitation but not SYNCRIP, STING, or control IgG pulldown samples or mock infected whole cell lysates. Three amplicons were designed against segment 5 (*1, 1.5, and 0.5 kb) and two amplicons against segment 7 (0.75 and 1 kb). **(C)** RNA integrity was checked after pulldowns with antibodies by extracting total RNA in the first washes of whole cell lysates incubated with antibodies and protein G Dynabeads™. Total RNA run on agarose gel confirms that 28S and 18S rRNA are intact suggesting little or no RNA degradation occurred during antibody incubation steps.

5.9 – SYNCRIP protein levels and localisation during IAV infection

The interaction between virus and host can be thought of in the context of an evolutionary arms race in which host cells have evolved to detect and restrict viral infection, while viruses have evolved to inhibit host cell detection and improve proliferation (Hoffmann et al. 2015). As already mentioned, the NS1 protein of IAV is a major antagonist of the host cell immune response through inhibition of RIG-I activation and IFN translation (Ayllon and García-Sastre 2015). Furthermore, the HA fusion peptide binds STING directly preventing STING dimerization and activation during infection with IAV (Holm et al. 2016). Since I have found that SYNCRIP restricts IAV infection it is reasonable to speculate that IAV strains with

mutations that enable the inhibition of SYNCRIP antiviral functions will be selected. This is supported by the finding that IAV grows to higher titres in SYNCRIP knockdown cells compared to control cells infected with PR8 NS1 mutant strains relative to cells infected with wild type PR8 (Figure 5.3 and 5.4). That no such difference is seen for control and SYNCRIP knockdown cells infected with Udorn (Figure 5.5) might suggest that Udorn has evolved to be able to restrict SYNCRIP antiviral functions more effectively than PR8. In order to look at whether IAV targets SYNCRIP, I assessed SYNCRIP protein levels by Western blotting during infection with PR8, anticipating that SYNCRIP might be degraded during the time-course of infection. However, no reduction of SYNCRIP isoforms was apparent in cells infected with PR8, marked by the detection of NS1 and NP protein at later timepoints, compared to mock infected cells or earlier timepoints (Figure 5.8 A). It is possible that no changes in SYNCRIP protein levels during infection were detected because only a subset of cells are infected and so any changes in infected cells are masked by a background of mostly non-infected cells. Therefore, immunofluorescence against viral protein NP was performed to assess the proportion of cells that were infected 24 hpi and different MOI were used to get more cells infected. When using an MOI of 3 as for detection of viral protein in cell lysates, surprisingly few cells stained positively for NP protein in HT1080 cells, since an MOI of 3 should result in nearly all cells in culture being infected (Figure 5.8 B). HEK293T cells similarly infected at an MOI of 3 showed more NP positive cells 24 hpi, although notably not all cells were infected as would be expected at this MOI. The proportion of NP positive cells at 24 hpi could be increased in HT1080 cells by increasing the inoculum to an MOI of 10, although still some cells remained infected. Therefore, it is possible that when assessing whole cell lysates for an effect on SYNCRIP protein levels during infection any decrease or increase was not seen at an MOI of 3. That HT1080 cells are less readily infected than HEK293T cells is interesting and could be due to a lower abundance of suitable cell surface receptors for IAV to bind or because HT1080 cells more effectively restrict IAV infection.

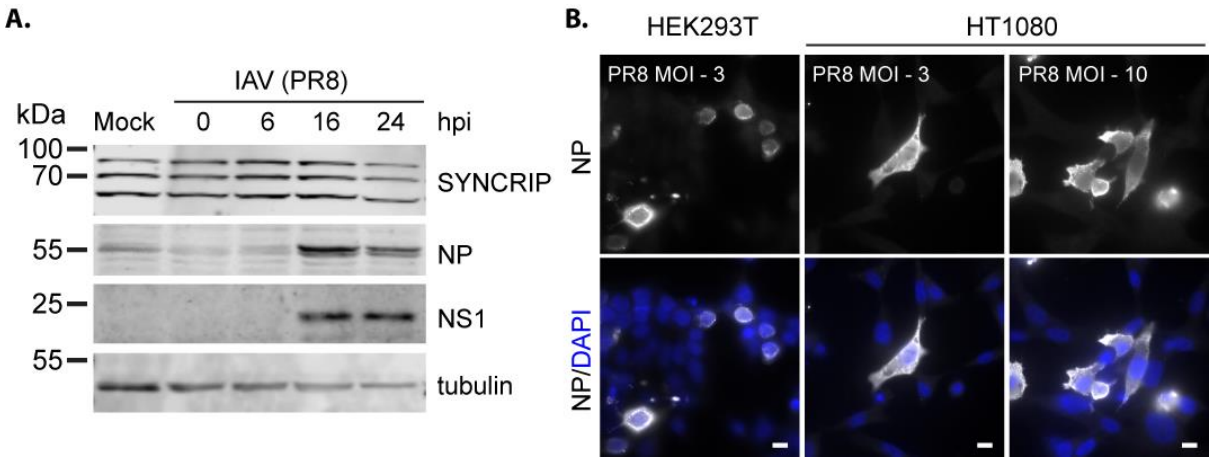

Figure 5.8 – SYNCRIP protein levels do not change during influenza A virus (IAV) infection. ***(A)*** *Western blotting shows that SYNCRIP protein levels are unaltered during infection with IAV (PR8) compared to mock infected cells, staining against NP and NS1 viral proteins confirms IAV infection. MOI – 3.* ***(B)*** *Immunofluorescence against NP in IAV (PR8) infected HEK293T and HT1080 cells shows that most HT1080 cells are not infected at an MOI of 3 and even increasing to an MOI of 10 does not result in all cells showing infection. MOI indicated in figure, cells fixed and stained 24 hpi. Scale = 10 μM.*

Since no alteration in SYNCRIP protein levels was evident by Western blot, I also used immunofluorescence staining to study the localisation of SYNCRIP during an infection time course with IAV. Although, immunofluorescence is not especially suitable for commenting on protein abundance, any changes in SYNCRIP localisation could be informative as to the mechanism through which SYNRIP restricts IAV infection. No consistent difference was seen for SYNCRIP localisation in IAV infected cells compared to mock infected cells (Figure 5.9 A). However, in several cells infected with IAV, SYNCRIP localisation to the cytoplasm appears reduced relative to non-infected cells in the same field of view (Figure 5.9 B, white arrows). This phenotype was only seen at later timepoints during infection (16 and 24 hpi) and was not apparent in all infected cells. From this data it is not possible to say whether this change in SYNCRIP localisation by immunofluorescence is actually reflective in a redistribution to the nucleus or a reduction in cytoplasmic SYNCRIP as a result of specific isoform degradation. Alternatively, cell membrane integrity may be compromised at later timepoints during infection leading to a loss of protein from the cytoplasm, or epitopes recognised by anti-SYNCRIP antibody could be masked at specific time points during infection. Nonetheless, whether or not SYNCRIP localisation changes during infection or whether specific SYNCRIP isoforms are targeted during infection warrants further study. In particular, future experiments should use expression of FLAG-tagged isoforms of SYNCRIP to evaluate whether

particular isoforms change distribution during infection. As noted in the previous chapter, the different isoforms of SYNCRIP localise to different cellular compartments, with the Q1 isoform predominantly cytoplasmic while Q2 and Q3 are mostly nuclear, while the highly homologous hnRNP R also recognised by the SYNCRIP antibody is a nuclear protein (Chen et al. 2008; Cappelli et al. 2018). Since the Q1 isoform is the most depleted by siRNA treatment (Figure 4.3) and there is some evidence that cytoplasmic SYNCRIP staining is reduced during IAV infection I would hypothesise that the Q1 isoform is required for restriction of IAV and may also be targeted specifically by IAV during infection.

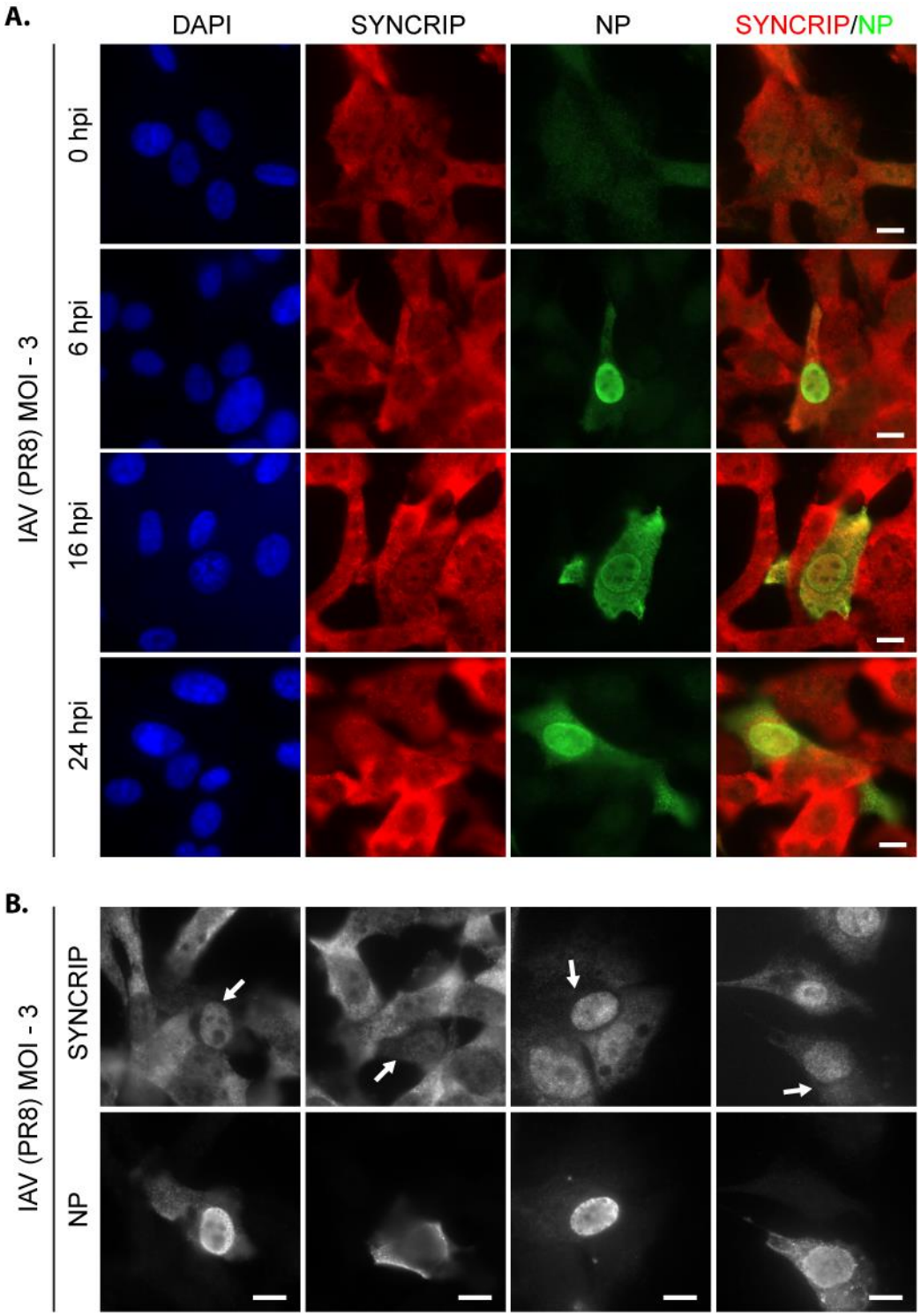

Figure 5.9 – SYNCRIP localisation during influenza A virus (IAV) infection. (A) *In most infected cells (marked by NP antibody staining) SYNCRIP localisation is not altered at various time points in infection.* ***(B)*** *In some cells, at later timepoints in infection (16 and 24 hpi), SYNCRIP antibody staining appears more nuclear with a loss of cytoplasmic staining (white arrows) compared to non-infected cells (no NP staining) in the same field of view. Scale = 10 µM.*

5.10 – Generation of SYNCRIP-knockout HT1080 cells

In order to confirm that the effect of SYNCRIP knockdown on IAV titres was a result of reducing SYNCRIP protein levels and not an indirect effect of the siRNA itself, I decided to generate a SYNCRIP knockout cell line using CRISPR/Cas9. Two guide RNAs (gRNA) targeting exons 3 and 6 of the SYNCRIP gene in the human genome were selected using the Synthego CRISPR Design Tool (Synthego, CA https://www.synthego.com/products/bioinformatics/crispr-design-tool) (Figure 5.10 A). Both exons are included in the majority of SYNCRIP isoforms and so knockout should affect all major isoforms (Q1, Q2, and Q3). Two gRNAs were designed because gRNA#1, which targets a region in exon 3, was not predicted to have high activity while gRNA#2, which targets a region in exon 6, was predicted to have high activity but does not target an early exon and may result in truncated SYNCRIP proteins which retain some activity. gRNAs were cloned into individual plasmids which co-express Cas9 fused to GFP allowing for selection of positively transfected cells based on GFP signal (Ran et al. 2013). HT1080 cells were transfected either with plasmids encoding gRNA#1 or gRNA#2 alone or with both plasmids and subject to fluorescence activated cell sorting (FACS) 24 h after transfection. Cells were gated to select for GFP-positive single cells and sorted to single cells in a 96-well plate (Figure 5.10 B). After growing up single cells, clones were screened by Western blotting using anti-SYNCRIP antibody. Although the success rate of growing up single cells to colonies was quite low, several clones were identified that showed a loss of SYNCRIP immunoreactive bands (Figure 5.10 C). Notably, the highest molecular weight band detected by the SYNCRIP antibody which is most likely an isoform of hnRNP R was not lost in any of the SYNCRIP knockout clones, confirming my earlier suggestion that this band is not a SYNCRIP isoform. Both clones that were transfected with gRNA#2 alone (2H6 and 2E2) retained weak SYNCRIP immunoreactive bands around the same molecular weight of Q3, Q2, and Q1 isoforms and so are likely not pure clones derived from a single cell. This can occur when GFP positive (and so Cas9 expressing) cells which have not been edited or are only edited at one allele, are sorted and then subsequently divide and because Cas9 and gRNA are present in the cell for several days after transient transfection of CRISPR plasmid editing occurs in only one of the daughter cells resulting in a colony which is not genetically identical (Mehravar et al. 2019).

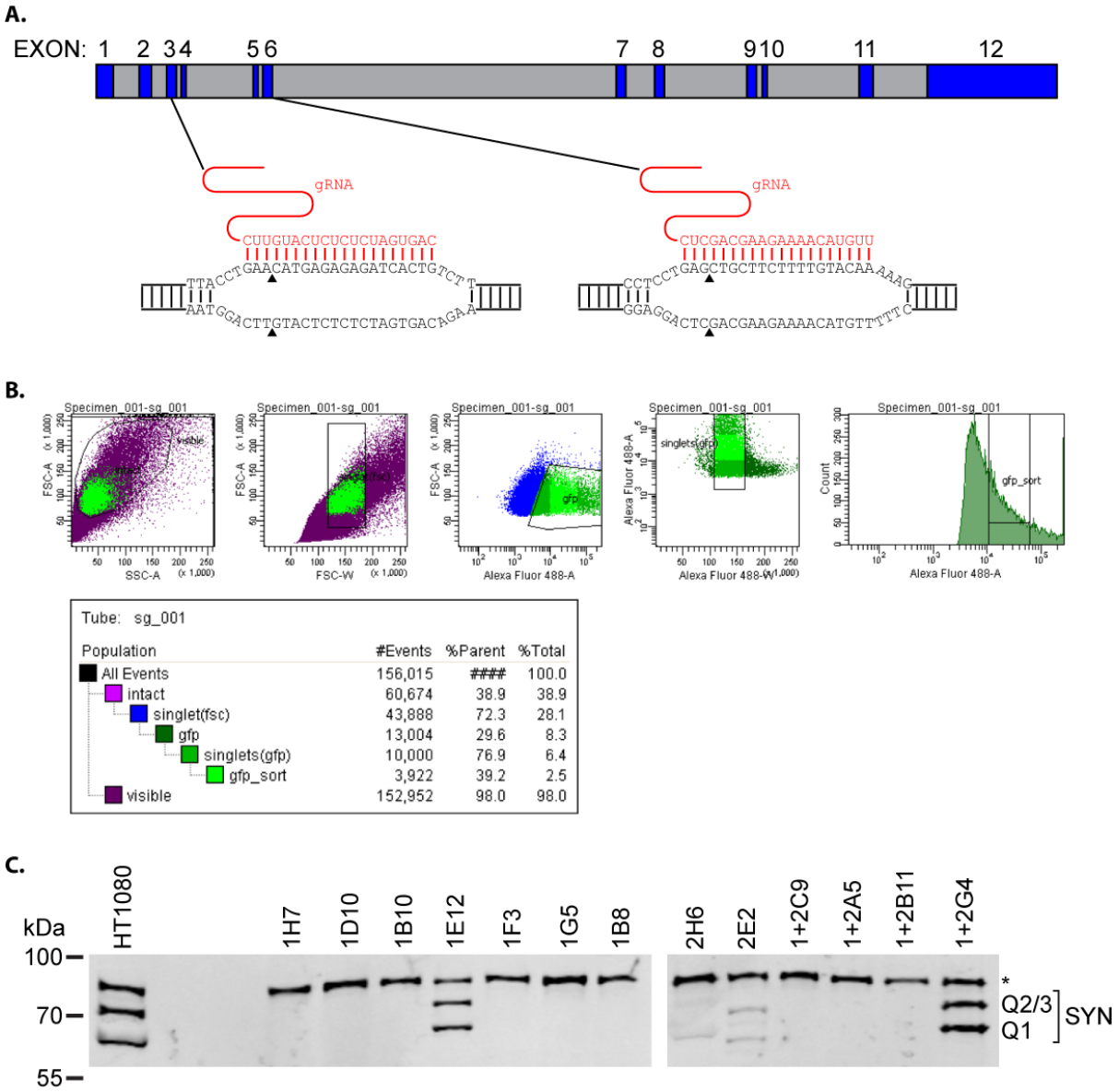

Figure 5.10 – Generation of SYNCRIP knockout HT1080 cell lines by CRISPR/Cas9 gene editing. (A) *Schematic showing two guide RNAs (gRNA) designed to target human SYNCRIP gene. Exons marked in blue and numbered 1 – 12, introns coloured grey. Black arrowheads show site of double-strand break.* ***(B)*** *Example FACS scatterplots showing gating for sorting of Cas9-GFP positive cells. Since Cas9-GFP and gRNA are encoded by the same plasmid, GFP positive cells are the only cells in which genome editing should occur. Gating left to right is as follows: scatter-plot 1 forward scatter area (FSC-A) and side scatter area (SSC-A) to select intact cells based on size and complexity, scatter-plot 2 FSC-A and forward scatter width (FSC-W) to select single cells, scatter-plot 3 FSC-A and Alexa Fluor 488-A to select GFP positive cells, scatter-plot 4 Alexa Fluor 488-A and Alexa Fluor 488-W to select GFP positive single cells, and histogram to gate the medium GFP expressing cells and leave out the highest and lowest intensity GFP positive cells. Table shows number of cells (events) within each gate and percentage of these in total cell population.* ***(C)*** *Western blotting showing SYNCRIP protein levels in colonies grown from FACS sorted single cells compared to wild type HT1080 cells. Western blotting confirms knockout of SYNCRIP (SYN) in several colonies with undetectable levels of SYNCRIP isoforms Q3, Q2, and Q1. * indicates probable hnRNP R band.*

5.11 – IAV proliferation in SYNCRIP-knockout cells

Having generated SYNCRIP-knockout HT1080 cells I next wanted to test the proliferation of IAV in a subset of these clonal cell lines. Clones 1H7, 2H6, 1+2B11 were chosen as SYNCRIP-knockout cell lines to test while clone 1+2G4 was chosen as a *SYNCRIP*$^{+/+}$ cell line that had undergone the same treatment as knockout clones but still expressed all major SYNCRIP isoforms (Figure 5.11 A). All these cell lines were also confirmed to express similar levels of STING and so any differences between them would not be a result of variable levels of STING expression. Immunofluorescence staining in these cells using an anti-SYNCRIP antibody shows that in clones 1H7 and 1+2B11 any cytoplasmic signal is completely lost while clone 1+2G4 retains cytoplasmic staining. Some cytoplasmic staining is still evident in clone 2H6 again indicating that this clone retains some SYNCRIP expression. All clones show strong nuclear signal likely equivalent to the highest molecular weight band recognised in Western blotting with SYNCRIP antibody, which is probably hnRNP R. All four clones were infected with IAV (PR8) at an MOI of 3 and viral titres at multiple time points during infection determined by plaque assay. Surprisingly, only in SYNCRIP knockout clone 1H7 infected cells did IAV grow to significantly higher titres than the *SYNCRIP*$^{+/+}$ control clone 1+2G4 at 16 hpi (Figure 5.11 C and D). IAV titres were slightly higher in SYNCRIP-knockout clone 1H7 compared to the control, ~2.5x higher, which was not quite as strong as the effect seen with SYNCRIP siRNA knockdown in which titres were ~3x higher compared to control cells (Figure 5.3). That IAV titres grown in clones 2H6 and 1+2B11 are no higher than titres grown in the control clone 1+2G4 at 16 hpi is unexpected and does not support the data seen for increased IAV titres in SYNCRIP knockdown cells compared to control knockdown cells. That only one of the SYNCRIP knockout clones replicates the siRNA results could suggest that SYNCRIP function is more complex, and this therefore requires further investigation. Firstly, it is possible that the effect seen for SYNCRIP knockdown on IAV titres is an indirect effect of the siRNA treatment and not the reduction in SYNCRIP protein levels detected by Western blotting. Therefore, SYNCRIP siRNA knockdown experiments should be repeated using a different siRNA. Secondly, it is possible that the lack of a difference between IAV titres grown in SYNCRIP knockout clones 2H6 and 1+2B11 compared to IAV titres grown in control clone 1+2G4 is a result of off-target gene editing directed by the gRNAs used. It is interesting to note that both of these clones

were edited using gRNA#2, which could explain why an increase in viral titres was seen in clone 1H7 which was edited using gRNA#1 only. It is also possible that clones 2H6 and 1+2B11 are not complete SYNCRIP knockouts and so retain some SYNCRIP protein which is functional in restricting IAV. Indeed, cell lysates from clone 2H6 retain immunoreactive bands detected by SYNCRIP antibody, albeit at lower levels than in the control clone 1+2G4. It is also possible that the process of generating knockout clones impaired some aspect of immune signalling and so even the control clone 1+2G4 is ineffective in restricting IAV and so no difference in titres is seen between this clone and SYNCRIP-knockout clones 2H6 and 1+2B11. In order to resolve these inconsistencies, more SYNCRIP-knockout clones should be screened for an effect on IAV titres. Furthermore, titres from clones should be compared to those from wild type HT1080 cells infected in parallel as well as a control clone which still expressed SYNCRIP to rule out the possibility that IAV grows to higher titres in all CRISPR clones regardless of SYNCRIP expression. Infection experiments could also be repeated using IAV PR8 NS1 mutants since the difference in viral titres was enhanced between SYNCRIP knockdown and control knockdown cells (Figure 5.4). Since not all of the SYNCRIP knockout clones tested showed an increase in IAV titres, sequencing around the gRNA cut sites was performed to verify the Western blotting data showing SYNCRIP knockout (Figure 5.11 E). Amplification of a 500 bp region around the gRNA#1 site of genomic DNA isolated from clones was successful and sequencing confirmed that gene editing had occurred in clones 1H7 and 1+2B11. In the case of 1H7 an homozygous insertion of 145 nt was detected which results in a frameshift and knockout, while for 1+2B11 there is a 4 nt deletion which will also result in a frameshift. Unfortunately, I was unable to amplify a region around the gRNA#2 cut site and so whether any editing occurs in clones treated with this gRNA cannot be stated. In the future it will be essential to perform this sequencing in order to determine the status of the SYNCRIP genomic sequences in clones treated using gRNA#2 (2H6, 1+2B11, 1+2G4). Finally, it would also be pertinent to confirm that SYNCRIP-knockout clones retain functional dsDNA and dsRNA sensing pathways by transfecting cells with dsDNA or poly(I:C) and measuring IRF3 activation because this could account for differences seen with regard to IAV proliferation.

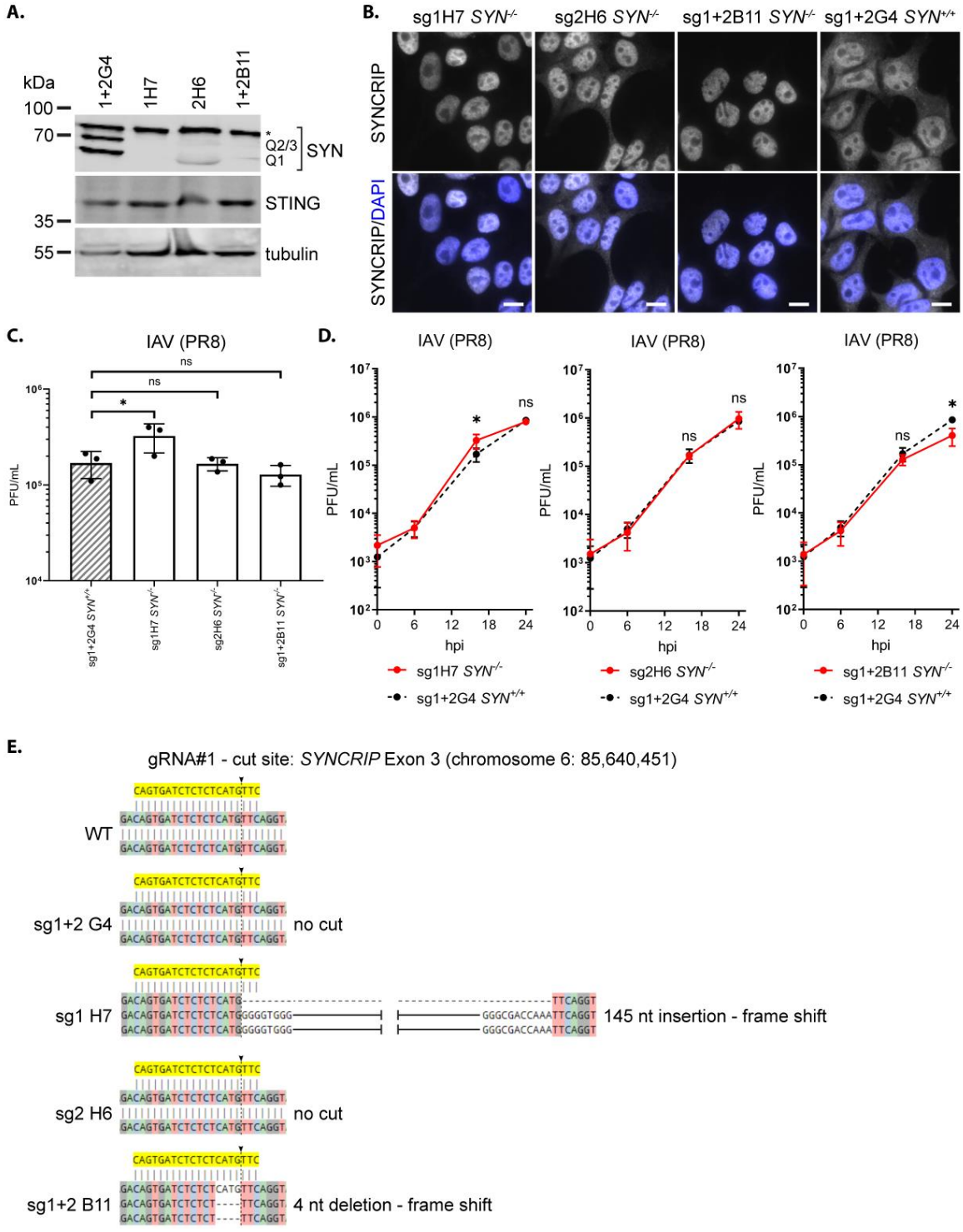

Figure 5.11 – Influenza A titres are significantly higher in one but not all SYNCRIP knockout HT1080 cell lines. (A) *Western blotting confirms detectable levels of STING protein in selected SYNCRIP knockout clones.* ***(B)*** *Immunofluorescence shows loss of SYNCRIP staining from the cytoplasm of SYNCRIP knockout clones 1H7 and 1+2B11 but only partial reduction in 2H6, likely corresponding to low levels of SYNCRIP detectable by Western blot for this clone (A). Scale = 10 µM.* ***(C)*** *IAV (PR8) titres are significantly higher (~2.5x) in SYNCRIP knockout clones 1H7 compared to control SYNCRIP positive clone 1+2G4 but are unaffected in SYNCRIP knockout clones 2H6 and 1+2B11 at 16 hpi.* ***(D)*** *Time course experiments shows viral growth in SYNCRIP*

*knockout clones compared to SYNCRIP positive clone (1+2G4). MOI – 3. Ordinary one-way ANOVA with Dunnett's multiple comparisons test. * p < 0.05. n = 3.* ***(E)*** *Sequencing of amplicons around the sgRNA#1 cut site produced from genomic DNA isolated from SYNCRIP knockout clones. Wild-type (WT) genomic sequence.*

5.12 – Chapter Summary

In this chapter I have screened several newly identified NE STING partners for a role in restricting RNA virus infection, showing that SYNCRIP is a novel antagonist of IAV in HT1080 cells, with IAV growing to higher titres in SYNCRIP knockdown cells. This seems to be a strain specific effect with only the H1N1 PR8 strain replicating to higher titres and not the H3N2 Udorn strain. Moreover, I have also confirmed that STING restricts IAV with the PR8 strain growing to higher viral titres in STING knockdown cells. Interestingly, STING knockdown similarly had no effect on Udorn proliferation suggesting that STING and SYNCRIP could restrict IAV through similar mechanisms. Alternatively, it is possible that SYNCRIP and STING mediate their antiviral effects independently of one another and that Udorn is able to inhibit both while PR8 is not. That PR8 titres were increased in cells treated with both SYNCRIP and STING siRNAs simultaneously compared to cells treated with STING siRNAs (and control siRNA so final siRNA concentrations were the same) would suggest that SYNCRIP is able to restrict IAV independently of STING. In support of this interpretation of the data an interaction between STING and SYNCRIP was not seen by co-immunoprecipitation experiments during viral infection.

One potential limitation of this study is the use of HT1080 cells, a fibrosarcoma cell line. Since IAV typically infects cells of the respiratory system a more appropriate cell line to use would be a lung cell line. Nonetheless, IAV was confirmed to infect HT1080 cells and so the findings presented in this chapter are still informative. The A549 epithelial cell line derived from a lung adenocarcinoma was initially considered for use in IAV infection experiments. However, A549 cells do not express detectable levels of STING protein (Figure 3.1) and since I wanted to test whether STING partners were involved in restricting an RNA virus, I postulated that any partner protein functions in viral restriction would require STING. It would now be interesting to confirm that SYNCRIP knockdown affects proliferation of IAV in A549 cells or another lung cell line. Since A549 cells do not express detectable levels of STING protein this would further inform as to whether STING is required for SYNCRIP antiviral functions.

The NS1 protein of IAV is thought to be the major antagonist of the host cell immune response and has been shown to inhibit the IFN response through several different mechanisms (Ayllon and García-Sastre 2015). There are some key differences between the NS1 proteins of PR8 and Udorn which affect the inhibition of the IFN response. PR8 NS1 does not bind to CPSF30 as a result of amino acid differences at positions 103 and 106 (S103/I106 PR8) compared with Udorn NS1 (F103/M106) (Kochs et al. 2007; Ayllon and García-Sastre 2015), and so does not inhibit cellular mRNA polyadenylation and expression of cellular genes while Udorn does. On the other hand, PR8 inhibits RIG-I signalling and IRF3 activation (Mibayashi et al. 2007; Opitz et al. 2007) while Udorn NS1 does not inhibit IRF3 activation (Kuo et al. 2010; Krug 2015). That PR8 titres are increased in SYNCRIP or STING knockdown cells but Udorn titres are not increased could indicate that both SYNCRIP and STING are involved in restricting viral infection independently of the RIG-I signalling pathway since PR8 NS1 restricts RIG-I activation. However, this restriction is not total so some activation of STING and SYNCRIP could still occur, which would explain why SYNCRIP knockdown enhanced the titres of PR8 NS1 mutant viruses which are incapable of inhibiting RIG-I, relative to wild type PR8. These results could indicate that SYNCRIP at least partially restricts IAV through a mechanism involving the RIG-I signalling pathway. Interestingly, STING has been reported not to be required for IFN expression during RNA virus infection but instead to restrict viral infection through a mechanism resulting in translational inhibition (Franz et al. 2018). This STING-dependent mechanism required RIG-I/MDA-5 but was distinct from the well-described PKR mediated inhibition of translation. My results showing an increase in PR8 titres in STING knockdown cells are consistent with a STING-dependent mechanism of viral restriction. However, that PR8 titres were elevated in STING knockdown cells compared to control knockdown cells suggests either PR8 NS1 cannot completely inhibit this STING mediated viral restriction or that STING also functions outside of RIG-I mediated signalling in its restriction of IAV. In order to test whether the NS1 proteins of PR8 and Udorn strains account for the differences seen in titres with SYNCRIP or STING knockdown I tried to make a recombinant PR8 virus encoding the Udorn NS1 protein by swapping the NS1 encoding genome segments from the two strains when producing the virus. I used a reverse genetics system to produce virus, in which individual plasmids encoding each of the 8 genome segments of IAV are simultaneously transfected into HEK293T cells resulting in the formation of functional virions (De Wit et al. 2004). Therefore, generation of the chimeric virus only required swapping PR8

segment 8 (encodes NS1/NEP) for Udorn segment 8. However, while this was tried several times, the virus generated was consistently of too low concentration to use in experiments. It would be interesting to try and optimise production of this virus in the future as it would reveal whether differences in the NS1 proteins explain the lack of effect with SYNCRIP or STING knockdown on Udorn viral titres. Alternatively, segment 8 of PR8 could be used to create a chimeric IAV with the other genome segments coming from Udorn.

As well as NS1, the fusion peptide (FP) of IAV has recently been shown to have immunosuppressive activity in the monocytic THP-1 cell line (Bahrami et al. 2016) and to bind to STING thus inhibiting IFN responses specifically triggered by fusogenic liposomes (Holm et al. 2016). Although the FP is highly conserved across IAV strains, there are three amino acid differences between the FP of PR8 and Udorn (Figure 5.12) and it is possible these differences affect the immunosuppressive qualities of the two FP during infection, explaining differences in PR8 and Udorn viral titres between control and STING knockdown cells. Interestingly, the recombinant FP (Flu ISU) found to inhibit STING dimerization (Holm et al. 2016) is more similar to the FP of Udorn than PR8 so it is possible that Udorn FP is more effective at inhibiting STING than that of PR8 which could explain differences in viral titres seen for the two viruses. This could be tested by infecting with a chimeric IAV in which the HA of PR8 is replaced with Udorn or vice versa.

Recombinant Flu ISU	GLFGAIAGFIENGWEGCGGEKEKEK
A/Puerto Rico/8/1934 (H1N1)	GLFGAIAGFIEGGWTGMIDGWYG
A/Udorn/1972 (H3N2)	GLFSAIAGFIENGWEGMIDGWYG

Figure 5.12 – Fusion Peptides of PR8 and Udorn compared to recombinant fusion peptide found to inhibit STING dimerization. *Amino acid sequences of HA fusion peptides from PR8 and Udorn strains compared to recombinant Flu ISU fusion peptide found to bind STING and inhibit dimerization in* (Holm et al. 2016)*. Residues in PR8 and Udorn fusion peptides that differ from recombinant Flu ISU are highlighted in yellow.*

In order to better understand the mechanisms through which STING and SYNCRIP restrict PR8 it would be interesting to look at IRF3 activation and IFNβ expression in cells treated with siRNAs against STING or SYNCRIP and infected with PR8. This would reveal whether either STING or SYNCRIP are required for IRF3 activation and IFNβ expression in HT1080 cells infected with IAV. Although I did not establish whether SYNCRIP is targeted by IAV during infection, some cells show a loss of SYNCRIP staining from the cytoplasm at later timepoints

in infection which could hint at a mechanism through which SYNCRIP restricts IAV or that IAV is targeting SYNCRIP in the cytoplasm to inhibit antiviral effects. Western blotting experiments against SYNCRIP should be repeated either infecting at a higher MOI to ensure a larger proportion of cells are infected or using a different cell line which is more readily infected by IAV, such as HEK293T or A549 cells, to see if there are any differences in SYNCRIP levels during infection. It would also be interesting to repeat immunofluorescence experiments using individual FLAG-tagged SYNCRIP isoforms so that whether a particular isoform is redistributed during infection could be better quantified. For this it would be pertinent to start with Q1 and Q3 isoforms as these are the isoforms knocked down by siRNA treatment.

Whether IAV targets SYNCRIP to restrict its antiviral properties could also be investigated by performing co-immunoprecipitation assays to assess binding of SYNCRIP by NS1. Interestingly, SYNCRIP has been identified as an interactor of NS1 from PR8 but not Udorn strain in pulldown experiments followed by mass spectrometry (Pichlmair et al. 2012; Bösl et al. 2019). This is supportive of my findings that SYNCRIP plays a role in IAV infection and might explain why only a difference in PR8 viral titres was identified in SYNCRIP knockdown cells and not Udorn viral titres. For example, SYNCRIP antiviral functions might need to be targeted by PR8 NS1 but not Udorn NS1 in the same way PR8 inhibits RIG-I but Udorn does not because Udorn NS1 inhibition of CPSF30 prevents host cell mRNA translation so upstream signalling pathway activation becomes irrelevant. Moreover, SYNCRIP has been identified as being a significantly differentially expressed gene in a meta-study which analysed cell-based gene expression profiles during IAV infection from ten published studies again suggesting a role for SYNCRIP during viral infection. Interestingly, in this meta-study SYNCRIP gene expression was down-regulated in some of the datasets and up-regulated in others perhaps indicating that SYNCRIP is up-regulated by the host cell but targeted by IAV for down-regulation (Forst et al. 2017). If binding between SYNCRIP and PR8 NS1 can be confirmed through co-immunoprecipitation, subsequent experiments should look at whether Udorn NS1 is unable to immunoprecipitate SYNCRIP and vice versa before point mutation studies to identify residues required for any such interaction.

While RNA immunoprecipitation experiments failed to identify binding of viral mRNAs encoded by IAV segments 5 and 7 the use of endogenous protein and lack of cross-linking in these experiments may not have been sensitive enough to identify an interaction between

SYNCRIP and viral RNA. RNA immunoprecipitation should therefore be repeated with overexpressed FLAG-tagged isoforms of SYNCRIP and the use of UV or formaldehyde crosslinking prior to immunoprecipitation to preserve RNA-protein interactions. Furthermore, primers should be designed against all segments of the IAV genome in case SYNCRIP is binding to specific viral mRNAs.

Finally, HT1080 SYNCRIP knockout cell lines showed mixed results for SYNCRIP having an effect on IAV titres with only clone 1H7 growing higher viral titres compared to the control SYNCRIP clone. Further clones should be screened to better clarify whether SYNCRIP knockout affects IAV titres. However, prior to doing this all clones should be sequenced at the gRNA target sites in the SYNCRIP gene to confirm whether gene editing has taken place. Although Western blotting suggests that SYNCRIP knockout has occurred in many clones due to a loss of SYNCRIP antibody immunoreactive bands, two of the clones tested with IAV infection retained weak immunoreactive bands which could explain why IAV titres were no higher in these cell lines compared to the control cell line. IAV infections of SYNCRIP knockout clones should also be repeated with a wild type HT1080 control to rule out the possibility that even SYNCRIP positive clones are impaired in their ability to restrict IAV infection. Once SYNCRIP knockout cell lines are verified and providing that IAV grows to higher titres in SYNCIRP knockout cells compared to SYNCRIP positive cells, it will be necessary to perform rescue experiments by transiently expressing different isoforms of SYNCRIP to see if they restrict IAV proliferation. These experiments should reveal if a particular isoform is critical for viral restriction and may inform on which domains of SYNCRIP are required for antiviral activity.

Considered together, my data show that STING restricts IAV infection and identify SYNCRIP as a novel viral antagonist. Future experiments should focus on establishing the mechanism through which SYNCRIP exerts its antiviral effect. In particular whether SYNCRIP interacts with NS1 should be confirmed through immunoprecipitation experiments and whether SYNCRIP binds viral RNA should be investigated more thoroughly. Moreover, immunofluorescence experiments studying localisation of SYNCRIP during infection should be performed using FLAG-tagged SYNCRIP isoforms so that localisation of individual SYNCRIP variants can be determined.

Chapter 6

Discussion

The work described in this thesis demonstrates unequivocally for the first time that a pool of endogenous STING is present in the inner nuclear membrane in addition to localising to the outer nuclear membrane and its well-known localisation throughout the ER. Moreover, I have shown through several assays that some partners of STING in the nuclear envelope are novel regulators of immune responses stimulated by both dsDNA and dsRNA ligands. Finally, NE STING partner SYNCRIP which has multiple functions in RNA processing is shown to be a restriction factor of the RNA virus, influenza A. These findings affect the way we should think about the roles STING plays as the key adaptor protein in dsDNA stimulated IIR as well as its functions in restricting RNA viruses.

6.1 – Implications of an inner nuclear membrane pool of STING

The identification of an INM pool of STING has implications for the interpretation of previous data from many labs describing STING functions. While cytoplasmic sensing of dsDNA by the cGAS-STING pathway is likely unaffected by STING's presence in the INM, the nuclear pool could also provide a mechanism for virus detection of transcripts in the nucleus to separately activate IIR so that the contribution of the cytoplasmic pool to measured effects might be exaggerated. Furthermore, a cGAS-independent function of STING in sensing DNA damage has been described (Dunphy et al. 2018). In this study *Dunphy et al.* found that DNA damage induced by etoposide treatment results in a STING-dependent response that is distinct from that of cytosolic dsDNA stimulated STING responses in human keratinocytes. Etoposide treatment resulted in a distinct signalling response to DNA damage compared to cytosolic dsDNA stimulated IIR. As well as activating an IFNβ response which was independent of cGAS but still required some trafficking of STING to perinuclear foci and TBK1 function, etoposide treatment activated a strong NF-κB signalling response, with upregulation of a distinct set of NF-κB dependent genes such as IL-6 and CCL20 inflammatory cytokines. Interestingly, this NF-κB dominant signalling response did not require redistribution of STING to perinuclear foci or the activity of cGAS and TBK1. Instead, this response required the DNA damage kinase ATM and PARP-1 and resulted in the assembly of a STING-IFI16-TRAF6-p53 signalling complex

which primarily activated NF-κB signalling. Moreover, this response is distinct from the delayed cGAS-STING response that occurs due to the sensing of cytosolic DNA originating from micronuclei (Glück et al. 2017; Mackenzie et al. 2017; Harding et al. 2017), with IFNβ, IL-6, and CCL20 gene expression occurring within 4 h of DNA damage and peaking after 8-12 h. *Dunphy et al.* propose that such a signalling complex assembles in the ER because both TRAF6 and p53 accumulate in membrane fractions 2-4 h after etoposide treatment and IFI16, TRAF6, and p53 are all able to shuttle between nucleus and cytoplasm. However, my data showing that STING is present in the INM suggest that such a complex could initially form at the INM since all components are present in the nucleus and this is the site of DNA damage. It would therefore be interesting to test whether INM localised STING is required for such a response and to test whether STING localisation within the NE changes following etoposide induced DNA damage.

While I found that knockdown of STING in HT1080 cells did not result in elevated HSV-1 titres, likely explained by a recent report suggesting that the TLR3-TRIF pathway is mainly responsible for antagonism of STING in HT1080 cells (Latif et al. 2020), STING has been shown to be involved in the restriction of herpesviruses including HSV-1 and Cytomegalovirus (CMV) (Ishikawa et al. 2009; Orzalli et al. 2012; West et al. 2015; Reinert et al. 2016). All herpesviruses are nuclear replicating and as such sensing of viral DNA occurs at least partially in the nucleus, principally through the DNA sensor IFI16 (Orzalli et al. 2012), although the recent reports establishing that cGAS also localises to the nucleus (Orzalli et al. 2015; Gentili et al. 2019; Volkman et al. 2019) would suggest that nuclear cGAS could also be involved in the recognition of viral DNA in the nucleus. Thus, it would make sense that a pool of STING at the INM would be activated first by nuclear recognition of herpesvirus DNA in by cGAS/IFI16 and could initiate immune responses before activation of ER resident STING. Herpesvirus infection is also detected by cGAS and IFI16 in the cytoplasm due to release of genomic DNA from proteasomal degradation of viral capsids (Horan et al. 2013) as well as the detection of mtDNA released as a consequence of viral induced mitochondrial stress (West et al. 2015). IFI16 has been shown to associate with to herpesvirus DNA in both the cytoplasm and nucleus (Kerur et al. 2011; Orzalli et al. 2012; Horan et al. 2013; Orzalli et al. 2013) and to associate with STING following immune stimulation with dsDNA or herpes simplex virus (HSV1) infection to activate antiviral gene expression (Unterholzner et al. 2010; Horan et al.

2013). Moreover, at least in a subset of human cells, cGAS and IFI16 act cooperatively to induce immune responses to cytosolic DNA and DNA viruses, with both proteins required for full STING activation and induction of IFN (Orzalli et al. 2015; Almine et al. 2017; Jønsson et al. 2017). Therefore, at least in cells other than HT1080 fibrosarcoma cells, STING at the INM could be the first site of STING activation following detection of nuclear replicating DNA viruses. In support of a nuclear function of STING during HSV-1 infection, in their earlier study *Orzalli et al.* found that IFI16 did not relocalise from the nucleus to cytoplasm during HSV-1 infection of human fibroblasts and moreover, in experiments in which cells were infected with a higher MOI there was an increase in nuclear STING as by detected by cellular fractionation and Western blotting (Orzalli et al. 2012).

STING at the NE redistributes similarly to STING localised throughout the ER following immune stimulation with dsDNA, as seen by immunofluorescence showing a loss of NE STING staining and accumulation in perinuclear foci in my studies. Moreover, I have shown that STING in the INM relocalises to the ONM within 2 h of dsDNA stimulation using smFRAP microscopy. The simplest explanation for this would be that cGAMP produced by cGAS sensing of cytoplasmic DNA, enters the nucleus and activates STING similarly to STING in the ER. Alternatively, plasmid DNA may enter the nucleus and be detected by nuclear localised cGAS. While plasmid DNA is typically thought to only enter the nucleus following nuclear envelope breakdown during mitosis, it has been shown that plasmid DNA can actively be transported into the nucleus by importins in the absence of mitosis (Bai et al. 2017). For example, biotin-labelled plasmid DNA microinjected into the cytoplasm of terminally differentiated rat myotubes is able to enter the nucleus and direct gene expression (Dowty et al. 1995). A number of so called 'DNA nuclear targeting sequences' or DNTs have been shown to direct targeting to the nucleus of plasmids microinjected into the cytoplasm including the SV40 enhancer sequence which has been shown to contain binding sites for multiple ubiquitously expressed transcription factors. The transcription factors that recognise such sequences bind the plasmid DNA in the cytoplasm and then NLSs in these transcription factors are recognised by transport receptors that in the process of transporting the transcription factors also carry the plasmid DNA into the nucleus (Bai et al. 2017). The pcDNA3.1 plasmid used in my experiments to stimulate IIR against dsDNA contains the SV40 enhancer sequence and so could be directed to the nucleus and be recognised by nuclear DNA sensors including cGAS. That said,

transfected DNA must enter the cytoplasm first and so an IIR is extremely likely to be initiated from cytoplasmic DNA sensing before this process of nuclear transport has time to occur. However, it would be interesting to test if cGAS/other nuclear DNA sensors could initiate IIR in the nucleus by nuclear delivery of biotin-labelled DNA by microinjection. Likewise, whether STING redistributes from the INM to ONM in response to nuclear microinjection of DNA or herpesvirus infection should be tested using single molecule FRAP. Interestingly, previous work in the Schirmer lab found that STING mobility at the NE was increased in cells 2 hpi with HSV-1 compared to mock infected HT1080 cells stably expressing STING-GFP using FRAP (Dixon et al. 2020) (Figure 1.5). Since FRAP of NET proteins has been shown to principally measure translocation through nuclear pores this likely indicates a redistribution of STING from the INM to ONM as seen with dsDNA stimulation (Zuleger et al. 2011). Intriguingly, in this experiment HSV-1 infection did not result in the accumulation of STING in perinuclear foci. This could be explained by HSV-1 protein $\gamma_1$34.5 inhibition of STING translocation to perinuclear foci (Pan et al. 2018) or since STING appears not to be the principal antagonist of HSV-1 infection in HT1080 cells (Latif et al. 2020). Nonetheless, that STING mobility in the NE was found to increase with HSV-1 infection points to a specific NE role for STING in HSV-1 infection that warrants further investigation.

I also found that STING in the INM redistributed to the ONM following immune stimulation with the dsRNA mimic, poly(I:C). This is an especially intriguing finding given that STING's functions in the restriction of RNA viruses remain to be fully elucidated and that STING is not required for the induction of IFNβ in response to poly(I:C) transfection (Ishikawa and Barber 2008; Franz et al. 2018). However, *Franz et al.* have shown that STING is partly responsible for translational inhibition triggered by infection with the RNA virus, vesicular stomatitis virus (VSV), or transfection of poly(I:C), as determined by polysome analysis. The mechanism of STING translational inhibition could not be resolved but is distinct from translational inhibition mediated by PKR, which phosphorylates eIF2α inhibiting translational initiation (Sidrauski et al. 2015). Thus, STING redistribution from the INM to ONM following immune stimulation with poly(I:C) could be related to STING-dependent translational inhibition, particularly given that no obvious changes are seen in STING localisation throughout the ER. It would now be pertinent to test whether STING redistribution in the NE that occurred with poly(I:C)

stimulation also occurs during infection with an RNA virus such as VSV or influenza A virus (IAV).

Previous work in the Schirmer lab uncovered a role for STING in promoting chromatin compaction, with levels of STING expression positively correlating with levels of compacted chromatin (Malik et al. 2014). Furthermore, STING overexpression was also associated with an increase in histone 3 lysine 9 trimethylation (H3K9me3) at the nuclear periphery. Thus, it seems that STING in the INM directs changes in chromatin structure. Several other NETs have been shown to tether genomic loci to the nuclear periphery (Meaburn et al. 2007; Zuleger et al. 2013; Robson et al. 2016). In fact, in a previous study from the Schirmer lab, *Zuleger et al.* found that overexpression of a STING-RFP construct in HT1080 cells caused a slight effect on the recruitment of a lacO array inserted into chromosome 5 to the nuclear periphery. Although this was not pursued further because other NETs had stronger effects on chromosome repositioning, it would now be interesting to investigate whether STING at the INM is involved in recruiting particular genomic loci to the nuclear periphery. Whether any recruited loci are released as a result of STING redistribution from INM to ONM during IIR would be a particularly exciting angle to explore. For example, in resting cells STING at the NE might hold loci encoding immune response genes at the nuclear periphery in a transcriptionally repressive environment. Following activation by either dsDNA or dsRNA ligands, STING redistribution to the ONM could release such loci into a more transcriptionally active nuclear compartment, aiding the expression of immune response genes.

One question raised by my data showing that STING is present in the INM is, how is STING targeted to the INM? Localisation of transmembrane proteins to the INM has been proposed to occur via several mechanisms (Zuleger et al. 2012; Katta et al. 2014; Dixon and Schirmer 2018), however, two principal models explain targeting of most NETs. In the first, NETs diffuse passively in the ER membrane to the ONM and then through the peripheral channels of the NPC into the INM, followed by retention at the INM through binding nuclear lamins, chromatin, and/or other proteins (Worman et al. 1988; Senior and Gerace 1988; Ye and Worman 1996; Brachner et al. 2005; Brachner and Foisner 2011; Boni et al. 2015; Ungricht et al. 2015). Alternatively, trafficking of some NETs to the INM has been shown to depend, at least partially, on nuclear localisation signal (NLS) dependent receptor-mediated transport, in which karyopherins that are required for central channel active transport are also required

for active transport of membrane bound NETs (King et al. 2006; Lusk et al. 2007; Ma et al. 2007; Zuleger et al. 2011; Meinema et al. 2011; Mudumbi et al. 2020). In the case of LBR and LAP2β which both contain an NLS, a recent study by *Mudumbi et al.* showed that these proteins traffic through the NPC simultaneously accessing central and peripheral channels and deletion of the NLS of either restricts their trafficking to the peripheral channel of the NPC (Mudumbi et al. 2020). In the case of STING, earlier work in the Schirmer lab demonstrated that STING fails to target to the NE in Lamin A/C knockout MEFs (Malik et al. 2010) suggesting an interaction between STING and Lamin A/C in STING retention at the INM, though this could be consistent with both modes of translocation. My data showing that FRET occurs in cells transfected with STING-RFP and Lamin A-GFP also supports the notion that STING interacts with the nuclear lamina and suggests that binding of STING to lamins could explain its INM localisation. The idea that Lamin A/C plays a role in targeting/retention is further supported by its identification as a STING interactor in the cross-linked pulldown, mass spectrometry experiment; however, this experiment also identified lamins B1 and B2 as STING interactors which is not necessarily consistent with the first experiment in the lamin A/C knockout MEFs since the other lamins were still present. Also, determining whether STING interactions with lamins are really direct will require *in vitro* interaction studies using bacterially expressed STING and Lamin fragments to map the domains required for interaction.

Interestingly, STING also contains a predicted bipartite NLS in its N terminus (amino acids 14-46) according to an NLS prediction tool (Kosugi et al. 2009) which might suggest that its mechanism for INM localisation is the receptor-mediated route (Figure 6.1). However, this NLS spans the first transmembrane domain of STING and so whether it could be recognised by karyopherins is questionable. Moreover, the N terminal domain of STING is only 18 amino acid residues long and so this would not be able to reach into the central channel of the NPC through which karyopherins transport their cargo (Mudumbi et al. 2020). Nonetheless, in support of this idea both importin β1 and importin α2 were identified as STING interactors and so whether STING traffics to the INM in an NLS-dependent manner should be tested as this will be important for understanding mechanisms for signalling and activating innate immune responses (IIR) that may require its translocation between the nucleus and cytoplasm. For example, point mutation of the basic residues in STING's predicted bipartite

NLS should abrogate its function if indeed it is receptor mediated and STING mutant targeting could be assessed by immunofluorescence in conjunction with detergent pre-extraction assay or by immunogold-EM. Alternatively, the dominant-negative Ran GTPase mutant, Q69L, could be used to inhibit NLS-dependent transport (Zuleger et al. 2011) and localisation of STING at the INM assessed. In doing so, if one could separate pools of STING at the NE and ER it would be incredibly valuable in dissecting potential NE-specific functions of STING discussed above. STING also contains a predicted nuclear export signal (NES) at amino acid residues 54-60 (LQLGLLL), although this is embedded within the second transmembrane domain and so it seems improbable that this sequence really functions as an NES since it would not be able to bind the soluble exportin CRM1 (La Cour et al. 2004).

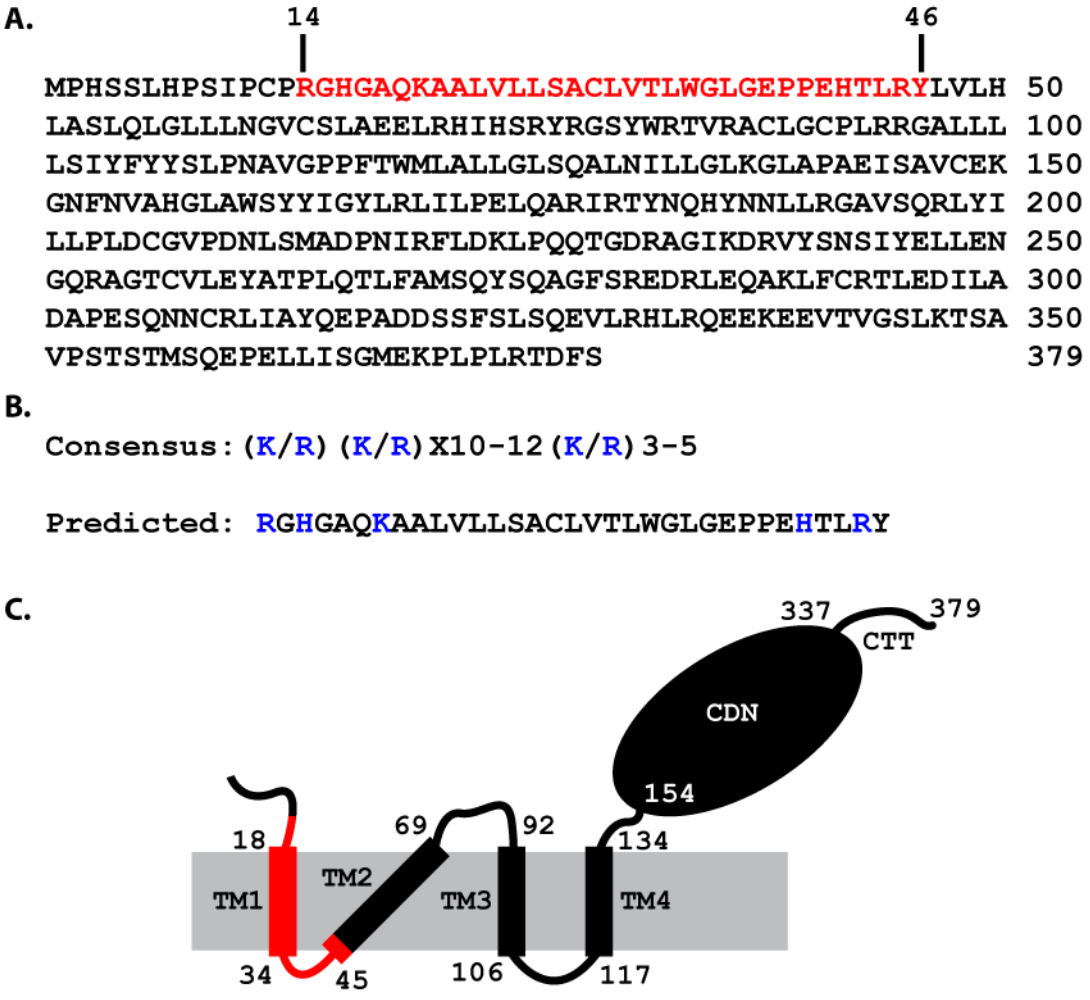

Figure 6.1 – STING contains a predicted bipartite nuclear localisation signal (NLS). (A) *Amino acid sequence of human STING showing predicted bipartite NLS (red), amino acid residues 14-46.* ***(B)*** *Consensus sequence of a bipartite NLS in which two clusters of basic residues (blue) are separated by a 10-12 amino acid linker. X indicates any amino acid, (K/R)3-5 represents at least three of either lysine or arginine in five consecutive amino acids. Predicted bipartite NLS*

of STING with basic amino acids coloured blue. Note that the linker region of bipartite NLS of some proteins has been shown to be longer than the classical 10-12 amino acids. ***(C)*** *Schematic of STING structural domains showing localisation of predicted NLS (red). Transmembrane (TM), cyclic dinucleotide binding (CDN), and C terminal tail (CTT) domains and the residues they encompass are shown. NLS predicted using cNLS mapper tool*(Kosugi et al. 2009)*. Schematic based on STING cryo-EM structure determined by Shang et al.*(Shang et al. 2019)

6.2 – The nuclear envelope STING interactome is distinct from that of STING in the ER

Much of the work completed in this thesis was founded on a mass spectrometry dataset of co-immunoprecipitated STING-GFP from isolated cross-linked NEs. When this experiment was performed less was known about STING's functions other than its critical role in immune responses stimulated by cytosolic DNA through activation of the key immune transcription factor IRF3. Therefore, we focussed on investigating IIR functions of NE STING partners that were found to have indirect links to IRF3/7 transcription factors according to the Human Protein Reference Database (HPRD, Johns Hopkins University). However, several other proteins were identified by mass spectrometry which could be interesting for further study based on more recently identified roles of STING in the DNA damage response, chromatin compaction, and inhibition of translation in response to RNA virus infection. By plotting normalised spectral counts for proteins detected in the STING-GFP sample compared to the mock transfected sample the proteins most enriched in the STING-GFP sample can be analysed (Figure 6.2, below dashed line).

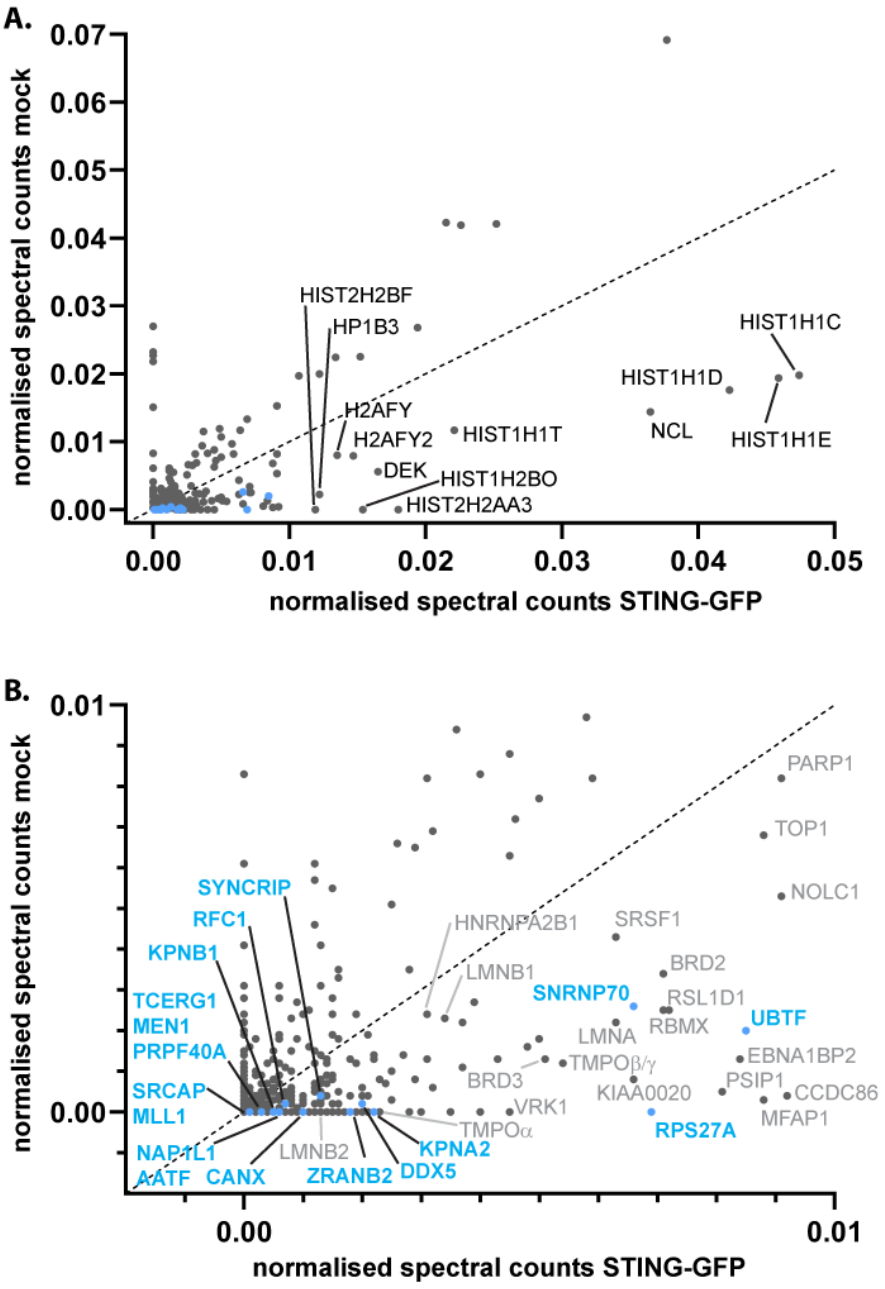

Figure 6.2 – The STING-GFP NE interactome is distinct from STING in the ER. (A) *Relative abundance of proteins identified by mass spectrometry in STING-GFP and mock pulldown samples were plotted against one another as normalised spectral counts (dnormS = normS/sum(normS)). Where normS is the number of spectra divided by protein molecular weight (in hundreds of kDa) and sum(normS) is the sum of normS in that sample. Proteins below dashed line are enriched in STING-GFP pulldown sample.* ***(B)*** *Most enriched proteins in STING-GFP pulldown sample after histone variants shown in (A). STING NE partners known to interact indirectly with IRF3/7 are highlighted in blue. Mass spectrometry experiment performed by Poonam Malik, Ravi Badwe, and Eric Schirmer; normalisation of data by Jose de las Heras; graphs plotted and data analysis by me.*

Interestingly the interactome of STING in the NE seems to be distinct from that of STING in the ER since our mass spectrometry data identified only 4 of a reported 102 STING interactors according to the HitPredict database of experimentally identified physical protein-protein interactions (López et al. 2015) (see Table 6.1). These are: CCDC47 (Li et al. 2011), an ER resident transmembrane protein proposed to be involved in calcium homeostasis (Thapa et al. 2018); DDX41, which has been shown to bind to dsDNA and STING and promote STING signalling (Zhang et al. 2011; Lee et al. 2015); histone H2B, which was recently reported to associate with IFI16-BRCA1 complexes in the nucleus which redistribute to the cytoplasm and associate with STING during infection with herpesviruses KSHV or HSV-1 (Iqbal et al. 2016); nucleoprotein TPR, which was identified as a STING interactor during HSV-1 infection (Shang et al. 2018). Notable STING interactors such as TBK1, IFI16, IRF3, MAVS, RIG-I, and STIM1 were not identified by mass spectrometry in the STING-GFP immunoprecipitated samples. This is unsurprising for MAVS which localises to the mitochondria and STIM1 which is resident in the ER since isolated NEs were used for pulldowns. Meanwhile IFI16 and IRF3 are only reported to associate with STING following immune stimulation and similarly STING-TBK1, STING-MAVS, and STING-RIG-I interactions are enhanced during IIR (Ishikawa and Barber 2008; Zhong et al. 2008; Tanaka and Chen 2012; Liu et al. 2015a; Almine et al. 2017). Since many known STING interactions only occur during an immune response or are enhanced following immune stimulation it would be worth performing pulldowns of STING from isolated NEs after immune stimulation with dsDNA, poly(I:C), or viral infection to identify partner interactions that are enhanced during an immune response to different immune stimuli. Moreover, HEK293T cells are impaired in their dsDNA sensing capability, and lack detectable expression of cGAS and IFI16, and express only very low levels of STING (Sun et al. 2013; Orzalli et al. 2015; Jønsson et al. 2017), thus, other known STING interactors may also not be expressed in the HEK293T cell line and so they would not be detected in our mass spectrometry dataset. Therefore, it would be now prudent to identify the NE STING interactome in additional cell lines which have a functional cGAS-STING pathway to ensure all potential interactors can be identified, for example HT1080 cells and THP1 cells.

Table 6.1 – Experimentally validated STING interactors identified in NE STING mass spectrometry

gene_name	isoform	p.mock	s.mock	p.STING-GFP	s.STING-GFP
CCDC47		0	0.0	2	2.0
DDX41*		0	0.0	4	4.0
H2B	HIST1H2BO	0	0.0	8	22.0
	HIST2H2BF	0	0.0	8	17.0
TPR		0	0.0	4	4.0

*DDX41-STING interaction identified in mouse. p, peptide s, spectra.

As well as a few previously reported STING interactors, our mass spectrometry dataset also includes several well-known NE proteins which were enriched in STING-GFP pulldown samples compared to mock samples: Lamin A/C (LMNA), Lamins B1 and B2 (LMNB1, LMNB2), LAP2α and LAP2β/γ (TMPOα, TMPOβ/γ) (see Table 6.2). An enrichment of these but not NE proteins, SUN2, Nesprin2, or LBR in STING-GFP pulldown samples suggests that interactions with nuclear lamin proteins and LAP2 isoforms are specific as opposed to simply pulling down the most abundant NE proteins because SUN2 and nesprins repeatedly were recovered at much higher spectral abundance than LAP2 in experiments identifying the NE proteome (Schirmer et al. 2003; Korfali et al. 2012). That STING pulled-down LAP2α is interesting since this LAP2 isoform is a nucleoplasmic protein sharing only its N-terminus with the other membrane associated LAP2 isoforms (Foisner and Gerace 1993; Furukawa et al. 1998). LAP2β binds lamin B at the NE while LAP2α binds A-type lamins in the nucleoplasm (Dechat et al. 1998; Dechat et al. 2000) and so an interaction with both could suggest that STING interacts with the N-terminal domain of LAP2. However, equally they could have been pulled down by virtue of a direct association with lamin proteins. That STING-GFP did not pulldown Nesprin proteins supports the interpretation of STING's resistance to detergent extraction in the NE being due to an interaction with the nuclear lamina rather than ONM localised Nesprin proteins which have also been shown to resist detergent extraction (Starr and Fischer 2005).

Table 6.2 – Well-known NE proteins identified in NE STING mass spectrometry

gene_name	protein_name	p.mock	s.mock	p.STING-GFP	s.STING-GFP
LMNA	Lamin A/C	6	11.0	28	48.0
LMNB1	Lamin B1	9	10.0	17	23.0
LMNB2	Lamin B2	0	0.0	6	9.0
TMPO	LAP2α	0	0.0	7	18.0
TMPO	LAP2β/y	3	4.0	13	28.0
SUN2	SUN2	3	3.0	1	1.0
SYNE2	Nesprin 2	1	1.0	0	0.0
LBR	LBR	2	2.0	0	0.0

p, peptide s, spectra.

Several proteins involved in the DNA damage response or DNA repair pathways were also identified as partners of STING in the NE (Table 6.3). Notably, these include PARP1, which was found to be required for recognition of etoposide induced DNA damage and assembly of a STING-IFI16-TRAF6-p53 signalling complex (Dunphy et al. 2018), as well as, subunits of the DNA-PK complex (DNA-PKcs, Ku70, and Ku80) which have been shown to activate STING-dependent IFNβ induction (Ferguson et al. 2012; Wang et al. 2017a). It is therefore probable that STING at the NE is involved in mediating these responses to DNA damage. It would now be interesting to test whether these interactions are enhanced following etoposide induced DNA damage by pulldowns of STING from isolated NEs or nuclei. Additionally, proximity ligation assays could be performed with and without etoposide treatment to assess whether interactions between STING and DNA damage response proteins occur at the INM.

Table 6.3 – DNA damage response and repair proteins identified in NE STING mass spectrometry

gene_name	protein_name	p.mock	s.mock	p.STING	s.STING
PARP1	PARP1	37	62.0	44	106.0
PRKDC	DNA-PKcs	17	17.0	18	20.0
TOP1	DNA topoisomerase I	20	41.0	32	82.0
TOP2A	DNA topoisomerase 2-alpha	25	41.0	32	51.0
LIG3	DNA Ligase III	2	2.0	9	9.0
PARP2	PARP2	0	0.0	8	10.0
XRCC6	Ku70	1	1.0	5	5.0
MRE11	MRE11	0	0.0	1	1.0
XRCC1	XRCC1	0	0.0	1	1.0
HMGB2	HMGB2	0	0.0	1	1.0
RUVBL2	RUVBL2	0	0.0	2	2.0
ACTL6A	ACTL6A	0	0.0	1	1.0

p, peptide s, spectra.

Although, the Schirmer lab previously identified a role for STING in chromatin compaction, with STING protein levels correlating with the amount of compacted chromatin and STING overexpression increasing levels of chromatin compaction, the mechanism through which STING mediates this effect is unclear. STING-GFP pulldown samples were most enriched for histone proteins with histone H1 and H2B variants particularly enriched compared to mock pulldown samples (Figure 6.2 A and Table 6.4). Interestingly, these histone variants have been reported to have immune functions. In particular, HIST1H1C is reported to antagonise IAV replication through interacting with IRF3 and upregulating IFNβ expression with HIST1H1C phosphorylation promoting IRF3 binding to the IFNβ promoter and methylation of HIST1H1C bringing nucleosomes into closer proximity to the IFNβ promoter and inhibiting IRF3 binding (Liu et al. 2017). While histone H2B has an extrachromosomal function in promoting dsDNA stimulated immune responses by forming complexes with IFI16-BRCA1 and with cGAS and STING during infection with herpesviruses (Iqbal et al. 2016). Additionally, H2B was reported to interact with MAVS and upregulate IFNβ expression following stimulation with dsDNA (Kobiyama et al. 2010). Thus, STING interaction with these histones at the INM could direct histone modifications which promote innate immune signalling or modification of these histones could affect interactions with STING at the NE leading to its activation and redistribution from the INM to ONM.

Table 6.4 – Histone proteins identified in NE STING mass spectrometry

gene_name	protein_name	p.mock	s.mock	p.STING	s.STING
HIST1H1C	Histone H1.2	7	28.0	13	104.0
HIST1H1E	Histone H1.4	7	28.0	13	103.0
HIST1H1D	Histone H1.3	6	26.0	10	97.0
HP1BP3	HP1BP3	6	9.0	23	77.0
HIST1H1T	Histone H1.6	3	17.0	5	50.0
HIST1H1B	Histone H1.5	0	0.0	5	7.0
H1F0	Histone H1.0	2	3.0	4	8.0
H1FX	Histone H1x	1	2.0	4	10.0
H2AFY	Core histone macro-H2A.1	10	21.0	17	55.0
H2AFY2	Core histone macro-H2A.2	11	21.0	19	61.0
HIST2H2AA3	Histone H2A type 2	0	0.0	6	26.0
HIST1H2BO	Histone H2B type 1-O	0	0.0	8	22.0
HIST2H2BF	Histone H2B type 2-F	0	0.0	8	17.0

p, peptide s, spectra.

Multiple chromatin modifying proteins were also enriched in the STING-GFP pulldown samples which could implement epigenetic chromatin modifications seen with STING overexpression (Malik et al. 2014). These include bromodomain proteins BRD2 and BRD3, knockdown of which results in reduced expression of multiple inflammatory cytokines in macrophages following immune stimulation with LPS (Nicodeme et al. 2010). Additionally, BAZ2A a subunit of the nucleolar remodelling complex which mediates the formation of perinucleolar heterochromatin was identified and could have a similar function at the NE (Guetg et al. 2010). Curiously, nucleolin (NCL) which is predominantly localised to the nucleolus bound to pre-ribosomal RNA was also identified as one of the most enriched proteins in the STING-GFP pulldown samples. STING interactions with such nucleolar proteins could hint at the mechanism through which STING is able to direct inhibition of cellular translation during infection with RNA viruses (Franz et al. 2018), since the nucleolus is the site of ribosome biogenesis.

Table 6.5 – Chromatin modifiers identified in NE STING mass spectrometry

gene_name	protein_name	p.mock	s.mock	p.STING	s.STING
BRD2	BRD2	12	20.0	26	64.0
BRD3	BRD3	5	7.0	20	42.0
BRD4	BRD4	10	12.0	11	30.0
KIAA0020	KIAA0020/PUM3	3	4.0	25	50.0
BAZ2A	BAZ2A	4	4.0	23	28.0
MECP2	MECP2	0	0.0	10	19.0
HELLS	HELLS	1	1.0	14	16.0
RSF1	RSF1	2	2.0	10	12.0

p, peptide s, spectra.

Finally, while undertaking the research submitted in this thesis, another research group separately published a NE STING interactome on bioRχiv (Cheradame et al. 2020). In this study *Cheradame at al.* report that STING partially localises at the INM in breast cancer cell lines and interacts with several DNA damage response proteins including DNA-PKcs, Ku70, and Ku80. Interestingly, they also show that depletion of STING results in reduction of 53BP1 and yH2AX foci and that STING colocalises with these foci following treatment with the DNA damaging agent mafosfamide. Thus, they conclude that STING is involved in the DNA damage response and DNA repair. While they similarly show that STING is present in the INM by immunogold-EM, this is only done with tagged and overexpressed STING and so my data is the first to show that endogenous STING partially localises at the INM. Moreover, they did

not investigate whether STING localisation within the NE changes in response to different stimuli. I would thus consider my data and theirs to be complementary and supportive of each other. To identify NE STING partners in their study, MCF7 breast cancer cells were stably transfected with a FLAG-STING-HA construct from which nuclei were isolated and treated with benzonase before immunoprecipitation using an anti-FLAG antibody. This differs slightly from the approach used in our study in which HEK293T cells were transiently transfected with a STING-GFP construct, NEs isolated and treated with DNase/RNase, and then reversibly cross-linked before immunoprecipitation using an anti-GFP antibody. Therefore, I decided to compare their STING NE interactome to ours to see if these two approaches identified the same binding partners. *Cheradame et al.* identified 126 high confidence interactors of NE localised STING and similarly did not identify canonical STING interactors (e.g. TBK1, IFI16, IRF3, MAVS, RIG-I, STIM1). Comparing their dataset to ours 57 of their 126 top hits are present in our mass spectrometry dataset (Figure 6.3, red highlight), with 34 of those proteins enriched in the STING-GFP pulldown sample compared to mock. SYNCRIP, SNRNP70, and UBTF proteins that we identified as NE STING partners with indirect links to IRF3/7 transcription factors were identified as enriched in STING pulldowns by *Cheradame et al.* while DDX5, TCERG1, and RPS27A were also identified but did not make the cut-off of being statistically significantly enriched in their study. Thus, their mass spectrometry data supports our identification of these proteins as NE STING partners. While the datasets do not overlap completely, this can be explained by the different cell lines and approaches used for identification of NE STING partners.

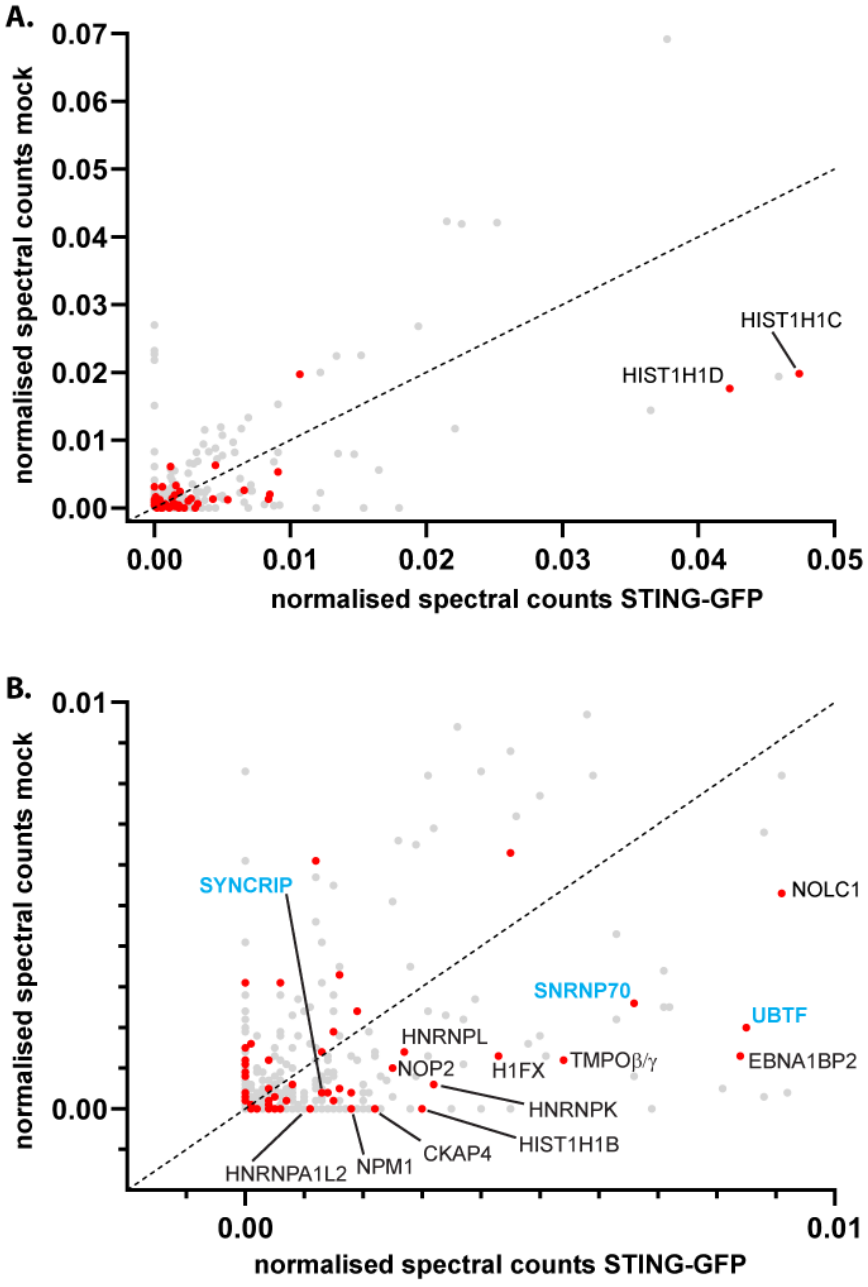

Figure 6.3 – NE STING partners identified by Cheradame et al. are present in our mass spectrometry dataset. (A) *Relative abundance of proteins identified by mass spectrometry in STING-GFP and mock pulldown samples were plotted against one another as normalised spectral counts (dnormS = normS/sum(normS)). Where normS is the number of spectra divided by protein molecular weight (in hundreds of kDa) and sum(normS) is the sum of normS in that sample. Proteins below dashed line are enriched in STING-GFP pulldown sample.* ***(B)*** *Most enriched proteins in STING-GFP pulldown sample after histone variants shown in (A). STING NE partners known to interact indirectly with IRF3/7 are highlighted in blue. NE STING interactors identified by Cheradame et al. are coloured red.*

6.3 – How do NE STING partners function in IIRs?

In this thesis I have shown that several NE STING partners are involved in the IIR with SYNCRIP, MEN1, SNRNP70, and RPS27A all found to be required for proper immune signalling following immune stimulation with dsDNA. While DDX5 appears to function antagonistically in immune signalling stimulated by either dsDNA or dsRNA ligands, with its knockdown leading to elevated IFNβ mRNA levels after immune stimulation with either plasmid DNA or poly(I:C). However, the mechanism through which these proteins mediate their effects on IIR signalling has not been completely elucidated and could occur at a number of levels in the signalling pathway.

Firstly, proteins could be directly involved in DNA/RNA sensing and the activation of downstream signalling partners. As all of these proteins predominantly localise to the nucleus, except for SYNCRIP for which isoforms Q2 and Q3 localise to the nucleus while Q1 localises to the cytoplasm, we initially proposed that these proteins could function in sensing of viral DNA or RNA in the nucleus. That said, transfection of dsDNA or poly(I:C) used to stimulate IIR in this study initially results in the release of transfected material into the cytoplasm and hence the initiation of IIR signalling likely occurs here. Indeed, in the cGAS-STING pathway, transfection of dsDNA results in the formation of cGAS foci around cytoplasmic DNA which initiates the production of cGAMP to activate STING (Hu et al. 2019). For SYNCRIP, MEN1, and SNRNP70 cytoplasmic localisation is also evident and so they could directly sense cytoplasmic DNA/RNA without requiring redistribution from the nucleus. In contrast, DDX5 is almost exclusively localised to the nucleus and so it is less likely to be involved in directly sensing DNA/RNA in the cytoplasm, particularly as no redistribution of DDX5 to the cytoplasm was evident after transfection with DNA or poly(I:C). Although, DDX5 has been shown to shuttle between the nucleus and cytoplasm and so could, under certain circumstances, be involved in cytoplasmic DNA/RNA sensing (Wang et al. 2009). Whether SYNCRIP, MEN1, DDX5, or SNRNP70 bind to transfected DNA/RNA in the cytoplasm and/or nucleus should be tested in the future by transfecting biotin labelled DNA/poly(I:C) and performing pulldown assays on nuclear and cytoplasmic cellular fractions.

Although when this study was started the notion of nuclear pathogen DNA/RNA sensors was novel and unexplored, over the last few years several proteins have been identified that function in nuclear DNA sensing and activation of STING signalling. These include IFI16, which

in conjunction with cGAS recognises plasmid DNA and HSV-1 genomic DNA at least partially in the nucleus as well as in the cytoplasm (Orzalli et al. 2015); hnRNPA2B1 which binds HSV-1 genomic DNA in the nucleus and subsequently relocalises to the cytoplasm where it activates TBK1-IRF3 signalling, as well as separately promoting translation of cGAS, IFI16, and STING mRNAs (Wang et al. 2019); and NONO which recognises HIV-2 capsids in the nucleus and associates with nuclear cGAS enabling the recognition of HIV-2 DNA (Lahaye et al. 2018). Therefore, there is a precedent for nuclear DNA sensors, and it is likely that the proteins identified here could also fulfil such a role and this should be investigated further.

The next stage at which NE STING partners could influence IIR signalling in response to cytoplasmic DNA could be at the level of cGAS activation. For example, NE STING partners could assist detection of dsDNA by cGAS or the formation of phase separated signalling foci (Du and Chen 2018). Several proteins have already been reported to act with cGAS to promote cGAMP production and downstream signalling including: G3BP1, which promotes cGAS oligomerisation and primes it for DNA sensing (Liu et al. 2019), ZCCHC3, which binds dsDNA and enhances cGAS dsDNA binding (Lian et al. 2018), and IFI16, which augments cGAS production of cGAMP (Jønsson et al. 2017). Thus, whether NE STING partners interact with cGAS or are required for efficient cGAMP production should be tested in the future by immunoprecipitation assays and detection of cGAMP levels should be assessed by quantitative mass spectrometry.

Downstream of cGAS, NE STING partners could be required for the activation of STING, STING translocation out of the ER, or recruitment of kinases to STING signalling complexes to activate IRF3, NF-κB, or AP-1 transcription factors. Knockdown of SYNCRIP, MEN1, DDX5, or SNRNP70 were all found to inhibit activation of IRF3 as measured by levels of IRF3 phosphorylation and accumulation of IRF3 in the nucleus following immune stimulation with dsDNA. Thus, these proteins are likely playing a role in immune signalling upstream of IRF3 activation which would explain the data showing that their knockdown impairs IFNβ and CCL5 expression following immune stimulation with dsDNA, since IRF3 is required for induction of these genes. To determine whether NE STING partners are required for functional STING signalling complexes, levels of STING phosphorylation (S366) and accumulation of STING in perinuclear foci should be measured by immunoblotting and immunofluorescence, respectively, following partner knockdown and immune stimulation with dsDNA. Additionally,

it would be interesting to measure levels of endogenous NF-κB activation after partner knockdown to support findings from the luciferase assay which showed that knockdown of SYNCRIP, MEN1, DDX5, or SNRNP70 reduced activation of an NF-κB activated luciferase reporter. While this was attempted by measuring accumulation of NF-κB (p65) in the nucleus of HT1080 cells after transfection of dsDNA, little or no nuclear accumulation of NF-κB was detected 4 h after stimulation. This could be due to reports that transfection of dsDNA more strongly activates STING mediated IRF3 activation rather than NF-κB activation (Dunphy et al. 2018; de Oliveira Mann et al. 2019), in agreement with my luciferase assay data showing less activation of the NF-κB luciferase reporter compared to the IFNβ luciferase reporter. Therefore, for this purpose it would be better to use etoposide treatment to induce DNA damage and STING signalling since this was found to more robustly activate NF-κB (Dunphy et al. 2018). Alternatively, NF-κB (p65) phosphorylation and accumulation in the nucleus could be measured at a later timepoint post-immune stimulation by plasmid DNA transfection. Levels of TBK1 activation, the kinase required for phosphorylation of IRF3 in activated STING signalling complexes (Liu et al. 2015a), should also be determined with STING partner knockdown and following immune stimulation by measuring levels of phosphorylated TBK1 by Western blot, since STING partners could be required for proper TBK1 activation or recruitment. Ubiquitination of STING has also been shown to be important for regulation of STING activity (Motwani et al. 2019) and so whether STING ubiquitination is altered in the absence of NE STING partners could also be tested.

Alternative mechanisms through which NE STING partners might influence IIR

Finally, it is possible that NE STING partners exert the effects on IRF3 activation and IFNβ expression through a novel mechanism or mechanisms. SYNCRIP is a member of the heterogenous nuclear ribonucleotide (hnRNP) family of proteins and is a multifunctional protein which is involved in the regulation of multiple aspects of RNA maturation including: splicing (Mourelatos et al. 2001; Chen et al. 2008), mRNA editing through association with APOBEC1 (Blanc et al. 2001; Shimizu et al. 2014; Beuck et al. 2016), vesicle-based mRNA transport through interaction with synaptogamins (Mizutani et al. 2000), sorting of miRNAs into exosomes (Santangelo et al. 2016; Hobor et al. 2018), competing with PABP for polyA binding and thus inhibiting translation (Svitkin et al. 2013), transcript-specific translational inhibition in myeloid cells stimulated with IFNy as a component of the GAIT complex

(Mukhopadhyay et al. 2009; Arif et al. 2012; Arif et al. 2018), and the regulation of HCV and MHV viral replication (Choi et al. 2004; Kim et al. 2004; Liu et al. 2009). Therefore, SYNCRIP could affect levels of IRF3 phosphorylation or IFNβ mRNA expression through these functions.

MEN1 is a tumour suppressor and regulates multiple signalling pathways including inhibiting the activity of NF-κB (Heppner et al. 2001) and AP1 (JunD) transcription factors (Agarwal et al. 1999). In some cell lines/organs MEN1 functions as a transcriptional repressor yet in others it is a transcriptional activator (Matkar et al. 2013). For example, MEN1 is an essential component of the MLL/SET1 histone methyltransferase complex that tri-methylates lysine 4 of histone H3, an activating chromatin mark which promotes transcription (Yokoyama et al. 2004; Milne et al. 2005). Interestingly, in the original study that identified MEN1 as directly interacting with JunD and thereby inhibiting JunD mediated transcription, co-expression of c-Jun and MEN1 led to increased activity of an AP1 driven luciferase reporter (Agarwal et al. 1999). Since an AP1 transcription complex heterodimer of ATF2/c-Jun is required for induction of IFNβ (Wathelet et al. 1998) the loss of MEN1 inhibiting activation of the IFNβ promoter triggered by cGAS-STING signalling, as seen in my results, would be consistent with these findings. In this context, MEN1 could normally be interacting with and repressing activity of JunD but not c-Jun, following immune stimulation with dsDNA c-Jun is required for induction of IFNβ, however, in the absence of MEN1 JunD is now free to form AP1 complexes and compete with c-Jun for doing so, thus resulting in less ATF2/c-Jun complexes to activate IFNβ and this reduces levels of IFNβ expression. However, this does not explain the reduction in IRF3 phosphorylation I see in MEN1 knockdown cells stimulated with dsDNA, suggesting that MEN1 has additional functions in IIR signalling beyond regulating NF-κB and AP1 transcription factors.

In the case of DDX5 which was recently reported to be a negative regulator of type-I IFN responses against RNA or DNA virus infection, with DDX5 knockdown resulting in higher levels of IFNβ protein levels in mouse macrophages (Zan et al. 2020), it has been suggested that DDX5 deactivates IRF3 by recruiting PP2A-Cβ to dephosphorylate IRF3 and thus inhibit type-I IFN. Interestingly, DDX5 is a positive regulator of the replication of multiple RNA viruses including HCV, Japanese encephalitis virus (JEV) and human immunodeficiency virus 1 (HIV-1) (Goh et al. 2004; Li et al. 2013a; Zhou et al. 2013; Cheng et al. 2018). Conversely, DDX5 appears to be a negative regulator of some DNA viruses and restricts Myxoma virus (MYXV)

replication in human cell lines (Rahman et al. 2017), as well as Hepatitis B virus (HBV) replication in human cancer cells (HeLa and A549) (Zhang et al. 2016), but a positive regulator of other DNA viruses including HSV-1 (Zan et al. 2020). My data showing that DDX5 knockdown results in higher levels of IFNβ mRNA and IRF3 phosphorylation following immune stimulation with poly(I:C) are consistent with DDX5 being a positive regulator of RNA viruses, potentially through inhibiting IRF3 activation by recruitment of PP2A-Cβ. However, DDX5 function in the case of dsDNA stimulated immune responses appears more complex with luciferase assay data showing that DDX5 knockdown decreases IFNβ or NF-κB luciferase construct activation and levels of IRF3 phosphorylation, while endogenous levels of IFNβ mRNA increased and HSV-1 proliferation was restricted. DDX5 is a DEAD-box RNA helicase family member and known to be involved in most aspects of RNA metabolism including translation, splicing, transcriptional regulation, ribosome biogenesis, mRNA export, and micro-RNA processing (Liu 2002; Wilson et al. 2004; Lin et al. 2005; Zonta et al. 2013; Dardenne et al. 2014). Thus, it is possible that DDX5 knockdown disrupts one or more of these fundamental RNA processes resulting in an alteration of IRF3 phosphorylation and IFNβ mRNA levels during an IIR. However, the closely related DDX17, which was also identified in our mass spectrometry dataset, has been shown to function partially redundantly with DDX5 in these processes (Germann et al. 2012; Dardenne et al. 2014) and so it is likely that DDX5 also performs a specific function in IIR triggered by DNA/RNA.

SNRNP70/U1-70K associates with U1 splicesomal RNA and Sm proteins, forming the U1-snRNP core component of the spliceosome which is essential for the recognition of the pre-mRNA 5’ splice site and assembly of the spliceosome (Hinterberger et al. 1983; Pomeranz Krummel et al. 2009; Kondo et al. 2015). Depletion of SNRNP70 could therefore disrupt expression of other innate immune signalling proteins by inhibiting transformation of pre-mRNA into mRNA. However, Western blotting against STING and cGAS showed that SNRNP70 knockdown did not affect protein levels and similarly IRF3 protein levels were not altered in SNRNP70 knockdown cells. Therefore, the core components of the cGAS-STING signalling pathway remain intact in SNRNP70 knockdown cells and this coupled with the reduced expression of IFNβ and activation of IRF3 I see in SNRNP70 knockdown cells suggests SNRNP70 plays a role in IIR signalling. Importantly, the *IFNβ* gene lacks intronic sequences and so does not undergo splicing in its expression pathway (Zago et al. 2009), so SNRNP70 knockdown

effects on IFNβ levels are likely independent of its role in splicing. Further testing of protein expression and activation of other known components of the cGAS-STING signalling pathway, such as the kinase TBK1, are required to rule out the possibility that SNRNP70 knockdown indirectly affects IIR signalling as a consequence of disrupted spliceosome function.

RPS27A is a component of the 40S subunit of the ribosome, encoded by the *RPS27A* gene the protein is expressed as a fusion protein with ubiquitin which is cleaved into the RPS27A protein and ubiquitin monomer (Kenmochi et al. 1998). While RPS27A knockdown significantly reduced induction of IFNβ and NF-κB luciferase reporters, its role in IIR was not investigated further here since knockdown caused high levels of cell death. However, RPS27A has been proposed to perform extra-ribosomal functions in promoting cell proliferation in leukaemia cell lines (Wang et al. 2014a). More intriguingly, RPS27A was recently identified as a candidate nuclear DNA-sensor in a study which identified proteins binding to biotinylated HSV-1 genomic DNA and that relocalised from the nucleus to the cytoplasm (Wang et al. 2019). Although the authors of this study did not focus on the role of RPS27A here and instead focused on another candidate DNA-sensor, hnRNPA2/B1, identifying it as a novel nuclear viral DNA sensor which activates cGAS-STING signalling (Wang et al. 2019). That their strategy identified RPS27A as one of 23 candidate HSV-1 nuclear DNA sensors and that I found that RPS27A knockdown impaired IFNβ and NF-κB luciferase reporter activation suggest it may play a role in DNA sensing and the cGAS-STING pathway, a function which should now be investigated. Moreover, hnRNPA2B1 was also identified as a NE STING partner in our mass spectrometry dataset (mock sample: 3 peptides, 7 spectra, STING-GFP sample: 7 peptides, 12 spectra) (Figure 6.2 B) while *Wang et al.* found that it immunoprecipitated the constitutive STING binding partner, TBK1 (Zhang et al. 2019; Wang et al. 2019). Although, they did not test whether hnRNPA2B1 immunoprecipitated STING itself, their data and ours suggest that hnRNPA2B1 is a component of STING signalling complexes and their data supports our approach for identifying NE DNA/RNA sensors.

Currently, one of the outstanding questions in the cGAS-STING field is how nuclear resident cGAS is able to detect dsDNA in the cytoplasm. While cGAS also has a cytoplasmic pool, recent studies suggest that the larger proportion of cGAS resides in the nucleus (Orzalli et al. 2015; Gentili et al. 2019; Volkman et al. 2019; Sun et al. 2021). Some nuclear cGAS is exported to the cytoplasm in response to DNA stimulation in a manner dependent on a cGAS nuclear

export signal (NES) and the nuclear export receptor CRM1 (Sun et al. 2021) and, correspondingly, inactivation of CRM1 or mutation of the cGAS NES results in a failure of this pool to leave the nucleus and severely attenuates the IFN response following cytosolic DNA immune stimulation (Sun et al. 2021). Therefore, it is unclear how cytosolic DNA results in the translocation of cGAS from the nucleus, although it is possible that in resting cells cGAS translocates back and forth between cytoplasm and nucleus and binding to DNA in the cytoplasm results in cGAS aggregation and accumulation in the cytoplasm. Similarly, it is unclear how NE STING partners contribute to IIR signalling in the cytoplasm when they exist predominantly in the nucleus. One possibility is that STING redistribution from the INM to ONM following immune stimulation alters STING-partner interactions allowing them to function in IIR signalling. We had initially hypothesised that STING could direct the redistribution of NE partners to the cytoplasm through physically trafficking them through the peripheral channels of the NPC, because preliminary data from the lab suggested that SYNCRIP and MEN1 redistributed from the nucleus to the cytoplasm following immune stimulation with plasmid DNA or poly(I:C) in a manner dependent on STING. However, my immunofluorescence experiments testing NE STING partner localisation during IIR showed only modest alterations in NE STING partner distributions following immune stimulation with DNA/poly(I:C). Therefore, this hypothesis was not pursued further. However, it is possible that the issues with antibodies recognising multiple isoforms of Syncrip as well as the cross-reactivity I noted in chapter 4 with hnRNP R reduced the effects observed. Accordingly, it would be interesting to investigate this hypothesis further through the use of fluorescently tagged protein constructs and using biotinylated DNA/poly(I:C) to determine whether NE STING partners associate with transfected nucleic acids. Moreover, I only looked at whether an alteration in protein localisation occurred 2 h post-immune stimulation, thus, it would be worth testing different timepoints (both earlier and later) to see if a redistribution occurs. Additionally, different immune stimuli could be tested such as DNA damage through etoposide treatment, nuclear microinjected DNA/poly(I:C), and viral genomic DNA/RNA in order to further elucidate the role of NE STING partners in IIR.

6.4 – How does SYNCRIP antagonise influenza A virus?

One of the major findings of the work presented in thesis is that SYNCRIP is a novel antagonist of the RNA virus influenza A (IAV), with IAV replicating to higher titres in SYNCRIP knockdown

and SYNCRIP knockout HT1080 cells. Interestingly, this appears to be a strain-specific effect with a loss of SYNCRIP only benefitting the H1N1 PR8 strain of IAV and not the H3N2 Udorn strain. Moreover, this effect was greater in PR8 mutant strains which have a defective NS1 protein, the main protein used by IAV to inhibit the host immune response. This suggests that the role SYNCRIP is playing in IIR against IAV infection is antagonised by NS1. In support of this notion, SYNCRIP has been identified as an interactor of NS1 from the PR8 but not the Udorn strain in pulldown experiments followed by mass spectrometry (Pichlmair et al. 2012; Bösl et al. 2019). This could explain why I only see a difference in IAV titres with SYNCRIP knockdown for the PR8 strain but not the Udorn strain. It is also consistent with the differences reported for how the NS1 proteins of these two strains antagonise innate immune signalling i.e. PR8 NS1 inhibits IRF3 activation to prevent IFNβ expression while Udorn NS1 targets host cell mRNA translation to downregulate IFNβ expression; thus, it may be that the Udorn strain has no need to target SYNCRIP. These findings, coupled with my data showing that SYNCRIP is required for optimal IRF3 activation, and IFNβ and CCL5 expression in cells stimulated with dsDNA, could suggest that SYNCRIP is similarly involved in the activation of IRF3 and subsequent induction of immune response genes during IAV infection. Further evidence of SYNCRIP playing a role in IAV infection comes from a meta study which analysed cell-based gene expression profiles during IAV infection from ten published studies and found that SYNCRIP is a significantly differentially expressed gene during IAV infection (Forst et al. 2017). Interestingly, in this study SYNCRIP gene expression was found to be down-regulated in some of the datasets and up-regulated in others, perhaps indicating that SYNCRIP is up-regulated by the host cell but targeted by IAV for down-regulation (Forst et al. 2017).

Despite showing that SYNCRIP is a novel factor in restricting IAV infection, the mechanism through which it does so requires further investigation. Based on my own research and what is already known about SYNCRIP functions from the literature several mechanisms might explain how SYNCRIP is able to antagonise viral infection. Firstly, it is possible that SYNCRIP is involved in STING-dependent dsDNA sensing of mtDNA in the cytoplasm released as a consequence of IAV infection (Moriyama et al. 2019). My data showing that SYNCRIP is required for optimal activation of IRF3 and IFNβ expression in response dsDNA transfection would support this since both transfection and mtDNA leakage result in the release of dsDNA into the cytoplasm. Secondly, STING has been shown to inhibit cellular translation in response

to infection with the RNA virus, VSV, or poly(I:C) stimulation through a mechanism that was independent of PKR and eIF2a (Franz et al. 2018). Given that we identify SYNCRIP as a partner of STING at the NE and that SYNCRIP is known to regulate translation (Kim et al. 2004; Cho et al. 2007; Kim et al. 2012; Svitkin et al. 2013; Lai et al. 2017), it is possible that SYNCRIP is responsible for restricting translation downstream of STING during RNA virus infection. Specifically, SYNCRIP is able to bind to the 5' UTR of mRNAs to upregulate translation of some mRNAs (Kim et al. 2012; Lai et al. 2017), and/or to increase internal ribosome entry site (IRES)-dependent translation through binding IRES sites (Kim et al. 2004; Cho et al. 2007), and/or to compete with PABP for binding to poly(A) tails of mRNAs thereby inhibiting translation (Svitkin et al. 2013). It would thus be interesting to test whether translation is affected in SYNCRIP knockdown cells following IAV infection or poly(I:C)/dsDNA transfection. This could be done using polysome profiling to determine the quantity of ribosomes bound to mRNAs in each condition.

Another mechanism through which SYNCRIP might influence IIR and inhibit IAV infection could be through packaging of miRNAs/mRNAs/cGAMP into extra-cellular vesicles (EV) for cell-to-cell transport. SYNCRIP is known to facilitate the sorting of specific miRNAs into EVs (Santangelo et al. 2016; Hobor et al. 2018) and so it is conceivable that it may be involved in sorting miRNAs with immune modulatory functions into EVs that could prime neighbouring cells for viral defence. Similarly cGAMP is packaged into EVs and viral particles of cells infected with DNA viruses or HIV-1 (Bridgeman et al. 2015; Gentili et al. 2015). Therefore, it would be interesting to test whether SYNCRIP can bind cGAMP or is involved in packaging cGAMP into EVs or viral particles. In addition to future experiments to unpick the mechanism through which SYNCRIP restricts IAV infection, whether SYNCRIP restricts the proliferation of other RNA viruses and DNA viruses should be tested. While SYNCRIP knockdown did not strongly affect HSV-1 viral titres in my experiments, this could have been due to a report that the cGAS-STING signalling pathway is not the principal signalling pathway through which HT1080 cells restrict HSV-1, instead relying on TLR3-TRIF mediated immune signalling (Latif et al. 2020). Thus, assuming that SYNCRIP restricts viruses in a manner dependent on STING, SYNCRIP knockdown in another cell line, such as THP-1 cells, should be tested for an effect on HSV-1 proliferation. My data, showing that SYNCRIP is a restriction factor of IAV adds to a literature already reporting SYNCRIP functions during viral infection. Interestingly, SYNCRIP is a pro-viral

factor during murine hepatitis virus (MHV) or HCV infection with SYNCRIP promoting virus RNA replication (Choi et al. 2004; Liu et al. 2009). Additionally, SYNCRIP promotes translation of HCV RNA through directly binding HCV mRNA and promoting IRES-dependent translation (Kim et al. 2004). Since IAV does not rely on IRES-dependent translation for production of viral proteins but instead IAV mRNAs acquire 5' mRNA caps from the host cell and so translation occurs in a cap-dependent manner (Plotch et al. 1979; Plotch et al. 1981; Garfinkel and Katze 1992), this could explain why SYNCRIP can be pro-viral in the case of HCV infection but anti-viral during IAV infection.

Intriguingly, several other hnRNP family members are also involved in antagonising viral infection (Valente and Goff 2006; Wang et al. 2014b; Wang et al. 2019; Kaur and Lal 2020), perhaps most notably hnRNPA2B1 which, in addition to being a nuclear sensor of HSV1 DNA (Wang et al. 2019), also binds to IAV NS1 and inhibits IAV replication partly through suppressing NS1 protein/RNA levels (Wang et al. 2014b). hnRNPA2B1 and SYNCRIP are also both involved in sorting of specific miRNAs into exosomes (Villarroya-Beltri et al. 2013; Santangelo et al. 2016), albeit recognising slightly different RNA sequences, making them two of only four proteins so far identified to have this capability (Hobor et al. 2018). These functional similarities could indicate that SYNCRIP and hnRNPA2B1 function in IIR and viral restriction through similar mechanisms.

6.5 – Final Remarks

The initial goal of this project was to investigate the role of STING in the NE. In the work submitted in this thesis, I have shown for the first time that a pool of endogenous STING resides in the INM and that STING localisation within the NE changes following immune stimulation with either dsDNA or, somewhat surprisingly, the dsRNA mimic poly(I:C). These findings have implications for the role STING plays in immune responses stimulated by nuclear DNA damage or DNA virus infection, as well as promoting chromatin compaction from the NE. Moreover, they could provide insight as to how STING functions in restricting cellular translation after immune stimulation with poly(I:C) or RNA virus infection. A key question to answer going forward will be to determine how STING localises to the INM, since this should enable the separation of ER and INM STING pools to better investigate STING function specifically within the INM. Moreover, in this work I have identified SYNCRIP, MEN1, DDX5, SNRNP70, and to a lesser extent RPS27A and AATF, as novel modulators of the cGAS-STING

immune signalling pathway. SYNCRIP, MEN1, DDX5, and SNRNP70 all effect IFNβ mRNA levels and IRF3 phosphorylation after immune stimulation with dsDNA while DDX5 also negatively regulates IFNβ mRNA levels after immune stimulation with poly(I:C). Further, experiments will be required to elucidate the exact mechanisms through which these proteins influence innate immune signalling. Finally, I have shown that SYNCRIP is a novel restriction factor of the RNA virus IAV, specifically antagonising the proliferation of the H1N1 strain, PR8, but not the H3N2 strain, Udorn. A finding that coupled with experiments showing that PR8 mutant strains expressing a defective NS1 protein are more strongly impaired by the presence of SYNCRIP, hints at a role for SYNCRIP in promoting IRF3 activation during IAV infection. I have also re-examined our NE STING mass spectrometry dataset to identify other protein candidates in the interactome that could mediate STING functions in the DNA damage response, chromatin compaction, and translational inhibition. Future experiments should seek to determine how the NE STING interactome changes following stimulation of cells with different immune stimuli including dsDNA transfection, etoposide treatment, poly(I:C) transfection, DNA virus infection, or RNA virus infection.

Considered together, my data are consistent with the notion that STING plays a wider role in immune signalling than its initial description as an adaptor protein in cytosolic dsDNA sensing, initiating different responses based on diverse inputs from DNA damage to RNA virus infection. The wide range of STING nuclear partners and the finding that STING translocates out of the nucleus with poly(I:C) or dsDNA treatment potentially provide novel mechanisms for STING functions in response to different innate immune challenges.

References

Abe T, Barber GN (2014) Cytosolic-DNA-Mediated, STING-Dependent Proinflammatory Gene Induction Necessitates Canonical NF- B Activation through TBK1. J Virol 88:5328–5341. doi: 10.1128/JVI.00037-14

Abe T, Harashima A, Xia T, Konno H, Konno K, Morales A, Ahn J, Gutman D, Barber GN (2013) STING Recognition of Cytoplasmic DNA Instigates Cellular Defense. Mol Cell 50:5–15. doi: 10.1016/j.molcel.2013.01.039

Ablasser A, Bauernfeind F, Hartmann G, Latz E, Fitzgerald K a, Hornung V (2009) RIG-I dependentsensing f poly(dA-dT) via the induction of an RNA polymerase III transcribed RNA intermediate. Nat Immunol. doi: 10.1038/ni.1779.RIG-I

Ablasser A, Chen ZJ (2019) CGAS in action: Expanding roles in immunity and inflammation. Science (80-). doi: 10.1126/science.aat8657

Ablasser A, Goldeck M, Cavlar T, Deimling T, Witte G, Röhl I, Hopfner K-PP, Ludwig J, Hornung V (2013a) CGAS produces a 2′-5′-linked cyclic dinucleotide second messenger that activates STING. Nature 498:380–384. doi: 10.1038/nature12306

Ablasser A, Schmid-Burgk JL, Hemmerling I, Horvath GL, Schmidt T, Latz E, Hornung V (2013b) Cell intrinsic immunity spreads to bystander cells via the intercellular transfer of cGAMP. Nature 503:530–534. doi: 10.1038/nature12640

Adam SA, Marr RS, Gerace L (1990) Nuclear protein import in permeabilized mammalian cells requires soluble cytoplasmic factors. J Cell Biol 111:807–816. doi: 10.1083/jcb.111.3.807

Agarwal SK, Guru SC, Heppner C, Erdos MR, Collins RM, Park SY, Saggar S, Chandrasekharappa SC, Collins FS, Spiegel AM, Marx SJ, Burns AL (1999) Menin Interacts with the AP1 Transcription Factor JunD and Represses JunD-Activated Transcription. Cell 96:143–152. doi: 10.1016/S0092-8674(00)80967-8

Aguirre S, Luthra P, Sanchez-Aparicio MT, Maestre AM, Patel J, Lamothe F, Fredericks AC, Tripathi S, Zhu T, Pintado-Silva J, Webb LG, Bernal-Rubio D, Solovyov A, Greenbaum B, Simon V, Basler CF, Mulder LCF, García-Sastre A, Fernandez-Sesma A (2017) Dengue virus NS2B protein targets cGAS for degradation and prevents mitochondrial DNA sensing during infection. Nat Microbiol 2:1–11. doi: 10.1038/nmicrobiol.2017.37

Aguirre S, Maestre AM, Pagni S, Patel JR, Savage T, Gutman D, Maringer K, Bernal-Rubio D, Shabman RS, Simon V, Rodriguez-Madoz JR, Mulder LCF, Barber GN, Fernandez-Sesma A (2012) DENV Inhibits Type I IFN Production in Infected Cells by Cleaving Human STING. PLoS Pathog 8:e1002934. doi: 10.1371/journal.ppat.1002934

Ahmad S, Hur S (2015) Helicases in Antiviral Immunity: Dual Properties as Sensors and Effectors. Trends Biochem Sci 40:576–585. doi: 10.1016/j.tibs.2015.08.001

Ahn J, Barber GN (2019) STING signaling and host defense against microbial infection. Exp Mol Med. doi: 10.1038/s12276-019-0333-0

Ahn J, Xia T, Konno H, Konno K, Ruiz P, Barber GN (2014) Inflammation-driven carcinogenesis is mediated through STING. Nat Commun. doi: 10.1038/ncomms6166

Aitchison JD, Rout MP (2012) The yeast nuclear pore complex and transport through it. Genetics 190:855–883. doi: 10.1534/genetics.111.127803

Almine JF, O'Hare CAJ, Dunphy G, Haga IR, Naik RJ, Atrih A, Connolly DJ, Taylor J, Kelsall IR, Bowie AG, Beard PM, Unterholzner L (2017) IFI16 and cGAS cooperate in the activation of STING during DNA sensing in human keratinocytes. Nat Commun 8:14392. doi: 10.1038/ncomms14392

Andreeva L, Hiller B, Kostrewa D, Lässig C, De Oliveira Mann CC, Jan Drexler D, Maiser A, Gaidt M, Leonhardt H, Hornung V, Hopfner K-PP (2017) CGAS senses long and HMGB/TFAM-bound U-turn DNA by forming protein-DNA ladders. Nature 549:394–398. doi: 10.1038/nature23890

Arif A, Chatterjee P, Moodt RA, Fox PL (2012) Heterotrimeric GAIT Complex Drives Transcript-Selective Translation Inhibition in Murine Macrophages. Mol Cell Biol 32:5046–5055. doi: 10.1128/MCB.01168-12

Arif A, Yao P, Terenzi F, Jia J, Ray PS, Fox PL (2018) The GAIT translational control system. Wiley Interdiscip Rev RNA. doi: 10.1002/wrna.1441

Ayllon J, García-Sastre A (2015) The NS1 Protein: A Multitasking Virulence Factor. Curr Top Microbiol Immunol 386:73–107. doi: 10.1007/82

Bagchi S, Fredriksson R, Wallén-Mackenzie Å (2015) In Situ Proximity Ligation Assay (PLA). In: Hnasko R (ed) ELISA: Methods and Protocols. Springer New York, New York, NY, pp 149–159

Bahrami S, Laska MJ, Pedersen FS, Duch M (2016) Immune suppressive activity of the influenza fusion peptide. Virus Res 211:126–132. doi: 10.1016/j.virusres.2015.10.012

Bai H, Lester GMS, Petishnok LC, Dean DA (2017) Cytoplasmic transport and nuclear import of plasmid DNA. Biosci Rep 37:1–17. doi: 10.1042/BSR20160616

Bajar BT, Wang ES, Zhang S, Lin MZ, Chu J (2016) A guide to fluorescent protein FRET pairs. Sensors (Switzerland) 16:1–24. doi: 10.3390/s16091488

Bannai H, Fukatsu K, Mizutani A, Natsume T, Iemura SI, Ikegami T, Inoue T, Mikoshiba K (2004) An RNA-interacting protein, SYNCRIP (heterogeneous nuclear ribonuclear protein Q1/NSAP1) is a component of mRNA granule transported with inositol 1,4,5-trisphosphate receptor type 1 mRNA in neuronal dendrites. J Biol Chem 279:53427–53434. doi: 10.1074/jbc.M409732200

Bartoszewski R, Sikorski AF (2019) Editorial focus: Understanding off-target effects as the key to successful RNAi therapy. Cell Mol Biol Lett 24:1–23. doi: 10.1186/s11658-019-0196-3

Bartsch K, Knittler K, Borowski C, Rudnik S, Damme M, Aden K, Spehlmann ME, Frey N, Saftig P, Chalaris A, Rabe B (2017) Absence of RNase H2 triggers generation of immunogenic micronuclei removed by autophagy. Hum Mol Genet 26:3960–3972. doi: 10.1093/hmg/ddx283

Batrakou DG, Kerr ARWW, Schirmer EC (2009) Comparative proteomic analyses of the nuclear envelope and pore complex suggests a wide range of heretofore unexpected

functions. J Proteomics 72:56–70. doi: 10.1016/j.jprot.2008.09.004

Beck M, Hurt E (2016) The nuclear pore complex: understanding its function through structural insight. Nat Rev Mol Cell Biol 18:73–89. doi: 10.1038/nrm.2016.147

Beck M, Lǔí V, Förster F, Baumeister W, Medalia O (2007) Snapshots of nuclear pore complexes in action captured by cryo-electron tomography. Nature 449:611–615. doi: 10.1038/nature06170

Bergsbaken T, Fink SL, Cookson BT (2009) Pyroptosis: Host cell death and inflammation. Nat Rev Microbiol 7:99–109. doi: 10.1038/nrmicro2070

Beuck C, Williamson JR, Kurt W, Serrano P, Wüthrich K, Serrano P, Wuthrich K, Serrano P, Kurt W, Serrano P, Wüthrich K, Serrano P (2016) The acidic domain is a unique structural feature of the splicing factor SYNCRIP. Protein Sci 25:1545–1550. doi: 10.1002/pro.2935

Bevilacqua PC, Cech TR (1996) Minor-groove recognition of double-stranded RNA by the double-stranded RNA-binding domain from the RNA-activated protein kinase PKR. Biochemistry 35:9983–9994. doi: 10.1021/bi9607259

Bhatelia K, Singh A, Tomar D, Singh K, Sripada L, Chagtoo M, Prajapati P, Singh R, Godbole MM, Singh R (2014) Antiviral signaling protein MITA acts as a tumor suppressor in breast cancer by regulating NF-κB induced cell death. Biochim Biophys Acta - Mol Basis Dis 1842:144–153. doi: 10.1016/j.bbadis.2013.11.006

Blanc V, Navaratnam N, Henderson JO, Anant S, Kennedy S, Jarmuz A, Scott J, Davidson NO (2001) Identification of GRY-RBP as an Apolipoprotein B RNA-binding Protein that Interacts with Both Apobec-1 and Apobec-1 Complementation Factor to Modulate C to U Editing. J Biol Chem 276:10272–10283. doi: 10.1074/jbc.M006435200

Boni A, Politi AZ, Strnad P, Xiang W, Hossain MJ, Ellenberg J (2015) Live imaging and modeling of inner nuclear membrane targeting reveals its molecular requirements in mammalian cells. J Cell Biol 209:705–720. doi: 10.1083/jcb.201409133

Boshart M, Gissmann L, Ikenberg H, Kleinheinz A, Scheurlen W, zur Hausen H (1984) A new type of papillomavirus DNA, its presence in genital cancer biopsies and in cell lines derived from cervical cancer. EMBO J 3:1151–1157. doi: 10.1002/j.1460-2075.1984.tb01944.x

Bösl K, Ianevski A, Than TT, Andersen PI, Kuivanen S, Teppor M, Zusinaite E, Dumpis U, Vitkauskiene A, Cox RJ, Kallio-Kokko H, Bergqvist A, Tenson T, Oksenych V, Bjørås M, Anthonsen MW, Shum D, Kaarbø M, Vapalahti O, Windisch MP, Superti-Furga G, Snijder B, Kainov D, Kandasamy RK (2019) Critical Nodes of Virus–Host Interaction Revealed Through an Integrated Network Analysis. bioRxiv 1–23. doi: 10.1101/548909

Brachner A, Foisner R (2011) Evolvement of LEM proteins as chromatin tethers at the nuclear periphery. Biochem Soc Trans 39:1735–1741. doi: 10.1042/BST20110724

Brachner A, Reipert S, Foisner R, Gotzmann J (2005) LEM2 is a novel MAN1-related inner nuclear membrane protein associated with A-type lamins. J Cell Sci 118:5797–5810. doi: 10.1242/jcs.02701

Braunagel SC, Williamson ST, Ding Q, Wu X, Summers MD (2007) Early sorting of inner nuclear membrane proteins is conserved. Proc Natl Acad Sci U S A 104:9307–12. doi: 10.1073/pnas.0703186104

Bridgeman A, Maelfait J, Davenne T, Partridge T, Peng Y, Mayer A, Dong T, Kaever V, Borrow P, Rehwinkel J (2015) Viruses transfer the antiviral second messenger cGAMP between cells. Science (80-) 349:19–23. doi: 10.1126/science.aab3632

Broers JLV, Peeters EAG, Kuijpers HJH, Endert J, Bouten CVC, Oomens CWJ, Baaijens FPT, Ramaekers FCS (2004) Decreased mechanical stiffness in LMNA-/- cells is caused by defective nucleo-cytoskeletal integrity: implications for the development of laminopathies. Hum Mol Genet 13:2567–2580. doi: 10.1093/hmg/ddh295

Bruno T, De Nicola F, Iezzi S, Lecis D, D'Angelo C, Di Padova M, Corbi N, Dimiziani L, Zannini L, Jekimovs C, Scarsella M, Porrello A, Chersi A, Crescenzi M, Leonetti C, Khanna KK, Soddu S, Floridi A, Passananti C, Delia D, Fanciulli M (2006) Che-1 phosphorylation by ATM/ATR and Chk2 kinases activates p53 transcription and the G2/M checkpoint. Cancer Cell 10:473–486. doi: 10.1016/j.ccr.2006.10.012

Bu Y, Liu F, Jia QA, Yu SN (2016) Decreased expression of TMEM173 predicts poor prognosis in patients with hepatocellular carcinoma. PLoS One 11:1–11. doi: 10.1371/journal.pone.0165681

Bui KH, Von Appen A, Diguilio AL, Ori A, Sparks L, Mackmull MT, Bock T, Hagen W, Andrés-Pons A, Glavy JS, Beck M, Andres-Pons A, Glavy JS, Beck M (2013) Integrated structural analysis of the human nuclear pore complex scaffold. Cell 155:1233–1243. doi: 10.1016/j.cell.2013.10.055

Bürckstümmer T, Baumann C, Blüml S, Dixit E, Dürnberger G, Jahn H, Planyavsky M, Bilban M, Colinge J, Bennett KL, Superti-Furga G (2009) An orthogonal proteomic-genomic screen identifies AIM2 as a cytoplasmic DNA sensor for the inflammasome. Nat Immunol 10:266–272. doi: 10.1038/ni.1702

Burdette DL, Monroe KM, Sotelo-troha K, Iwig JS, Eckert B, Hyodo M, Hayakawa Y, Vance RE, Figure S (2011) STING is a direct innate immune sensor of cyclic di-GMP. Nature 478:515–518. doi: 10.1038/nature10429

Burke B, Stewart CL (2013) The nuclear lamins: flexibility in function. Nat Rev Mol Cell Biol 14:13–24. doi: 10.1038/nrm3488

Callan HG, Randall JT, Tomlin SG (1949) An Electron Microscope Study of the Nuclear Membrane. Nature 163:280–280. doi: 10.1038/163280a0

Callan HG, Tomlin SG (1950) Investigation of the structure of the nuclear membrane by means of the electron microscope. Exp Stud Amphib oocyte Nucl 137:367–378.

Caneparo V, Landolfo S, Gariglio M, De Andrea M (2018) The absent in melanoma 2-like receptor IFN-inducible protein 16 as an inflammasome regulator in systemic lupus erythematosus: The dark side of sensing microbes. Front Immunol 9:1–14. doi: 10.3389/fimmu.2018.01180

Cao D, Han X, Fan X, Xu RM, Zhang X (2020) Structural basis for nucleosome-mediated inhibition of cGAS activity. Cell Res 30:1088–1097. doi: 10.1038/s41422-020-00422-4

Cappelli S, Romano M, Buratti E (2018) Systematic Analysis of Gene Expression Profiles Controlled by hnRNP Q and hnRNP R, Two Closely Related Human RNA Binding Proteins Implicated in mRNA Processing Mechanisms. Front Mol Biosci 5:1–17. doi: 10.3389/fmolb.2018.00079

Chen H-H, Chang J-G, Lu R-M, Peng T-Y, Tarn W-Y, And T-YP, Tarn W-Y (2008) The RNA binding protein hnRNP Q modulates the utilization of exon 7 in the survival motor neuron 2 (SMN2) gene. Mol Cell Biol 28:6929–38. doi: 10.1128/MCB.01332-08

Chen H, Sun H, You F, Sun W, Zhou X, Chen L, Yang J, Wang Y, Tang H, Guan Y, Xia W, Gu J, Ishikawa H, Gutman D, Barber G, Qin Z, Jiang Z (2011) Activation of STAT6 by STING is critical for antiviral innate immunity. Cell 147:436–446. doi: 10.1016/j.cell.2011.09.022

Chen IY, Ichinohe T (2015) Response of host inflammasomes to viral infection. Trends Microbiol 23:55–63. doi: 10.1016/j.tim.2014.09.007

Chen Q, Boire A, Jin X, Valiente M, Er EE, Lopez-Soto A, Jacob LS, Patwa R, Shah H, Xu K, Cross JR, Massague J (2016) Carcinoma-astrocyte gap junctions promote brain metastasis by cGAMP transfer. Nature 533:493–498. doi: 10.1038/nature18268

Chen X, Yang X, Zheng Y, Yang Y, Xing Y, Chen Z (2014) SARS coronavirus papain-like protease inhibits the type I interferon signaling pathway through interaction with the STING-TRAF3-TBK1 complex. Protein Cell 5:369–381. doi: 10.1007/s13238-014-0026-3

Chen YA, Shen YL, Hsia HY, Tiang YP, Sung TL, Chen LY (2017) Extrachromosomal telomere repeat DNA is linked to ALT development via cGAS-STING DNA sensing pathway. Nat Struct Mol Biol 24:1124–1131. doi: 10.1038/nsmb.3498

Cheng W, Chen G, Jia H, He X, Jing Z (2018) DDX5 RNA helicases: Emerging roles in viral infection. Int J Mol Sci. doi: 10.3390/ijms19041122

Cheng Y, Sun Y, Wang H, Yan Y, Ding C, Sun J (2015) Chicken STING Mediates Activation of the IFN Gene Independently of the RIG-I Gene. J Immunol 195:3922–3936. doi: 10.4049/jimmunol.1500638

Cheradame L, Guerrera IC, Gaston J, Schmitt A, Jung V, Pouillard M, Radosevic-Robin N, Modesti M, Judde JG, Cairo S, Goffin V (2020) STING promotes breast cancer cell survival by an inflammatory-independent nuclear pathway enhancing the DNA damage response. bioRxiv 1–44. doi: 10.1101/2020.07.11.196790

Chiang JJ, Davis ME, Gack MU (2014) Regulation of RIG-I-like receptor signaling by host and viral proteins. Cytokine Growth Factor Rev 25:491–505. doi: 10.1016/j.cytogfr.2014.06.005

Chiu YH, MacMillan JB, Chen ZJ (2009) RNA Polymerase III Detects Cytosolic DNA and Induces Type I Interferons through the RIG-I Pathway. Cell 138:576–591. doi: 10.1016/j.cell.2009.06.015

Cho S, Park SM, Kim TD, Kim JH, Kim K-T, Jang SK (2007) BiP Internal Ribosomal Entry Site Activity Is Controlled by Heat-Induced Interaction of NSAP1. Mol Cell Biol 27:368–383. doi: 10.1128/mcb.00814-06

Choi KS, Mizutani A, Lai MMC (2004) SYNCRIP , a Member of the Heterogeneous Nuclear

Ribonucleoprotein Family , Is Involved in Mouse Hepatitis Virus RNA Synthesis. J Virol 78:13153–13162. doi: 10.1128/JVI.78.23.13153

Chow J, Franz KM, Kagan JC (2015) PRRs are watching you: Localization of innate sensing and signaling regulators. Virology 479–480:104–109. doi: 10.1016/j.virol.2015.02.051

Christensen MH, Jensen SB, Miettinen JJ, Luecke S, Prabakaran T, Reinert LS, Mettenleiter T, Chen ZJ, Knipe DM, Sandri-Goldin RM, Enquist LW, Hartmann R, Mogensen TH, Rice SA, Nyman TA, Matikainen S, Paludan SR (2016) HSV -1 ICP 27 targets the TBK 1-activated STING signalsome to inhibit virus-induced type I IFN expression . EMBO J 35:1385–1399. doi: 10.15252/embj.201593458

Civril F, Deimling T, De Oliveira Mann CC, Ablasser A, Moldt M, Witte G, Hornung V, Hopfner K-PP (2013) Structural mechanism of cytosolic DNA sensing by cGAS. Nature 498:332–337. doi: 10.1038/nature12305

Clayton P, Fischer B, Mann A, Mansour S, Rossier E, Veen M, Lang C, Baasanjav S, Kieslich M, Brossuleit K, Gravemann S, Schnipper N, Karbasyian M, Demuth I, Zwerger M, Vaya A, Utermann G, Mundlos S, Stricker S, Sperling K, Hoffmann K (2010) Mutations causing Greenberg dysplasia but not pelger anomaly uncouple enzymatic from structural functions of a nuclear membrane protein. Nucleus 1:354–366. doi: 10.4161/nucl.1.4.12435

Clements L, Manilal S, Love DR, Morris GE (2000) Direct Interaction between Emerin and Lamin A. Biochem Biophys Res Commun 267:709–714. doi: 10.1006/bbrc.1999.2023

Clementz MA, Chen Z, Banach BS, Wang Y, Sun L, Ratia K, Baez-Santos YM, Wang J, Takayama J, Ghosh AK, Li K, Mesecar AD, Baker SC (2010) Deubiquitinating and Interferon Antagonism Activities of Coronavirus Papain-Like Proteases. J Virol 84:4619–4629. doi: 10.1128/jvi.02406-09

Coiras M, Montes M, Montanuy I, López-Huertas MR, Mateos E, Le Sommer C, Garcia-Blanco MA, Hernández-Munain C, Alcamí J, Suñé C (2013) Transcription elongation regulator 1 (TCERG1) regulates competent RNA polymerase II-mediated elongation of HIV-1 transcription and facilitates efficient viral replication. Retrovirology 10:1–18. doi: 10.1186/1742-4690-10-124

Cook A, Bono F, Jinek M, Conti E (2007) Structural biology of nucleocytoplasmic transport. Annu Rev Biochem 76:647–671. doi: 10.1146/annurev.biochem.76.052705.161529

Crisp M, Liu Q, Roux K, Rattner JB, Shanahan C, Burke B, Stahl PD, Hodzic D (2006) Coupling of the nucleus and cytoplasm: Role of the LINC complex. J Cell Biol 172:41–53. doi: 10.1083/jcb.200509124

Crow YJ, Hayward BE, Parmar R, Robins P, Leitch A, Ali M, Black DN, Van Bokhoven H, Brunner HG, Hamel BC, Corry PC, Cowan FM, Frints SG, Klepper J, Livingston JH, Lynch SA, Massey RF, Meritet JF, Michaud JL, Ponsot G, Voit T, Lebon P, Bonthron DT, Jackson AP, Barnes DE, Lindahl T (2006) Mutations in the gene encoding the 3’-5’ DNA exonuclease TREX1 cause Aicardi-Goutières syndrome at the AGS1 locus. Nat Genet 38:917–920. doi: 10.1038/ng1845

Crow YJ, Manel N (2015) Aicardi-Goutières syndrome and the type I interferonopathies. Nat

Rev Immunol 15:429–440. doi: 10.1038/nri3850

Crowl JT, Gray EE, Pestal K, Volkman HE, Stetson DB (2017) Intracellular Nucleic Acid Detection in Autoimmunity. Annu Rev Immunol 35:annurev-immunol-051116-052331. doi: 10.1146/annurev-immunol-051116-052331

Dambuza IM, Brown GD (2015) C-type lectins in immunity: Recent developments. Curr Opin Immunol 32:21–27. doi: 10.1016/j.coi.2014.12.002

Dardenne E, PolayEspinoza M, Fattet L, Germann S, Lambert MP, Neil H, Zonta E, Mortada H, Gratadou L, Deygas M, Chakrama FZ, Samaan S, Desmet FO, Tranchevent LC, Dutertre M, Rimokh R, Bourgeois CF, Auboeuf D (2014) RNA Helicases DDX5 and DDX17 Dynamically Orchestrate Transcription, miRNA, and Splicing Programs in Cell Differentiation. Cell Rep 7:1900–1913. doi: 10.1016/j.celrep.2014.05.010

Dauber B, Saffran HA, Smiley JR (2019) The herpes simplex virus host shutoff (vhs) RNase limits accumulation of double stranded RNA in infected cells: Evidence for accelerated decay of duplex RNA. PLoS Pathog 15:1–23. doi: 10.1371/journal.ppat.1008111

Dauletbaev N, Cammisano M, Herscovitch K, Lands LC (2015) Stimulation of the RIG-I/MAVS Pathway by Polyinosinic:Polycytidylic Acid Upregulates IFN-β in Airway Epithelial Cells with Minimal Costimulation of IL-8. J Immunol 195:2829–2841. doi: 10.4049/jimmunol.1400840

de Las Heras JI, Meinke P, Batrakou DG, Srsen V, Zuleger N, Kerr AR, Schirmer EC (2013) Tissue specificity in the nuclear envelope supports its functional complexity. Nucleus 4:460–77. doi: 10.4161/nucl.26872

de Oliveira Mann CC, Orzalli MH, King DS, Kagan JC, Lee ASY, Kranzusch PJ (2019) Modular Architecture of the STING C-Terminal Tail Allows Interferon and NF-κB Signaling Adaptation. Cell Rep 27:1165-1175.e5. doi: 10.1016/j.celrep.2019.03.098

De Wit E, Spronken MIJ, Bestebroer TM, Rimmelzwaan GF, Osterhaus ADME, Fouchier RAM (2004) Efficient generation and growth of influenza virus A/PR/8/34 from eight cDNA fragments. Virus Res 103:155–161. doi: 10.1016/j.virusres.2004.02.028

Dechat T, Gotzmann J, Stockinger A, Harris CA, Talle MA, Siekierka JJ, Foisner R (1998) Detergent-salt resistance of LAP2α in interphase nuclei and phosphorylation-dependent association with chromosomes early in nuclear assembly implies functions in nuclear structure dynamics. EMBO J 17:4887–4902. doi: 10.1093/emboj/17.16.4887

Dechat T, Korbei B, Vaughan OA, Vlcek S, Hutchison CJ, Foister R (2000) Lamina-associated polypeptide 2α binds intranuclear A-type lamins. J Cell Sci 113:3473–3484.

Demmerle J, Koch AJ, Holaska JM (2012) The nuclear envelope protein emerin binds directly to histone deacetylase 3 (HDAC3) and activates HDAC3 activity. J Biol Chem 287:22080–22088. doi: 10.1074/jbc.M111.325308

Denais CM, Gilbert RM, Isermann P, McGregor AL, Te Lindert M, Weigelin B, Davidson PM, Friedl P, Wolf K, Lammerding J (2016) Nuclear envelope rupture and repair during cancer cell migration. Science (80-) 352:353–358. doi: 10.1126/science.aad7297

Deng L, Liang H, Xu M, Yang X, Burnette B, Arina A, Li XD, Mauceri H, Beckett M, Darga T,

Huang X, Gajewski TF, Chen ZJ, Fu YX, Weichselbaum RR (2014) STING-dependent cytosolic DNA sensing promotes radiation-induced type I interferon-dependent antitumor immunity in immunogenic tumors. Immunity 41:843–852. doi: 10.1016/j.immuni.2014.10.019

Deschamps T, Kalamvoki M (2017a) Impaired STING Pathway in Human Osteosarcoma U2OS Cells Contributes to the Growth of ICP0-Null Mutant Herpes Simplex Virus. J Virol 91:1–14. doi: 10.1128/jvi.00006-17

Deschamps T, Kalamvoki M (2017b) Evasion of the STING DNA-Sensing Pathway by VP11/12 of Herpes Simplex Virus 1. 91:1–17.

Diamond MS, Kinder M, Matsushita H, Mashayekhi M, Dunn GP, Archambault JM, Lee H, Arthur CD, White JM, Kalinke U, Murphy KM, Schreiber RD (2011) Type I interferon is selectively required by dendritic cells for immune rejection of tumors. J Exp Med 208:1989–2003. doi: 10.1084/jem.20101158

Diner BA, Lum KK, Cristea IM (2015) The emerging role of nuclear viral DNA sensors. J Biol Chem 290:26412–26421. doi: 10.1074/jbc.R115.652289

Diner EJ, Burdette DL, Wilson SC, Monroe KM, Kellenberger CA, Hyodo M, Hayakawa Y, Hammond MC, Vance RE (2013) The Innate Immune DNA Sensor cGAS Produces a Noncanonical Cyclic Dinucleotide that Activates Human STING. Cell Rep 3:1355–1361. doi: 10.1016/j.celrep.2013.05.009

Ding Q, Cao X, Lu J, Huang B, Liu YJ, Kato N, Shu HB, Zhong J (2013) Hepatitis C virus NS4B blocks the interaction of STING and TBK1 to evade host innate immunity. J Hepatol 59:52–58. doi: 10.1016/j.jhep.2013.03.019

Ding Q, Gaska JM, Douam F, Wei L, Kim D, Balev M, Heller B, Ploss A (2018) Species-specific disruption of STING-dependent antiviral cellular defenses by the Zika virus NS2B3 protease. Proc Natl Acad Sci U S A 115:E6310–E6318. doi: 10.1073/pnas.1803406115

Dixon CR, Malik P, de las Heras JI, Saiz-Ros N, de Lima Alves F, Tingey M, Gaunt E, Christine Richardson A, Kelly DA, Goldberg MW, Towers GJ, Yang W, Rappsilber J, Digard P, Schirmer EC (2020) STING Nuclear Partners Contribute to Innate Immune Signalling Responses. bioRxiv 44:1–51. doi: 10.1101/2020.12.21.423744

Dixon CR, Schirmer EC (2018) Navigating the Nuclear Envelope: One or Multiple Transport Mechanisms for Integral Membrane Proteins? In: Yang W (ed) Nuclear-Cytoplasmic Transport. Springer International Publishing, Cham, pp 151–177

Dobbs N, Burnaevskiy N, Chen D, Gonugunta VK, Alto NM, Yan N (2015) STING activation by translocation from the ER is associated with infection and autoinflammatory disease. Cell Host Microbe 18:157–68. doi: 10.1016/j.chom.2015.07.001

Dou D, Revol R, Östbye H, Wang H, Daniels R (2018) Influenza A virus cell entry, replication, virion assembly and movement. Front Immunol 9:1–17. doi: 10.3389/fimmu.2018.01581

Dowty ME, Williams P, Zhang G, Hagstrom JE, Wolff JA (1995) Plasmid DNA entry into postmitotic nuclei of primary rat myotubes. Proc Natl Acad Sci U S A 92:4572–4576. doi: 10.1073/pnas.92.10.4572

Du M, Chen ZJ (2018) DNA-induced liquid phase condensation of cGAS activates innate immune signaling. Science (80-). doi: 10.1126/science.aat1022

Dunphy G, Flannery SM, Almine JF, Connolly DJ, Paulus C, Jønsson KL, Jakobsen MR, Nevels MM, Bowie AG, Unterholzner L (2018) Non-canonical Activation of the DNA Sensing Adaptor STING by ATM and IFI16 Mediates NF-κB Signaling after Nuclear DNA Damage. Mol Cell 71:745-760.e5. doi: 10.1016/j.molcel.2018.07.034

Ellis DJ, Jenkins H, Whitfield WG, Hutchison CJ (1997) GST-lamin fusion proteins act as dominant negative mutants in Xenopus egg extract and reveal the function of the lamina in DNA replication. J Cell Sci 2507–18.

Erdal E, Haider S, Rehwinkel J, Harris AL, McHugh PJ (2017) A prosurvival DNA damage-induced cytoplasmic interferon response is mediated by end resection factors and is limited by Trex1. Genes Dev 31:353–369. doi: 10.1101/gad.289769.116

Ergun SL, Fernandez D, Weiss TM, Li L (2019) STING Polymer Structure Reveals Mechanisms for Activation, Hyperactivation, and Inhibition. Cell 178:290-301.e10. doi: 10.1016/j.cell.2019.05.036

Fang R, Wang C, Jiang Q, Lv M, Gao P, Yu X, Mu P, Zhang R, Bi S, Feng J-M, Jiang Z (2017) NEMO–IKKβ Are Essential for IRF3 and NF-κB Activation in the cGAS–STING Pathway. J Immunol 199:ji1700699. doi: 10.4049/jimmunol.1700699

Fatima G, Mathan G, Kumar V (2012) The HBx protein of hepatitis B virus regulates the expression, intracellular distribution and functions of ribosomal protein S27a. J Gen Virol 93:706–15. doi: 10.1099/vir.0.035691-0

Fenech M, Kirsch-Volders M, Natarajan AT, Surralles J, Crott JW, Parry J, Norppa H, Eastmond DA, Tucker JD, Thomas P (2011) Molecular mechanisms of micronucleus, nucleoplasmic bridge and nuclear bud formation in mammalian and human cells. Mutagenesis 26:125–132. doi: 10.1093/mutage/geq052

Ferguson BJ, Mansur DS, Peters NE, Ren H, Smith GL (2012) DNA-PK is a DNA sensor for IRF-3-dependent innate immunity. Elife 2012:1–17. doi: 10.7554/eLife.00047

Fernandes-Alnemri T, Yu JW, Datta P, Wu J, Alnemri ES (2009) AIM2 activates the inflammasome and cell death in response to cytoplasmic DNA. Nature 458:509–513. doi: 10.1038/nature07710

Fiserova J, Richards SA, Wente SR, Goldberg MW (2010) Facilitated transport and diffusion take distinct spatial routes through the nuclear pore complex. J Cell Sci 123:2773–2780. doi: 10.1242/jcs.070730

Fitzgerald KA, Rowe DC, Barnes BJ, Caffrey DR, Visintin A, Latz E, Monks B, Pitha PM, Golenbock DT (2003) LPS-TLR4 signaling to IRF-3/7 and NF-κB involves the toll adapters TRAM and TRIF. J Exp Med 198:1043–1055. doi: 10.1084/jem.20031023

Fodor E (2013) The RNA polymerase of influenza A virus: Mechanisms of viral transcription and replication. Acta Virol 57:113–122. doi: 10.4149/av_2013_02_113

Foisner R, Gerace L (1993) Integral membrane proteins of the nuclear envelope interact with lamins and chromosomes, and binding is modulated by mitotic phosphorylation. Cell

73:1267–1279. doi: 10.1016/0092-8674(93)90355-T

Forst C V., Zhou B, Wang M, Chou T-W, Mason G, Song W, Schadt E, Ghedin E, Zhang B (2017) Integrative gene network analysis identifies key signatures, intrinsic networks and host factors for influenza virus A infections. npj Syst Biol Appl 3:35. doi: 10.1038/s41540-017-0036-x

Franz KM, Neidermyer WJ, Tan Y-JJ, Whelan SPJJ, Kagan JC (2018) STING-dependent translation inhibition restricts RNA virus replication. Proc Natl Acad Sci 115:201716937. doi: 10.1073/pnas.1716937115

Frenkiel-Krispin D, Maco B, Aebi U, Medalia O (2010) Structural Analysis of a Metazoan Nuclear Pore Complex Reveals a Fused Concentric Ring Architecture. J Mol Biol 395:578–586. doi: 10.1016/j.jmb.2009.11.010

Fried H, Kutay U (2003) Nucleocytoplasmic transport: Taking an inventory. Cell Mol Life Sci 60:1659–1688. doi: 10.1007/s00018-003-3070-3

Fuertes MB, Kacha AK, Kline J, Woo SR, Kranz DM, Murphy KM, Gajewski TF (2011) Host type I IFN signals are required for antitumor CD8+ T cell responses through CD8α+ dendritic cells. J Exp Med 208:2005–2016. doi: 10.1084/jem.20101159

Furukawa K, Fritze CE, Gerace L (1998) The major nuclear envelope targeting domain of LAP2 coincides with its lamin binding region but is distinct from its chromatin interaction domain. J Biol Chem 273:4213–4219. doi: 10.1074/jbc.273.7.4213

Gack MU, Shin YC, Joo CH, Urano T, Liang C, Sun L, Takeuchi O, Akira S, Chen Z, Inoue S, Jung JU (2007) TRIM25 RING-finger E3 ubiquitin ligase is essential for RIG-I-mediated antiviral activity. Nature 446:916–920. doi: 10.1038/nature05732

Gall JG (1967) Octagonal nuclear pores. J Cell Biol 32:391–9. doi: 10.1083/JCB.32.2.391

Gao D, Wu J, Wu Y-T, Du F, Aroh C, Yan N, Sun L, Chen ZJ (2013a) Cyclic GMP-AMP Synthase Is an Innate Immune Sensor of HIV and Other Retroviruses. Science (80-). doi: 10.1126/science.1240933

Gao P, Ascano M, Wu Y, Barchet W, Gaffney BL, Zillinger T, Serganov AA, Liu Y, Jones RA, Hartmann G, Tuschl T, Patel DJ (2013b) Cyclic [G(2',5')pA(3',5')p] is the metazoan second messenger produced by DNA-activated cyclic GMP-AMP synthase. Cell 153:1094–1107. doi: 10.1016/j.cell.2013.04.046

Garfinkel MS, Katze MG (1992) Translational control by influenza virus. Selective and cap-dependent translation of viral mRNAs in infected cells. J Biol Chem 267:9383–9390. doi: 10.1016/s0021-9258(19)50435-5

Gentili M, Kowal J, Tkach M, Satoh TT, Lahaye X, Conrad C, Boyron M, Lombard B, Durand S, Kroemer G, Loew D, Dalod M, Théry C, Manel N (2015) Transmission of innate immune signaling by packaging of cGAMP in viral particles. Science (80-) 349:1232–1236. doi: 10.1126/science.aab3628

Gentili M, Lahaye X, Nadalin F, Nader GFP, Puig Lombardi E, Herve S, De Silva NS, Rookhuizen DC, Zueva E, Goudot C, Maurin M, Bochnakian A, Amigorena S, Piel M, Fachinetti D, Londoño-Vallejo A, Manel N (2019) The N-Terminal Domain of cGAS

Determines Preferential Association with Centromeric DNA and Innate Immune Activation in the Nucleus. Cell Rep 26:2377-2393.e13. doi: 10.1016/j.celrep.2019.01.105

Gerace L, Blum A, Blobel G (1978) Immunocytochemical localization of the major polypeptides of the nuclear pore complex-lamina fraction: Interphase and mitotic distribution. J Cell Biol 79:546–566. doi: 10.1083/jcb.79.2.546

Germann S, Gratadou L, Zonta E, Dardenne E, Gaudineau B, Fougère M, Samaan S, Dutertre M, Jauliac S, Auboeuf D (2012) Dual role of the ddx5/ddx17 RNA helicases in the control of the pro-migratory NFAT5 transcription factor. Oncogene 31:4536–4549. doi: 10.1038/onc.2011.618

Ginsbach C, Fahimi HD (1987) Labeling of cholesterol with filipin in cellular membranes of parenchymatous organs - Standardization of incubation conditions. Histochemistry 86:241–248. doi: 10.1007/BF00490254

Gitlin L, Barchet W, Gilfillan S, Cella M, Beutler B, Flavell RA, Diamond MS, Colonna M (2006) Essential role of mda-5 in type I IFN responses to polyriboinosinic: polyribocytidylic acid and encephalomyocarditis picornavirus. Proc Natl Acad Sci U S A 103:8459–8464. doi: 10.1073/pnas.0603082103

Glück S, Guey B, Gulen MF, Wolter K, Kang T-W, Schmacke NA, Bridgeman A, Rehwinkel J, Zender L, Ablasser A (2017) Innate immune sensing of cytosolic chromatin fragments through cGAS promotes senescence. Nat Cell Biol. doi: 10.1038/ncb3586

Goh P-Y, Tan Y-J, Lim SP, Tan YH, Lim SG, Fuller-Pace F, Hong W (2004) Cellular RNA Helicase p68 Relocalization and Interaction with the Hepatitis C Virus (HCV) NS5B Protein and the Potential Role of p68 in HCV RNA Replication. J Virol 78:5288–5298. doi: 10.1128/JVI.78.10.5288-5298.2004

Gonugunta VK, Sakai T, Pokatayev V, Yang K, Wu J, Dobbs N, Yan N (2017) Trafficking-Mediated STING Degradation Requires Sorting to Acidified Endolysosomes and Can Be Targeted to Enhance Anti-tumor Response. Cell Rep 21:3234–3242. doi: 10.1016/j.celrep.2017.11.061

Gonzalo S, Coll-Bonfill N (2019) Genomic instability and innate immune responses to self-DNA in progeria. GeroScience 41:255–266. doi: 10.1007/s11357-019-00082-2

Goubau D, Deddouche S, Reis e Sousa C (2013) Cytosolic Sensing of Viruses. Immunity 38:855–869. doi: 10.1016/j.immuni.2013.05.007

Graham FL, Smiley J, Russell WC, Nairn R (1977) Characteristics of a human cell line transformed by DNA from human adenovirus type 5. J Gen Virol 36:59–72. doi: 10.1099/0022-1317-36-1-59

Gray EE, Winship D, Snyder JM, Child SJ, Geballe AP, Stetson DB (2016) The AIM2-like Receptors Are Dispensable for the Interferon Response to Intracellular DNA. Immunity 45:255–266. doi: 10.1016/j.immuni.2016.06.015

Graziano S, Kreienkamp R, Coll-Bonfill N, Gonzalo S (2018) Causes and consequences of genomic instability in laminopathies: Replication stress and interferon response. Nucleus 9:289–306. doi: 10.1080/19491034.2018.1454168

Grivennikov SI, Greten FR, Karin M (2010) Immunity, Inflammation, and Cancer. Cell 140:883–899. doi: 10.1016/j.cell.2010.01.025

Grossman E, Medalia O, Zwerger M (2012) Functional Architecture of the Nuclear Pore Complex. Annu Rev Biophys 41:557–584. doi: 10.1146/annurev-biophys-050511-102328

Gruenbaum Y, Foisner R (2015) Lamins: Nuclear Intermediate Filament Proteins with Fundamental Functions in Nuclear Mechanics and Genome Regulation. Annu Rev Biochem 84:131–164. doi: 10.1146/annurev-biochem-060614-034115

Guetg C, Lienemann P, Sirri V, Grummt I, Hernandez-Verdun D, Hottiger MO, Fussenegger M, Santoro R (2010) The NoRC complex mediates the heterochromatin formation and stability of silent rRNA genes and centromeric repeats. EMBO J 29:2135–2146. doi: 10.1038/emboj.2010.17

Gui X, Yang H, Li T, Tan X, Shi P, Li M, Du F, Chen ZJ (2019) Autophagy induction via STING trafficking is a primordial function of the cGAS pathway. Nature 567:262–266. doi: 10.1038/s41586-019-1006-9

Gürtler C, Carty M, Kearney J, Schattgen SA, Ding A, Fitzgerald KA, Bowie AG (2014) SARM Regulates CCL5 Production in Macrophages by Promoting the Recruitment of Transcription Factors and RNA Polymerase II to the Ccl5 Promoter €. doi: 10.4049/jimmunol.1302980

Güttler T, Görlich D (2011) Ran-dependent nuclear export mediators: a structural perspective. EMBO J 30:3457–74. doi: 10.1038/emboj.2011.287

Harding SM, Benci JL, Irianto J, Discher DE, Minn AJ, Greenberg RA (2017) Mitotic progression following DNA damage enables pattern recognition within micronuclei. Nat Publ Gr 548:466–470. doi: 10.1038/nature23470

Harris LJ, Larson SB, Hasel KW, McPherson A (1997) Refined structure of an intact IgG2a monoclonal antibody. Biochemistry 36:1581–1597. doi: 10.1021/bi962514+

Härtlova A, Erttmann SF, Raffi FAM, Schmalz AM, Resch U, Anugula S, Lienenklaus S, Nilsson LM, Kröger A, Nilsson JA, Ek T, Weiss S, Gekara NO (2015) DNA Damage Primes the Type I Interferon System via the Cytosolic DNA Sensor STING to Promote Anti-Microbial Innate Immunity. Immunity 42:332–343. doi: 10.1016/j.immuni.2015.01.012

Hatch EM, Fischer AH, Deerinck TJ, Hetzer MW (2013) Catastrophic Nuclear Envelope Collapse in Cancer Cell Micronuclei. Cell 154:47. doi: 10.1016/j.cell.2013.06.007

Hemmi H, Takeuchi O, Kawai T, Kaisho T, Sato S, Sanjo H, Matsumoto M, Hoshino K, Wagner H, Takeda K, Akira S (2000) A Toll-like receptor recognizes bacterial DNA. Nature 408:740–745. doi: 10.1038/35047123

Heppner C, Bilimoria KY, Agarwal SK, Kester MB, Whitty LJ, Guru SC, Chandrasekharappa SC, Collins FS, Spiegel AM, Marx SJ, Burns AL (2001) The tumor suppressor protein menin interacts with NF-κb proteins and inhibits NF-κb-mediated transactivation. Oncogene 20:4917–4925. doi: 10.1038/sj.onc.1204529

Herbert A (2014) Single Molecule Light Microscopy ImageJ Plugins. 1–156.

Hinshaw JE, Carragher BO, Milligan R a (1992) Architecture and design of the nuclear pore complex. Cell 69:1133–1141. doi: 10.1016/0092-8674(92)90635-P

Hinterberger M, Pettersson I, Steitz JA (1983) Isolation of small nuclear ribonucleoproteins containing U1, U2, U4, U5, and U6 RNAs. J Biol Chem 258:2604–2613. doi: 10.1016/s0021-9258(18)32969-7

Ho CY, Jaalouk DE, Vartiainen MK, Lammerding J (2013) Lamin A/C and emerin regulate MKL1–SRF activity by modulating actin dynamics. Nature 497:507–511. doi: 10.1038/nature12105

Hobor F, Dallmann A, Ball NJ, Cicchini C, Battistelli C, Ogrodowicz RW, Christodoulou E, Martin SR, Castello A, Tripodi M, Taylor IA, Ramos A (2018) A cryptic RNA-binding domain mediates Syncrip recognition and exosomal partitioning of miRNA targets. Nat Commun. doi: 10.1038/s41467-018-03182-3

Hodzic DM, Yeater DB, Bengtsson L, Otto H, Stahl PD (2004) Sun2 is a novel mammalian inner nuclear membrane protein. J Biol Chem 279:25805–12. doi: 10.1074/jbc.M313157200

Hoffmann HH, Schneider WM, Rice CM (2015) Interferons and viruses: An evolutionary arms race of molecular interactions. Trends Immunol 36:124–138. doi: 10.1016/j.it.2015.01.004

Holm CK, Jensen SB, Jakobsen MR, Cheshenko N, Horan KA, Moeller HB, Gonzalez-Dosal R, Rasmussen SB, Christensen MH, Yarovinsky TO, Rixon FJ, Herold BC, Fitzgerald KA, Paludan SR (2012) Virus-cell fusion as a trigger of innate immunity dependent on the adaptor STING. Nat Immunol 13:737–743. doi: 10.1038/ni.2350

Holm CK, Rahbek SH, Gad HH, Bak RO, Jakobsen MR, Jiang Z, Hansen AL, Jensen SK, Sun C, Thomsen MK, Laustsen A, Nielsen CG, Severinsen K, Xiong Y, Burdette DL, Hornung V, Lebbink RJ, Duch M, Fitzgerald KA, Bahrami S, Mikkelsen JG, Hartmann R, Paludan SR (2016) Influenza A virus targets a cGAS-independent STING pathway that controls enveloped RNA viruses. Nat Commun 7:10680. doi: 10.1038/ncomms10680

Honda K, Takaoka A, Taniguchi T (2006) Type I Inteferon Gene Induction by the Interferon Regulatory Factor Family of Transcription Factors. Immunity 25:349–360. doi: 10.1016/j.immuni.2006.08.009

Horan KA, Hansen K, Jakobsen MR, Holm CK, Søby S, Unterholzner L, Thompson M, West JA, Iversen MB, Rasmussen SB, Ellermann-Eriksen S, Kurt-Jones E, Landolfo S, Damania B, Melchjorsen J, Bowie AG, Fitzgerald KA, Paludan SR (2013) Proteasomal Degradation of Herpes Simplex Virus Capsids in Macrophages Releases DNA to the Cytosol for Recognition by DNA Sensors. J Immunol 190:2311–2319. doi: 10.4049/jimmunol.1202749

Hornung V, Ablasser A, Charrel-Dennis M, Bauernfeind F, Horvath G, Caffrey DR, Latz E, Fitzgerald KA (2009) AIM2 recognizes cytosolic dsDNA and forms a caspase-1-activating inflammasome with ASC. Nature 458:514–518. doi: 10.1038/nature07725

Hornung V, Ellegast J, Kim S, Brzozka K, Jung A, Kato H, Poeck H, Akira S, Conzelmann K-K, Schlee M, Endres S, Hartmann G (2006) 5’-Triphosphate RNA Is the Ligand for RIG-I.

Science (80-) 314:994–997. doi: 10.1126/science.1132505

Hornung V, Hartmann R, Ablasser A, Hopfner K-P (2014) OAS proteins and cGAS: unifying concepts in sensing and responding to cytosolic nucleic acids. Nat Rev Immunol 14:521–528. doi: 10.1038/nri3719

Hou F, Sun L, Zheng H, Skaug B, Jiang QX, Chen ZJ (2011) MAVS forms functional prion-like aggregates to activate and propagate antiviral innate immune response. Cell 146:448–461. doi: 10.1016/j.cell.2011.06.041

Hu S, Sun H, Yin L, Li J, Mei S, Xu F, Wu C, Liu X, Zhao F, Zhang D, Huang Y, Ren L, Cen S, Wang J, Liang C, Guo F (2019) PKR-dependent cytosolic cGAS foci are necessary for intracellular DNA sensing. Sci Signal 12:1–14. doi: 10.1126/scisignal.aav7934

Hur S (2019) Double-Stranded RNA Sensors and Modulators in Innate Immunity. Annu Rev Immunol 37:349–375. doi: 10.1146/annurev-immunol-042718-041356

Iezzi S, Fanciulli M (2015) Discovering Che-1/AATF: A new attractive target for cancer therapy. Front Genet 6:1–7. doi: 10.3389/fgene.2015.00141

Iqbal J, Ansari MA, Kumar B, Dutta D, Roy A, Chikoti L, Pisano G, Dutta S, Vahedi S, Veettil MV, Chandran B (2016) Histone H2B-IFI16 Recognition of Nuclear Herpesviral Genome Induces Cytoplasmic Interferon-β Responses. PLoS Pathog 12:1–40. doi: 10.1371/journal.ppat.1005967

Ishii KJ, Coban C, Kato H, Takahashi K, Torii Y, Takeshita F, Ludwig H, Sutter G, Suzuki K, Hemmi H, Sato S, Yamamoto M, Uematsu S, Kawai T, Takeuchi O, Akira S (2006) A toll-like receptor-independent antiviral response induced by double-stranded B-form DNA. Nat Immunol 7:40–48. doi: 10.1038/ni1282

Ishikawa H, Barber GN (2008) STING is an endoplasmic reticulum adaptor that facilitates innate immune signalling. Nature 455:674–678. doi: 10.1038/nature07317

Ishikawa H, Ma Z, Barber GN (2009) STING regulates intracellular DNA-mediated, type I interferon-dependent innate immunity. Nature 461:788–92. doi: 10.1038/nature08476

Ivorra C, Kubicek M, González JM, Sanz-González SM, Alvarez-Barrientos A, O'Connor J-E, Burke B, Andrés V (2006) A mechanism of AP-1 suppression through interaction of c-Fos with lamin A/C. Genes Dev 20:307–320. doi: 10.1101/gad.349506

Jacques DA, McEwan WA, Hilditch L, Price AJ, Towers GJ, James LC (2016) HIV-1 uses dynamic capsid pores to import nucleotides and fuel encapsidated DNA synthesis. Nature 536:349–353. doi: 10.1038/nature19098

Jakobsen MR, Bak RO, Andersen A, Berg RK, Jensen SB, Jin T, Laustsen A, Hansen K, Ostergaard L, Fitzgerald KA, Xiao TS, Mikkelsen JG, Mogensen TH, Paludan SR (2013) IFI16 senses DNA forms of the lentiviral replication cycle and controls HIV-1 replication. Proc Natl Acad Sci 110:E4571–E4580. doi: 10.1073/pnas.1311669110

Janeway, C.A. J (1989) Evolution and revolution in immunology. LI:54 Pt 1, 1–13.

Jeremiah N, Neven B, Gentili M, Callebaut I, Maschalidi S, Stolzenberg M, Goudin N, Frémond M, Nitschke P, Molina TJ, Blanche S, Picard C, Rice GI, Crow YJ, Manel N,

Fischer A, Bader-meunier B, Rieux-laucat F (2014) Inherited STING-activating mutation underlies a familial inflammatory. J Clin Invest 124:5516–5520. doi: 10.1172/JCI79100DS1

Jiang Y, Zhu Y, Qiu W, Liu YJ, Cheng G, Liu ZJ, Ouyang S (2017) Structural and functional analyses of human DDX41 DEAD domain. Protein Cell 8:72–76. doi: 10.1007/s13238-016-0351-9

Jin L, Waterman PM, Jonscher KR, Short CM, Reisdorph NA, Cambier JC (2008) MPYS, a novel membrane tetraspanner, is associated with major histocompatibility complex class II and mediates transduction of apoptotic signals. Mol Cell Biol 28:5014–5026. doi: 10.1128/MCB.00640-08

Jin T, Perry A, Jiang J, Smith P, Curry JA, Unterholzner L, Jiang Z, Horvath G, Rathinam V, Ricky W, Hornung V, Latz E, Bowie AG, Fitzgerald KA, Xiao TS (2013) Structures of The HIN Domain:DNA Complexes Reveal Ligand Binding and Activation Mechanisms of The AIM2 Inflammasome and IFI16 Receptor. 36:561–571. doi: 10.1016/j.immuni.2012.02.014.Structures

Jønsson KL, Laustsen A, Krapp C, Skipper KA, Thavachelvam K, Hotter D, Egedal JH, Kjolby M, Mohammadi P, Prabakaran T, Sørensen LK, Sun C, Jensen SB, Holm CK, Lebbink RJ, Johannsen M, Nyegaard M, Mikkelsen JG, Kirchhoff F, Paludan SR, Jakobsen MR (2017) IFI16 is required for DNA sensing in human macrophages by promoting production and function of cGAMP. Nat Publ Gr 8:1–17. doi: 10.1038/ncomms14391

Kabat JL, Barberan-soler S, Zahler AM (2009) HRP-2 , the Caenorhabditis elegans Homolog of Mammalian Heterogeneous Nuclear Ribonucleoproteins Q and R , Is an Alternative Splicing Factor That Binds to UCUAUC Splicing Regulatory Elements *. 284:28490–28497. doi: 10.1074/jbc.M109.023101

Kanai Y, Dohmae N, Hirokawa N (2004) Kinesin transports RNA: Isolation and characterization of an RNA-transporting granule. Neuron 43:513–525. doi: 10.1016/j.neuron.2004.07.022

Kang D, Gopalkrishnan R V, Wu Q, Jankowsky E, Pyle AM, Fisher PB (2002) mda-5: An interferon-inducible putative RNA helicase with double-stranded RNA-dependent ATPase activity and melanoma growth-suppressive properties. Proc Natl Acad Sci U S A 99:637–42. doi: 10.1073/pnas.022637199

Kato H, Fujita T (2014) Autoimmunity caused by constitutive activation of cytoplasmic viral RNA sensors. Cytokine Growth Factor Rev 25:739–743. doi: 10.1016/j.cytogfr.2014.08.003

Kato H, Takeuchi O, Mikamo-Satoh E, Hirai R, Kawai T, Matsushita K, Hiiragi A, Dermody TS, Fujita T, Akira S (2008) Length-dependent recognition of double-stranded ribonucleic acids by retinoic acid-inducible gene-I and melanoma differentiation-associated gene 5. J Exp Med 205:1601–1610. doi: 10.1084/jem.20080091

Kato H, Takeuchi O, Sato S, Yoneyama M, Yamamoto M, Matsui K, Uematsu S, Jung A, Kawai T, Ishii KJ, Yamaguchi O, Otsu K, Tsujimura T, Koh C-SS, Reis e Sousa C, Matsuura Y, Fujita T, Akira S (2006) Differential roles of MDA5 and RIG-I helicases in the recognition of RNA viruses. Nature 441:101–105. doi: 10.1038/nature04734

Katta SS, Smoyer CJ, Jaspersen SL (2014) Destination: inner nuclear membrane. Trends Cell Biol 24:221–229. doi: 10.1016/j.tcb.2013.10.006

Kaur R, Lal SK (2020) The multifarious roles of heterogeneous ribonucleoprotein A1 in viral infections. Rev Med Virol 30:1–10. doi: 10.1002/rmv.2097

Kawai T, Akira S (2011) Toll-like Receptors and Their Crosstalk with Other Innate Receptors in Infection and Immunity. Immunity 34:637–650. doi: 10.1016/j.immuni.2011.05.006

Kawai T, Takahashi K, Sato S, Coban C, Kumar H, Kato H, Ishii KJ, Takeuchi O, Akira S (2005) IPS-1, an adaptor triggering RIG-I- and Mda5-mediated type I interferon induction. Nat Immunol 6:981–8. doi: 10.1038/ni1243

Kenmochi N, Kawaguchi T, Rozen S, Davis E, Goodman N, Hudson TJ, Tanaka T, Page DC (1998) A map of 75 human ribosomal protein genes. Genome Res 8:509–523. doi: 10.1101/gr.8.5.509

Kennedy BK, Barbie DA, Classon M, Dyson N, Harlow E (2000) Nuclear organization of DNA replication in primary mammalian cells. Genes Dev 14:2855–68.

Kersse K, Bertrand MJM, Lamkanfi M, Vandenabeele P (2011) NOD-like receptors and the innate immune system: Coping with danger, damage and death. Cytokine Growth Factor Rev 22:257–276. doi: 10.1016/j.cytogfr.2011.09.003

Kerur N, Veettil MV, Sharma-Walia N, Bottero V, Sadagopan S, Otageri P, Chandran B (2011) IFI16 acts as a nuclear pathogen sensor to induce the inflammasome in response to Kaposi Sarcoma-associated herpesvirus infection. Cell Host Microbe 9:363–375. doi: 10.1016/j.chom.2011.04.008

Kim D, Kim W, Lee K, Kim S, Lee H, Kim H, Jung Y, Choi J, Kim K (2012) hnRNP Q regulates translation of p53 in normal and stress conditions. Cell Death Differ 20:226–234. doi: 10.1038/cdd.2012.109

Kim JH, Paek KY, Ha SH, Cho S, Choi K, Kim CS, Ryu SH, Jang SK (2004) A Cellular RNA-Binding Protein Enhances Internal Ribosomal Entry Site-Dependent Translation through an Interaction Downstream of the Hepatitis C Virus Polyprotein Initiation Codon. Mol Cell Biol 24:7878–7890. doi: 10.1128/MCB.24.18.7878-7890.2004

Kim YM, Brinkmann MM, Paquet ME, Ploegh HL (2008) UNC93B1 delivers nucleotide-sensing toll-like receptors to endolysosomes. Nature 452:234–238. doi: 10.1038/nature06726

King KR, Aguirre AD, Ye YX, Sun Y, Roh JD, Ng RP, Kohler RH, Arlauckas SP, Yoshiko V, Savo A, Sadreyev RI, Kelly M, Fitzgibbons TP, Fitzgerald KA, Mitchison T, Libby P, Nahrendorf M, Weissleder R (2017) IRF3 and type i interferons fuel a fatal response to myocardial infarction. Nat Med 23:1481–1487. doi: 10.1038/nm.4428

King MC, Lusk CP, Blobel G (2006) Karyopherin-mediated import of integral inner nuclear membrane proteins. Nature 442:1003–1007. doi: 10.1038/nature05075

Kobiyama K, Takeshita F, Jounai N, Sakaue-Sawano A, Miyawaki A, Ishii KJ, Kawai T, Sasaki S, Hirano H, Ishii N, Okuda K, Suzuki K (2010) Extrachromosomal Histone H2B Mediates Innate Antiviral Immune Responses Induced by Intracellular Double-Stranded DNA. J

Virol 84:822–832. doi: 10.1128/jvi.01339-09

Kochs G, García-Sastre A, Martínez-Sobrido L (2007) Multiple Anti-Interferon Actions of the Influenza A Virus NS1 Protein. J Virol 81:7011–7021. doi: 10.1128/jvi.02581-06

Kondo T, Kobayashi J, Saitoh T, Maruyama K, Ishii KJ, Barber GN, Komatsu K, Akira S, Kawai T (2013) DNA damage sensor MRE11 recognizes cytosolic double-stranded DNA and induces type i interferon by regulating STING trafficking. Proc Natl Acad Sci U S A 110:2969–2974. doi: 10.1073/pnas.1222694110

Kondo Y, Oubridge C, Van Roon AMM, Nagai K (2015) Crystal structure of human U1 snRNP, a small nuclear ribonucleoprotein particle, reveals the mechanism of 5' splice site recognition. Elife 2015:1–19. doi: 10.7554/eLife.04986.001

Konno H, Konno K, Barber GN (2013) Cyclic Dinucleotides Trigger ULK1 (ATG1) Phosphorylation of STING to Prevent Sustained Innate Immune Signaling. Cell 155:688–698. doi: 10.1016/j.cell.2013.09.049

Korfali N, Wilkie GS, Swanson SK, Srsen V, Batrakou DG, Fairley EAL, Malik P, Zuleger N, Goncharevich A, de Las Heras J, Kelly DA, Kerr ARW, Florens L, Schirmer EC (2010) The leukocyte nuclear envelope proteome varies with cell activation and contains novel transmembrane proteins that affect genome architecture. Mol Cell Proteomics 9:2571–85. doi: 10.1074/mcp.M110.002915

Korfali N, Wilkie GS, Swanson SK, Srsen V, de las Heras J, Batrakou DG, Malik P, Zuleger N, Kerr ARW, Florens L, Schirmer EC (2012) The nuclear envelope proteome differs notably between tissues. Nucl (United States) 3:552–564. doi: 10.4161/nucl.22257

Kosugi S, Hasebe M, Tomita M, Yanagawa H (2009) Systematic identification of cell cycle-dependent yeast nucleocytoplasmic shuttling proteins by prediction of composite motifs. Proc Natl Acad Sci U S A 106:10171–10176. doi: 10.1073/pnas.0900604106

Kowalinski E, Lunardi T, McCarthy AA, Louber J, Brunel J, Grigorov B, Gerlier D, Cusack S (2011) Structural basis for the activation of innate immune pattern-recognition receptor RIG-I by viral RNA. Cell 147:423–435. doi: 10.1016/j.cell.2011.09.039

Kralt A, Jagalur NB, van den Boom V, Lokareddy RK, Steen A, Cingolani G, Fornerod M, Veenhoff LM (2015) Conservation of inner nuclear membrane targeting sequences in mammalian Pom121 and yeast Heh2 membrane proteins. Mol Biol Cell 26:3301–12. doi: 10.1091/mbc.E15-03-0184

Kranzusch PJ, Wilson SC, Lee ASY, Berger JM, Doudna JA, Vance RE (2015) Ancient Origin of cGAS-STING Reveals Mechanism of Universal 2',3' cGAMP Signaling. Mol Cell 59:891–903. doi: 10.1016/j.molcel.2015.07.022

Kreienkamp R, Graziano S, Coll-Bonfill N, Bedia-Diaz G, Cybulla E, Vindigni A, Dorsett D, Kubben N, Batista LFZ, Gonzalo S (2018) A Cell-Intrinsic Interferon-like Response Links Replication Stress to Cellular Aging Caused by Progerin. Cell Rep 22:2006–2015. doi: 10.1016/j.celrep.2018.01.090

Krishnamurthy S, Takimoto T, Scroggs RA, Portner A (2006) Differentially Regulated Interferon Response Determines the Outcome of Newcastle Disease Virus Infection in Normal and Tumor Cell Lines. J Virol 80:5145–5155. doi: 10.1128/jvi.02618-05

Krug RM (2015) Functions of the influenza A virus NS1 protein in antiviral defense. Curr Opin Virol 12:1–6. doi: 10.1016/j.coviro.2015.01.007

Kuchler L, Giegerich AK, Sha LK, Knape T, Wong MSK, Schröder K, Brandes RP, Heide H, Wittig I, Brüne B, Von Knethen A (2014) SYNCRIP-dependent Nox2 mRNA destabilization impairs ROS formation in M2-polarized macrophages. Antioxidants Redox Signal 21:2483–2497. doi: 10.1089/ars.2013.5760

Kujirai T, Zierhut C, Takizawa Y, Kim R, Negishi L, Uruma N, Hirai S, Funabiki H, Kurumizaka H (2020) Structural basis for the inhibition of cGAS by nucleosomes. Science (80-) 370:455–458. doi: 10.1126/science.abd0237

Kumar KP, McBride KM, Weaver BK, Dingwall C, Reich NC (2000) Regulated nuclear-cytoplasmic localization of interferon regulatory factor 3, a subunit of double-stranded RNA-activated factor 1. Mol Cell Biol 20:4159–4168. doi: 10.1128/MCB.20.11.4159-4168.2000

Kuo RL, Zhao C, Malur M, Krug RM (2010) Influenza A virus strains that circulate in humans differ in the ability of their NS1 proteins to block the activation of IRF3 and interferon-β transcription. Virology 408:146–158. doi: 10.1016/j.virol.2010.09.012

La Cour T, Kiemer L, Mølgaard A, Gupta R, Skriver K, Brunak S (2004) Analysis and prediction of leucine-rich nuclear export signals. Protein Eng Des Sel 17:527–536. doi: 10.1093/protein/gzh062

La P, Silva AC, Hou Z, Wang H, Schnepp RW, Yan N, Shi Y, Hua X (2004) Direct Binding of DNA by Tumor Suppressor Menin. J BiolChem 279.47:49045–49054. doi: 10.1007/s11103-011-9767-z.Plastid

Laba J, Steen A, Popken P, Chernova A, Poolman B, Veenhoff L (2015) Active Nuclear Import of Membrane Proteins Revisited. Cells 4:653–673. doi: 10.3390/cells4040653

Laba JK, Steen A, Veenhoff LM (2014) Traffic to the inner membrane of the nuclear envelope. Curr Opin Cell Biol 28:36–45. doi: 10.1016/j.ceb.2014.01.006

Lahaye X, Gentili M, Silvin A, Conrad C, Picard L, Jouve M, Zueva E, Maurin M, Nadalin F, Knott GJ, Zhao B, Du F, Rio M, Amiel J, Fox AH, Li P, Etienne L, Bond CS, Colleaux L, Manel N (2018) NONO Detects the Nuclear HIV Capsid to Promote cGAS-Mediated Innate Immune Activation. Cell 175:488-501.e22. doi: 10.1016/j.cell.2018.08.062

Lahaye X, Satoh T, Gentili M, Cerboni S, Conrad C, Hurbain I, ElMarjou A, Lacabaratz C, Lelièvre JD, Manel N (2013) The Capsids of HIV-1 and HIV-2 Determine Immune Detection of the Viral cDNA by the Innate Sensor cGAS in Dendritic Cells. Immunity 39:1132–1142. doi: 10.1016/j.immuni.2013.11.002

Lai CH, Huang YC, Lee JC, Tseng JTC, Chang KC, Chen YJ, Ding NJ, Huang PH, Chang WC, Lin BW, Chen RY, Wang YC, Lai YC, Hung LY (2017) Translational upregulation of Aurora-A by hnRNP Q1 contributes to cell proliferation and tumorigenesis in colorectal cancer. Cell Death Dis 8:1–12. doi: 10.1038/cddis.2016.479

Lammerding J, Fong LG, Ji JY, Reue K, Stewart CL, Young SG, Lee RT (2006) Lamins A and C but Not Lamin B1 Regulate Nuclear Mechanics. J Biol Chem 281:25768–25780. doi: 10.1074/jbc.M513511200

Lammerding J, Schulze PC, Takahashi T, Kozlov S, Sullivan T, Kamm RD, Stewart CL, Lee RT (2004) Lamin A/C deficiency causes defective nuclear mechanics and mechanotransduction. J Clin Invest 113:370–8. doi: 10.1172/JCI19670

Lan YY, Londoño D, Bouley R, Rooney MS, Hacohen N (2014) Dnase2a deficiency uncovers lysosomal clearance of damaged nuclear DNA via autophagy. Cell Rep 9:180–192. doi: 10.1016/j.celrep.2014.08.074

Latif MB, Raja R, Kessler PM, Sen GC (2020) Relative Contributions of the cGAS-STING and TLR3 Signaling Pathways to Attenuation of Herpes Simplex Virus 1 Replication. J Virol 94:1–16. doi: 10.1128/JVI.01717-19

Latz E, Schoenemeyer A, Visintin A, Fitzgerald KA, Monks BG, Knetter CF, Lien E, Nilsen NJ, Espevik T, Golenbock DT (2004) TLR9 signals after translocating from the ER to CpG DNA in the lysosome. Nat Immunol 5:190–198. doi: 10.1038/ni1028

Lau A, Gray EE, Brunette RL, Stetson DB (2015) DNA tumor virus oncogenes antagonize the cGAS-STING DNA-sensing pathway. Science (80-) 350:568–571. doi: 10.1126/science.aab3291

Lee JSH, Hale CM, Panorchan P, Khatau SB, George JP, Tseng Y, Stewart CL, Hodzic D, Wirtz D (2007) Nuclear Lamin A/C Deficiency Induces Defects in Cell Mechanics, Polarization, and Migration. Biophys J 93:2542–2552. doi: 10.1529/biophysj.106.102426

Lee K-GG, Kim SS-YY, Kui L, Voon DC-CC, Mauduit M, Bist P, Bi X, Pereira NA, Liu C, Sukumaran B, Rénia L, Ito Y, Lam K-PP (2015) Bruton's Tyrosine Kinase Phosphorylates DDX41 and Activates Its Binding of dsDNA and STING to Initiate Type 1 Interferon Response. Cell Rep 10:1055–1065. doi: 10.1016/j.celrep.2015.01.039

Lee Y, Auh SL, Wang Y, Burnette B, Wang Y, Meng Y, Beckett M, Sharma R, Chin R, Tu T, Weichselbaum RR, Fu YX (2009) Therapeutic effects of ablative radiation on local tumor require CD8 + T cells: Changing strategies for cancer treatment. Blood 114:589–595. doi: 10.1182/blood-2009-02-206870

Levin D, London IM (1978) Regulation of protein synthesis: activation by double-stranded RNA of a protein kinase that phosphorylates eukaryotic initiation factor 2. Proc Natl Acad Sci U S A 75:1121–1125. doi: 10.1073/pnas.75.3.1121

Li C, Ge LL, Li PP, Wang Y, Sun MX, Huang L, Ishag H, Di DD, Shen ZQ, Fan WX, Mao X (2013a) The DEAD-box RNA helicase DDX5 acts as a positive regulator of Japanese encephalitis virus replication by binding to viral 3' UTR. Antiviral Res 100:487–499. doi: 10.1016/j.antiviral.2013.09.002

Li S, Min JY, Krug RM, Sen GC (2006) Binding of the influenza A virus NS1 protein to PKR mediates the inhibition of its activation by either PACT or double-stranded RNA. Virology 349:13–21. doi: 10.1016/j.virol.2006.01.005

Li S, Wang L, Berman M, Kong YY, Dorf ME (2011) Mapping a Dynamic Innate Immunity Protein Interaction Network Regulating Type I Interferon Production. Immunity 35:426–440. doi: 10.1016/j.immuni.2011.06.014

Li T, Diner B a., Chen J, Cristea IM (2012) Acetylation modulates cellular distribution and DNA sensing ability of interferon-inducible protein IFI16. Proc Natl Acad Sci 109:10558–

10563. doi: 10.1073/pnas.1203447109

Li T, Huang T, Du M, Chen X, Du F, Ren J, Chen ZJ (2021) Phosphorylation and chromatin tethering prevent cGAS activation during mitosis. Science (80-). doi: 10.1126/science.abc5386

Li X-D, Wu J, Gao D, Wang H, Sun L, Chen ZJ (2013b) Pivotal Roles of cGAS-cGAMP Signaling in Antiviral Defense and Immune Adjuvant Effects. Science (80-) 341:1390–1394. doi: 10.1126/science.1244040

Li X, Shu C, Yi G, Chaton CT, Shelton CL, Diao J, Zuo X, Kao CC, Herr AB, Li P (2013c) Cyclic GMP-AMP Synthase Is Activated by Double-Stranded DNA-Induced Oligomerization. Immunity 39:1019–1031. doi: 10.1016/j.immuni.2013.10.019

Lian H, Wei J, Zang R, Ye W, Yang Q, Zhang XN, Chen Y Da, Fu YZ, Hu MM, Lei CQ, Luo WW, Li S, Shu HB (2018) ZCCHC3 is a co-sensor of cGAS for dsDNA recognition in innate immune response. Nat Commun. doi: 10.1038/s41467-018-05559-w

Lin C, Yang L, Yang JJ, Huang Y, Liu Z-R (2005) ATPase/Helicase Activities of p68 RNA Helicase Are Required for Pre-mRNA Splicing but Not for Assembly of the Spliceosome. Mol Cell Biol 25:7484–7493. doi: 10.1128/mcb.25.17.7484-7493.2005

Lin R, Heylbroeck C, Pitha PM, Hiscott J (1998) Virus-Dependent Phosphorylation of the IRF-3 Transcription Factor Regulates Nuclear Translocation, Transactivation Potential, and Proteasome-Mediated Degradation. Mol Cell Biol 18:2986–2996. doi: 10.1128/mcb.18.5.2986

Liu H, Zhang H, Wu X, Ma D, Wu J, Wang L, Jiang Y, Fei Y, Zhu C, Tan R, Jungblut P, Pei G, Dorhoi A, Yan Q, Zhang F, Zheng R, Liu S, Liang H, Liu Z, Yang H, Chen J, Wang P, Tang T, Peng W, Hu Z, Xu Z, Huang X, Wang J, Li H, Zhou Y, Liu F, Yan D, Kaufmann SHEE, Chen C, Mao Z, Ge B (2018) Nuclear cGAS suppresses DNA repair and promotes tumorigenesis. Nature 563:131–136. doi: 10.1038/s41586-018-0629-6

Liu HM, Aizaki H, Choi KS, Machida K, Ou JJ-HJHJ-H, Lai MMCC (2009) SYNCRIP (synaptotagmin-binding, cytoplasmic RNA-interacting protein) is a host factor involved in hepatitis C virus RNA replication. Virology 386:249–256. doi: 10.1016/j.virol.2009.01.018

Liu S, Cai H, Xue W, Wang M, Xia T, Li WJ, Xing JQ, Zhao M, Huang YJ, Chen S, Wu SM, Wang X, Liu X, Pang X, Zhang ZY, Li T, Dai J, Dong F, Xia Q, Li AL, Zhou T, Liu ZSZ gang ZS, Zhang X-M, Li T (2019) G3BP1 promotes DNA binding and activation of cGAS. Nat Immunol. doi: 10.1038/s41590-018-0262-4

Liu S, Cai X, Wu J, Cong Q, Chen X, Li T, Du F, Ren J, Wu YT, Grishin N V., Chen ZJ (2015a) Phosphorylation of innate immune adaptor proteins MAVS, STING, and TRIF induces IRF3 activation. Science (80-) 347:aaa2630. doi: 10.1126/science.aaa2630

Liu S, Cai X, Wu J, Cong Q, Chen X, Li T, Du F, Ren J, Wu YT, Grishin N V, Chen ZJ (2015b) Phosphorylation of innate immune adaptor proteins MAVS, STING, and TRIF induces IRF3 activation. Science 347:aaa2630. doi: 10.1126/science.aaa2630

Liu X, Yang C, Hu Y, Lei E, Lin X, Zhao L, Zou Z, Zhang A, Zhou H, Chen H, Qian P, Jin M (2017) HIST1H1C regulates interferon-β and inhibits influenza virus replication by interacting

with IRF3. Front Immunol 8:1–14. doi: 10.3389/fimmu.2017.00350

Liu Y, Jesus AA, Marrero B, Yang D, Ramsey SE, Montealegre Sanchez GA, Tenbrock K, Wittkowski H, Jones OY, Kuehn HS, Lee CCR, DiMattia MA, Cowen EW, Gonzalez B, Palmer I, DiGiovanna JJ, Biancotto A, Kim HJ, Tsai WL, Trier AM, Huang Y, Stone DL, Hill S, Kim HJ, St Hilaire C, Gurprasad S, Plass N, Chapelle D, Horkayne-Szakaly I, Foell D, Barysenka A, Candotti F, Holland SM, Hughes JD, Mehmet H, Issekutz AC, Raffeld M, McElwee J, Fontana JR, Minniti CP, Moir S, Kastner DL, Gadina M, Steven AC, Wingfield PT, Brooks SR, Rosenzweig SD, Fleisher TA, Deng Z, Boehm M, Paller AS, Goldbach-Mansky R (2014) Activated STING in a vascular and pulmonary syndrome. N Engl J Med 371:507–518. doi: 10.1056/NEJMoa1312625

Liu Z-R (2002) p68 RNA Helicase Is an Essential Human Splicing Factor That Acts at the U1 snRNA-5′ Splice Site Duplex. Mol Cell Biol 22:5443–5450. doi: 10.1128/mcb.22.15.5443-5450.2002

López Y, Nakai K, Patil A (2015) HitPredict version 4: Comprehensive reliability scoring of physical protein-protein interactions from more than 100 species. Database 2015:1–10. doi: 10.1093/database/bav117

Luecke S, Holleufer A, Christensen MH, Jønsson KL, Boni GA, Sørensen LK, Johannsen M, Jakobsen MR, Hartmann R, Paludan SR (2017) cGAS is activated by DNA in a length-dependent manner . EMBO Rep 18:1707–1715. doi: 10.15252/embr.201744017

Lusk CP, Blobel G, King MC (2007) Highway to the inner nuclear membrane: rules for the road. Nat Rev Mol Cell Biol 8:414–20. doi: 10.1038/nrm2165

Ma Y, Cai S, Lv Q, Jiang Q, Zhang Q, Sodmergen, Zhai Z, Zhang C (2007) Lamin B receptor plays a role in stimulating nuclear envelope production and targeting membrane vesicles to chromatin during nuclear envelope assembly through direct interaction with importin beta. J Cell Sci 120:520–30. doi: 10.1242/jcs.03355

Ma Z, Damania B (2016) The cGAS-STING Defense Pathway and Its Counteraction by Viruses. Cell Host Microbe 19:150–158. doi: 10.1016/j.chom.2016.01.010

Ma Z, Ni G, Damania B (2018) Innate Sensing of DNA Virus Genomes. Annu Rev Virol 5:341–362. doi: 10.1146/annurev-virology-092917-043244

Mackenzie KJ, Carroll P, Lettice L, Tarnauskaitė Ž, Reddy K, Dix F, Revuelta A, Abbondati E, Rigby RE, Rabe B, Kilanowski F, Grimes G, Fluteau A, Devenney PS, Hill RE, Reijns MA, Jackson AP (2016) Ribonuclease H2 mutations induce a cGAS/STING-dependent innate immune response. EMBO J 35:831–844. doi: 10.15252/embj.201593339

Mackenzie KJ, Carroll P, Martin C-A, Murina O, Fluteau A, Simpson DJ, Olova N, Sutcliffe H, Rainger JK, Leitch A, Osborn RT, Wheeler AP, Nowotny M, Gilbert N, Chandra T, Reijns MAM, Jackson AP (2017) cGAS surveillance of micronuclei links genome instability to innate immunity. Nature. doi: 10.1038/nature23449

Maimon T, Elad N, Dahan I, Medalia O (2012) The Human Nuclear Pore Complex as Revealed by Cryo-Electron Tomography. Structure 20:998–1006. doi: 10.1016/j.str.2012.03.025

Makatsori D, Kourmouli N, Polioudaki H, Shultz LD, McLean K, Theodoropoulos PA, Singh PB, Georgatos SD (2004) The inner nuclear membrane protein lamin B receptor forms

distinct microdomains and links epigenetically marked chromatin to the nuclear envelope. J Biol Chem 279:25567–73. doi: 10.1074/jbc.M313606200

Malathi K, Dong B, Gale M, Silverman RH (2007) Small self-RNA generated by RNase L amplifies antiviral innate immunity. Nature 448:816–819. doi: 10.1038/nature06042

Malik P, Korfali N, Vlastimil S, Lazou V, Dzmitry B, Nikolaj Z, Kavanagh DM, Wilkie GS, Goldberg MW, Schirmer EC (2010) Cell-specific and lamin-dependent targeting of novel transmembrane proteins in the nuclear envelope. Cell Mol Life Sci 67:1353–1369. doi: 10.1007/s00018-010-0257-2

Malik P, Zuleger N, De Heras JI Las, Saiz-Ros N, Makarov AA, Lazou V, Meinke P, Waterfall M, Kelly DA, Schirmer EC (2014) NET23/STING promotes chromatin compaction from the nuclear envelope. PLoS One. doi: 10.1371/journal.pone.0111851

Marckmann S, Wiesemann E, Hilse R, Trebst C, Stangel M, Windhagen A (2004) Interferon-β up-regulates the expression of co-stimulatory molecules CD80, CD86 and CD40 on monocytes: Significance for treatment of multiple sclerosis. Clin Exp Immunol 138:499–506. doi: 10.1111/j.1365-2249.2004.02624.x

Maringer K, Fernandez-Sesma A (2014) Message in a bottle: Lessons learned from antagonism of STING signalling during RNA virus infection. Cytokine Growth Factor Rev 25:669–679. doi: 10.1016/j.cytogfr.2014.08.004

Marques JT, Devosse T, Wang D, Zamanian-Daryoush M, Serbinowski P, Hartmann R, Fujita T, Behlke MA, Williams BRG (2006) A structural basis for discriminating between self and nonself double-stranded RNAs in mammalian cells. Nat Biotechnol 24:559–565. doi: 10.1038/nbt1205

Matkar S, Thiel A, Hua X (2013) Menin: A scaffold protein that controls gene expression and cell signaling. Trends Biochem Sci 38:394–402. doi: 10.1016/j.tibs.2013.05.005

Meaburn KJ, Cabuy E, Bonne G, Levy N, Morris GE, Novelli G, Kill IR, Bridger JM (2007) Primary laminopathy fibroblasts display altered genome organization and apoptosis. Aging Cell 6:139–153. doi: 10.1111/j.1474-9726.2007.00270.x

Medzhitov R (2009) Approaching the Asymptote: 20 Years Later. Immunity 30:766–775. doi: 10.1016/j.immuni.2009.06.004

Mehravar M, Shirazi A, Nazari M, Banan M (2019) Mosaicism in CRISPR/Cas9-mediated genome editing. Dev Biol 445:156–162. doi: 10.1016/j.ydbio.2018.10.008

Meier J, Campbell KH, Ford CC, Stick R, Hutchison CJ (1991) The role of lamin LIII in nuclear assembly and DNA replication, in cell-free extracts of Xenopus eggs. J Cell Sci 98 (Pt 3):271–9.

Meinema AC, Laba JK, Hapsari RA, Otten R, Mulder FAA, Kralt A, van den Bogaart G, Lusk CP, Poolman B, Veenhoff LM (2011) Long Unfolded Linkers Facilitate Membrane Protein Import Through the Nuclear Pore Complex. Science (80-) 333:90–93. doi: 10.1126/science.1205741

Meinema AC, Poolman B, Veenhoff LM (2013) Quantitative Analysis of Membrane Protein Transport Across the Nuclear Pore Complex. Traffic 14:487–501. doi:

10.1111/tra.12048

Meinke P, Schirmer EC (2015) LINC'ing form and function at the nuclear envelope. FEBS Lett 589:2514–2521. doi: 10.1016/j.febslet.2015.06.011

Meylan E, Curran J, Hofmann K, Moradpour D, Binder M, Bartenschlager R, Tschopp J (2005) Cardif is an adaptor protein in the RIG-I antiviral pathway and is targeted by hepatitis C virus. Nature 437:1167–72. doi: 10.1038/nature04193

Mibayashi M, Martínez-Sobrido L, Loo Y-M, Cárdenas WB, Gale M, García-Sastre A (2007) Inhibition of Retinoic Acid-Inducible Gene I-Mediated Induction of Beta Interferon by the NS1 Protein of Influenza A Virus. J Virol 81:514–524. doi: 10.1128/jvi.01265-06

Michalski S, de Oliveira Mann CC, Stafford CA, Witte G, Bartho J, Lammens K, Hornung V, Hopfner KP (2020) Structural basis for sequestration and autoinhibition of cGAS by chromatin. Nature 587:678–682. doi: 10.1038/s41586-020-2748-0

Milne TA, Hughes CM, Lloyd R, Yang Z, Rozenblatt-Rosen O, Dou Y, Schnepp RW, Krankel C, LiVolsi VA, Gibbs D, Hua X, Roeder RG, Meyerson M, Hess JL (2005) Menin and MLL cooperatively regulate expression of cyclin-dependent kinase inhibitors. Proc Natl Acad Sci U S A 102:749–754. doi: 10.1073/pnas.0408836102

Min JY, Krug RM (2006) The primary function of RNA binding by the influenza A virus NS1 protein in infected cells: Inhibiting the 2'-5' oligo (A) synthetase/RNase L pathway. Proc Natl Acad Sci U S A 103:7100–7105. doi: 10.1073/pnas.0602184103

Min JY, Li S, Sen GC, Krug RM (2007) A site on the influenza A virus NS1 protein mediates both inhibition of PKR activation and temporal regulation of viral RNA synthesis. Virology 363:236–243. doi: 10.1016/j.virol.2007.01.038

Mizutani A, Fukuda M, Ibata K, Shiraishi Y, Mikoshiba K (2000) SYNCRIP, a cytoplasmic counterpart of heterogeneous nuclear ribonucleoprotein R, interacts with ubiquitous synaptotagmin isoforms. J Biol Chem 275:9823–31. doi: 10.1074/JBC.275.13.9823

Moir RD, Montag-Lowy M, Goldman RD (1994) Dynamic properties of nuclear lamins: lamin B is associated with sites of DNA replication. J Cell Biol 125:1201–12.

Mole RH (1953) Whole body irradiation; radiobiology or medicine? Br J Radiol 26:234–241. doi: 10.1259/0007-1285-26-305-234

Morchikh M, Cribier A, Raffel R, Amraoui S, Cau J, Severac D, Dubois E, Schwartz O, Bennasser Y, Benkirane M (2017) HEXIM1 and NEAT1 Long Non-coding RNA Form a Multi-subunit Complex that Regulates DNA-Mediated Innate Immune Response. Mol Cell 67:387-399.e5. doi: 10.1016/j.molcel.2017.06.020

Moretti J, Roy S, Bozec D, Martinez J, Chapman JR, Ueberheide B, Lamming DW, Chen ZJ, Horng T, Yeretssian G, Green DR, Blander JM (2017) STING Senses Microbial Viability to Orchestrate Stress-Mediated Autophagy of the Endoplasmic Reticulum. Cell 171:809-823.e13. doi: 10.1016/j.cell.2017.09.034

Moriyama M, Koshiba T, Ichinohe T (2019) Influenza A virus M2 protein triggers mitochondrial DNA-mediated antiviral immune responses. Nat Commun. doi: 10.1038/s41467-019-12632-5

Morrone SR, Wang T, Constantoulakis LM, Hooy RM, Delannoy MJ, Sohn J (2014) Cooperative assembly of IFI16 filaments on dsDNA provides insights into host defense strategy. Proc Natl Acad Sci U S A 111:E62-71. doi: 10.1073/pnas.1313577111

Motwani M, Pesiridis S, Fitzgerald KA (2019) DNA sensing by the cGAS–STING pathway in health and disease. Nat Rev Genet 20:657–674. doi: 10.1038/s41576-019-0151-1

Mourelatos Z, Abel L, Yong J, Kataoka N, Dreyfuss G (2001) SMN interacts with a novel family of hnRNP and spliceosomal proteins. EMBO J 20:5443–5452. doi: 10.1093/emboj/20.19.5443

Mudumbi KC, Czapiewski R, Ruba A, Junod SL, Li Y, Luo W, Ngo C, Ospina V, Schirmer EC, Yang W (2020) Nucleoplasmic signals promote directed transmembrane protein import simultaneously via multiple channels of nuclear pores. Nat Commun 11:1–14. doi: 10.1038/s41467-020-16033-x

Mudumbi KC, Schirmer EC, Yang W (2016) Single-point single-molecule FRAP distinguishes inner and outer nuclear membrane protein distribution. Nat Commun. doi: 10.1038/ncomms12562

Mukai K, Konno H, Akiba T, Uemura T, Waguri S, Kobayashi T, Barber GN, Arai H, Taguchi T (2016) Activation of STING requires palmitoylation at the Golgi. Nat Commun 7:11932. doi: 10.1038/ncomms11932

Mukhopadhyay R, Jia J, Arif A, Ray PS, Fox PL (2009) The GAIT system: a gatekeeper of inflammatory gene expression. Trends Biochem Sci 34:324–331. doi: 10.1016/j.tibs.2009.03.004

Munoz J, Rodière M, Jeremiah N, Rieux-Laucat F, Oojageer A, Rice GI, Rozenberg F, Crow YJ, Bessis D (2015) Stimulator of interferon genes-associated vasculopathy with onset in infancy: A mimic of childhood granulomatosis with polyangiitis. JAMA Dermatology 151:872–877. doi: 10.1001/jamadermatol.2015.0251

Nakabayashi T, Wang HP, Kinjo M, Ohta N (2008) Application of fluorescence lifetime imaging of enhanced green fluorescent protein to intracellular pH measurements. Photochem Photobiol Sci 7:668–670. doi: 10.1039/b800391b

Nazmi A, Mukhopadhyay R, Dutta K, Basu A (2012) STING mediates neuronal innate immune response following japanese encephalitis virus infection. Sci Rep 2:1–10. doi: 10.1038/srep00347

Nemeroff ME, Barabino SML, Li Y, Keller W, Krug RM (1998) Influenza virus NS1 protein interacts with the cellular 30 kDa subunit of CPSF and inhibits 3′ end formation of cellular pre-mRNAs. Mol Cell 1:991–1000. doi: 10.1016/S1097-2765(00)80099-4

Nguyen TA, Smith BRC, Tate MD, Belz GT, Barrios MH, Elgass KD, Weisman AS, Baker PJ, Preston SP, Whitehead L, Garnham A, Lundie RJ, Smyth GK, Pellegrini M, O'Keeffe M, Wicks IP, Masters SL, Hunter CP, Pang KC (2017) SIDT2 Transports Extracellular dsRNA into the Cytoplasm for Innate Immune Recognition. Immunity 47:498-509.e6. doi: 10.1016/j.immuni.2017.08.007

Nicodeme E, Jeffrey KL, Schaefer U, Beinke S, Dewell S, Chung CW, Chandwani R, Marazzi I, Wilson P, Coste H, White J, Kirilovsky J, Rice CM, Lora JM, Prinjha RK, Lee K,

Tarakhovsky A (2010) Suppression of inflammation by a synthetic histone mimic. Nature 468:1119–1123. doi: 10.1038/nature09589

Nitta S, Sakamoto N, Nakagawa M, Kakinuma S, Mishima K, Kusano-Kitazume A, Kiyohashi K, Murakawa M, Nishimura-Sakurai Y, Azuma S, Tasaka-Fujita M, Asahina Y, Yoneyama M, Fujita T, Watanabe M (2013) Hepatitis C virus NS4B protein targets STING and abrogates RIG-I-mediated type I interferon-dependent innate immunity. Hepatology 57:46–58. doi: 10.1002/hep.26017

Noah DL, Twu KY, Krug RM (2003) Cellular antiviral responses against influenza A virus are countered at the posttranscriptional level by the viral NS1A protein via its binding to a cellular protein required for the 3' end processing of cellular pre-mRNAS. Virology 307:386–395. doi: 10.1016/S0042-6822(02)00127-7

Ohba T, Schirmer EC, Nishimoto T, Gerace L (2004) Energy- and temperature-dependent transport of integral proteins to the inner nuclear membrane via the nuclear pore. J Cell Biol 167:1051–1062. doi: 10.1083/jcb.200409149

Olins AL, Rhodes G, Welch DBM, Zwerger M, Olins DE (2010) Lamin B receptor multi-tasking at the nuclear envelope. Nucleus 1:53–70. doi: 10.4161/nucl.1.1.10515

Omura H, Oikawa D, Nakane T, Kato M, Ishii R, Ishitani R, Tokunaga F, Nureki O (2016) Structural and functional analysis of DDX41: A bispecific immune receptor for DNA and cyclic dinucleotide. Sci Rep 6:1–4. doi: 10.1038/srep34756

Opitz B, Rejaibi A, Dauber B, Eckhard J, Vinzing M, Schmeck B, Hippenstiel S, Suttorp N, Wolff T (2007) IFNβ induction by influenza A virus is mediated by RIG-I which is regulated by the viral NS1 protein. Cell Microbiol 9:930–938. doi: 10.1111/j.1462-5822.2006.00841.x

Orzalli MH, Broekema NM, Diner BA, Hancks DC, Elde NC, Cristea IM, Knipe DM (2015) cGAS-mediated stabilization of IFI16 promotes innate signaling during herpes simplex virus infection. Proc Natl Acad Sci 112:201424637. doi: 10.1073/pnas.1424637112

Orzalli MH, Conwell SE, Berrios C, DeCaprio JA, Knipe DM (2013) Nuclear interferon-inducible protein 16 promotes silencing of herpesviral and transfected DNA. Proc Natl Acad Sci U S A 110:E4492-501. doi: 10.1073/pnas.1316194110

Orzalli MH, DeLuca N a., Knipe DM (2012) Nuclear IFI16 induction of IRF-3 signaling during herpesviral infection and degradation of IFI16 by the viral ICP0 protein. Proc Natl Acad Sci 109:E3008–E3017. doi: 10.1073/pnas.1211302109

Oshiumi H, Matsumoto M, Hatakeyama S, Seya T (2009) Riplet/RNF135, a RING finger protein, ubiquitinates RIG-I to promote interferon-β induction during the early phase of viral infection. J Biol Chem 284:807–817. doi: 10.1074/jbc.M804259200

Ouyang S, Song X, Wang YYY, Ru H, Shaw N, Jiang Y, Niu F, Zhu Y, Qiu W, Parvatiyar K, Li Y, Zhang R, Cheng G, Liu Z-J (2012) Structural Analysis of the STING Adaptor Protein Reveals a Hydrophobic Dimer Interface and Mode of Cyclic di-GMP Binding. Immunity 36:1073–1086. doi: 10.1016/j.immuni.2012.03.019

Palchetti S, Starace D, De Cesaris P, Filippini A, Ziparo E, Riccioli A (2015) Transfected poly(I:C) activates different dsRNA receptors, leading to apoptosis or immunoadjuvant

response in androgen-independent prostate cancer cells. J Biol Chem 290:5470–5483. doi: 10.1074/jbc.M114.601625

Palm NW, Medzhitov R (2009) Pattern recognition receptors and control of adaptive immunity. Immunol Rev 227:221–233. doi: 10.1111/j.1600-065X.2008.00731.x

Pan S, Liu X, Ma Y, Cao Y, He B (2018) Herpes Simplex Virus 1 γ 1 34.5 Protein Inhibits STING Activation That Restricts Viral Replication. J Virol 92:1–11. doi: 10.1128/JVI.01015-18

Pantelidou C, Sonzogni O, Taveira MDO, Mehta AK, Kothari A, Wang D, Visal T, Li MK, Pinto J, Castrillon JA, Cheney EM, Bouwman P, Jonkers J, Rottenberg S, Guerriero JL, Wulf GM, Shapiro GI (2019) Parp inhibitor efficacy depends on CD8+ T-cell recruitment via intratumoral sting pathway activation in brca-deficient models of triple-negative breast cancer. Cancer Discov 9:722–737. doi: 10.1158/2159-8290.CD-18-1218

Parvatiyar K, Zhang Z, Teles RM, Ouyang S, Jiang Y, Iyer SS, Zaver SA, Schenk M, Zeng S, Zhong W, Liu ZJ, Modlin RL, Liu YJ, Cheng G (2012) The helicase DDX41 recognizes the bacterial secondary messengers cyclic di-GMP and cyclic di-AMP to activate a type i interferon immune response. Nat Immunol 13:1155–1161. doi: 10.1038/ni.2460

Pfaller CK, Li Z, George CX, Samuel CE (2011) Protein kinase PKR and RNA adenosine deaminase ADAR1: New roles for old players as modulators of the interferon response. Curr Opin Immunol 23:573–582. doi: 10.1016/j.coi.2011.08.009

Pichlmair A, Kandasamy K, Alvisi G, Mulhern O, Sacco R, Habjan M, Binder M, Stefanovic A, Eberle CA, Goncalves A, Bürckstümmer T, Müller AC, Fauster A, Holze C, Lindsten K, Goodbourn S, Kochs G, Weber F, Bartenschlager R, Bowie AG, Bennett KL, Colinge J, Superti-Furga G (2012) Viral immune modulators perturb the human molecular network by common and unique strategies. Nature 487:486–490. doi: 10.1038/nature11289

Pinto RM, Lycett S, Gaunt E, Digard P (2020) Accessory Gene Products of Influenza A Virus. Cold Spring Harb Perspect Med a038380. doi: 10.1101/cshperspect.a038380

Plotch SJ, Bouloy M, Krug RM (1979) Transfer of 5'-terminal cap of globin mRNA to influenza viral complementary RNA during transcription in vitro. Proc Natl Acad Sci U S A 76:1618–1622.

Plotch SJ, Bouloy M, Ulmanen I, Krug RM (1981) A unique cap(m7GpppXm)-dependent influenza virion endonuclease cleaves capped RNAs to generate the primers that initiate viral RNA transcription. Cell 23:847–858. doi: 10.1016/0092-8674(81)90449-9

Pomeranz Krummel DA, Oubridge C, Leung AKW, Li J, Nagai K (2009) Crystal structure of human spliceosomal U1 snRNP at 5.5 resolution. Nature 458:475–480. doi: 10.1038/nature07851

Powell L, Burke B (1990) Internuclear exchange of an inner nuclear membrane protein (p55) in heterokaryons: In vivo evidence for the interaction of p55 with the nuclear lamina. J Cell Biol 111:2225–2234. doi: 10.1083/jcb.111.6.2225

Prabakaran T, Bodda C, Krapp C, Zhang B, Christensen MH, Sun C, Reinert L, Cai Y, Jensen SB, Skouboe MK, Nyengaard JR, Thompson CB, Lebbink RJ, Sen GC, van Loo G, Nielsen R, Komatsu M, Nejsum LN, Jakobsen MR, Gyrd-Hansen M, Paludan SR (2018) Attenuation

of cGAS-STING signaling is mediated by a p62/SQSTM1-dependent autophagy pathway activated by TBK1. EMBO J. doi: 10.15252/embj.201797858

Quaresma AJC, Bressan GC, Gava LM, Lanza DCF, Ramos CHI, Kobarg J (2009) Human hnRNP Q re-localizes to cytoplasmic granules upon PMA, thapsigargin, arsenite and heat-shock treatments. Exp Cell Res 315:968–980. doi: 10.1016/j.yexcr.2009.01.012

Raab M, Gentili M, De Belly H, Thiam HR, Vargas P, Jimenez AJ, Lautenschlaeger F, Voituriez R, Lennon-Duménil AM, Manel N, Piel M (2016) ESCRT III repairs nuclear envelope ruptures during cell migration to limit DNA damage and cell death. Science (80-) 352:359–362. doi: 10.1126/science.aad7611

Rahman MM, Bagdassarian E, Ali MAM, McFadden G (2017) Identification of host DEAD-box RNA helicases that regulate cellular tropism of oncolytic Myxoma virus in human cancer cells. Sci Rep 7:1–14. doi: 10.1038/s41598-017-15941-1

Rajgor D, Shanahan CM (2013) Nesprins: from the nuclear envelope and beyond. Expert Rev Mol Med 15:1–17. doi: 10.1017/erm.2013.6

Rajsbaum R, Albrecht RA, Wang MK, Maharaj NP, Versteeg GA, Nistal-Villán E, García-Sastre A, Gack MU (2012) Species-Specific Inhibition of RIG-I Ubiquitination and IFN Induction by the Influenza A Virus NS1 Protein. PLoS Pathog. doi: 10.1371/journal.ppat.1003059

Ran FA, Hsu PD, Wright J, Agarwala V, Scott DA, Zhang F (2013) Genome engineering using the CRISPR-Cas9 system. Nat Protoc 8:2281–2308. doi: 10.1038/nprot.2013.143

Ran Y, Shu H-BB, Wang Y-YY (2014) MITA/STING: A central and multifaceted mediator in innate immune response. Cytokine Growth Factor Rev 25:631–639. doi: 10.1016/j.cytogfr.2014.05.003

Rasaiyaah J, Tan CP, Fletcher AJ, Price AJ, Blondeau C, Hilditch L, Jacques DA, Selwood DL, James LC, Noursadeghi M, Towers GJ (2013) HIV-1 evades innate immune recognition through specific cofactor recruitment. Nature 503:402–405. doi: 10.1038/nature12769

Reinert LS, Lopušná K, Winther H, Sun C, Thomsen MK, Nandakumar R, Mogensen TH, Meyer M, Vægter C, Nyengaard JR, Fitzgerald KA, Paludan SR (2016) Sensing of HSV-1 by the cGAS-STING pathway in microglia orchestrates antiviral defence in the CNS. Nat Commun. doi: 10.1038/ncomms13348

Roberts TL, Idris A, Dunn JA, Kelly GM, Burnton CM, Hume DA, Stacey KJ (2010) HIN-200 Proteins Regulate Caspase. Science (80-) 1057:1057–1061. doi: 10.1126/science.1169841

Robson MII, de las Heras JI, Czapiewski R, Lê Thành P, Booth DGG, Kelly DAA, Webb S, Kerr ARWRW, Schirmer ECC, de las Heras JI, Czapiewski R, Lê Thành P, Booth DGG, Kelly DAA, Webb S, Kerr ARWRW, Schirmer ECC (2016) Tissue-Specific Gene Repositioning by Muscle Nuclear Membrane Proteins Enhances Repression of Critical Developmental Genes during Myogenesis. Mol Cell 62:834–847. doi: 10.1016/j.molcel.2016.04.035

Rodero MP (2017) Type i interferon-mediated autoinflammation due to DNase II deficiency. Nat Commun. doi: 10.1038/s41467-017-01932-3

Rodriguez-Madoz JR, Belicha-Villanueva A, Bernal-Rubio D, Ashour J, Ayllon J, Fernandez-

Sesma A (2010) Inhibition of the Type I Interferon Response in Human Dendritic Cells by Dengue Virus Infection Requires a Catalytically Active NS2B3 Complex. J Virol 84:9760–9774. doi: 10.1128/jvi.01051-10

Roers A, Hiller B, Hornung V (2016) Recognition of Endogenous Nucleic Acids by the Innate Immune System. Immunity 44:739–754. doi: 10.1016/j.immuni.2016.04.002

Rongvaux A (2018) Innate immunity and tolerance toward mitochondria. Mitochondrion 41:14–20. doi: 10.1016/j.mito.2017.10.007

Rongvaux A, Jackson R, Harman CCD, Li T, West AP, De Zoete MR, Wu Y, Yordy B, Lakhani SA, Kuan CY, Taniguchi T, Shadel GS, Chen ZJ, Iwasaki A, Flavell RA (2014) Apoptotic caspases prevent the induction of type i interferons by mitochondrial DNA. Cell 159:1563–1577. doi: 10.1016/j.cell.2014.11.037

Rotem BZ, Cox RA, Isaacs A (1963) Inhibition of Virus Multiplication by Foreign Nucleic Acid. Nature 564–566.

Saitoh T, Fujita N, Hayashi T, Takahara K, Satoh T, Lee H (2009) Atg9a controls dsDNA-driven dynamic translocation. Pnas 106:20842–46.

Saksena S, Shao Y, Braunagel SC, Summers MD, Johnson AE (2004) Cotranslational integration and initial sorting at the endoplasmic reticulum translocon of proteins destined for the inner nuclear membrane. Proc Natl Acad Sci U S A 101:12537–42. doi: 10.1073/pnas.0404934101

Salpingidou G, Smertenko A, Hausmanowa-Petrucewicz I, Hussey PJ, Hutchison CJ (2007) A novel role for the nuclear membrane protein emerin in association of the centrosome to the outer nuclear membrane. J Cell Biol 178:897–904. doi: 10.1083/jcb.200702026

Samji T (2009) Influenza A: Understanding the viral life cycle. Yale J Biol Med 82:153–159.

Santangelo L, Giurato G, Cicchini C, Alonzi T, Weisz A, Tripodi M (2016) The RNA-Binding Protein SYNCRIP Is a Component of the Hepatocyte Exosomal Machinery Controlling MicroRNA Sorting. Cell Rep 17:799–808. doi: 10.1016/j.celrep.2016.09.031

Sato R, Kato A, Chimura T, Saitoh SI, Shibata T, Murakami Y, Fukui R, Liu K, Zhang Y, Arii J, Sun-Wada GH, Wada Y, Ikenoue T, Barber GN, Manabe T, Kawaguchi Y, Miyake K (2018) Combating herpesvirus encephalitis by potentiating a TLR3–mTORC2 axis. Nat Immunol 19:1071–1082. doi: 10.1038/s41590-018-0203-2

Schermelleh L, Carlton PM, Haase S, Shao L, Winoto L, Kner P, Burke B, Cardoso MC, Agard D a, Gustafsson MGL, Leonhardt H, Sedat JW (2008) Subdiffraction multicolor imaging of the nuclear periphery with 3D structured illumination microscopy. Science 320:1332–6. doi: 10.1126/science.1156947

Schindelin J, Arganda-Carreras I, Frise E, Kaynig V, Longair M, Pietzsch T, Preibisch S, Rueden C, Saalfeld S, Schmid B, Tinevez JY, White DJ, Hartenstein V, Eliceiri K, Tomancak P, Cardona A (2012) Fiji: An open-source platform for biological-image analysis. Nat Methods 9:676–682. doi: 10.1038/nmeth.2019

Schirmer EC, Florens L, Guan T, Yates JR, Gerace L (2003) Nuclear Membrane Proteins with Potential Disease Links Found by Subtractive Proteomics. Science (80-) 1380:10–13.

doi: 10.1126/science.1088176

Schirmer EC, Guan T, Gerace L (2001) Involvement of the lamin rod domain in heterotypic lamin interactions important for nuclear organization. J Cell Biol 152:479–489. doi: 10.1083/jcb.153.3.479

Schlee M, Hartmann G (2016) Discriminating self from non-self in nucleic acid sensing. Nat Rev Immunol 16:566–580. doi: 10.1038/nri.2016.78

Schlee M, Roth A, Hornung V, Hagmann CA, Wimmenauer V, Barchet W, Coch C, Janke M, Mihailovic A, Wardle G, Juranek S, Kato H, Kawai T, Poeck H, Fitzgerald KA, Takeuchi O, Akira S, Tuschl T, Latz E, Ludwig J, Hartmann G (2009) Recognition of 5′ Triphosphate by RIG-I Helicase Requires Short Blunt Double-Stranded RNA as Contained in Panhandle of Negative-Strand Virus. Immunity 31:25–34. doi: 10.1016/j.immuni.2009.05.008

Schneider WM, Chevillotte MD, Rice CM (2014) Interferon-Stimulated Genes: A Complex Web of Host Defenses. Annu Rev Immunol 32:513–545. doi: 10.1146/annurev-immunol-032713-120231

Schoggins JW, MacDuff D a, Imanaka N, Gainey MD, Shrestha B, Eitson JL, Mar KB, Richardson RB, Ratushny A V, Litvak V, Dabelic R, Manicassamy B, Aitchison JD, Aderem A, Elliott RM, García-Sastre A, Racaniello V, Snijder EJ, Yokoyama WM, Diamond MS, Virgin HW, Rice CM (2014) Pan-viral specificity of IFN-induced genes reveals new roles for cGAS in innate immunity. Nature 505:691–5. doi: 10.1038/nature12862

Schoggins JW, Wilson SJ, Panis M, Murphy MY, Jones CT, Bieniasz P, Rice CM, Wilson SJ, Rice CM, Murphy MY, Panis M, Jones CT (2011) A diverse range of gene products are effectors of the type I interferon antiviral response. Nature 472:481–5. doi: 10.1038/nature09907

Senior A, Gerace L (1988) Integral membrane proteins specific to the inner nuclear membrane and associated with the nuclear lamina. J Cell Biol 107:2029–36. doi: 10.1083/JCB.107.6.2029

Servant MJ, Grandvaux N, Hiscott J (2002) Multiple signaling pathways leading to the activation of interferon regulatory factor 3. Biochem Pharmacol 64:985–992. doi: 10.1016/S0006-2952(02)01165-6

Seth RB, Sun L, Ea C-K, Chen ZJ (2005) Identification and characterization of MAVS, a mitochondrial antiviral signaling protein that activates NF-kappaB and IRF 3. Cell 122:669–82. doi: 10.1016/j.cell.2005.08.012

Shaklai S, Amariglio N, Rechavi G, Simon AJ (2007) Gene silencing at the nuclear periphery. FEBS J 274:1383–1392. doi: 10.1111/j.1742-4658.2007.05697.x

Shang G, Zhang C, Chen ZJ, Bai X chen, Zhang X (2019) Cryo-EM structures of STING reveal its mechanism of activation by cyclic GMP–AMP. Nature 567:

Shang G, Zhu D, Li N, Zhang J, Zhu C, Lu D, Liu C, Yu Q, Zhao Y, Xu S, Gu L (2012) Crystal structures of STING protein reveal basis for recognition of cyclic di-GMP. Nat Struct Mol Biol 19:725–7. doi: 10.1038/nsmb.2332

Shang J, Xia T, Han QQ, Zhao X, Hu MM, Shu HB, Guo L (2018) Quantitative Proteomics

Identified TTC4 as a TBK1 Interactor and a Positive Regulator of SeV-Induced Innate Immunity. Proteomics. doi: 10.1002/pmic.201700403

Shen YJ, LeBert N, Chitre AA, Koo CXE, Nga XH, Ho SSW, Khatoo M, Tan NY, Ishii KJ, Gasser S (2015) Genome-derived cytosolic DNA mediates type I interferon-dependent rejection of B cell lymphoma cells. Cell Rep 11:460–473. doi: 10.1016/j.celrep.2015.03.041

Shimizu Y, Nishitsuji H, Marusawa H, Ujino S, Takaku H, Shimotohno K (2014) The RNA-editing Enzyme APOBEC1 Requires heterogeneous nuclear ribonucleoprotein Q Isoform 6 for efficient interaction with interleukin-8 mRNA. J Biol Chem 289:26226–26238. doi: 10.1074/jbc.M114.563221

Shirota H, Ishii KJ, Takakuwa H, Klinman DM (2006) Contribution of interferon-β to the immune activation induced by double-stranded DNA. Immunology 118:302–310. doi: 10.1111/j.1365-2567.2006.02367.x

Sidrauski C, McGeachy AM, Ingolia NT, Walter P (2015) The small molecule ISRIB reverses the effects of eIF2α phosphorylation on translation and stress granule assembly. Elife 2015:1–16. doi: 10.7554/eLife.05033

Sieben C, Sezgin E, Eggeling C, Manley S (2020) Influenza a viruses use multivalent sialic acid clusters for cell binding and receptor activation. PLoS Pathog 16:1–27. doi: 10.1371/journal.ppat.1008656

Sliter DA, Martinez J, Hao L, Chen X, Sun N, Fischer TD, Burman JL, Li Y, Zhang Z, Narendra DP, Cai H, Borsche M, Klein C, Youle RJ (2018) Parkin and PINK1 mitigate STING-induced inflammation. Nature 561:258–262. doi: 10.1038/s41586-018-0448-9

Smith S, Blobel G (1993) The first membrane spanning region of the lamin B receptor is sufficient for sorting to the inner nuclear membrane. J Cell Biol 120:631–637. doi: 10.1083/jcb.120.3.631

Song S, Peng P, Tang Z, Zhao J, Wu W, Li H, Shao M, Li L, Yang C, Duan F, Zhang M, Zhang J, Wu H, Li C, Wang X, Wang H, Ruan Y, Gu J (2017) Decreased expression of STING predicts poor prognosis in patients with gastric cancer. Sci Rep 7:1–13. doi: 10.1038/srep39858

Soullam B, Worman HJ (1995) Signals and structural features involved in integral membrane protein targeting to the inner nuclear membrane. J Cell Biol 130:15–27. doi: 10.1083/jcb.130.1.15

Soullam B, Worman HJ (1993) The amino-terminal domain of the lamin B receptor is a nuclear envelope targeting signal. J Cell Biol 120:1093–1100.

Spann TP, Moir RD, Goldman AE, Stick R, Goldman RD (1997) Disruption of nuclear lamin organization alters the distribution of replication factors and inhibits DNA synthesis. J Cell Biol 136:1201–12.

Sparrer KMJ, Gack MU (2015) Intracellular detection of viral nucleic acids. Curr Opin Microbiol 26:1–9. doi: 10.1016/j.mib.2015.03.001

Srikanth S, Woo JS, Wu B, El-sherbiny YM, Leung J, Chupradit K, Rice L, Seo GJ, Calmettes G, Ramakrishna C, Cantin E, An DS, Sun R, Wu T, Jung JU, Savic S, Gwack Y (2019) The Ca2+

sensor STIM1 regulates the type I interferon response by retaining the signaling adaptor STING at the endoplasmic reticulum. Nat Immunol 20:152–162. doi: 10.1038/s41590-018-0287-8

Stabell AC, Meyerson NR, Gullberg RC, Gilchrist AR, Webb KJ, Old WM, Perera R, Sawyer SL (2018) Dengue viruses cleave STING in humans but not in nonhuman primates, their presumed natural reservoir. Elife 7:1–25. doi: 10.7554/eLife.31919

Starr DA, Fischer JA (2005) KASH 'n Karry: The KASH domain family of cargo-specific cytoskeletal adaptor proteins. BioEssays 27:1136–1146. doi: 10.1002/bies.20312

Stejskalova E, Stane D (2014) The splicing factor U1-70K interacts with the SMN complex and is required for nuclear gem integrity. 3909–3915. doi: 10.1242/jcs.155838

Stetson DB, Ko JS, Heidmann T, Medzhitov R (2008) Trex1 Prevents Cell-Intrinsic Initiation of Autoimmunity. Cell 134:587–598. doi: 10.1016/j.cell.2008.06.032

Stetson DB, Medzhitov R (2006) Recognition of cytosolic DNA activates an IRF3-dependent innate immune response. Immunity 24:93–103. doi: 10.1016/j.immuni.2005.12.003

Su C, Zheng C (2017) Herpes Simplex Virus 1 Abrogates the cGAS/STING-Mediated Cytosolic DNA-Sensing Pathway via its Virion Host Shutoff Protein, UL41. J Virol 91:1–9.

Sumner RP, Thorne LG, Fink DL, Khan H, Milne RS, Towers GJ (2017) Are evolution and the intracellular innate immune system key determinants in HIV transmission? Front Immunol 8:1–23. doi: 10.3389/fimmu.2017.01246

Sun B, Sundström KB, Chew JJ, Bist P, Gan ES, Tan HC, Goh KC, Chawla T, Tang CK, Ooi EE (2017) Dengue virus activates cGAS through the release of mitochondrial DNA. Sci Rep 7:1–8. doi: 10.1038/s41598-017-03932-1

Sun H, Huang Y, Mei S, Xu F, Liu X, Zhao F, Yin L, Zhang D, Wei L, Wu C, Ma S, Wang J, Cen S, Liang C, Hu S, Guo F (2021) A Nuclear Export Signal Is Required for cGAS to Sense Cytosolic DNA. Cell Rep 34:108586. doi: 10.1016/j.celrep.2020.108586

Sun L, Wu J, Du F, Chen X, Chen ZJ (2013) Cyclic GMP-AMP Synthase Is a Cytosolic DNA Sensor That Activates the Type I Interferon Pathway. Science 339:786–791. doi: 10.1126/science.1229963

Sun L, Xing Y, Chen X, Zheng Y, Yang Y, Nichols DB, Clementz MA, Banach BS, Li K, Baker SC, Chen Z (2012) Coronavirus papain-like proteases negatively regulate antiviral innate immune response through disruption of STING-mediated signaling. PLoS One. doi: 10.1371/journal.pone.0030802

Sun W, Li Y, Chen L, Chen H, You F, Zhou X, Zhou Y, Zhai Z, Chen D, Jiang Z (2009) ERIS, an endoplasmic reticulum IFN stimulator, activates innate immune signaling through dimerization. Proc Natl Acad Sci U S A 106:8653–8658. doi: 0900850106 [pii]\r10.1073/pnas.0900850106

Suzuki J, Yamada T, Inoue K, Nabe S, Kuwahara M, Takemori N, Takemori A, Matsuda S, Kanoh M, Imai Y, Yasukawa M, Yamashita M (2018) The tumor suppressor menin prevents effector CD8 T-cell dysfunction by targeting mTORC1-dependent metabolic activation. Nat Commun 9:1–12. doi: 10.1038/s41467-018-05854-6

Svitkin Y V, Yanagiya A, Karetnikov AE, Alain T, Fabian MR, Khoutorsky A, Perreault S, Topisirovic I, Sonenberg N (2013) Control of Translation and miRNA-Dependent Repression by a Novel Poly (A) Binding Protein , hnRNP-Q. doi: 10.1371/journal.pbio.1001564

Swift J, Ivanovska IL, Buxboim A, Harada T, Dingal PCDP, Pinter J, Pajerowski JD, Spinler KR, Shin J-W, Tewari M, Rehfeldt F, Speicher DW, Discher DE (2013) Nuclear Lamin-A Scales with Tissue Stiffness and Enhances Matrix-Directed Differentiation. Science 341:1240104–1240104. doi: 10.1126/science.1240104

Tanaka Y, Chen ZJ (2012) STING specifies IRF3 phosphorylation by TBK1 in the cytosolic DNA signaling pathway. Sci Signal 5:ra20. doi: 10.1126/scisignal.2002521

Te Velthuis AJW, Fodor E (2016) Influenza virus RNA polymerase: Insights into the mechanisms of viral RNA synthesis. Nat Rev Microbiol 14:479–493. doi: 10.1038/nrmicro.2016.87

Thapa K, Wu KC, Sarma A, Grund EM, Szeto A, Mendez AJ, Gesta S, Vishnudas VK, Narain NR, Sarangarajan R (2018) Dysregulation of the calcium handling protein, CCDC47, is associated with diabetic cardiomyopathy. Cell Biosci 8:1–13. doi: 10.1186/s13578-018-0244-0

Tokuyasu KT (1973) A technique for ultracryotomy of cell suspensions and tissues. J Cell Biol 57:551–565. doi: 10.1083/jcb.57.2.551

Tsuchida T, Zou J, Saitoh T, Kumar H, Abe T, Matsuura Y, Kawai T, Akira S (2010) The ubiquitin ligase TRIM56 regulates innate immune responses to intracellular double-stranded DNA. Immunity 33:765–776. doi: 10.1016/j.immuni.2010.10.013

Turgay Y, Ungricht R, Rothballer A, Kiss A, Csucs G, Horvath P, Kutay U (2010) A classical NLS and the SUN domain contribute to the targeting of SUN2 to the inner nuclear membrane. EMBO J 29:2262–2275. doi: 10.1038/emboj.2010.119

Ungricht R, Klann M, Horvath P, Kutay U (2015) Diffusion and retention are major determinants of protein targeting to the inner nuclear membrane. J Cell Biol 209:687–704. doi: 10.1083/jcb.201409127

Unterholzner L (2013) The interferon response to intracellular DNA: Why so many receptors? Immunobiology 218:1312–1321. doi: 10.1016/j.imbio.2013.07.007

Unterholzner L, Keating SE, Baran M, Horan KA, Jensen SB, Sharma S, Sirois CM, Jin T, Latz E, Xiao TS, Fitzgerald KA, Paludan SR, Bowie AG (2010) IFI16 is an innate immune sensor for intracellular DNA. Nat Immunol 11:997–1004. doi: 10.1038/ni.1932

Valente ST, Goff SP (2006) Inhibition of HIV-1 Gene Expression by a Fragment of hnRNP U. Mol Cell 23:597–605. doi: 10.1016/j.molcel.2006.07.021

Van Deursen JM (2014) The role of senescent cells in ageing. Nature 509:439–446. doi: 10.1038/nature13193

Villarroya-Beltri C, Gutiérrez-Vázquez C, Sánchez-Cabo F, Pérez-Hernández D, Vázquez J, Martin-Cofreces N, Martinez-Herrera DJ, Pascual-Montano A, Mittelbrunn M, Sánchez-Madrid F (2013) Sumoylated hnRNPA2B1 controls the sorting of miRNAs into exosomes

through binding to specific motifs. Nat Commun 4:1–10. doi: 10.1038/ncomms3980

Volkman HE, Cambier S, Gray EE, Stetson DB (2019) Tight nuclear tethering of cGAS is essential for preventing autoreactivity. Elife 8:1–21. doi: 10.7554/eLife.47491

von Appen A, Beck M (2016) Structure Determination of the Nuclear Pore Complex with Three-Dimensional Cryo electron Microscopy. J Mol Biol 428:2001–2010. doi: 10.1016/j.jmb.2016.01.004

von Appen A, Kosinski J, Sparks L, Ori A, DiGuilio AL, Vollmer B, Mackmull M-T, Banterle N, Parca L, Kastritis P, Buczak K, Mosalaganti S, Hagen W, Andres-Pons A, Lemke EA, Bork P, Antonin W, Glavy JS, Bui KH, Beck M (2015) In situ structural analysis of the human nuclear pore complex. Nature 526:140–143. doi: 10.1038/nature15381

Vu LP, Prieto C, Amin EM, Chhangawala S, Krivtsov A, Nieves Calvo-Vidal M, Chou T, Chow A, Minuesa G, Mi Park S, Barlowe TS, Taggart J, Tivnan P, Deering RP, Chu LP, Kwon J-A, Meydan C, Perales-Paton J, Arshi A, Gönen M, Famulare C, Patel M, Paietta E, Tallman MS, Lu Y, Glass J, Garret-Bakelman FE, Melnick A, Levine R, Al-Shahrour F, Järås M, Hacohen N, Hwang A, Garippa R, Lengner CJ, Armstrong SA, Cerchietti L, Cowley GS, Root D, Doench J, Leslie C, Ebert BL, Kharas MG (2017) Functional screen of MSI2 interactors identifies an essential role for SYNCRIP in myeloid leukemia stem cells. Nat Publ Gr. doi: 10.1038/ng.3854

Wang H, Gao X, Huang Y, Yang J, Liu ZR (2009) P68 RNA helicase is a nucleocytoplasmic shuttling protein. Cell Res 19:1388–1400. doi: 10.1038/cr.2009.113

Wang H, Yu J, Zhang L, Xiong Y, Chen S, Xing H, Tian Z, Tang K, Wei H, Rao Q, Wang M, Wang J (2014a) RPS27a promotes proliferation, regulates cell cycle progression and inhibits apoptosis of leukemia cells. Biochem Biophys Res Commun 446:1204–1210. doi: 10.1016/j.bbrc.2014.03.086

Wang J, Kang L, Song D, Liu L, Yang S, Ma L, Guo Z, Ding H, Wang H, Yang B (2017a) Ku70 Senses HTLV-1 DNA and Modulates HTLV-1 Replication. J Immunol 199:2475–2482. doi: 10.4049/jimmunol.1700111

Wang L, Wen M, Cao X (2019) Nuclear hnRNPA2B1 initiates and amplifies the innate immune response to DNA viruses. Science (80-). doi: 10.1126/science.aav0758

Wang T, Birsoy K, Hughes NW, Krupczak KM, Post Y, Wei JJ, Lander ES, Sabatini DM (2015) Identification and characterization of essential genes in the human genome. Science (80-) 350:1096–1101. doi: 10.1126/science.aac7041

Wang W, Riedel K, Lynch P, Chien CY, Montelione GT, Krug RM (1999) RNA binding by the novel helical domain of the influenza virus NS1 protein requires its dimer structure and a small number of specific basic amino acids. Rna 5:195–205. doi: 10.1017/S1355838299981621

Wang X, Majumdar T, Kessler P, Ozhegov E, Zhang Y, Chattopadhyay S, Barik S, Sen GC (2016) STING Requires the Adaptor TRIF to Trigger Innate Immune Responses to Microbial Infection. Cell Host Microbe 20:329–341. doi: 10.1016/j.chom.2016.08.002

Wang Y, Ning X, Gao P, Wu S, Sha M, Lv M, Zhou X, Gao J, Fang R, Meng G, Su X, Jiang Z (2017b) Inflammasome Activation Triggers Caspase-1-Mediated Cleavage of cGAS to

Regulate Responses to DNA Virus Infection. Immunity 46:393–404. doi: 10.1016/j.immuni.2017.02.011

Wang Y, Zhou J, Du Y (2014b) HnRNP A2/B1 interacts with influenza A viral protein NS1 and inhibits virus replication potentially through suppressing NS1 RNA/protein levels and NS1 mRNA nuclear export. Virology 449:53–61. doi: 10.1016/j.virol.2013.11.009

Wathelet MG, Lin CH, Parekh BS, Ronco L V, Howley PM, Maniatis T (1998) Virus Infection Induces the Assembly of Coordinately Activated Transcription Factors on the IFN-β Enhancer In Vivo. Mol Cell 1:507–518. doi: 10.1016/S1097-2765(00)80051-9

Watson RO, Bell SL, MacDuff DA, Kimmey JM, Diner EJ, Olivas J, Vance RE, Stallings CL, Virgin HW, Cox JS (2015) The Cytosolic Sensor cGAS Detects Mycobacterium tuberculosis DNA to Induce Type I Interferons and Activate Autophagy. Cell Host Microbe 17:811–819. doi: 10.1016/j.chom.2015.05.004

Watson RO, Manzanillo PS, Cox JS (2012) Extracellular M. tuberculosis DNA targets bacteria for autophagy by activating the host DNA-sensing pathway. Cell 150:803–815. doi: 10.1016/j.cell.2012.06.040

Welcker D, Jain M, Khurshid S, Jokić M, Höhne M, Schmitt A, Frommolt P, Niessen CM, Spiro J, Persigehl T, Wittersheim M, Büttner R, Fanciulli M, Schermer B, Reinhardt HC, Benzing T, Höpker K (2018) AATF suppresses apoptosis, promotes proliferation and is critical for Kras-driven lung cancer. Oncogene 37:1503–1518. doi: 10.1038/s41388-017-0054-6

West AP, Khoury-Hanold W, Staron M, Tal MC, Pineda CM, Lang SM, Bestwick M, Duguay BA, Raimundo N, MacDuff DA, Kaech SM, Smiley JR, Means RE, Iwasaki A, Shadel GS (2015) Mitochondrial DNA stress primes the antiviral innate immune response. Nature 520:553–557. doi: 10.1038/nature14156

White MJ, McArthur K, Metcalf D, Lane RM, Cambier JC, Herold MJ, Van Delft MF, Bedoui S, Lessene G, Ritchie ME, Huang DCS, Kile BT (2014) Apoptotic caspases suppress mtDNA-induced STING-mediated type i IFN production. Cell 159:1549–1562. doi: 10.1016/j.cell.2014.11.036

Wiens KE, Ernst JD (2016) The Mechanism for Type I Interferon Induction by Mycobacterium tuberculosis is Bacterial Strain-Dependent. PLoS Pathog 12:1–20. doi: 10.1371/journal.ppat.1005809

Wilkie GS, Korfali N, Swanson SK, Malik P, Srsen V, Batrakou DG, de las Heras J, Zuleger N, Kerr ARWW, Florens L, Schirmer EC (2011) Several Novel Nuclear Envelope Transmembrane Proteins Identified in Skeletal Muscle Have Cytoskeletal Associations. Mol Cell Proteomics 10:M110.003129. doi: 10.1159/000350240

Willis ND, Cox TR, Rahman-Casañs SF, Smits K, Przyborski SA, van den Brandt P, van Engeland M, Weijenberg M, Wilson RG, de Bruïne A, Hutchison CJ (2008) Lamin A/C Is a Risk Biomarker in Colorectal Cancer. PLoS One 3:e2988. doi: 10.1371/journal.pone.0002988

Wilson BJ, Bates GJ, Nicol SM, Gregory DJ, Perkins ND, Fuller-Pace F V. (2004) The p68 and p72 DEAD box RNA helicases interact with HDAC1 and repress transcription in a

promoter-specific manner. BMC Mol Biol 5:1–15. doi: 10.1186/1471-2199-5-11

Woo SR, Fuertes MB, Corrales L, Spranger S, Furdyna MJ, Leung MYK, Duggan R, Wang Y, Barber GN, Fitzgerald KA, Alegre ML, Gajewski TF (2014) STING-dependent cytosolic DNA sensing mediates innate immune recognition of immunogenic tumors. Immunity 41:830–842. doi: 10.1016/j.immuni.2014.10.017

Woodward JJ, Lavarone AT, Portnoy DA (2010) C-di-AMP secreted by intracellular Listeria monocytogenes activates a host type I interferon response. Science (80-) 328:1703–1705. doi: 10.1126/science.1189801

Worman HJ, Schirmer EC (2015) Nuclear membrane diversity: Underlying tissue-specific pathologies in disease? Curr Opin Cell Biol 34:101–112. doi: 10.1016/j.ceb.2015.06.003

Worman HJ, Yuan J, Blobel G, Georgatos SD (1988) A lamin B receptor in the nuclear envelope. Proc Natl Acad Sci U S A 85:8531–8534. doi: 10.1073/pnas.85.22.8531

Wu B, Peisley A, Richards C, Yao H, Zeng X, Lin C, Chu F, Walz T, Hur S (2013a) Structural basis for dsRNA recognition, filament formation, and antiviral signal activation by MDA5. Cell 152:276–289. doi: 10.1016/j.cell.2012.11.048

Wu B, Peisley A, Tetrault D, Li Z, Egelman EH, Magor KE, Walz T, Penczek PA, Hur S (2014) Molecular imprinting as a signal-activation mechanism of the viral RNA sensor RIG-I. Mol Cell 55:511–523. doi: 10.1016/j.molcel.2014.06.010

Wu J, Sun L, Chen X, Du F, Shi H, Chen C, Chen ZJ (2013b) Cyclic GMP-AMP Is an Endogenous Second Messenger in Innate Immune Signaling by Cytosolic DNA. Science (80-) 339:826–830. doi: 10.1126/science.1229963

Xia T, Konno H, Ahn J, Barber GN (2016a) Deregulation of STING Signaling in Colorectal Carcinoma Constrains DNA Damage Responses and Correlates With Tumorigenesis. Cell Rep 14:282–297. doi: 10.1016/j.celrep.2015.12.029

Xia T, Konno H, Barber GN (2016b) Recurrent Loss of STING Signaling in Melanoma Correlates with Susceptibility to Viral Oncolysis. Cancer Res 76:6747–6759. doi: 10.1158/0008-5472.CAN-16-1404

Xing Y, Chen J, Tu J, Zhang B, Chen X, Shi H, Baker SC, Feng L, Chen Z (2013) The papain-like protease of porcine epidemic diarrhea virus negatively regulates type I interferon pathway by acting as a viral deubiquitinase. J Gen Virol 94:1554–1567. doi: 10.1099/vir.0.051169-0

Yamada T, Kanoh M, Nabe S, Yasuoka T, Suzuki J, Matsumoto A, Kuwahara M, Maruyama S, Fujimoto T, Sakisuka R, Yasukawa M, Yamashita M (2016) Menin Plays a Critical Role in the Regulation of the Antigen-Specific CD8 + T Cell Response upon Listeria Infection . J Immunol 197:4079–4089. doi: 10.4049/jimmunol.1502295

Yamamoto M, Sato S, Mori K, Hoshino K, Takeuchi O, Takeda K, Akira S (2002) Cutting Edge: A Novel Toll/IL-1 Receptor Domain-Containing Adapter That Preferentially Activates the IFN-β Promoter in the Toll-Like Receptor Signaling. J Immunol 169:6668–6672. doi: 10.4049/jimmunol.169.12.6668

Yang H, Wang H, Ren U, Chen Q, Chena ZJ (2017) CGAS is essential for cellular senescence.

Proc Natl Acad Sci U S A 114:E4612–E4620. doi: 10.1073/pnas.1705499114

Yang L, Wang L, Ketkar H, Ma J, Yang G, Cui S, Geng T, Mordue DG, Fujimoto T, Cheng G, You F, Lin R, Fikrig E, Wang P (2018) UBXN3B positively regulates STING-mediated antiviral immune responses. Nat Commun 9:1–12. doi: 10.1038/s41467-018-04759-8

Yang W (2013) Distinct, but not completely separate spatial transport routes in the nuclear pore complex. Nucleus 4:166–75. doi: 10.4161/nucl.24874

Ye Q, Worman HJ (1996) Interaction between an integral protein of the nuclear envelope inner membrane and human chromodomain proteins homologous to Drosophila HP1. J Biol Chem 271:14653–6. doi: 10.1074/JBC.271.25.14653

Ye Q, Worman HJ (1994) Primary structure analysis and lamin B and DNA binding of human LBR, an integral protein of the nuclear envelope inner membrane. J Biol Chem 269:11306–11.

Yi G, Wen Y, Shu C, Han Q, Konan K V., Li P, Kao CC (2015) The Hepatitis C Virus NS4B Can Suppress STING Accumulation to Evade Innate Immune Responses. J Virol 90:JVI.01720-15. doi: 10.1128/JVI.01720-15

Yokoyama A, Wang Z, Wysocka J, Sanyal M, Aufiero DJ, Kitabayashi I, Herr W, Cleary ML (2004) Leukemia Proto-Oncoprotein MLL Forms a SET1 like Complex with Menin to Regulate Hox Gene Expression. Blood 104:2550–2550. doi: 10.1182/blood.v104.11.2550.2550

Yoneyama M, Fujita T (2009) RNA recognition and signal transduction by RIG-I-like receptors. Immunol Rev 227:54–65. doi: 10.1111/j.1600-065X.2008.00727.x

Yoneyama M, Kikuchi M, Natsukawa T, Shinobu N, Imaizumi T, Miyagishi M, Taira K, Akira S, Fujita T (2004) The RNA helicase RIG-I has an essential function in double-stranded RNA-induced innate antiviral responses. Nat Immunol 5:730–737. doi: 10.1038/ni1087

Yoneyama M, Onomoto K, Jogi M, Akaboshi T, Fujita T (2015) Viral RNA detection by RIG-I-like receptors. Curr Opin Immunol 32:48–53. doi: 10.1016/j.coi.2014.12.012

Yoneyama M, Suhara W, Fukuhara Y, Fukuda M, Nishida E, Fujita T (1998) Direct triggering of the type I interferon system by virus infection: Activation of a transcription factor complex containing IRF-3 and CBP/p300. EMBO J 17:1087–1095. doi: 10.1093/emboj/17.4.1087

Yu CY, Chang TH, Liang JJ, Chiang RL, Lee YL, Liao CL, Lin YL (2012) Dengue virus targets the adaptor protein MITA to subvert host innate immunity. PLoS Pathog. doi: 10.1371/journal.ppat.1002780

Yu X, Zhang L, Shen J, Zhai Y, Jiang Q, Yi M, Deng X, Ruan Z, Fang R, Chen Z, Ning X, Jiang Z (2021) The STING phase-separator suppresses innate immune signalling. Nat Cell Biol 23:330–340. doi: 10.1038/s41556-021-00659-0

Yum S, Li M, Chen ZJ (2020) Old dogs, new trick: classic cancer therapies activate cGAS. Cell Res 30:639–648. doi: 10.1038/s41422-020-0346-1

Yum S, Li M, Frankel AE, Chen ZJ (2019) Roles of the cGAS-STING pathway in cancer

immunosurveillance and immunotherapy. Annu Rev Cancer Biol 3:323–344. doi: 10.1146/annurev-cancerbio-030518-055636

Zago P, Baralle M, Ayala YM, Skoko N, Zacchigna S, Buratti E, Tisminetzky S (2009) Improving human interferon-β production in mammalian cell lines by insertion of an intronic sequence within its naturally uninterrupted gene. Biotechnol Appl Biochem 52:191. doi: 10.1042/ba20080046

Zan J, Xu R, Tang X, Lu M, Xie S, Cai J, Huang Z, Zhang J (2020) RNA helicase DDX5 suppresses IFN-I antiviral innate immune response by interacting with PP2A-Cβ to deactivate IRF3. Exp Cell Res. doi: 10.1016/j.yexcr.2020.112332

Zhang C, Shang G, Gui X, Zhang X, Bai X chen, Chen ZJ (2019) Structural basis of STING binding with and phosphorylation by TBK1. Nature 567:394–398. doi: 10.1038/s41586-019-1000-2

Zhang H, Xing Z, Mani SKK, Bancel B, Durantel D, Zoulim F, Tran EJ, Merle P, Andrisani O (2016) RNA helicase DEAD box protein 5 regulates Polycomb repressive complex 2/Hox transcript antisense intergenic RNA function in hepatitis B virus infection and hepatocarcinogenesis. Hepatology 64:1033–1048. doi: 10.1002/hep.28698

Zhang J, Hu MM, Wang YY, Shu HB (2012) TRIM32 protein modulates type I interferon induction and cellular antiviral response by targeting MITA/STING protein for K63-linked ubiquitination. J Biol Chem 287:28646–28655. doi: 10.1074/jbc.M112.362608

Zhang X, Shi H, Wu J, Zhang X, Sun L, Chen C, Chen ZJ (2013) Cyclic GMP-AMP containing mixed Phosphodiester linkages is an endogenous high-affinity ligand for STING. Mol Cell 51:226–235. doi: 10.1016/j.molcel.2013.05.022

Zhang Z, Yuan B, Bao M, Lu N, Kim T, Liu Y-J (2011) The helicase DDX41 senses intracellular DNA mediated by the adaptor STING in dendritic cells. Nat Immunol 12:959–65. doi: 10.1038/ni.2091

Zheng C (2018) Evasion of Cytosolic DNA-Stimulated Innate Immune Responses by Herpes Simplex Virus 1. J Virol 92:1–6. doi: 10.1128/jvi.00099-17

Zheng J, Yong HY, Panutdaporn N, Liu C, Tang K, Luo D (2015) High-resolution HDX-MS reveals distinct mechanisms of RNA recognition and activation by RIG-I and MDA5. Nucleic Acids Res 43:1216–1230. doi: 10.1093/nar/gku1329

Zhong B, Yang Y, Li S, Wang Y-YY, Li Y, Diao F, Lei C, He X, Zhang L, Tien P, Shu H-BB (2008) The Adaptor Protein MITA Links Virus-Sensing Receptors to IRF3 Transcription Factor Activation. Immunity 29:538–550. doi: 10.1016/j.immuni.2008.09.003

Zhong L, Hu MM, Bian LJ, Liu Y, Chen Q, Shu HB (2020) Phosphorylation of cGAS by CDK1 impairs self-DNA sensing in mitosis. Cell Discov. doi: 10.1038/s41421-020-0162-2

Zhou W, Whiteley AT, de Oliveira Mann CC, Morehouse BR, Nowak RP, Fischer ES, Gray NS, Mekalanos JJ, Kranzusch PJ (2018) Structure of the Human cGAS–DNA Complex Reveals Enhanced Control of Immune Surveillance. Cell 174:300-311.e11. doi: 10.1016/j.cell.2018.06.026

Zhou X, Luo J, Mills L, Wu S, Pan T, Geng G, Zhang J, Luo H, Liu C, Zhang H (2013) DDX5

Facilitates HIV-1 Replication as a Cellular Co-Factor of Rev. PLoS One 8:e65040. doi: 10.1371/journal.pone.0065040

Zhu M, Fang T, Li S, Meng K, Guo D (2015) Bipartite Nuclear Localization Signal Controls Nuclear Import and DNA-Binding Activity of IFN Regulatory Factor 3. J Immunol 195:289–297. doi: 10.4049/jimmunol.1500232

Zonta E, Bittencourt D, Samaan S, Germann S, Dutertre M, Auboeuf D (2013) The RNA helicase DDX5/p68 is a key factor promoting c-fos expression at different levels from transcription to mRNA export. Nucleic Acids Res 41:554–564. doi: 10.1093/nar/gks1046

Zuleger N, Boyle S, Kelly DA, de las Heras JI, Lazou V, Korfali N, Batrakou DG, Randles KN, Morris GE, Harrison DJ, Bickmore WA, Schirmer EC (2013) Specific nuclear envelope transmembrane proteins can promote the location of chromosomes to and from the nuclear periphery. Genome Biol 14:R14. doi: 10.1186/gb-2013-14-2-r14

Zuleger N, Kelly DA, Richardson AC, Kerr ARW, Goldberg MW, Goryachev AB, Schirmer EC (2011) System analysis shows distinct mechanisms and common principles of nuclear envelope protein dynamics. J Cell Biol 193:109–123. doi: 10.1083/jcb.201009068

Zuleger N, Kerr ARW, Schirmer EC (2012) Many mechanisms, one entrance: Membrane protein translocation into the nucleus. Cell Mol Life Sci 69:2205–2216. doi: 10.1007/s00018-012-0929-1

Appendix

Table 1 – Mass Spectrometry top hits

spectral counts/mw = normS (mw expressed as 100x kD)
dnormS = normS/sum(spectral counts)

p = number peptides
s = spectral counts with pep_score >=25

= 220 proteins

198 - STING-GFP peptides >=2

22 - STING-GFP peptides =1, spectral counts >=2

gene_name	dnormS. mock	dnormS. STING	dnormS (STING/mock)	p.mock	s.mock	p.STING	s.STING	average. abundance
HIST1H1C	0.0198	0.0474	2.3911	7	28	13	104	0.0336
HIST1H1E	0.0194	0.0459	2.3682	7	28	13	103	0.03265
HIST1H1D	0.0176	0.0423	2.4018	6	26	10	97	0.02995
NCL	0.0144	0.0365	2.5310	24	73	38	287	0.02545
DEK	0.0056	0.0165	2.9372	9	16	20	73	0.01105
HIST2H2AA3	0.0000	0.0180	Inf	0	0	6	26	0.009
HIST1H2BO	0.0000	0.0154	Inf	0	0	8	22	0.0077
HP1BP3	0.0022	0.0122	5.5078	6	9	23	77	0.0072
HIST2H2BF	0.0000	0.0119	Inf	0	0	8	17	0.00595
BRD2	0.0034	0.0071	2.0601	12	20	26	64	0.00525
UBTF	0.0020	0.0085	4.1845	7	12	25	78	0.00525
RSL1D1	0.0025	0.0072	2.9327	7	9	19	41	0.00485
EBNA1BP2	0.0013	0.0084	6.4377	2	3	14	30	0.00485
RBMX	0.0025	0.0071	2.8510	4	7	10	31	0.0048
CCDC86	0.0004	0.0092	24.4632	1	1	13	38	0.0048
SNRNP70	0.0026	0.0066	2.5035	6	9	18	35	0.0046
MFAP1	0.0003	0.0088	30.2571	1	1	15	47	0.00455
PSIP1	0.0005	0.0081	16.0942	2	2	22	50	0.0043
LMNA	0.0022	0.0063	2.8092	6	11	28	48	0.00425
KIAA0020	0.0008	0.0066	8.0471	3	4	25	50	0.0037
RPS27A	0.0000	0.0069	Inf	0	0	7	13	0.00345
SRSF2	0.0018	0.0050	2.7897	2	3	4	13	0.0034
TMPO	0.0012	0.0054	4.5064	3	4	13	28	0.0033
BRD3	0.0013	0.0051	3.8626	5	7	20	42	0.0032
CDK11B	0.0016	0.0048	2.9613	7	10	28	46	0.0032
H1FX	0.0013	0.0043	3.2188	1	2	4	10	0.0028
RBM28	0.0011	0.0037	3.5407	5	6	21	33	0.0024
VRK1	0.0000	0.0045	Inf	0	0	13	21	0.00225
HNRNPR	0.0013	0.0031	2.4678	5	6	14	23	0.0022
IGHG1	0.0000	0.0040	Inf	0	0	3	15	0.002
HNRNPK	0.0006	0.0032	5.4720	2	2	11	17	0.0019
PAF1	0.0008	0.0029	3.8626	3	3	13	18	0.00185
NOP2	0.0010	0.0025	2.4678	5	6	14	23	0.00175
MECP2	0.0000	0.0035	Inf	0	0	10	19	0.00175
RBMXL1	0.0000	0.0035	Inf	0	0	7	15	0.00175
SRSF5	0.0010	0.0025	2.5751	1	2	4	8	0.00175
NOP58	0.0008	0.0023	3.0043	3	3	10	14	0.00155
LYAR	0.0007	0.0024	3.5407	2	2	9	11	0.00155

HIST1H1B	0.0000	0.0030	Inf	0	0	5	7	0.0015
RRP1B	0.0000	0.0028	Inf	0	0	15	24	0.0014
REXO4	0.0003	0.0025	7.7252	1	1	7	12	0.0014
RNPS1	0.0000	0.0028	Inf	0	0	6	10	0.0014
CTDSPL2	0.0006	0.0020	3.5407	1	2	7	11	0.0013
KIF22	0.0004	0.0021	5.1502	2	2	12	16	0.00125
HDGFRP2	0.0004	0.0020	4.8283	1	2	12	15	0.0012
TMPO	0.0000	0.0023	Inf	0	0	7	18	0.00115
CKAP4	0.0000	0.0022	Inf	0	0	11	15	0.0011
DDX5	0.0002	0.0020	9.0128	1	1	11	14	0.0011
KPNA2	0.0000	0.0022	Inf	0	0	10	13	0.0011
HSPA1A	0.0004	0.0018	4.1845	2	2	10	13	0.0011
ILF3	0.0005	0.0016	3.4334	3	3	9	16	0.00105
UHRF1	0.0007	0.0014	2.0922	4	4	10	13	0.00105
GPATCH4	0.0000	0.0021	Inf	0	0	7	11	0.00105
RRP1	0.0000	0.0020	Inf	0	0	7	11	0.001
C16orf88	0.0000	0.0019	Inf	0	0	9	10	0.00095
BOLA2	0.0000	0.0019	Inf	0	0	1	2	0.00095
HELLS	0.0002	0.0016	10.3003	1	1	14	16	0.0009
MCM7	0.0004	0.0014	3.8626	2	2	11	12	0.0009
TAF15	0.0005	0.0013	2.5751	1	2	6	8	0.0009
ZRANB2	0.0000	0.0018	Inf	0	0	6	7	0.0009
NPM1	0.0000	0.0018	Inf	0	0	4	6	0.0009
DDX17	0.0002	0.0015	7.0815	1	1	10	11	0.00085
GNL3	0.0000	0.0017	Inf	0	0	8	11	0.00085
SYNCRIP	0.0004	0.0013	2.8970	2	2	6	9	0.00085
SRSF10	0.0005	0.0012	2.5751	1	1	2	4	0.00085
RBBP7	0.0000	0.0016	Inf	0	0	6	8	0.0008
BAZ2A	0.0003	0.0013	4.5064	4	4	23	28	0.0008
FTSJ3	0.0000	0.0015	Inf	0	0	10	15	0.00075
PARP2	0.0000	0.0015	Inf	0	0	8	10	0.00075
NOP56	0.0002	0.0013	5.7939	1	1	8	9	0.00075
CENPB	0.0000	0.0015	Inf	0	0	7	10	0.00075
LEO1	0.0002	0.0013	6.4377	1	1	6	10	0.00075
SUZ12	0.0002	0.0012	6.4377	1	1	8	10	0.0007
HNRNPD	0.0004	0.0010	2.5751	1	1	2	4	0.0007
SNRPD3	0.0000	0.0014	Inf	0	0	1	2	0.0007
MCM2	0.0003	0.0010	3.5407	2	2	8	11	0.00065
LMNB2	0.0000	0.0013	Inf	0	0	6	9	0.00065
DDX50	0.0004	0.0008	2.2532	2	2	7	7	0.0006
SDAD1	0.0002	0.0010	5.1502	1	1	6	8	0.0006
GTF2I	0.0000	0.0012	Inf	0	0	11	14	0.0006
C14orf21	0.0000	0.0012	Inf	0	0	8	9	0.0006
C17orf85	0.0000	0.0012	Inf	0	0	7	9	0.0006
RRS1	0.0000	0.0012	Inf	0	0	4	5	0.0006
KRT74	0.0000	0.0012	Inf	0	0	3	7	0.0006
TCL6	0.0000	0.0012	Inf	0	0	1	2	0.0006

LIG3	0.0003	0.0008	2.8970	2	2	9	9	0.00055
KRT75	0.0000	0.0011	Inf	0	0	4	7	0.00055
HNRNPA1L2	0.0000	0.0011	Inf	0	0	2	4	0.00055
HNRNPAB	0.0000	0.0011	Inf	0	0	2	4	0.00055
TPX2	0.0000	0.0010	Inf	0	0	9	9	0.0005
KIF20A	0.0001	0.0009	5.7939	1	1	8	9	0.0005
SCML2	0.0000	0.0010	Inf	0	0	7	8	0.0005
CANX	0.0000	0.0010	Inf	0	0	5	7	0.0005
DNTTIP2	0.0002	0.0008	4.5064	1	1	5	7	0.0005
KRT72	0.0000	0.0010	Inf	0	0	2	6	0.0005
RSF1	0.0002	0.0007	3.8626	2	2	10	12	0.00045
RFC1	0.0002	0.0007	2.8970	2	2	9	9	0.00045
MCM4	0.0002	0.0007	4.5064	1	1	7	7	0.00045
MCM6	0.0002	0.0007	4.5064	1	1	6	7	0.00045
KRI1	0.0000	0.0009	Inf	0	0	5	8	0.00045
XRCC6	0.0002	0.0007	3.2188	1	1	5	5	0.00045
HSPA5	0.0002	0.0007	3.2188	1	1	5	5	0.00045
HIRIP3	0.0000	0.0009	Inf	0	0	4	6	0.00045
SURF6	0.0000	0.0009	Inf	0	0	3	4	0.00045
MTA2	0.0000	0.0008	Inf	0	0	6	6	0.0004
API5	0.0000	0.0008	Inf	0	0	5	5	0.0004
HNRPDL	0.0000	0.0008	Inf	0	0	2	4	0.0004
CWC22	0.0001	0.0006	4.5064	1	1	5	7	0.00035
STRBP	0.0000	0.0007	Inf	0	0	3	5	0.00035
CDCA7	0.0000	0.0007	Inf	0	0	3	3	0.00035
SLC9A2	0.0000	0.0007	Inf	0	0	1	7	0.00035
SNRPA1	0.0000	0.0007	Inf	0	0	1	2	0.00035
THOC4	0.0000	0.0007	Inf	0	0	1	2	0.00035
TCOF1	0.0002	0.0004	2.2532	2	2	6	7	0.0003
LARP7	0.0000	0.0006	Inf	0	0	4	4	0.0003
HSPA1L	0.0000	0.0006	Inf	0	0	4	4	0.0003
DDX41	0.0000	0.0006	Inf	0	0	4	4	0.0003
PNN	0.0000	0.0006	Inf	0	0	3	5	0.0003
CKAP2	0.0000	0.0006	Inf	0	0	3	5	0.0003
AATF	0.0000	0.0006	Inf	0	0	3	4	0.0003
LUC7L3	0.0000	0.0006	Inf	0	0	3	3	0.0003
NAP1L1	0.0000	0.0006	Inf	0	0	3	3	0.0003
CLASRP	0.0000	0.0006	Inf	0	0	2	5	0.0003
RPL4	0.0000	0.0006	Inf	0	0	2	3	0.0003
AZGP1	0.0000	0.0006	Inf	0	0	2	2	0.0003
SRSF12	0.0000	0.0006	Inf	0	0	1	2	0.0003
SF3B1	0.0000	0.0005	Inf	0	0	6	7	0.00025
ACIN1	0.0001	0.0004	3.8626	1	1	6	6	0.00025
CUL4B	0.0000	0.0005	Inf	0	0	5	5	0.00025
KPNB1	0.0000	0.0005	Inf	0	0	5	5	0.00025
GTPBP4	0.0000	0.0005	Inf	0	0	4	4	0.00025
YTHDC1	0.0000	0.0005	Inf	0	0	4	4	0.00025

CHAF1A	0.0001	0.0004	2.5751	1	1	4	4	0.00025
GNL2	0.0000	0.0005	Inf	0	0	3	4	0.00025
GTF2F1	0.0000	0.0005	Inf	0	0	2	3	0.00025
CDCA7L	0.0000	0.0005	Inf	0	0	2	3	0.00025
TMEM173	0.0000	0.0005	Inf	0	0	2	2	0.00025
	0.0000	0.0005	Inf	0	0	1	3	0.00025
YBX1	0.0000	0.0005	Inf	0	0	1	2	0.00025
KDM1B	0.0000	0.0004	Inf	0	0	4	4	0.0002
PPIG	0.0000	0.0004	Inf	0	0	4	4	0.0002
SRRT	0.0000	0.0004	Inf	0	0	4	4	0.0002
EZH2	0.0000	0.0004	Inf	0	0	4	4	0.0002
GANAB	0.0000	0.0004	Inf	0	0	4	4	0.0002
SFRS18	0.0000	0.0004	Inf	0	0	3	4	0.0002
HSPA8	0.0000	0.0004	Inf	0	0	3	3	0.0002
TOR1AIP1	0.0000	0.0004	Inf	0	0	3	3	0.0002
RNF6	0.0000	0.0004	Inf	0	0	3	3	0.0002
LUC7L2	0.0000	0.0004	Inf	0	0	2	2	0.0002
RRP8	0.0000	0.0004	Inf	0	0	2	2	0.0002
RCOR1	0.0000	0.0004	Inf	0	0	2	2	0.0002
LUC7L	0.0000	0.0004	Inf	0	0	2	2	0.0002
GLTSCR2	0.0000	0.0004	Inf	0	0	2	2	0.0002
GRWD1	0.0000	0.0004	Inf	0	0	2	2	0.0002
RUVBL2	0.0000	0.0004	Inf	0	0	2	2	0.0002
KRT84	0.0000	0.0004	Inf	0	0	1	3	0.0002
RBM23	0.0000	0.0004	Inf	0	0	1	2	0.0002
AHCTF1	0.0001	0.0002	3.2188	1	1	5	5	0.00015
ATAD5	0.0000	0.0003	Inf	0	0	6	6	0.00015
BCORL1	0.0000	0.0003	Inf	0	0	5	5	0.00015
TCERG1	0.0000	0.0003	Inf	0	0	4	4	0.00015
PRPF40A	0.0000	0.0003	Inf	0	0	3	3	0.00015
ZNF512B	0.0000	0.0003	Inf	0	0	3	3	0.00015
MEN1	0.0000	0.0003	Inf	0	0	2	2	0.00015
HSPD1	0.0000	0.0003	Inf	0	0	2	2	0.00015
HSPA9	0.0000	0.0003	Inf	0	0	2	2	0.00015
CCDC47	0.0000	0.0003	Inf	0	0	2	2	0.00015
HSPA2	0.0000	0.0003	Inf	0	0	2	2	0.00015
RANGAP1	0.0000	0.0003	Inf	0	0	2	2	0.00015
DNAJC21	0.0000	0.0003	Inf	0	0	2	2	0.00015
SCMH1	0.0000	0.0003	Inf	0	0	2	2	0.00015
GLYR1	0.0000	0.0003	Inf	0	0	2	2	0.00015
SMARCD1	0.0000	0.0003	Inf	0	0	2	2	0.00015
UTP18	0.0000	0.0003	Inf	0	0	2	2	0.00015
MLLT1	0.0000	0.0003	Inf	0	0	2	2	0.00015
SFPQ	0.0000	0.0003	Inf	0	0	2	2	0.00015
MSL3	0.0000	0.0003	Inf	0	0	2	2	0.00015
SMARCD2	0.0000	0.0003	Inf	0	0	2	2	0.00015
SF3A3	0.0000	0.0003	Inf	0	0	2	2	0.00015

DPYSL5	0.0000	0.0003	Inf	0	0	1	2	0.00015
RAI1	0.0000	0.0002	Inf	0	0	3	5	0.0001
SCAF11	0.0000	0.0002	Inf	0	0	3	3	0.0001
INTS3	0.0000	0.0002	Inf	0	0	3	3	0.0001
SMARCA2	0.0000	0.0002	Inf	0	0	3	3	0.0001
ADNP	0.0000	0.0002	Inf	0	0	2	2	0.0001
NOC2L	0.0000	0.0002	Inf	0	0	2	2	0.0001
TTF1	0.0000	0.0002	Inf	0	0	2	2	0.0001
U2SURP	0.0000	0.0002	Inf	0	0	2	2	0.0001
C19orf29	0.0000	0.0002	Inf	0	0	2	2	0.0001
ESF1	0.0000	0.0002	Inf	0	0	2	2	0.0001
RBM25	0.0000	0.0002	Inf	0	0	2	2	0.0001
DNMT3A	0.0000	0.0002	Inf	0	0	2	2	0.0001
HSP90B1	0.0000	0.0002	Inf	0	0	2	2	0.0001
TRIM28	0.0000	0.0002	Inf	0	0	2	2	0.0001
MPHOSPH10	0.0000	0.0002	Inf	0	0	2	2	0.0001
POTEJ	0.0000	0.0002	Inf	0	0	2	2	0.0001
DDX42	0.0000	0.0002	Inf	0	0	2	2	0.0001
DDX23	0.0000	0.0002	Inf	0	0	2	2	0.0001
VCP	0.0000	0.0002	Inf	0	0	2	2	0.0001
ITPR2	0.0000	0.0002	Inf	0	0	1	7	0.0001
BRDT	0.0000	0.0002	Inf	0	0	1	2	0.0001
TMEM214	0.0000	0.0002	Inf	0	0	1	2	0.0001
BPTF	0.0000	0.0001	Inf	0	0	4	4	0.00005
TPR	0.0000	0.0001	Inf	0	0	4	4	0.00005
TNRC18	0.0000	0.0001	Inf	0	0	3	3	0.00005
MLL	0.0000	0.0001	Inf	0	0	2	3	0.00005
TIMELESS	0.0000	0.0001	Inf	0	0	2	2	0.00005
SRCAP	0.0000	0.0001	Inf	0	0	2	2	0.00005
CECR2	0.0000	0.0001	Inf	0	0	2	2	0.00005
ZMYND8	0.0000	0.0001	Inf	0	0	2	2	0.00005
TCF20	0.0000	0.0001	Inf	0	0	2	2	0.00005
KIF4A	0.0000	0.0001	Inf	0	0	2	2	0.00005
CENPF	0.0000	0.0001	Inf	0	0	2	2	0.00005
MYH4	0.0000	0.0001	Inf	0	0	1	3	0.00005
MYH8	0.0000	0.0001	Inf	0	0	1	3	0.00005
MYH1	0.0000	0.0001	Inf	0	0	1	3	0.00005
NAV3	0.0000	0.0001	Inf	0	0	1	2	0.00005
VARS	0.0000	0.0001	Inf	0	0	1	2	0.00005
VWA3A	0.0000	0.0001	Inf	0	0	1	2	0.00005
COL5A1	0.0000	0.0001	Inf	0	0	1	2	0.00005